# Roles of the Autism Candidate Genes Neuroligin-3, Neuroligin-4, and Neurobeachin in Synaptic Plasticity and Excitation-Inhibition Balance in the Dentate Gyrus

# *Die Rollen der Autismus-Kandidatengene Neuroligin-3, Neuroligin-4 und Neurobeachin in der Synaptischen Plastizität und der Exzitations-Inhibitions-Balance im Gyrus Dentatus*

PhD dissertation submitted to the Faculty of Biosciences of the

*Dissertation zur Erlangung des Doktorgrades der Naturwissenschaften vorgelegt beim Fachbereich Biowissenschaften der*

Johann Wolfgang Goethe-Universität in Frankfurt am Main


by / *von*

**Julia Muellerleile**

from / *aus*

Augsburg



Frankfurt am Main, 2022
(D30)

Vom Fachbereich Biowissenschaften der

Johann Wolfgang Goethe-Universität als Dissertation angenommen

Dekan: Prof. Dr. Sven Klimpel

Gutachter:

Prof. Dr. Manfred Kössl
Prof. Dr. Peter Jedlička

Datum der Disputation: 13.06.2022

# Contents

**Zusammenfassung / Summary (Deutsch / English)** **1**

**1 Introduction** **11**
1.1 Clinical Features of ASD . . . 12
1.1.1 Behavioral Symptoms of ASD . . . 12
1.1.2 Neuroanatomical Abnormalities in Individuals with ASD . . . 13
1.1.3 Comorbidities of ASD with Other Disorders . . . 14
1.1.4 Prognosis and Treatment . . . 15
1.1.5 Etiology . . . 15
1.2 Animal Models of ASD . . . 16
1.2.1 Model Species . . . 17
1.2.2 Behavioral Testing . . . 17
Assessing Social Deficits . . . 18
Assessing Communication Deficits . . . 19
Assessing Repetitive Behaviors and the ″Insistence on Sameness″ . . . 20
Assessing Sensory Symptoms . . . 20
1.3 Overview of the ASD Mouse Models Investigated in this Dissertation . . . 21
1.3.1 The Neurobeachin Haploinsufficient Mouse Model . . . 21
1.3.2 The Neuroligin-3 Knockout Mouse Model . . . 23
1.3.3 The Neuroligin-4 Knockout Mouse Model . . . 26
1.4 Assessing E-I Balance in the Hippocampal Dentate Gyrus . . . 28
1.5 Aims and Objectives . . . 31

**2 Discussion** **33**

**Bibliography** **41**

**3 Manuscript 1** **55**

**4 Manuscript 2** **79**

**5 Manuscript 3** **109**

# List of Figures

1.1 Dentate Gyrus Circuitry and fEPSP . . . . . 29

1 Manuscript 1 - Figure 1 . . . . . 61
2 Manuscript 1 - Figure 2 . . . . . 63
2 Manuscript 1 - Figure 2 . . . . . 64
3 Manuscript 1 - Figure 3 . . . . . 64
4 Manuscript 1 - Figure 4 . . . . . 66
S1 Manuscript 1 - Figure S1 . . . . . 78

1 Publication 2 - Figure 1 . . . . . 88
2 Publication 2 - Figure 2 . . . . . 89
3 Publication 2 - Figure 3 . . . . . 91
4 Publication 2 - Figure 4 . . . . . 92
5 Publication 2 - Figure 5 . . . . . 94
S1 Publication 2 - Figure S1 . . . . . 107

1 Publication 3 - Figure 1 . . . . . 119
2 Publication 3 - Figure 2 . . . . . 120
3 Publication 3 - Figure 3 . . . . . 121
4 Publication 3 - Figure 4 . . . . . 122
5 Publication 3 - Figure 5 . . . . . 124
6 Publication 3 - Figure 6 . . . . . 127
7 Publication 3 - Figure 7 . . . . . 128
8 Publication 3 - Figure 8 . . . . . 130
9 Publication 3 - Figure 9 . . . . . 133
S1 Publication 3 - Figure S1 . . . . . 141

# List of Tables

1 Publication 2 - Table 1 . . . . . 94

1 Publication 3 - Table 1 . . . . . 126
2 Publication 3 - Table 2 . . . . . 131
3 Publication 3 - Table 3 . . . . . 131

# List of Abbreviations

| | |
|---|---|
| **ADHD** | **A**ttention **D**eficit/**H**yperactivity **D**isorder |
| **AKAP** | **A**-**K**inase **A**nchor **P**rotein |
| **AMPA** | **A**lpha-amino-3-hydroxy-5-**M**ethyl-4-isoxazole-**P**ropionic **A**cid |
| **ASD** | **A**utism **S**pectrum **D**isorder |
| **BEACH** | **BE**ige **A**nd **C**hediak-**H**igashi |
| **CA** | **C**ornu **A**mmonis |
| **CCK** | **C**hole**C**ysto**K**inin |
| **DFG** | **D**eutsche **F**orschungs**G**emeinschaft |
| **DOI** | **D**igital **O**bject **I**dentifier |
| **DSM** | **D**iagnostic and **S**tatistical **M**anual |
| **E-I** | **E**xcitation-**I**nhibition |
| **EM** | **E**lectron **M**icroscopy |
| **E-S** | EPSP-Population **S**pike |
| **EPSC** | **E**xcitatory **P**ost**S**ynaptic **C**urrent |
| **FELASA** | **F**ederation of **E**uropean **L**aboratory **A**nimal **S**cience **A**ssociations |
| **fEPSP** | field **E**xcitatory **P**ost**S**ynaptic **P**otential |
| **GABA** | **G**amma-**A**mino**B**utyric **A**cid |
| **HCN** | **H**yperpolarization-activated **C**yclic **N**ucleotide-gated |
| **I-O** | **I**nput-**O**utput |
| **IPSC** | **I**nhibitory **P**ost**S**ynaptic **C**urrent |
| **KO** | **K**nock**O**ut |
| **LPP** | **L**ateral **P**erforant **P**ath |
| **LRRTM** | **L**eucine-**R**ich-**R**epeat **T**rans**M**embrane Protein |
| **LTP** | **L**ong-**T**erm **P**otentiation |
| **mEPSC** | **m**iniature **E**xcitatory **P**ost**S**ynaptic **C**urrent |
| **mGluR** | **m**etabotropic **Glu**tamate **R**eceptor |
| **MPP** | **M**edial **P**erforant **P**ath |
| **MRI** | **M**agnetic **R**esonance **I**maging |
| **Nbea** | **N**euro**bea**chin |
| **Nlgn** | **N**euro**ligin** |
| **NMDA** | **N**-**M**ethyl-**D**-**A**spartate |
| **OTC** | **O**rgano**T**ypic entorhino-hippocampal slice **C**ulture |
| **PAR** | **P**seudo-**A**utosomal **R**egion |
| **pCREB** | **p**hosphorylated **c**AMP **R**esponse-**E**lement **B**inding protein |
| **PKA** | **P**rotein **K**inase **A** |
| **PPI** | **P**aired-**P**ulse **I**nhibition |
| **PTP** | **P**rotein **T**yrosine **P**hosphatase |
| **RM-ANOVA** | **R**epeated **M**easures-**AN**alysis **O**f **VA**riance |
| **RMP** | **R**esting **M**embrane **P**otential |
| **SEM** | **S**tandard **E**rror of the **M**ean |
| **SFARI** | **S**imons **F**oundation **A**utism **R**esearch **I**nitiative |
| **SI** | **S**upplementary **I**nformation |
| **SOM** | **SOM**atostatin |
| **TBS** | **T**heta-**B**urst **S**timulation |

| | |
|---|---|
| **TLE** | **T**emporal **L**obe **E**pilepsy |
| **TTX** | **T**etrodo**T**o**X**in |
| **VTA** | **V**entral **T**egmental **A**rea |
| **WT** | **W**ild-**T**ype |

# Zusammenfassung / Summary (Deutsch / English)

Autismus-Spektrum-Störung (ASS) ist eine häufig vorkommende neurologische Entwicklungsstörung mit einem mannigfaltigen klinischen Erscheinungsbild. Obwohl schon viele genetische Risikofaktoren identifiziert und in Mausmodellen untersucht worden sind, sind die neurophysiologischen Mechanismen, die zu einer Ausbildung von einem autistischen Phänotyp führen, immer noch unklar. Basierend auf der hohen Komorbiditätsrate von ASS und Epilepsie wurde die Hypothese aufgestellt, dass das Gleichgewicht zwischen der Exzitation und Inhibition in neuronalen Netzwerken der betroffenen Personen gestört sein könnte. In dieser Dissertation wurde die Aktivität von Neuronen im Netzwerk und an der Synapse in drei genetisch veränderten Mausmodellen, die charakteristische Verhaltensauffälligkeiten der autistischen Störung aufzeigen, untersucht: im Neurobeachin (Nbea) haploinsuffizienten, im Neuroligin-3 (Nlgn3) Knock-out (KO), und im Nlgn4 KO Mausmodell. Diese Proteine sind alle an der Synapsenbildung und/oder -funktion im zentralen Nervenystem beteiligt. Daher wurde vermutet, dass die Reduktion oder Deletion dieser Proteine die Balance zwischen exzitatorischer und inhibitorischer synaptischer Übertragung in einzelnen Neuronen sowie in neuronalen Netzwerken ändern könnte. Extrazelluläre Ableitungen im hippocampalen Gyrus dentatus von anästhesierten Mäusen haben gezeigt, dass das Exzitations-Inhibitions(E-I)-Gleichgewicht in Nbea haploinsuffizienten sowie Nlgn4 KO-Mäusen reduziert war, aber in Nlgn3 KO-Mäusen trotz einer Verminderung der exzitatorischen synaptischen Übertragung unverändert war. Unerwarteterweise war die intrinsische Erregbarkeit der Körnerzellen in allen drei Mausmodellen verändert. Diese Ergebnisse weisen darauf hin, dass eine homöostatische Erhöhung der intrinsischen Erregbarkeit die Reduktion der exzitatorischen synaptischen Transmission in Nlgn3 KO-Mäusen kompensieren kann, wohingegen die verminderte intrinsische Erregbarkeit in Nbea haploinsuffizienten sowie Nlgn4 KO-Mäusen das E-I-Ungleichgewicht verursacht. Insgesamt zeigen diese Befunde, dass der Einfluss von genetischen Faktoren auf das E-I-Gleichgewicht ein potenzieller Mechanismus ist, der zur Ausbildung von ASS führen könnte.

Charakteristisch für ASS sind Probleme in zwei Bereichen des Verhaltens: (1) Soziale Interaktion und Kommunikation, sowie (2) sensorische und motorische Funktionen. Beispiele für Probleme in den sozialen Fähigkeiten und der Kommunikation sind Defizite in der Entwicklung sozialer Beziehungen und in der non-verbalen Kommunikation, sowie eine verzögerte Sprachentwicklung. Zu den sensorisch-motorischen Auffälligkeiten gehören repetitive Verhaltensweisen, eng begrenzte Interessensbereiche, ein ungewöhnlich hoher Widerstand gegen Veränderungen und eine gesteigerte oder verminderte Wahrnehmung sensorischer Stimuli. Im Allgemeinen treten die Symptome in der frühen Kindheit auf und frühzeitige Verhaltensinterventionen können den Verlauf der Symptome günstig beeinflussen. Allerdings gibt es keinerlei vollständige Heilung von ASS und während viele der betroffenen Personen im Erwachsenenalter ohne größere Einschränkungen leben können, benötigen andere lebenslange Unterstützung. Die Entwicklung von effektiven Therapien ist deshalb sehr wichtig und bedarf der Identifizierung der grundsätzlichen biologischen Mechanismen, die bei autistischen Personen gestört sind.

Dies wird allerdings dadurch erschwert, dass die Ursachen für die Entstehung von ASS multifaktoriell sind: genetische, epigenetische und Umweltfaktoren tragen zum Risiko der

Entwicklung von ASS bei. Allerdings haben Zwillingsstudien gezeigt, dass die größten Risikofaktoren genetischen Ursprungs sind. Gene, die an der Synaptogenese beteiligt sind, wurden im Zusammenhang mit ASS beschrieben und sprechen für eine Manifestation der Störungen während der Gehirnentwicklung. Interessanterweise treten ASS und Epilepsie häufig zusammen auf und haben viele genetische Risikofaktoren gemeinsam. Die genetische Gemeinsamkeit deutet darauf hin, dass ähnliche biologische Prozesse wie etwa die neuronale Migration und die synaptische Funktion in beiden Erkrankungen eine Rolle spielen. Eine relative Zunahme der Exzitation in den neuronalen Netzwerken autistischer Personen könnte eine Prädisposition für Epilepsie darstellen und die erhöhte Komorbidität der Erkrankungen erklären. Da eine relative Erhöhung der Exzitation im Netzwerk sowohl durch gesteigerte exzitatorische synaptische Übertragung als auch verminderte inhibitorische synaptische Übertragung entstehen kann, ist das Ungleichgewicht von Exzitation und Inhibition ein hypothetischer Mechanismus für die Entwicklung von ASS.

Mittels Genomsequenzierung konnten hunderte Gene identifiziert werden, die potenziell an der Entwicklung von ASS beteiligt sind. Welche dieser Gene ASS auslösen wird durch die Ausprägung tausender verschiedener Genvarianten, die in sehr vielen Personen vorkommen, erschwert. Jede einzelne dieser häufig vorkommenden Varianten erhöht das Risiko für die Entwicklung von ASS nur leicht, aber in der Summe bestimmen diese Varianten die Prädisposition für ASS. Das Untersuchen einzelner ASS-assoziierter Gene in genetisch homogenen Tiermodellen wie z.B. in Inzucht-Mausstämmen reduziert die genetische Hintergrundvariabilität und ermöglicht somit die Evaluation des Effekts einzelner Genvarianten auf den Phänotyp.

Die Zweckmäßigkeit eines Tiermodells für eine menschliche Erkrankung wird nach den folgenden drei Kriterien beurteilt: (1) dieselben biologischen Prozesse, die in betroffenen Menschen verändert sind, müssen auch im Tiermodell verändert sein, (2) die Symptome müssen in Mensch und Tier gleich (oder ähnlich) sein, und (3) die gleiche medizinische Behandlung von Mensch und Tier muss beiderseits den gleichen Effekt haben. Auch wenn die meisten Gene in Menschen und Mäusen homolog sind und Verhaltensweisen analog zu den Verhaltenssymptomen in ASS auch in Mäusen beobachtet werden können, gibt es keinerlei zugelassene pharmakologische Behandlung der hauptsächlichen Symptome bei ASS. Entsprechend können Mausmodelle für ASS nur anhand der ersten zwei Kriterien bewertet werden. In solchen Mausmodellen werden Gene, die mit ASS in Zusammenhang stehen so manipuliert, dass dem Menschen verwandte biologische Prozesse beeinflusst werden und der Effekt der genetischen Modifikation auf ASS-relevante Verhaltensweisen in der Maus evaluiert werden kann.

Um den Zusammenhang zwischen potenziellen Autismus-Genen und deren Einfluss auf die synaptische Funktion und das E-I-Gleichgewicht zu verstehen, wurden in dieser Dissertation drei validierte genetische Mausmodelle für ASS untersucht: das Neurobeachin (Nbea) haploinsuffiziente (veröffentlichtes Manuskript 1), das Nlgn3 KO (veröffentlichtes Manuskript 2), und das Nlgn4 KO (Manuskript 3) Mausmodell. Jedes dieser Mausmodelle zeigt Defizite in der Synapsenbildung oder -funktion, jedoch wurde das E-I-Gleichgewicht zuvor nur in einem Modell systematisch untersucht (Nlgn4 KO). Sowohl die synaptische als auch die Netzwerkaktivität wurden mittels *whole-cell patch-clamp*-Messungen in hippocampalen Körnerzellen und extrazellulären Feldpotenzialmessungen im Gyrus dentatus erprobt; einer Hirnregion, die sowohl strukturelle als auch funktionelle Beeinträchtigungen in einigen autistischen Personen sowie in Personen, die an einer Temporallappenepilepsie leiden, aufweist.

Der Gyrus dentatus dient als zentrale Eingangsstruktur für die kortikalen und subkortikalen Afferenzen des Hippocampus, einer wichtigen Hirnstruktur für die Gedächtniskonsolidierung und das Abrufen von Erinnerungen. Der hauptsächliche Zelltyp im Gyrus dentatus ist die Körnerzelle, die sich durch ein niedriges Ruhepotenzial und starke Inhibition auszeichnet. Dadurch wird die Weiterleitung epilepsieartiger Aktivität in den Hippocampus verhindert. Diese Eigenschaften der Körnerzelle sind auch für eine kompakte Kodierung (engl. *sparse coding*) der Information im Gyrus dentatus verantwortlich, welche eine der mutmaßlichen

Funktionen dieser Hirnregion ermöglicht, nämlich die Unterscheidung ähnlicher synaptischer Aktivitätsmuster (die sogenannte Mustertrennung oder engl. *pattern separation*). Für die Fragestellung von maßgeblicher Bedeutung ist die Möglichkeit, die Körnerzellen und das lokale inhibitorische Netzwerk im Gyrus dentatus gleichzeitig durch die Stimulation des Tractus perforans, der aus den Axonen der Neurone des entorhinalen Kortex besteht, zu aktivieren. Der extrazellulär abgeleitete *population spike* spiegelt die Summe der Aktionspotenziale der einzelnen Körnerzellen wider und zeigt somit das relative Verhältnis zwischen Exzitation und Inhibition im Gyrus dentatus an. Durch den Vergleich des *population spike* in genetisch modifizierten Mäusen mit dem in Wildtyp-Mäusen konnten Störungen im E-I-Gleichgewicht der ASS Mausmodelle festgestellt werden. Die damit einhergehenden Änderungen der intrazellulären und Netzwerkaktivität im Gyrus dentatus konnten neue Erkenntnisse über die Funktion dieser drei Proteine in der Regulierung der synaptischen Übertragung und der intrinsischen Erregbarkeit in den Körnerzellen liefern.

**Im ersten Manuskript** wurde ein haploinsuffizientes Nbea ($Nbea^{+/-}$) Mausmodell untersucht. Nbea ist ein Protein mit mehreren Domänen, das in vielfältige neuronale Funktionen wie etwa die Vesikelsekretion, den Transport von Neurotransmitterrezeptoren, und die Organisation des Aktin-Zytoskeletts eingebunden ist. Die Störung dieser zellulären Prozesse durch den Verlust von Nbea führt in neruonalen Zellkulturen von Mäusen zu Problemen in der prä- und postsynaptischen Funktion sowie zu einer geringeren Anzahl von dendritischen Dornen; kleine Membranausstülpungen zur Bildung exzitatorischer Synapsen. Während der Verlust eines Nbea-Allels im Zusammenhang mit ASS und Epilepsie steht, ist ein homozygoter KO von Nbea in Mäusen hingegen tödlich, weil er zum Aussetzen der synaptischen Übertragung an den muskulären Endplatten der Atemmuskulatur führt. Da es bisher keinerlei klinische Berichte über homozygote Deletionen von Nbea gibt, ist es wahrscheinlich, dass Nbea auch ein letaler Faktor in Menschen ist. Vorangegangene Studien haben gezeigt, dass $Nbea^{+/-}$ Mäuse Unterschiede im sozialen Verhalten und eine Erhöhung repetitiver Verhaltensweisen im Vergleich zum Wildtyp und somit analoge Veränderungen zum pathologischen Phänotyp im Menschen zeigen. Außerdem wurde bereits festgestellt, dass haploinsuffiziente Mäuse weniger Synapsen sowie Störungen in der exzitatorischen synaptischen Übertragung und Plastizität aufweisen. Im Gegensatz dazu wurde in dieser Arbeit kein signifikanter Unterschied im exzitatorischen synaptischen Input zum Gyrus dentatus von $Nbea^{+/-}$ Mäusen im Vergleich zu Wildtyp-Mäusen festgestellt. Allerdings führte der gleiche synaptische Input zu einem schwächeren *population spike*, der entweder durch eine Steigerung der Inhibition oder durch eine Reduktion der intrinsischen Erregbarkeit der Körnerzellen zu erklären ist. Auch wenn diese Frage mittels extrazellulärer Messungen nicht komplett geklärt werden konnte, sprechen die Daten dieser Arbeit dafür, dass die inhibitorische Übertragung in $Nbea^{+/-}$ Mäusen nicht verändert ist. Zusätzlich konnte eine Dissoziation zwischen der synaptischen Potenzierung und der Potenzierung des *population spike* nach der Induktion einer Langzeitpotenzierung, einer Form der synaptischen Plastizität, festgestellt werden, die darauf hindeutet, dass die Regulation der intrinsischen Erregbarkeit der Körnerzellen in $Nbea^{+/-}$ Mäusen verändert ist. Die Reduktion der Nbea-Expression in den $Nbea^{+/-}$ Mäusen könnte zu Störungen des intradendritischen Proteintransports und/oder der Expression von Ionenkanälen in der Zellmembran führen und dadurch die intrinsische Erregbarkeit vermindern, wodurch das E-I-Gleichgewicht in $Nbea^{+/-}$ Mäusen in Richtung der Inhibition verschoben ist.

**Im zweiten Manuskript** wurde in Nlgn3 KO-Mäusen gezeigt, dass eine Reduktion des synaptischen Inputs zu einer Erhöhung der intrinsischen Erregbarkeit der Körnerzellen führt und somit zu einem Erhalt des E-I-Gleichgewichts im Gyrus dentatus. Nlgn3 wird als ein synaptisches Adhäsionsprotein an der postsynaptischen Membran exprimiert und führt dort durch Bindung an präsynaptische Neurexin-Proteine zu einer Stabilisierung der Synapse. Im Zusammenhang mit ASS wurden im Menschen sowohl *gain-of-function* als auch *loss-of-function* Mutationen im Nlgn3-Gen beobachtet. Aufgrund der Lokalisierung des Nlgn3-Gens auf dem

X-Chromosom sind die betroffenen Personen erwartungsgemäß meistens männlich. Ähnlich zu Menschen mit ASS, haben Nlgn3 KO-Mäuse Einschränkungen im sozialen Gedächtnis und eine gesteigerte Tendenz zur Entwicklung repetitiver motorischer Verhaltensroutinen. Neurophysiologisch zeigen sich in den KO-Mäusen regionale Beeinträchtigungen der exzitatorischen und inhibitorischen synaptischen Übertragung und/oder Plastizität in kortikalen, zerebellaren und Hirnstamm-Neuronen. In der vorliegenden Arbeit wurde eine Reduktion der synaptischen Übertragung vom Tractus perforans auf die Körnerzellen anhand von extrazellulären Feldpotenzialmessungen festgestellt und somit vorangegangene Befunde aus Studien an akuten Schnitten, die eine Reduktion der exzitatorischen synaptischen Ströme in Körnerzellen, in denen die Nlgn3-Expression heruntergeregelt worden war, gezeigt hatten, bestätigt. Die extrazellulären Ableitungen im Gyrus dentatus zeigten allerdings eine unveränderte Amplitude des *population spike* der Körnerzellen im Vergleich zum Wildtyp. Dieser Zusammenhang deutet auf eine homöostatische Erhöhung der intrinsischen Erregbarkeit der Körnerzellen in Nlgn3 KO-Mäusen hin, um den verminderten synaptischen Input zu kompensieren. Interessanterweise war die Inhibition in Nlgn3 KO-Mäusen ebenfalls leicht erhöht, allerdings nicht stark genug, um das E-I-Gleichgewicht im Gyrus dentatus zu beeinflussen. Diese Ergebnisse unterstreichen wie wichtig homöostatische Mechanismen für das E-I-Gleichgewicht sind und zeigen, dass Defekte in der synaptischen Funktion nicht notwendigerweise zu einer Veränderung des E-I-Gleichgewichts führen.

**Im dritten Manuskript** wurde die Funktion von Neuroligin-4 (Nlgn4) an Synapsen von Körnerzellen im Gyrus dentatus mittels extrazellulärer *in vivo* Ableitungen und *whole-cell patch-clamp*-Ableitungen von Körnerzellen in entorhino-hippocampalen Schnittkulturen (engl. *organotypic slice cultures*, kurz OTCs) untersucht. Nlgn4 ist ein weiteres synaptisches Adhäsionsprotein aus der Neuroligin-Familie, das im Menschen ebenfalls auf dem X-Chromosom lokalisiert ist. Interessanterweise ist das Nlgn4-Gen in Mäusen auf der pseudoautosomalen Region der Geschlechtschromosomen lokalisiert. Dementsprechend kann es genauso wie autosomale Gene homolog rekombiniert werden. Auch wenn es beträchtliche Unterschiede zwischen der Sequenz des Nlgn4-Gens in Menschen und Mäusen gibt, sind die entscheidenden funktionalen Regionen des Gens scheinbar konserviert. Mutationen des Nlgn4-Gens im Menschen stehen im Zusammenhang mit der Entwicklung von ASS, geistiger Behinderung und der Aufmerksamkeits- und Hyperaktivitätsstörung. Im Einklang mit diesen Symptomen in Menschen sind die Nlgn4 KO-Mäuse weniger sozial und zeigen Beeinträchtigungen im sozialen Gedächtnis und in der Kommunikation. Obwohl in erster Linie die inhibitorische synaptische Übertragung in Nlgn4 KO-Mäusen geschädigt ist, ist auch die exzitatorische synaptische Übertragung im somatosensorischen Kortex betroffen. Insgesamt kommt es dadurch zu einer Verminderung des E-I-Gleichgewichts. In den untersuchten OTCs von Nlgn4 KO-Mäusen konnten hingegen keine Veränderungen der exzitatorischen oder inhibitorischen Übertragung in individuellen Körnerzellen beobachtet werden. Allerdings war das Aktionspotenzial-Feuerungsmuster der Körnerzellen in Antwort auf intrazelluläre Strominjektionen in den OTCs von Nlgn4 KO-Mäuse verändert. Außerdem wurden leichte Unterschiede in der Schwelle des *population spike* sowie in der Netzwerk-Inhibition im Gyrus dentatus von Nlgn4 KO-Mäusen *in vivo* festgestellt. Möglicherweise ist die intrinsische Erregbarkeit der Körnerzellen in Nlgn4 KO-Mäusen reduziert. Dies würde zu einem späteren Eintreten des *population spike* führen und die relative Stärke der inhibitorischen Kontrolle über den Aktionspotenzials-Output der Körnerzellen erhöhen. Dementsprechend könnten Änderungen der intrinsischen Erregbarkeit das E-I-Gleichgewicht im Gyrus dentatus stören, obwohl das Level der exzitatorischen und inhibitorischen Übertragung nicht verändert ist.

Insgesamt sprechen die Ergebnisse der Einzelarbeiten dieser Dissertation für die Hypothese eines E-I-Ungleichgewichts bei ASS neben zwei weiteren wichtigen Beobachtungen: (1) Im Gegensatz zu Epilepsie scheint ASS auch mit einer Steigerung des relativen Levels der Inhibition in Verbindung zu stehen, und (2) Defizite in der synaptischen Übertragung können sowohl

zu einem E-I-Ungleichgewicht führen als auch durch Veränderungen der intrinsischen Erregbarkeit kompensiert werden. Diese Ergebnisse stehen im Einklang mit anderen Studien, die eine erhöhte Inhibition in ASS-Mausmodellen gezeigt haben. Allerdings ist zu beachten, dass viele verschiedene Klassen inhibitorischer Interneurone existieren, die unterschiedliche Funktionen übernehmen einschließlich der Regulation anderer Interneurone. Die Inhibition des *population spike* der Körnerzellen wird in erster Linie durch Interneurone vermittelt, deren Synapsen an der perisomatischen Region der Körnerzellen lokalisiert sind. Entsprechend beziehen sich die Ergebnisse dieser Arbeit nur auf eine spezifische Form der Inhibition. Andere Einschränkungen, die bei der Interpretation der Ergebnisse der durchgeführten Studien gemacht werden müssen, betreffen einerseits die verwendete Anästhesie der Versuchstiere, die erwartungsgemäß zu einer Veränderung des Levels von Exzitation und Inhibition führt und andererseits die Stimulationsmethode, die nur eine Afferenz des Gyrus dentatus beeinflusst.

Zusammenfassend lässt sich festhalten, dass die dargestellten Ergebnisse die Relevanz der intrinsischen Erregbarkeit der Körnerzellen auf das E-I-Gleichgewicht im Gyrus dentatus hervorheben. Sowohl im Nbea$^{+/-}$ als auch im Nlgn4 KO ASS-Mausmodell konnte eine Verminderung der intrinsischen Erregbarkeit, die zu mehr Inhibition führt, beobachtet werden, wohingegen die Reduktion der exzitatorischen synaptischen Übertragung im Nlgn3 KO ASS-Mausmodell durch einen Anstieg der intrinsischen Erregbarkeit der Körnerzellen kompensiert wurde. Zukünftige Untersuchungen der Netzwerkaktivität in wachen Mäusen könnten zeigen inwieweit die beschriebenen Veränderungen auf elektrophysiologischer Ebene mit dem veränderten Phänotyp der ASS-Mausmodelle im Zusammenhang stehen und ob sich diese auch auf andere Hirnregionen generalisieren lassen. Sollte sich eine Verbindung zwischen den Symptomen bei ASS und einem E-I-Ungleichgewicht bestätigen, könnte das Wiederherstellen des E-I-Gleichgewichts eine Behandlungsmöglichkeit für ASS darstellen.

Autism spectrum disorder (ASD) is a common neurodevelopmental disorder with a multifarious clinical presentation. Even though many genetic risk factors have been identified and studied in mouse models, the neurophysiological mechanisms underlying the autistic phenotype are still unclear. Based on the high rates of comorbidity with epilepsy, it was hypothesized that the balance between excitation and inhibition in neural circuits may be disrupted in autistic individuals. In this dissertation, synaptic and network activity was measured in three different genetically modified mouse models that exhibit the characteristic behavioral abnormalities of the disorder: the Neurobeachin (Nbea) haploinsufficient mouse, the Neuroligin-3 (Nlgn3) knockout (KO) mouse, and the Neuroligin-4 (Nlgn4) KO mouse. Each of the affected proteins is involved in the formation and/or function of synapses in the central nervous system. Therefore, it was posited that the reduction or deletion of these proteins might alter the balance of excitatory to inhibitory synaptic transmission in individual neurons and in neural circuits. Extracellular recordings in the hippocampal dentate gyrus of anesthetized mice revealed that the excitation-inhibition (E-I) balance was reduced in Nbea haploinsufficient and Nlgn4 KO mice, but unchanged in Nlgn3 KO mice despite a reduction in excitatory synaptic transmission to dentate granule cells. Unexpectedly, the intrinsic excitability of dentate granule cells was altered in all three mouse models. These results imply that a homeostatic increase in the intrinsic excitability is able to compensate for the decreased excitatory transmission in Nlgn3 KO mice, whereas the decreased intrinsic excitability in the Nbea haploinsufficient and Nlgn4 KO mice leads to a reduction in the E-I balance. Taken together, these findings suggest that the influence of genetic factors on the E-I balance might be a potential common mechanism underlying the development of ASD.

ASD is characterized by difficulties in two behavioral domains: (1) social interaction and communication and (2) sensory-motor function. Examples of social and communication difficulties in ASD include deficits in developing relationships, poor eye-contact, and delayed speech. In the sensory-motor domain, affected individuals may exhibit repetitive behaviors, highly restricted interests, a resistance to change, and an enhanced or a diminished response to sensory stimuli. Generally, the symptoms emerge during early childhood, and timely behavioral interventions help improve outcomes. However, there is no cure for ASD, and while many individuals go on to live independently, others require lifelong support. Therefore, the development of effective treatments is of the utmost importance and requires the identification of the common biological mechanisms that are disrupted in autistic individuals.

Identifying these mechanisms is complicated by the multifactorial etiology of ASD, with genetic, epigenetic and environmental factors contributing to the risk of developing ASD. However, twin studies have shown most ASD risk is due to genetic factors. In support of a manifestation of the disorder during brain development, mutations in many genes involved in synaptogenesis have been implicated in the development of ASD. Interestingly, epilepsy also frequently co-occurs with ASD and shares many risk genes, which indicates that similar biological processes, such as neuronal migration and synaptic function, are involved in both conditions. A relative increase in the level of excitation in the neuronal circuits of autistic individuals might predispose to epilepsy, thus accounting for the higher-than-average comorbidity. Both an increase in the level of excitatory synaptic transmission and a decrease in the level of inhibitory synaptic transmission could lead to relative increase in the relative level of excitation. Thus, an imbalance in the relative levels of excitation and inhibition in neuronal circuits is a hypothetical mechanism for the development of ASD.

Thanks to advances in whole genome sequencing, hundreds of potential candidate genes for ASD have been identified. Determining whether mutations in these genes cause ASD is complicated by the additional presence of thousands of genetic variants shared by many individuals, so-called common variants, which individually raise the ASD risk only slightly but together determine the susceptibility to developing ASD. Therefore, studying the function of specific candidate genes in animal models with a homogeneous genetic background, such as inbred mouse strains, reduces the background genetic variability and enables the evaluation of the

effect of the individual gene variants on the phenotype.

The utility of an animal model for a human disease is evaluated using the following three criteria: (1) the same biological processes disrupted in the human individual must be disrupted in the animal model, (2) the same (or similar) symptoms must be present in the human and the animal, and (3) the same treatments must be effective in both animal and human. While there are no approved pharmacological treatments for the core symptoms of ASD, humans and mice share most of their genes and mice show behaviors that are reminiscent of the behavioral symptoms of ASD. Thus, mouse models of ASD can only be evaluated based on the first and second criterion. To this end, ASD candidate genes can be modified in mice to mimic mutations observed in autistic individuals and the resulting phenotype can be assessed with standardized behavioral tests.

To understand the relationship between autism candidate genes and their impact on the neurophysiological processes mediating synaptic function and E-I balance, three validated genetic mouse models of ASD were investigated in this dissertation: the Nbea haploinsufficient (published manuscript 1), the Nlgn3 KO (published manuscript 2), and the Nlgn4 KO (submitted manuscript 3) mouse model. Each of these mouse models exhibits defects in synaptic formation and/or function, but E-I balance had been systematically studied in only one of these models (Nlgn4 KO). Both synaptic and network activity were measured using whole-cell patch clamp recordings of dentate granule cells and extracellular recordings of field potentials in the hippocampal dentate gyrus, a brain region that exhibits structural and functional abnormalities in some individuals with ASD and in individuals suffering from temporal lobe epilepsy.

The dentate gyrus serves as the main input structure for cortical and subcortical afferents to the hippocampus, an important brain region involved in memory encoding and retrieval. The principal cells of the dentate gyrus, the granule cells, are characterized by a low resting membrane potential and strong inhibition, which aid in preventing the propagation of epileptiform activity to the hippocampus. These properties are also responsible for sparse coding in the dentate gyrus, which enables one of the proposed functions of this brain region, the differentiation between similar input patterns (referred to as pattern separation). Importantly, it is possible to concurrently activate both the granule cells and the local inhibitory network by electrically stimulating the perforant path, which consists of axons from the entorhinal cortex. The extracellularly recorded population spike reflects the summed action potential output of the individual granule cells and provides information about the relative level of excitation to inhibition in the dentate gyrus. Thus, by comparing the population spike in genetically modified mouse models to that in their wildtype littermates, disruptions in the dentate E-I balance could be identified. The accompanying alterations in the intracellular and network activity in the dentate gyrus yielded new insights into the functional role of the three proteins in controlling the synaptic efficacy and intrinsic excitability in hippocampal granule cells.

**In manuscript 1**, the Nbea haploinsufficient ($Nbea^{+/-}$) mouse model of ASD and epilepsy was investigated. Nbea is a multidomain protein involved in a variety of neuronal functions such as vesicle secretion, neurotransmitter receptor trafficking, and the organization of the actin cytoskeleton. By disrupting these cellular processes, the deletion of Nbea in cultured mouse neurons leads to defects in pre- and postsynaptic function and a reduction in the number of dendritic spines, i.e. small, synapse-containing membranous protrusions. In humans, the monoallelic loss of Nbea is associated with ASD and epilepsy. However, the homozygous KO of Nbea is lethal in mice due to the absence of synaptic transmission at neuromuscular junctions in the respiratory system, which is likely to be the case in humans as well given the lack of a clinical report describing a homozygous deletion of Nbea. Previous work has revealed differences in sociability and an increase in repetitive behaviors in $Nbea^{+/-}$ mice compared to wildtype littermate controls, suggestive of the two core symptoms of ASD. Moreover, it was shown that haploinsufficient mice have fewer synapses and exhibit impairments in excitatory synaptic transmission and plasticity. In contrast, in this work, no significant differences in the excitatory

synaptic input to the dentate gyrus of Nbea$^{+/-}$ mice compared to wildtype littermates were detected. However, the same synaptic input produced weaker population spikes, indicating either an increase in inhibition or a decrease in the intrinsic excitability of the granule cells. While this question could not be fully resolved using extracellular recordings, our data suggest that inhibitory transmission is not altered in Nbea$^{+/-}$ mice. We also observed a dissociation between the synaptic potentiation and the potentiation of the population spike following the induction of long-term potentiation, a form of synaptic plasticity, indicating that the intrinsic excitability of the granule cells is differentially regulated in Nbea$^{+/-}$ mice. The reduction in Nbea expression in the mutant mice might lead to disruptions in the intradendritic trafficking and/or surface expression of ion channels, thereby altering the intrinsic excitability. Taken together, these results suggest that E-I balance is shifted towards inhibition in Nbea$^{+/-}$ mice due to a decrease in the intrinsic excitability of the granule cells.

**In manuscript 2**, we showed in Nlgn3 KO mice that the granule cell intrinsic excitability can be upregulated in response to a reduction in synaptic input, thereby preserving the E-I balance in the dentate gyrus. Nlgn3 is a synaptic adhesion protein which is expressed at the postsynaptic membrane, where it binds to presynaptic neurexin proteins to stabilize synapses. In humans, both gain- and loss-of-function mutations in Nlgn3 have been implicated in ASD. Most affected individuals are male, consistent with the location of Nlgn3 on the X-chromosome. Similarly to autistic individuals, Nlgn3 knockout (KO) mice exhibit defects in social memory and an increased tendency to develop repetitive motor routines, in addition to region-specific impairments in synaptogenesis, excitatory and/or inhibitory synaptic transmission and synaptic plasticity in cortical, cerebellar, and brainstem neurons. In accordance with previous results from acute brain slices showing decreased excitatory synaptic currents in granule cells in which Nlgn3 expression had been knocked down, we found that synaptic transmission from the perforant path to the granule cells was reduced in Nlgn3 KO mice. However, the population spike amplitude was similar to that of wildtype littermates, suggesting that the intrinsic excitability of the granule cells was homeostatically increased in Nlgn3 KO mice to compensate for the decreased synaptic input. Interestingly, inhibition was also slightly increased in Nlgn3 KO mice, but not enough to affect the E-I balance in the dentate gyrus. These results highlight the importance of homeostatic mechanisms in shaping the neuronal E-I balance and show that primary defects in synaptic function do not necessarily lead to alterations in the E-I balance.

**Manuscript 3** examined the synaptic function of Neuroligin-4 (Nlgn4) in dentate granule cells using extracellular recordings *in vivo* as well as whole-cell patch clamp recordings of granule cells in organotypic entorhino-hippocampal slice cultures (OTCs). Nlgn4 is another synaptic adhesion protein from the neuroligin family which is also located on the X chromosome in humans. Interestingly, the murine Nlgn4 gene is in the pseudo-autosomal region of the sex chromosomes, meaning that like autosomal genes, it can undergo homologous recombination. There are considerable sequence differences between the human and murine Nlgn4 genes, but it appears that the key functional regions of the protein are preserved. Loss-of-function mutations in the human X-chromosomal Nlgn4 gene are associated with ASD and intellectual disability. In accordance with these symptoms in humans, Nlgn4 KO mice are less sociable than wildtype mice and exhibit deficits in social memory and communication. While Nlgn4 KO mice primarily show defects in inhibitory synaptic transmission in hippocampal and retinal neurons, they additionally exhibit impairments in excitatory synaptic transmission in the somatosensory cortex, leading to a reduction in E-I balance. While we observed no alterations in excitatory or inhibitory transmission in individual granule cells, the pattern of action potential firing in response to intracellular current injections differed in the OTCs prepared from Nlgn4 KO mice. Furthermore, we found slight differences in the population spike threshold and network inhibition in the dentate gyrus of Nlgn4 KO mice *in vivo*. Therefore, it is possible that the intrinsic excitability of the granule cells is reduced in Nlgn4 KO mice, which would lead to a later onset of the population spike and increase the relative strength of the inhibitory control over the granule cell

output. Thus, changes in the intrinsic excitability could disrupt the E-I balance in the dentate gyrus even if the levels of excitatory and inhibitory transmission are unchanged.

Taken together, these results support the E-I imbalance hypothesis of ASD with two important qualifications. (1) Unlike epilepsy, ASD may also be associated with increases in the relative level of inhibition, and (2) while changes in the intrinsic excitability can compensate for deficits in synaptic transmission, they can also lead to E-I imbalance. These findings are consistent with reports of increased inhibition in other ASD mouse models. However, it is important to note that there are many different classes of inhibitory interneurons which serve varied functions, including the regulation of other interneurons. The inhibition of the granule cell population spike is primarily mediated by interneurons which target the perisomatic region of granule cells. Thus, our results only shed light on this specific form of inhibition. Other limitations concern the use of anesthesia, which is expected to alter the levels of excitation and inhibition, and the stimulation method, which targeted only one input to the dentate gyrus.

In conclusion, the presented results underscore the importance of the intrinsic excitability of the granule cells for the E-I balance in the dentate gyrus. Both the $Nbea^{+/-}$ and the Nlgn4 KO mouse model of ASD displayed decreases in the intrinsic excitability, resulting in a shift towards inhibition, while the reduction in excitatory synaptic transmission in the Nlgn3 KO mouse model was compensated by an increase in the intrinsic excitability of the granule cells. Future investigations of the network activity in awake mice could show to what extent the observed electrophysiological changes are involved in the behavioral phenotype of the ASD mouse models and whether they can be generalized to other brain regions. If a connection between the autistic symptoms and E-I imbalance is confirmed, restoring the E-I balance could be a possible treatment option for ASD.

# Chapter 1

# Introduction

Autism spectrum disorders (ASDs) are among the most common developmental disorders with an estimated median worldwide prevalence of 62 per 10,000 individuals (Elsabbagh et al., 2012). Males are diagnosed with ASD approximately three times more often than females (Loomes, Hull, and Mandy, 2017). While the severity of the disorder varies widely between individuals, the core symptoms which characterize ASD are deficits in social interaction and communication and the presence of repetitive behaviors (Lord et al., 2018). A meta-analysis of twin studies has revealed that ASD is highly heritable, with genetics accounting for between 64 and 91% of the ASD risk (Tick et al., 2016). At the same time, the inheritance of ASD is highly polygenic, with a mix of *de novo* mutations and inherited genetic variation contributing to the risk for developing ASD (Gaugler et al., 2014). One approach to studying the etiology of ASD is to identify shared molecular or developmental pathways that are disrupted by highly penetrant single-gene mutations in autistic individuals. Though the individual genetic variants are rare, such mutations are estimated to account for the autistic phenotype in 10-30% of individuals with ASD (Vorstman et al., 2017). Many of the heretofore identified autism candidate genes are involved in synapse formation or function (Gilman et al., 2011; Mahfouz et al., 2015; De Rubeis et al., 2014), suggesting that ASD is a synaptopathy (Bourgeron, 2009; Bourgeron, 2015).

A general impairment in synapse formation or function would have far-reaching consequences not only for the activity of individual neurons, but also for the functioning of neural circuits and overall brain activity. The excitation-inhibition (E-I) imbalance theory, first articulated by Rubenstein and Merzenich in 2003, is one of the most influential neurobiological models of ASD (Rubenstein and Merzenich, 2003; Nelson and Valakh, 2015; Lee, Lee, and Kim, 2017; Sohal and Rubenstein, 2019). The original hypothesis was inspired by the finding that ASD and epilepsy are highly comorbid, suggesting that the E-I balance might be shifted towards excitation in autistic individuals (Rubenstein and Merzenich, 2003). Indeed, there have been reports of reduced inhibitory signaling in individuals with ASD (Robertson, Ratai, and Kanwisher, 2016). However, more recent human (Port, Oberman, and Roberts, 2019) and animal (Nelson and Valakh, 2015; Lee, Lee, and Kim, 2017) studies have shown that both increases and decreases in the E-I ratio are associated with autistic phenotypes, prompting the reformulation of the original hypothesis from a unidimensional to a multidimensional view of E-I balance, which takes into account the many different mechanisms, including homeostatic compensation of the initial defects in excitation or inhibition, operating on different timescales (Sohal and Rubenstein, 2019).

Transgenic mice are invaluable tools for studying the functions of autism candidate genes *in vivo*. If a transgenic mouse expressing an autism-associated mutation also exhibits behavioral abnormalities reminiscent of autistic symptoms, the function of the gene is thought to be highly relevant to the development of ASD. While the behavioral repertoire of mice is smaller than that of humans, it is nevertheless possible to identify murine behaviors that are relevant to the core symptoms of ASD, such as deficits in social approach or an increase in repetitive behaviors (Servadio, Vanderschuren, and Trezza, 2015). Behaviorally validated genetic mouse models are also useful for identifying potential pharmacological targets for the treatment of autism-related

phenotypes.

In this dissertation, the E-I imbalance theory of ASD was evaluated using behaviorally validated genetic mouse models of ASD. To this end, disruptions in the E-I balance in the hippocampal dentate gyrus were determined in the Neurobeachin haploinsufficient mouse, the Neuroligin-3 knockout (KO) mouse, and the Neuroligin-4 KO mouse. Several lines of evidence support a role for these genes in synaptogenesis or synaptic function (Su et al., 2004; Medrihan et al., 2009; Niesmann et al., 2011; Nair et al., 2013; Farzana et al., 2016; Repetto et al., 2018; Etherton et al., 2011; Baudouin et al., 2012; Földy, Malenka, and Südhof, 2013; Rothwell et al., 2014; Hoon et al., 2017; Polepalli et al., 2017; Horn and Nicoll, 2018; Zhang et al., 2009; Chanda et al., 2016; Hoon et al., 2011; Delattre et al., 2013; Hammer et al., 2015; Unichenko et al., 2017; Gatford et al., 2021), and the reduction or loss of these proteins is implicated in the development of ASD in humans (Castermans et al., 2003; Jamain et al., 2003; Laumonnier et al., 2004; Reddy, 2005; Ritvo et al., 1988; Smith et al., 2002) and autism-like behaviors in mice (Nuytens et al., 2013; Norris et al., 2019; Radyushkin et al., 2009; Modi et al., 2019; Jamain et al., 2008; El-Kordi et al., 2013; Ju et al., 2014). *In vivo* and/or *in vitro* electrophysiological recordings showed that the intrinsic neuronal excitability was altered in each of these mouse models, underscoring the importance of non-synaptic mechanisms in regulating the neuronal E-I balance and suggesting a potential common mechanism disrupted in ASD.

## 1.1 Clinical Features of ASD

Autism was first included as a diagnostic category in version 3 of the American Psychiatric Association's Diagnostic and Statistical Manual for Mental Disorders (DSM), released in 1980 (Rosen, Lord, and Volkmar, 2021). The purely descriptive definition of what was termed "infantile autism" marked a departure from previous definitions which had relied on psychoanalytic theories of origin (Vivanti and Messinger, 2021). ASD is now understood to be a neurodevelopmental disorder with a highly heterogeneous presentation (from mild to severe) which first manifests in childhood, but is a lifelong condition (Lord et al., 2018). Despite considerable efforts to identify reliable biomarkers, the diagnosis of ASD is based entirely on behavioral features using standardized diagnostic tools as well as parent and caregiver reports (Campisi et al., 2018; Lord et al., 2018).

### 1.1.1 Behavioral Symptoms of ASD

ASD is characterized by deficits or abnormalities in two domains of behavior: (1) social interactions and communication and (2) sensory-motor function. The current DSM (version 5) further defines the types of behavior that are indicative of ASD. In the social domain, the individual must have deficits in social reciprocity, in non-verbal communication, and in developing relationships; and in the sensory-motor domain, the individual must exhibit two of the following behaviors: repetitive movements, speech, or use of objects; resistance to change; insistence on following an established routine; highly restricted interests; and hyper- or hyporeactivity to sensory stimuli (American Psychiatric Association, 2013). The current version of the World Health Organization's International Classification of Diseases (ICD-11) uses the same two diagnostc criteria as the DSM-5, but further subdivides ASD depending on the presence and severity of accompanying language and intellectual impairments (World Health Organization, 2021). Even though sensory abnormalities were mentioned in some of the earliest clinical descriptions of autism (Kanner, 1943), abnormal sensory perception was long considered an epiphenomenon of the defects in social cognition before being reintroduced as a core symptom of ASD in the DSM-5 (Robertson and Baron-Cohen, 2017). Indeed, a fascination with specific sensory stimuli might account for certain repetitive behaviors (Posar and Visconti, 2018). However, sensory

abnormalities often go unnoticed due to the communication difficulties of individuals with ASD (Posar and Visconti, 2018). Regarding visual perception, autistic individuals are often described as focusing more on the details and less on the scene as a whole, i.e. ignoring the global features in favor of the local features (Robertson and Baron-Cohen, 2017). In other sensory modalities (such as touch and hearing), autistic individuals exhibit temporal delays in neural processing (Robertson and Baron-Cohen, 2017). Psychophysical studies have shown that these differences in sensory perception are due to differences in the primary sensory cortices and higher-order areas (Robertson and Baron-Cohen, 2017). Researchers hope that these differences in sensory perception might serve as biomarkers for ASD, since these differences can be detected in infancy and have predictive value for the development of later cognitive symptoms (Robertson and Baron-Cohen, 2017). However, so far no reliable biomarkers have been established. While a recent meta-analysis showed that prepulse inhibition of the acoustic startle response, a measure of sensorimotor gating, was impaired in children and adolescents with ASD, the number of studies analyzed was very low so the results should be treated with caution (Cheng et al., 2018).

### 1.1.2 Neuroanatomical Abnormalities in Individuals with ASD

Besides the behavioral and sensory abnormalities that characterize ASD, a number of neuroanatomical differences have been identified in autistic individuals using modern brain imaging methods such as magnetic resonance imaging (MRI) and diffusion tensor imaging as well as post-mortem analyses of brain tissue. Cerebellar abnormalities are widespread in autistic individuals and may underlie some of the behavioral and motor symptoms (Fatemi et al., 2012). One of the most consistent observations in post-mortem brains of autistic individuals is a decrease in the number of cerebellar Purkinje cells, the only output neurons of the cerebellum (Fatemi et al., 2012). The cerebellum is involved in cognitive functions such as language processing in addition to its role in motor coordination (De Smet et al., 2013), so a reduction in cerebellar output might account for some of the language deficits in ASD.

ASD is also associated with structural alterations in the limbic system, though the evidence is less conclusive than for the cerebellum. The amygdala, which is important for processing emotion, has been shown to be enlarged (Mosconi et al., 2009) or decreased (Xu et al., 2020; Aylward et al., 1999) in ASD depending on the study, though these disparate results may be reconciled by the finding that the amygdala is larger initially, but fails to undergo an age-related increase in volume observed in typically developing individuals (Schumann et al., 2004). Several studies have found that the hippocampus, a brain structure in the temporal lobe which is important for the encoding and retrieval of memories (Buzsáki and Moser, 2013), is larger in autistic individuals (Xu et al., 2020; Rojas et al., 2006; Schumann et al., 2004), which could be a reflection of an increased activation of the hippocampus in response to sensory input (Maier et al., 2015). However, reductions in the hippocampal volume in ASD have also been reported (Aylward et al., 1999; Sussman et al., 2015), and there is evidence that the hippocampus is smaller in autistic children, but increases in volume with age (Xu et al., 2020).

Age-related differences in total brain size have also been associated with ASD, specifically, an overgrowth of the brain during early childhood which is followed by a phase of arrested growth in late childhood/early adolescence and a phase of accelerated degeneration compared to typically developing individuals in adulthood (Courchesne, Campbell, and Solso, 2011). Microanatomical abnormalities at the level of minicolumns and axon bundles have been detected in both higher-order association areas and primary sensory regions (McKavanagh, Buckley, and Chance, 2015). Autistic individuals had wider minicolumns, especially at younger ages, resulting in less overlap between dendritic trees of the cortical pyramidal cells, which could contribute to the bias towards local processing (McKavanagh, Buckley, and Chance, 2015). These studies suggest that brain development in individuals with ASD follows a different trajectory compared to that in typically developing individuals.

### 1.1.3 Comorbidities of ASD with Other Disorders

ASD is highly comorbid with other psychiatric and somatic conditions such as intellectual disability, attention-deficit/hyperactivity disorder (ADHD), and sensory impairments (Rydzewska et al., 2019). There are several forms of "syndromic" autism, where autistic features occur as part of an inherited condition. Fragile X syndrome and tuberous sclerosis complex are two prominent examples of syndromic autism. However, the distinction between syndromic and non-syndromic ASD is being eroded by an increasing number of findings that many non-syndromic forms of ASD are accompanied by various other conditions ranging from epilepsy to heart defects to gastrointestinal problems (Vorstman et al., 2017). Therefore, it is advised that clinicians broaden their focus in order to consider possible somatic comorbidities along with the behavioral symptoms (Vorstman et al., 2017). Changes in the diagnostic criteria in the DSM-5 replaced the previously used subtypes (autistic disorder, Asperger's disorder, Rett syndrome, and pervasive developmental disorder not otherwise specified) with the umbrella term of ASD and allowed for comorbid diagnoses (Grzadzinski, Huerta, and Lord, 2013). These changes show a gradual shift in the clinical perception of ASD from a behaviorally defined disorder to a medical condition with a likelihood of co-occurring psychiatric and somatic comorbidities (Vorstman et al., 2017).

Approximately 50% of individuals with ASD also have an intellectual disability (ID) (Loomes, Hull, and Mandy, 2017). Genome-wide association studies have shown that *de novo* loss-of-function mutations are more prevalent in females and males with below-average intelligence (Iossifov et al., 2014), which could indicate that these rare and highly penetrant mutations do not cause ASD, but make the autistic phenotype more visible by impairing the ability to mask their symptoms (Skuse, 2007; Bourgeron, 2015). Interestingly, a population-based study showed that even though females only made up approximately 20% of the ASD diagnoses, they were more than twice as likely to be diagnosed with ID, indicating that less severe forms of ASD without accompanying ID might be underdiagnosed in females (Rydzewska et al., 2019). Furthermore, individuals with ID are underrepresented in studies of ASD, which means that treatments tested on autistic individuals with unimpaired intellectual functioning might not be effective in autistic individuals with comorbid ID (Russell et al., 2019).

ASD, ADHD and schizophrenia are associated with copy number variations (CNVs) at common loci (Williams et al., 2012), which indicates that the same biological pathways might play a role in each of these disorders (Taurines et al., 2012). ADHD is the most common comorbidity in individuals with ASD, with an estimated prevalence of 28% (Lai et al., 2019), though higher numbers have been reported (Antshel and Russo, 2019). The previous version of the DSM, the DSM-IV TR, had classified ASD and ADHD as mutually exclusive disorders, but many studies had reported an overlap in the symptoms and a higher prevalence of ADHD in children with ASD (Taurines et al., 2012). Since the release of the DSM-5, which allowed for comorbid diagnoses of ASD and ADHD, the number of studies regarding the association between ASD and ADHD has been steadily increasing (Antshel and Russo, 2019). Like ASD, ADHD is a highly heritable neurodevelopmental disorder which first arises in childhood and is characterized by defects in executive function and lower levels of reciprocal social interactions (Antshel and Russo, 2019). ASD and schizophrenia have been reported to co-occur at higher-than-expected levels (prevalence estimated at 4% by Lai et al., 2019) and share several symptoms, such as deficits in social interaction and communication and a reduced emotional response (Chisholm et al., 2015). Historically, autism was considered a core feature or the infantile form of schizophrenia, and the term autism was often used interchangeably with schizophrenia until the 1970s (Chisholm et al., 2015). While they are now recognized as separate disorders, ASD and schizophrenia also share many genetic risk factors and exhibit similar changes in brain structure and cognition (Mastrovito, Hanson, and Hanson, 2018).

Epilepsy is the most frequently co-occurring neurological condition in autistic individuals,

with an estimated prevalence of 14% (Pan et al., 2021), a finding which has been explained by shared alterations in synaptic function and E-I balance in affected individuals (Keller et al., 2017). Furthermore, increased epileptiform EEG activity has been reported in individuals with ASD, even in the absence of seizures (Chez et al., 2006). A number of genes associated with ASD are mutated in individuals with epilepsy and vice versa. The affected genes and the proteins they encode are most commonly associated with neuronal migration (e.g., Reelin) and synaptic function (e.g., synapsin, neurexin, SHANK3) (Keller et al., 2017). Other genes are associated with syndromes that encompass both ASD and epilepsy, such as TSC1 and TSC2 (tuberous sclerosis complex), MECP2 (Rett syndrome), or UBE3A (Angelman syndrome) (Keller et al., 2017). Individuals with syndromic autism often present with more severe phenotypes than non-syndromic individuals, which indicates that syndromic mutations have a high penetrance. Many of the affected genes are involved in fundamental cellular functions, such as cell cycle progression (TSC1 and TSC2), DNA methylation (MECP2), and protein degradation (UBE3A), which might explain the severe phenotypes resulting from mutations in these genes.

Other common co-occurring conditions include anxiety, which has an estimated prevalence of 20% (Lai et al., 2019), sensory impairments (Rydzewska et al., 2019), and gastrointestinal symptoms (Holingue et al., 2018).

### 1.1.4 Prognosis and Treatment

ASD is a lifelong condition for which no cure exists. Many patients are prescribed psychotropic drugs to manage specific symptoms (such as repetitive behaviors) or co-occurring psychiatric conditions (such as anxiety), but the currently available evidence does not support the routine use of drugs for the treatment of the core symptoms of ASD (Howes et al., 2018). The response of the family members and caregivers to the diagnosis is just as important for the eventual outcome as any specific treatment (Lord et al., 2018). Even low-intensity interventions such as coaching parents and caregivers how to interact with their young child can improve the child's social and communicative behavior (Lord et al., 2018). For older children and adolescents, social skills groups using cognitive behavioral therapy are the most prevalent and promising behavioral intervention (Lord et al., 2018). Other treatments, such as chelation and hyperbaric oxygen therapies and different dietary interventions, lack empirical validity and can even be harmful (Campisi et al., 2018). More recently, the treatment with intranasally delivered oxytocin has shown promise in ameliorating the social deficits in autistic individuals (Bernaerts et al., 2020), but larger, standardized studies are needed before oxytocin can be recommended as a standard treatment for ASD (Alvares, Quintana, and Whitehouse, 2017).

### 1.1.5 Etiology

ASD is a heterogeneous condition with no single cause. Instead, ASD appears to be a multifactorial hereditary disorder that depends on genetic variations, environmental factors, and gene-environment interactions (Tordjman et al., 2014). The heritability of ASD is estimated to be between 64 and 91% based on a meta-analysis of twin studies (Tick et al., 2016). Environmental and epigenetic factors likely account for the remaining ASD risk (Tordjman et al., 2014). The strongest evidence for the existence of environmental risk factors comes from studies comparing the concordance rate of dizygotic twins to that of non-twin siblings. In each group, the sibling pairs share 50% of their genetics, but the uterine environment differs in non-twin siblings. Dizygotic twins have a higher concordance rate, which indicates that the uterine environment likely plays a role in the development of ASD (Bohm, Stewart, and Healy, 2013). To date, most of the studies on environmental risk factors suffer from methodological limitations (e.g., observational study design, confounding factors) and, for the most part, small sample sizes (Modabbernia, Velthorst, and Reichenberg, 2017). Some of the most robust associations with an

increased risk of ASD have been found for the parental age. Advanced parental age is known to increase the risk of chromosomal abnormalities, such as trisomies, in offspring, and there is evidence that parental age is positively correlated with the risk of developing ASD (Bölte, Girdler, and Marschik, 2019). A meta-analysis concluded that the highest maternal and paternal age categories were associated with a significantly increased risk of the offspring developing ASD compared to the reference age categories (i.e., the midpoint between the highest and the lowest age categories) (Wu et al., 2017). It has been proposed that autism risk genes predispose to certain personality traits (e.g., aloofness, anxiousness, hypersensitivity) that lead to a later age at procreation (Puleo et al., 2008), but support for this hypothesis is limited (Hultman et al., 2011). The use of anti-epileptic drugs during pregnancy is also strongly associated with the development of ASD in the offspring. One study found that the prevalence of ASD was higher in the group of children who had been exposed to the anti-epileptic drug valproate compared to children born to both non-epileptic mothers and epileptic, non-drug treated mothers (Bromley et al., 2013). A different study also concluded that children exposed to valproate had a higher risk of developing ASD, even after adjusting for parental epilepsy (Smith and Brown, 2014). The mechanism of action of valproate is not well understood, but it is known to inhibit histone deacetylase and thereby might interfere with epigenetic modifications (Modabbernia, Velthorst, and Reichenberg, 2017). However, a network meta-analysis of five studies reported that in addition to valproate, the other anti-epileptic drugs oxcarbazepine and lamotrigine were also significantly associated with ASD (Veroniki et al., 2017).

The recent advances in whole-exome and whole-genome sequencing have allowed researchers to identify hundreds of autism-associated gene variants (Nakanishi, Anderson, and Takumi, 2019). Such highly penetrant, inherited and *de novo* single gene variants probably account for between 10 and 30% of ASD cases (Vorstman et al., 2017), and are often associated with a more severe phenotype and comorbid conditions such as ID (Bourgeron, 2015). Common variants probably account for most cases of ASD (Gaugler et al., 2014), since ASD can also be caused by a high burden ($> 1,000$) of common, but low-risk, variants (Bourgeron, 2015). Even in individuals with a single, high-risk genetic variation, the effect of the common variants is not negligible (Nakanishi, Anderson, and Takumi, 2019). However, to date, most studies have investigated rare variants, which can be modified in otherwise genetically homogeneous mouse strains, thereby reducing the genetic background variability and providing functional insights into the etiology of ASD.

## 1.2 Animal Models of ASD

In the past few decades, hundreds of genetic and environmental risk factors that predispose to ASD have been discovered using whole genome sequencing and population-based studies. Psychophysical studies of autistic individuals have revealed differences in sensory perception, and brain imaging studies have shown abnormalities in gray matter volume and connectivity. There is evidence that certain neuronal processes, such as cell motility and synapse formation, are dysregulated in autistic individuals. However, despite these advances, our understanding of the underlying neurobiology that gives rise to the autistic phenotype is limited. One of the most promising approaches to elucidate these mechanisms is the generation and study of appropriate animal models of ASD.

Animal models can be used to test hypotheses regarding the etiology of ASD and possible treatments. The usefulness of animal models is described by three factors: construct (or etiological) validity, face validity, and predictive validity (Willner, 1984). Construct validity refers to the etiological similarity of the models, so the same biological processes would be affected in a construct-valid model. Face validity refers to the phenotypic similarity of the model. A face-valid model should exhibit the same symptoms as the human patient and should not

exhibit any other symptoms. Predictive validity refers to the responsiveness of the model to treatments that have been shown to be effective in human patients. A model has high predictive validity if treatments show the same effect in the model as in human patients. An ideal model would score highly in all three categories. Given the multifactorial etiology, variable clinical presentation, and current lack of pharmacological treatment for the core symptoms, there is no ASD animal model which fulfills all three criteria (Servadio, Vanderschuren, and Trezza, 2015). Nevertheless, a large number of animal models has been characterized. These models are based on genetic manipulations (e.g., introducing an autism-related mutation or knocking out an autism candidate gene), environmental exposure to ASD risk factors (e.g., *in utero* exposure to valproate), or are naturally occurring genetic variants exhibiting autistic-like symptoms (e.g., the BTBR mouse strain). Despite their lack of full validity, these models have been useful in establishing common underlying neurobiological processes altered in ASD (Chadman et al., 2019).

### 1.2.1 Model Species

The most common model species are the mouse (*Mus musculus*) and rat (*Rattus norvegicus*). While compelling arguments have been made in favor of other model species which are evolutionarily more closely related to humans, such as rhesus macaques (*Macaca mulatta*) (Bauman and Schumann, 2018; Zhao, Jiang, and Zhang, 2018), or which exhibit stronger behavioral similarities, such as domestic dogs (*Canis lupus familiaris*) (Topál, Román, and Turcsán, 2019), rodents offer several advantages over these species: they are small and relatively easy to house, have a short generation time and can be bred year-round, and are amenable to a variety of genetic and pharmacological manipulations. The use of genetically homogeneous (inbred) strains ensures much higher standardization than would be possible with outbred or wild strains, which in turn decreases the sample sizes needed to achieve appropriate statistical power; but an over-reliance on standardization may limit the generalizability of the results (Kafkafi et al., 2018). However, the standardization of the genetic background and home cage conditions by using littermates is still regarded the "gold standard" for assessing the phenotypic effects of a single-gene knockout. The following sections provide an overview of the types of behavioral tests used to assess the face validity of mouse models of ASD.

### 1.2.2 Behavioral Testing

Since there are no established biomarkers for the diagnosis of ASD, the face validity of ASD models is evaluated by the presence of behaviors that resemble the autistic symptoms in humans (social and communication deficits, repetitive behaviors, sensory abnormalities) (Chadman et al., 2019). Over the years, many behavioral tests have been developed for rodents (see Table I from (Chadman, Yang, and Crawley, 2009)), but there have been concerns regarding the validity of the underlying assumptions about the behaviors (Crusio, 2015) and the replicability of the outcomes of these tests (Kafkafi et al., 2018). Some of these concerns can be alleviated by using different tests of what is assumed to be the same behavior and by repeating tests in different cohorts and across laboratories. Before testing a potential new mouse model for disease-specific behaviors, the general health and sensory-motor abilities should be assessed to rule out any confounding neurological or motor abnormalities (Chadman, Yang, and Crawley, 2009). While there are no firm rules regarding what constitutes a valid mouse model, Chadman and colleagues recommend that at least two tests within the relevant behavioral domains be used to confirm the face validity of the model.

**Assessing Social Deficits**

A variety of behavioral paradigms have been designed to study autism-related social deficits in mice. Observing the reciprocal social interactions between mice (e.g., sniffing, following, mounting, etc.) provides the most detailed assessment of social behavior, but is time-consuming and subject to observer bias (Silverman et al., 2010). Therefore, more standardized measures of social interaction were developed (Moy et al., 2004). Sociability (or social approach) is commonly assessed using a three-chambered apparatus in which the subject mouse can freely choose to spend time with a novel object or a novel conspecific for a defined observation period (Yang, Silverman, and Crawley, 2011). In the classic version of the test, the stranger mouse is confined in an upside-down wire mesh pencil cup to deter aggressive behavior, and an identical cup serves as the novel object. Increased time spent interacting with the stranger mouse relative to the novel object is considered a sign of sociability. Sociability measured by this assay is impaired in several ASD models and bears some resemblance to the reduced social approach observed in autistic individuals (Möhrle et al., 2020). The preference for social novelty, which relies on social recognition and memory, can be tested in the same three-chambered apparatus by presenting the subject mouse with the same, now-familiar conspecific in one chamber and a second, unfamiliar conspecific in the second chamber (Yang, Silverman, and Crawley, 2011). Mice generally spend more time interacting with the unfamiliar conspecific and thus show a preference for social novelty, but several ASD model mice exhibit a reduced preference for social novelty (Silverman et al., 2010). However, since social recognition in mice and humans is dependent on different senses (olfaction in mice vs. vision and hearing in humans), the results of the social novelty test may not be directly translatable to the human behavior (Möhrle et al., 2020).

Over the years, there have been many improvements or variations of both the three-chambered test apparatus and the experimental paradigm. In the original version of the three-chamber sociability test, the subject mouse is first allowed to habituate to the testing apparatus for a total of 20 minutes before being presented with the choice between the novel mouse and the novel object for 10 minutes (Yang, Silverman, and Crawley, 2011). However, some researchers argue that the time spent near the novel mouse may simply reflect a preference for moving stimuli, rather than a preference for social interaction, and therefore suggest modifying the test to allow for habituation to both stimuli over several hours (Bader et al., 2011). While mice may exhibit normal social preference in the classic three-chamber test, their behavior may differ following a two-hour habituation phase (Bader et al., 2011). More recently, a modified protocol was proposed that includes a habituation phase in which the subject mouse can explore the chamber and the empty cups as well as a pre-test phase in which two identical objects are placed under the cups so the mouse is familiarized with the presence of objects within the cups (Rein, Ma, and Yan, 2020). Crucially, during the test phase, a different novel object is placed under one wire cup so the subject mouse has the choice between this novel object and the novel mouse. Rein and colleagues showed that this protocol was more sensitive to differences in sociability than the classic version of the three-chamber test, in which the same kind of cup that serves as the novel object is also part of the social stimulus. Therefore, an increase in interaction times with the social stimulus could be explained by the greater novelty of the cup paired with the mouse compared to the cup alone, and subtle differences in social preference would be masked (Rein, Ma, and Yan, 2020). The sensitivity of the classic three-chamber test is not very high when it comes to detecting subtle changes in social memory, since the required memory load is quite low. Therefore, researchers have developed a more demanding social memory task that requires distinguishing between five different mice at once (Krueger-Burg et al., 2016). This modified test revealed deficits in social memory in heterozygous PSD95-KO mice, which were expected to have a milder phenotype than the socially abnormal homozygous PSD-95 KO mice (Krueger-Burg et al., 2016).

Regardless of which sociability test is used, it is crucial to control for motor and sensory

function between experimental groups. The three-chamber sociability/social novelty test relies on active exploration of the test chamber and intact olfactory function, so motor or olfactory dysfunctions invalidate the test results. Confounding factors such as strain-specific differences in activity levels can also interfere with the outcomes of behavioral tests (Yang, Silverman, and Crawley, 2011). The genetic background can also critically affect sociability: transgenic mice generated using embryonic stem cell lines from 129 mice may behave differently from control mice with a different genetic background because some 129 substrains are generally less sociable and more anxious than other strains (Yang, Silverman, and Crawley, 2011). Interpreting the results of the three-chamber sociability test is also not straightforward: while some researchers argue that the outcome is categorical (either the subject mouse spends more time with the stranger mouse and is thus deemed sociable, or the subject mouse spends more time with the object and is deemed nonsocial) (Yang, Silverman, and Crawley, 2011), other researchers argue that sociability should be treated as a continuous variable in order to study possible dose-dependent effects of drug treatments on social approach behavior (Nygaard, Maloney, and Dougherty, 2019). More concerning is the finding by Nygaard and colleagues that almost half of the studies they analyzed used incorrect statistical inferences to interpret the three-chamber sociability test. Instead of using a normalized measure such as a sociability index to compare different genotypes or treatments, some researchers simply tested for significant differences between the time spent with the stranger mouse and the time spent with the object for each group and drew the erroneous conclusion that the absence of a significant difference within one group meant that this group was less sociable than the other group (Nygaard, Maloney, and Dougherty, 2019). However, the lack of a significant difference within one group does not correlate with a significant difference between groups. Nygaard and colleagues also recommend reporting the absolute time spent in each chamber for each group because a large difference in the interaction times could indicate a confounding influence in one group, such as motor abnormalities. These shortcomings notwithstanding, the three-chamber test remains a valuable tool for assessing defects in sociability and social recognition in mice.

#### Assessing Communication Deficits

Mice use a variety of sensory modalities to communicate, which, while not yet well understood, have nevertheless been used in behavioral assays of communication deficits (Silverman et al., 2010). There are well-established assays based on olfactory signals, such as urinary pheromones; and ultrasonic vocalizations, which are emitted by mice in social situations (Silverman et al., 2010). Most mice show an increased interest in the scent of another mouse compared to non-social scents, and the habituation to a novel social odor can be used as a measure of the social recognition and social interest (Silverman et al., 2010). Deficits in ultrasonic vocalizations can be tested at various ages in different situations, for instance, in pups that are separated from their mother and nest or in adult male mice in the presence of female urinary pheromones or female mice (Kazdoba et al., 2016). However, most assays simply compare the latency and frequency of calls rather than analyze the auditory waveform, which might reveal more subtle communication deficits. For instance, Scattoni and colleagues classified the types of calls made by pups separated from their mothers and found that the pups of the autistic-like BTBR mouse strain emitted a distinct pattern of vocalizations compared to pups of other strains, indicating that the call patterns may be a useful assay of the autistic phenotype (Scattoni et al., 2008). Newer methods for automatically classifying the call types (Premoli et al., 2021) may make this type of analysis more widespread. However, it should be noted that unlike human speech, rodent ultrasonic vocalization is a largely innate behavior and is not suitable as a model of speech impairment (Möhrle et al., 2020; Kazdoba et al., 2016). Rather, rodent calls should be viewed as a measure of emotionality and sociability.

**Assessing Repetitive Behaviors and the "Insistence on Sameness"**

Repetitive behaviors such as self-grooming, barbering, digging, chewing, and marble burying as well as stereotyped nest building occur more frequently in many rodent ASD models and are considered analogous to human motor or behavior stereotypies (Möhrle et al., 2020). Locomotor abilities and learning of a repetitive motor routine are commonly tested with the rotarod device, an accelerating rotating rod (Möhrle et al., 2020). The "insistence on sameness" observed in many autistic individuals is more difficult to measure in rodents, but reversal learning paradigms using spatial and visual/auditory cues (mazes) or only visual cues (touchscreen tasks) have been used to assess cognitive (in)flexibility or perseverance in rodents (Izquierdo et al., 2017). Touchscreen tasks have also been used to measure transitive inference in mice (Silverman et al., 2015; Norris et al., 2019), a form of learning that is dependent on the ability to memorize stimulus pairs and transfer previously learned relations to new stimulus pairings and which was shown to be impaired in a cohort of autistic adults (Solomon et al., 2011), but unimpaired in autistic adolescents (Solomon et al., 2015). However, the autistic adolescents showed a different functional connectivity pattern while performing the task, indicating that they might employ a less efficient cognitive strategy, i.e. reactive control, which is reflected by the transient activation of the lateral prefrontal cortex along with additional brain regions, such as the hippocampus (Solomon et al., 2015; Braver, 2012). In contrast, proactive control involves the sustained activation of the lateral prefrontal cortex in anticipation of the task demands (Braver, 2012). In mice, the response latency during the performance of a transitive inference tasks can serve as a proxy for the cognitive processing speed and was shown to be increased in two genetic ASD mouse models (Norris et al., 2019).

**Assessing Sensory Symptoms**

Differences in sensory perception can be easily studied in rodents with established behavioral paradigms. For example, changes in acoustic sensitivity and reactivity can be quantified using the acoustic startle response and prepulse inhibition of the startle response (Möhrle et al., 2020). However, prepulse inhibition is a reliable measure of sensorimotor gating only if hearing is normal, and should be carefully interpreted since a decrease in prepulse inhibition during repeated testing might be the result of stress-induced exhaustion rather than habituation (Degroote, Hunting, and Takser, 2017). General olfactory function can be assessed by the latency to find a buried treat (buried food test) and the ability to distinguish different odors is measured in the olfactory habituation/dishabituation test, wherein the mouse is repeatedly exposed to the same odor and the sniffing time is scored (Möhrle et al., 2020). Differences in pain thresholds can be determined using the hot plate test, where the mouse is placed on a hotplate set to a constant, uncomfortable temperature. The latency of the first paw lick or jump is used as a measure of acute pain sensitivity (Möhrle et al., 2020). Visual sensitivity can be measured by the velocity and latency of eyelid opening in response to light (Möhrle et al., 2020).

Further phenotypes that often accompany ASD are also found in genetic animal models. Deficits in learning or memory serve as proxies for intellectual disability. For instance, impaired long-term memory tested with object recognition tasks has been observed in Shank3 mutant mice (Yang et al., 2012). Several genetic mouse models exhibit impairments in spatial memory tested with the Morris water maze and associative learning tested with cued or contextual fear conditioning (Kazdoba et al., 2016; Möhrle et al., 2020). Other associated symptoms that have been identified in rodent models include anxiety, seizures, attention deficits/hyperactivity, and sleep disorders (Kazdoba et al., 2016).

## 1.3 Overview of the ASD Mouse Models Investigated in this Dissertation

Three different genetic animal models of ASD were investigated in this dissertation: Neurobeachin haploinsufficient ($Nbea^{+/-}$) mice, Neuroligin-3 (Nlgn3) KO mice, and Neuroligin-4 (Nlgn4) KO mice. The genes altered in these models correlate strongly with ASD in humans and represent some of the rare deleterious mutations that occur in a small percentage of autistic individuals. In a function-based ranking of 25,825 human genes, Nbea was ranked the 37th most probable ASD risk gene while Nlgn3 and Nlgn4 were ranked near the top 10% of genes, at ranks 2829 and 2439, respectively (Krishnan et al., 2016). Moreover, since each protein is involved in synaptogenesis and/or synaptic function, it was hypothesized that the reduction or deletion of these proteins might alter the balance of excitatory to inhibitory synaptic transmission in individual neurons and in neural circuits. What follows is a brief introduction to each mouse model and an overview of the current state of knowledge regarding the function of each protein.

### 1.3.1 The Neurobeachin Haploinsufficient Mouse Model

Multiple independent lines of evidence point to Neurobeachin (Nbea) as an autism candidate gene. Nbea was first implicated in ASD when a *de novo* balanced reciprocal translocation of one allele was discovered in a patient with a negative family history of autism and no neurological abnormalities (Castermans et al., 2003). The translocation was expected to lead to a complete loss of Nbea expression from the one allele, thus resulting in a haploinsufficient genotype. The Nbea gene resides in a common fragile site, meaning it is prone to chromosomal breakage (Savelyeva et al., 2006). Indeed, several translocations or deletions of the Nbea gene have been identified in individuals with autism (Reddy, 2005; Ritvo et al., 1988; Smith et al., 2002). *De novo* point mutations in Nbea have been implicated in developmental delay/intellectual disability (Bowling et al., 2017) and epilepsy (Mulhern et al., 2018; Boulin et al., 2021). Furthermore, a whole-exome sequencing study found that the load of disruptive mutations in the Nbea gene was quite low in a control cohort, which indicates that a gene is under purifying selection and that mutations have a very strong likelihood of causing ASD (Iossifov et al., 2015). If most disruptive mutations in Nbea led to the development of ASD, the number of disruptive mutations in the control cohort is expected to be low because the reduced fecundity in individuals with ASD would reduce the chance of these mutations being transmitted (Iossifov et al., 2015). The Simons Foundation Autism Research Initiative (SFARI) score, which gives an estimate of the the strength of the evidence in favor of autism candidate genes (Banerjee-Basu and Packer, 2010; Abrahams et al., 2013), is 1S (high confidence, syndromic), which indicates that Nbea has a high likelihood of causing ASD and is associated with additional symptoms (e.g., epilepsy) that are correlated with, but not required for an ASD diagnosis.

Nbea is a member of the BEACH (beige and Chediak-Higashi) domain-containing protein family that is expressed in neurons (Wang et al., 2000). The subcellular localization of Nbea near the trans-Golgi network (Wang et al., 2000) suggests it is involved in protein trafficking, like all BEACH-domain containing proteins (Cullinane, Schäffer, and Huizing, 2013). In addition to the BEACH domain, Nbea contains several WD40 motifs which mediate protein-protein interactions (Volders, Nuytens, and Creemers, 2011). Nbea also possesses a protein kinase A (PKA) binding site, which allows it to function as an A-kinase anchor protein (AKAP) (Wang et al., 2000). AKAPs regulate PKA signaling by sequestering PKA with its substrates at specific subcellular locations (Langeberg and Scott, 2005). Nbea is involved in regulated secretion, which occurs in neurons and blood platelets (Goubau et al., 2013), and the large, dense-core vesicles in blood platelets from a patient haploinsufficient for Nbea displayed an abnormal morphology (Castermans et al., 2010). While the number of synaptic vesicles appears to be unchanged in

two different Nbea KO mouse models (Su et al., 2004; Medrihan et al., 2009), stimulus-release coupling in presynaptic terminals is disrupted, leading to a loss of evoked synaptic transmission at neuromuscular junctions (Su et al., 2004). Thus, null-mutant mice suffocate shortly after birth due to a failure to initiate breathing (Su et al., 2004). Loss-of-function experiments using acute brain slices or cultured neurons from embryonic mice indicate that Nbea plays an important role in synaptogenesis and synaptic function (Nair et al., 2013; Farzana et al., 2016; Su et al., 2004; Medrihan et al., 2009; Niesmann et al., 2011; Repetto et al., 2018) as well as the formation of dendritic spines (Niesmann et al., 2011). In order to mimic the monoallelic Nbea deletions in autistic individuals, Nbea heterozygous ($Nbea^{+/-}$) mice, which exhibit a 30% reduction in Nbea expression (Niesmann et al., 2011), have been generated.

The first evidence for the face validity of the Nbea haploinsufficient ASD mouse model came from a study by Nuytens and coworkers, who performed a battery of behavioral tests aimed at uncovering possible autism-like phenotypes (Nuytens et al., 2013). Female $Nbea^{+/-}$ mice showed increased grooming behavior when sprayed with water mist, which is suggestive of autism-related repetitive behaviors (Nuytens et al., 2013). The three-chamber sociability test was analyzed by repeated-measures analysis of variance (RM-ANOVA) and revealed an effect of the chamber on the interaction time, with the Tukey post-hoc test showing a significant difference between the time spent with the stranger mouse and the time spent with the object for the wildtype (WT) mice, but not for the $Nbea^{+/-}$ mice (Nuytens et al., 2013). However, the sociability index was not reported, so a direct comparison of the genotypes was not possible. In the social novelty portion of the test, both the WT and the $Nbea^{+/-}$ mice showed a preference for the unfamiliar mouse over the familiar mouse, and no genotype effect on the interaction time was reported (Nuytens et al., 2013). Interestingly, a recent study reported an increase in sociability in one-year-old $Nbea^{+/-}$ mice, which the authors attributed to a possible age-related improvement in social function (Odent et al., 2021). Nbea was also shown to be involved in hippocampal-dependent forms of memory: spatial memory assessed by the Morris water maze was impaired in $Nbea^{+/-}$ mice, whereas contextual fear conditioning was enhanced, as evidenced by increased freezing levels (Nuytens et al., 2013). Reversal learning was not tested in this study, thus the contribution of Nbea to cognitive flexibility is unknown. A more recent study using a different $Nbea^{+/-}$ mouse line (but also on a C57BL6J background) provided further evidence for the involvement of Nbea in contextual fear conditioning, but in this case, only the extinction of the fear memory was affected, as evidenced by increased freezing levels during the extinction phase (Lee et al., 2018). The increased freezing levels were not due to differences in locomotor activity, in fact, $Nbea^{+/-}$ mice displayed slightly higher locomotor activity in the first five minutes of the open field test; and there was no genotype difference in the time spent in the center of the open field, indicating that baseline anxiety levels were not altered by Nbea haploinsufficiency. Fear extinction was also impaired in mice which had been injected with an adeno-associated virus carrying small hairpin RNA to selectively knock down Nbea expression in the cornu ammonis (CA1) region of the hippocampus, suggesting that Nbea plays a key role in regulating fear extinction (Lee et al., 2018). Interestingly, a functional MRI study revealed delayed fear extinction in autistic individuals, which the authors attributed to a difficulty in distinguishing safe cues from threat cues (Top et al., 2016). In conclusion, the Nbea haploinsufficient mouse models several autistic phenotypes and thus serves as a face- and construct-valid model of ASD.

In addition to the behavioral phenotype, $Nbea^{+/-}$ mice also exhibited a reduction in the number of spine synapses (Niesmann et al., 2011) and deficits in synaptic function (Nuytens et al., 2013). Specifically, the density of axo-spinous synapses as well as the frequency of miniature excitatory and inhibitory postsynaptic currents were reduced in the somatosensory cortex of adult $Nbea^{+/-}$ mice (Niesmann et al., 2011), and long-term potentiation (LTP) in hippocampal subregion CA1 was reduced in acute slices prepared from adult female $Nbea^{+/-}$ mice (Nuytens et al., 2013). These results are in line with findings that the complete deletion of Nbea interferes with the subcellular distribution of actin (Niesmann et al., 2011) and impairs the trafficking of

synaptic receptors (Nair et al., 2013; Farzana et al., 2016; Gromova et al., 2018). Taken together, these experiments suggest that the cognitive deficits in the haploinsufficient mice could be explained by impairments of synaptic function in the hippocampus.

### 1.3.2 The Neuroligin-3 Knockout Mouse Model

The neuroligins are a family of postsynaptic cell adhesion proteins which stabilize synapses by binding to presynaptic neurexin proteins (Südhof, 2017). There are four conserved neuroligin genes in vertebrates (Neuroligins 1-4) which encode proteins consisting of a large extracellular, esterase-homology domain which forms homo- and heterodimers with other neuroligins, a transmembrane domain, and a small intracellular domain (Südhof, 2017). A variety of different functions ranging from synaptogenesis and synapse stabilization to the regulation of synaptic transmission and plasticity have been reported for different neuroligins. However, it appears that the different isoforms perform synapse-type-specific, non-overlapping functions (Südhof, 2017). Nlgn3 is expressed at excitatory as well as inhibitory synapses in cultured hippocampal neurons (Budreck and Scheiffele, 2007) and was shown to form heterodimers with Nlgn1 (Poulopoulos et al., 2012), which raises the intriguing possibility that Nlgn3 could regulate both excitatory and inhibitory synaptic function, perhaps via its interactions with other neuroligins or other synaptic proteins.

The SFARI gene score for Nlgn3 is 1, implicating it in ASD with high confidence. Nlgn3 was first identified as an ASD candidate gene in a sibling study (Jamain et al., 2003). The mutation led to a change in the amino acid sequence within the esterase-homology domain which was expected to alter the structure and calcium-dependent functionality of the protein (Jamain et al., 2003). To study the effects of this mutation on brain function and behavior, several animal models were generated: a knock-in mouse line of the point mutation observed in the sibling study (referred to as the $Nlgn3^{R451C}$ mouse line, for the arginine-to-cysteine substitution at amino acid position 451) (Tabuchi et al., 2007), a Nlgn3 KO mouse line (Varoqueaux et al., 2006), and a Nlgn3 KO rat line (Hamilton et al., 2014). Each model displays some level of face validity, but there are important differences in the behavioral phenotypes that can be attributed to species or strain differences.

Nlgn3 KO mice exhibit several autism-related behaviors that have been validated with different strains and in different laboratories. One of the earliest studies of Nlgn3 KO mice reported hyperactivity in the open-field test, but normal sociability in the three-chamber test (Radyushkin et al., 2009). However, the Nlgn3 KO mice showed less preference for an unfamiliar mouse in the social novelty test and emitted fewer vocalizations in the presence of a female mouse in estrus. These results are complicated by a possibly confounding impairment in olfaction, which was assessed with the buried-food finding test (Radyushkin et al., 2009). The social memory deficits of the Nlgn3 KO ASD mouse model were confirmed in a different laboratory using a different background strain (129SvEv as opposed to C57BL6N in the 2009 study) and a different test design (Bariselli et al., 2018). In this version of the social novelty test, the subject mouse was exposed to the same stranger mouse for 15 minutes on four consecutive days, and the mice were allowed to freely interact. On the fifth day, a different stranger mouse was introduced into the cage and the social novelty response was quantified by the ratio of the interaction time on the fifth day to the interaction time on the fourth day. The habituation to the stranger mouse over the first four days was assessed by comparing the social interaction times on each day; this analysis revealed that Nlgn3 KO mice interacted less with the stranger mouse than their WT littermates did and also showed no significant habituation. Therefore, sociability was also judged to be lower in Nlgn3 KO mice. Furthermore, male Nlgn3 KO mice had a clear preference for social odors, but showed a decreased response to a novel social odor, mimicking the results from the three-chamber test. A more recent study also reported a significant difference between Nlgn3 KO and WT mice in sociability as well as social novelty

in the three-chamber test (Modi et al., 2019). Therefore, the difference in olfaction observed in the C57BL6N-Nlgn3 KO mice does not extend to other strains, which suggests that the social recognition deficits are predominantly mediated by the deletion of Nlgn3. Interestingly, Nlgn3 KO mice also exhibited enhanced rotarod learning, which could be related to an increased tendency to develop repetitive motor routines (Rothwell et al., 2014). Previous studies had shown no differences in rotarod performance between Nlgn3 KO and WT littermates (Radyushkin et al., 2009), but the number of trials and maximum speed of the rotating rod differed in these two studies, and it is possible that differences in motor learning might only become apparent in more challenging tasks. Intriguingly, there is evidence for enhanced cognitive flexibility in Nlgn3 KO mice: Nlgn3 KO mice exhibited enhanced reversal learning in the Morris water maze (Radyushkin et al., 2009) and enhanced behavioral flexibility in a test of visual transitive inference (Norris et al., 2019). However, the response latency was increased in Nlgn3 KO mice, indicating slower cognitive processing (Norris et al., 2019), which would be consistent with findings from autistic adolescents showing a difference in the functional connectivity during a transitive inference task (Solomon et al., 2015). In conclusion, while the sociability defects were not consistent between laboratories, the impairment of social memory in these mice is robust, as is the hyperactive phenotype, and an argument can be made in favor of an increase in repetitive behaviors and, possibly, increased cognitive flexibility and slower cognitive processing.

An initial study of Nlgn3$^{R451C}$ mice reported that the mutant mice spent less time with the stranger mouse in the three-chamber test than their WT littermates did, but both groups spent more time with the other mouse than with the object (Tabuchi et al., 2007). The sociability index, which would allow firm conclusions regarding the degree of sociability exhibited by each group, was not reported in this study. Interestingly, Nlgn3$^{R451C}$ mice exhibited faster initial and reversal learning in the Morris water maze, indicating an enhancement in spatial memory (Tabuchi et al., 2007). However, the behavioral phenotype of the R451C mutation appears to be dependent on the genetic background used in the 2007 study (a hybrid C57BL6J/129S2/SvPasCrl background) because the differences in sociability and spatial learning could not be replicated in two separate studies of Nlgn3$^{R451C}$ mice on a pure C57BL6J background (Chadman et al., 2008; Jaramillo et al., 2018). Further support for an influence of the background strain comes from two studies, one using the same background strain as Tabuchi and colleagues (Etherton et al., 2011) and one using Nlgn3$^{R451C}$ mice on a 129S2/SvPasCrl background (Jaramillo et al., 2014), which were able to independently replicate the reduced sociability in the mutant mice. The strain-specific differences also extended to motor-related abnormalities. Rothwell and colleagues observed an increase in exploratory behavior in the open field and enhanced motor learning on the rotarod in Nlgn3$^{R451C}$ mice on the hybrid C57BL6J/129S2/SvPasCrl background (Rothwell et al., 2014), and mice on a 129S2/SvPasCrl background also displayed increased locomotor activity in the open field (Jaramillo et al., 2014). However, Nlgn3$^{R451C}$ mice on a pure C57BL6J background only exhibited a slight increase in locomotor activity in a novel (cage) environment, and no increase in exploratory behavior in the open field (Jaramillo et al., 2018). In a visual transitive inference task, Nlgn3$^{R451C}$ mice also displayed enhanced cognitive flexibility and an increased response latency, similarly to Nlgn3 KO mice (Norris et al., 2019). In summary, the face validity of the Nlgn3$^{R451C}$ mouse model is highly dependent on the background strain, and the behavioral phenotype is less informative than that of the well-validated Nlgn3 KO mouse model. The discrepant results obtained from different background strains underscore the importance of testing for potential epistatic interactions of the mutant gene with the background strain when characterizing new mouse models.

The Nlgn3 KO rat was developed using zinc-finger nuclease-mediated genome editing and is one of the first transgenic rat models of ASD (Hamilton et al., 2014). Juvenile Nlgn3-KO rats displayed normal sociability in the three-chamber test, but engaged in fewer play behaviors with a juvenile conspecific (Hamilton et al., 2014). Sensory and locomotor function was normal in Nlgn3-KO rats, but prepulse inhibition was reduced, suggesting a defect in sensorimotor gating.

A newer study was not able to replicate the differences in sociability and sensorimotor gating observed by Hamilton and colleagues, but found differences in sleep patterns in Nlgn3 KO rats (Thomas et al., 2017). However, older rats which had been obtained from a commercial vendor were used in this study, so the differences could be due to age- or environment-related factors. Further corroborating evidence from a different laboratory or using a different background strain is necessary to validate the Nlgn3 KO rat as an ASD model.

Initial experiments using RNA-interference-mediated gene knockdown had suggested that Nlgn3 was involved in the formation of synapses (Chih, Engelman, and Scheiffele, 2005), but later experiments using constitutive knockout mice showed that Nlgn3 was dispensable for synapse formation (Varoqueaux et al., 2006). The conflicting *in vitro* results could be explained by a decease in synaptic efficacy at Nlgn-deficient synapses, which would disadvantage synapses in the competition for presynaptic contacts, and thereby lead to a reduction in the number of synapses (Varoqueaux et al., 2006). Indeed, Nlgn3 has been shown to regulate a variety of synaptic functions in a region-specific manner. Researchers have found evidence for an involvement of Nlgn3 in Alpha-amino-3-hydroxy-5-Methyl-4-isoxazole-Propionic Acid(AMPA)-receptor-mediated excitatory synaptic transmission in hippocampal area CA1 (Etherton et al., 2011), metabotropic glutamate receptor-mediated long-term depression at parallel fiber-Purkinje cell synapses in the cerebellum (Baudouin et al., 2012), tonic endocannabinoid signaling at cholecystokinin-positive (CCK) basket cell synapses in CA1 (Földy, Malenka, and Südhof, 2013), inhibitory synaptic transmission at D1-dopamine-receptor-expressing medium spiny neurons in the nucleus accumbens (Rothwell et al., 2014), the clustering of gamma-aminobutyric acid $(GABA)_A\alpha 2$ receptor subunits in the inner plexiform layer of the retina (Hoon et al., 2017), N-Methyl-D-Aspartate(NMDA)-receptor-mediated excitatory postsynaptic currents (EPSCs) in parvalbuminergic interneurons in hippocampal area CA1 (Polepalli et al., 2017), and somatostatin-expressing (SOM) interneuron function in CA1 (Horn and Nicoll, 2018). Furthermore, Nlgn3 appears to be involved in dendritic outgrowth in the somatosensory cortex (but not the hippocampus) (Xu et al., 2019) and developmental synaptic pruning in the cerebellum (Lai et al., 2021), suggesting that Nlgn3 may regulate synapse numbers without being involved in synapse formation *per se*.

In addition to these region- and synapse-specific functions, Nlgn3 also appears to exhibit age-specific functions. During the first two weeks of postnatal development, while synaptogenesis is ongoing, the synaptic functions of Nlgn1 and Nlgn3 can be compensated by a fellow neurexin binding partner, leucine-rich repeat transmembrane protein (LRRTM) 2, but not at later time points, when synaptogenesis is mostly complete (Soler-Llavina et al., 2011). These results suggest that the neuroligins serve different functions at developing and at mature synapses, and any results obtained from young Nlgn3-deficient neurons may suffer from confounding effects of compensation. These concerns were borne out in a study by Zhang and colleagues, who observed that a constitutive or prenatal conditional KO of Nlgn3 did not impair synaptic transmission at the calyx of Held, but a postnatal conditional KO of Nlgn3 significantly reduced AMPA-receptor-mediated synaptic transmission (Zhang et al., 2017). It was recently shown that the human NLGN3 protein is expressed at the leading edge of growth cones during early neuronal development and promotes neuritogenesis (Gatford et al., 2021). These findings could be replicated in mouse cortical neurons overexpressing Nlgn3, indicating that Nlgn3 has an important non-synaptic function during neuronal development (Gatford et al., 2021). Taken together, these results show that the age of the animal during experimental manipulation and the age during the manipulation of Nlgn3 expression likely affect the experimental outcome.

It is not yet fully understood how the remarkable age- and synapse-specificity of Nlgn3 function is achieved. The synaptic targeting and function of neuroligins appears to be partially controlled by alternative splicing (Uchigashima et al., 2020a; Oku et al., 2020). Specifically, the splice insert at site A1, which is present in Nlgn1 and Nlgn3, increases the binding selectivity for the heparan-sulfate chain of neurexin and thereby promotes synapse formation (Oku et al., 2020). Intriguingly, the deficits in presynaptic differentiation in cells expressing an autism-associated

Nlgn1 mutation were partially rescued by the expression of the A1 splice site insert, suggesting that increasing this splice variant might be a potential therapeutic intervention in individuals with deleterious mutations (Oku et al., 2020). Differences in the binding affinities of the different splice variants for their presynaptic binding partners, the neurexins, have been proposed to form a code determining the synaptic properties (Boucard et al., 2005), but more recent studies showed that the neuroligin splice variants had a weaker effect on neurexin binding than initially assumed (Koehnke et al., 2010; Reissner et al., 2008). However, different neurexin splice variants differentially affect neuroligin function (Uchigashima et al., 2020b; Futai et al., 2013), so the hypothesis of a neuroligin-neurexin splice code is still plausible. A non-canonical transsynaptic interaction between Nlgn3 and a type IIA receptor protein tyrosine phosphatase (PTP) $\delta$ was recently identified, which could potentially explain the behavioral differences between the Nlgn3 KO and Nlgn3$^{R451C}$ mice (Yoshida et al., 2021). The disruption of the non-canonical Nlgn3-PTP$\delta$ interaction recapitulated the enhanced motor learning, but not the social deficits, observed in the Nlgn3 ASD models; and the Nlgn3$^{R451C}$ mutation selectively impaired the non-canonical interaction, whereas the complete loss of Nlgn3 would impair both interactions. Yoshida and colleagues propose that PTP$\delta$ competes with neurexins for Nlgn3 binding at certain synapses, and the balance of these interactions determines the development of sociality.

Nlgn3 also appears to have several unexpected non-synaptic functions. The secretion of Nlgn3 ectodomains from active neurons was shown to activate the phosphoinositide-3-kinase pathway in glioma cells, leading to increased proliferation (Venkatesh et al., 2015). An activity-dependent cleavage pathway was recently identified by Bemben and colleagues: in synaptically active spines, metabotropic glutamate receptors (mGluRs) initiate protein kinase C signaling, which leads to the secretion of different proteases that cleave both Nlgn3 homodimers and Nlgn1-Nlgn3 heterodimers extracellularly (Bemben et al., 2019). A proteomic analysis revealed alterations in translation-related genes in the ventral tegmental area (VTA) of Nlgn3 KO mice, suggesting an unexpected involvement of Nlgn3 in protein translation (Hörnberg et al., 2020). In a series of elegant experiments, the authors demonstrated that treatment with a mitogen-activated protein kinase interacting kinase inhibitor was able to restore not only translational homeostasis, but also the response to oxytocin in VTA dopaminergic neurons and the social memory in juvenile Nlgn3 KO mice (Hörnberg et al., 2020). Oxytocin is a potential therapeutic agent for the social deficits in ASD, so these results indicate that the Nlgn3 KO model might also exhibit predictive validity. Recently, an interesting link between Nlgn3 and gastrointestinal function was found in mice: Nlgn3-deficient mice exhibited an increased colonic diameter and faster colonic migrating motor complexes (Leembruggen et al., 2020). While the mechanisms are not yet understood, an involvement of Nlgn3 in the regulation of the enteric nervous system could help explain the prevalence of gastrointestinal disturbances in autistic individuals (McElhanon et al., 2014).

In conclusion, the Nlgn3 KO mouse represents a face-, construct-, and (potentially) predictive-valid animal model of ASD. Its wide-ranging functions can explain both the ubiquity and specificity of Nlgn3 mutations in ASD: many different physiological processes, from synaptic transmission to gut motility, are disrupted by the loss of Nlgn3, so the deletion of Nlgn3 can account for social, motor, and gastrointestinal symptoms of ASD; but mutations that do not completely abolish Nlgn3 expression, such as the R451C mutation, might give rise to cell- and region-specific differences in Nlgn3 levels and distinct phenotypes.

### 1.3.3 The Neuroligin-4 Knockout Mouse Model

Nlgn4 was first identified as an autism candidate gene in the same sibling study that linked Nlgn3 to ASD (Jamain et al., 2003). A later study described a pedigree in which a mutant variant of the X-chromosome-linked Nlgn4 (NLGN4X) displayed complete penetrance for ASD in males, but not in carrier females, providing further evidence for an involvement of Nlgn4

in ASD (Laumonnier et al., 2004). These findings had puzzled researchers because it was assumed that the Y-linked Nlgn4 gene (NLGN4Y), which shares 97% sequence identity with NLGN4X, might be able to compensate for a dysfunctional NLGN4X in males (Nguyen et al., 2020). A recent study showed that the Y-linked Nlgn4 gene has an amino acid difference in the extracellular domain which prevents it from trafficking to the cell surface as efficiently as NLGN4X (Nguyen et al., 2020). Therefore, NLGN4Y is unable to compensate a loss-of-function mutation in NLGN4X, resulting in the complete penetrance of the ASD phenotype in males. So far, only one autism-related mutation in the NLGN4Y gene has been reported (Yan et al., 2008), whereas at least 19 different *de novo* or inherited mutations have been identified in NLGN4X (Nguyen, Lehr, and Roche, 2020). A partial deletion of the Y-chromosomal region containing the NLGN4Y and protocadherin 11 genes was recently discovered in a child with a gonadal development disorder (mixed gonadal dysgenesis 45,X/46,XY) alongside severe language and behavioral impairments characteristic of ASD (Nardello et al., 2021). While the evidence for an involvement of NLGN4Y in ASD is mounting, it is not yet as strong as the evidence in support of NLGN4X. While NLGN4X has a SFARI gene score of 1, NLGN4Y has a score of 3, which indicates that only one *de novo* likely gene-disrupting mutation has been identified so far. Therefore, most research is focused on NLGN4X.

The relevance of Nlgn4 KO mouse models to NLGN4X-linked ASD is complicated by sequence differences between the human NLGN4X gene and the mouse Nlgn4-like gene (Bolliger et al., 2008). The murine Nlgn4-like gene only has a sequence identity of approximately 60% with the human NLGN4X and NLGN4Y genes, which was unexpected given the strong homology of the other neuroligin genes between humans and mice (between 98 and 99%) (Bolliger et al., 2008). The chromosomal localization of mouse Nlgn4-like was only recently identified using fluorescent *in situ* hybridization. Surprisingly, the gene was localized to the sex chromosomes, but unlike human NLGN4X, the mouse Nlgn4 gene is located in the pseudoautosomal region (PAR) of the sex chromosomes and can therefore undergo homologous recombination in both males and females (Maxeiner et al., 2020). Furthermore, the authors found that while the Nlgn4-like gene has undergone considerable sequence changes (mostly insertions of short, repetitive sequences) within the eumuroidea clade (containing the mouse and hamster families), these differences are limited to introns or regions that likely do not affect the functionality of the Nlgn4 protein (Maxeiner et al., 2020). Thus, the mouse Nlgn4-like gene is one of the few genes to have withstood the "erosion" of the murine PAR, which is indicative of considerable evolutionary pressure to maintain the function of the Nlgn4 protein (Maxeiner et al., 2020).

In addition to genetic differences, there are differences in the localization and function of the mouse and human Nlgn4 protein. In mice, Nlgn4 is expressed mostly at inhibitory synapses and regulates glycinergic (Hoon et al., 2011) and GABAergic (Hammer et al., 2015) synaptic transmission (but see Delattre et al., 2013; Unichenko et al., 2017), whereas in humans, Nlgn4 was recently found to be predominantly localized to excitatory synapses (Marro et al., 2019). The overexpression of NLGN4X in induced human neuronal cells led to an increase in the number of synapses, but a decrease in the frequency of spontaneous EPSCs and the amplitude of evoked EPSCs, suggesting that Nlgn4 induces the formation of nonfunctional synapses (Marro et al., 2019). However, the overexpression of NLGN4X with an autism-linked Nlgn4 mutation, R704C, also led to an increase in synapse numbers, but concurrently increased the synaptic strength (Marro et al., 2019). In cultured mouse hippocampal neurons, the overexpression of NLGN4X also led to an increase in synapse numbers, but a decrease in the amplitude of miniature EPSCs (Zhang et al., 2009; Chanda et al., 2016) while overexpression of the R704C mutant gene increased the excitatory synaptic strength (Chanda et al., 2016). The comparison of the mouse and human gene function is somewhat complicated by the methodological differences: while the mouse studies relied on the constitutive genetic deletion of the Nlgn4 gene, the studies of the human protein relied on overexpression of NLGN4X in cultured cells. Generally speaking, if the same pathway is targeted, overexpression and deletion of a protein either cause the same

phenotype, opposite phenotypes, or no phenotype (Prelich, 2012). Neomorphic phenotypes, i.e., phenotypes that are not normally associated with an overexpressed protein, are rare (Prelich, 2012), but not unheard of, so it is possible that the overexpression of NLGN4X might lead to a mislocalization of Nlgn4 to excitatory synapses. Thus, the different phenotypes observed in the human overexpression and mouse KO experiments do not necessarily reflect a difference in function of the human and mouse protein. Furthermore, a cell-type-specific difference in function cannot be excluded. Delattre and colleagues observed a decrease in excitatory synaptic transmission in acute slices of the somatosensory cortex from Nlgn4 KO mice (Delattre et al., 2013), and Unichenko and coworkers observed a decrease in the frequency of mEPSCs in layer 4 spiny stellate neurons in the barrel cortex of Nlgn4-deficient mice, indicating that murine Nlgn4 also plays a role at certain excitatory synapse types. Furthermore, both human and murine Nlgn4 were shown to promote neuritogenesis in developing neurons (Gatford et al., 2021), indicating functional overlap during a critical period of neuronal development.

Despite the above-mentioned differences between murine and human Nlgn4, the Nlgn4 KO mouse model has strong face validity in the social and communication domain and could aid in understanding common pathomechanisms of ASD. Nlgn4 KO mice generated on a 129P2/OlaHsd background exhibited impairments in sociability and social memory in the three-chamber test and produced fewer ultrasonic calls in the presence of a female mouse in estrus than their WT littermates (Jamain et al., 2008). The validity of the Nlgn4 KO model were called into question by a later replication study which failed to detect impairments in social behavior or vocalization, despite using the same mouse line, three-chamber apparatus and experimental procedures (Ey et al., 2012). The authors attributed these differences to the increased number of backcrosses in the mouse lines used in the later experiments, which would have further reduced the expected percentage of the 129P2/OlaHsd genome still present in the Nlgn4 KO mice (Ey et al., 2012). Later experiments using revitalized frozen embryos from the Nlgn4 KO line that had been used in the original study (which had been backcrossed with C57BL/6J mice for six generations) and were backcrossed for two further generations for a total of eight backcrosses were able to replicate the social and vocalization defects in male Nlgn4 KO mice (El-Kordi et al., 2013) and extended these findings to female (El-Kordi et al., 2013) and juvenile (Ju et al., 2014) KO mice. The cohorts studied by Ey et al. (2012) had been backcrossed a maximum of eight times, so the phenotypic differences might reflect environmental, rather than genetic, differences. A replication study in a different laboratory could help allay remaining concerns regarding the face validity of the Nlgn4 KO mouse model.

## 1.4 Assessing E-I Balance in the Hippocampal Dentate Gyrus

While individual neurons may experience transient phases of increased excitation or inhibition, the global activity of neuronal circuits is usually maintained at a stable level (Sohal and Rubenstein, 2019). Since differences in the level of excitatory or inhibitory innervation to individual neurons can be compensated by intrinsic plasticity mechanisms (Nelson and Valakh, 2015), it is imperative to measure the global activity in neuronal circuits to determine whether an autism-related mutation actually leads to E-I imbalance. However, many studies of Nbea, Nlgn3 and Nlgn4 function have employed cultured neurons, which limits the conclusions that can be drawn regarding the effect of these proteins on E-I balance *in vivo*. Therefore, the aim of this dissertation was to assess the effect of Nbea haploinsufficiency and Nlgn3 or Nlgn4 loss on E-I balance in an intact neuronal circuit.

The hippocampal dentate gyrus is an anatomically and electrophysiologically well-defined region which is highly sensitive to changes in E-I balance. In order to assess behaviorally relevant changes in the E-I balance of the dentate gyrus, it is necessary to record population activity *in vivo*. It has been reported that inhibition is weaker in hippocampal slice preparations

compared to the *in vivo* situation because long-range inhibitory connections are severed during the slicing procedure (Buckmaster and Schwartzkroin, 1995). Therefore, it was decided to record local field potentials in the granule cell layer of the dentate gyrus while stimulating the perforant path, a method which had been successfully used to analyze E-I balance in different mouse models (Jedlicka et al., 2009; Jedlicka et al., 2011).

The dentate gyrus is characterized by a unidirectional excitatory input from the entorhinal cortex, which is transmitted to the dentate gyrus via the perforant path (Amaral and Lavenex, 2007). The axons of the perforant path form excitatory synapses onto the principal neurons of the dentate gyrus, the granule cells, and onto interneurons which extend their dendrites into the molecular layer (Figure 1.1a). This unique connectivity can be exploited in order to repeatedly stimulate the dentate granule cells and interneurons without eliciting feedback inhibition onto the spiny stellate cells of the entorhinal cortex, which give rise to the perforant path. In response to perforant path stimulation, a positive-going field excitatory postsynaptic potential (fEPSP) reflecting the strength of the synaptic transmission can be recorded in the dentate gyrus (Lømo, 1971; Bronzino et al., 1994)(Figure 1.1b). At higher stimulation intensities, the strength of the fEPSP increases until the granule cells begin firing action potentials, which can be recorded as the negative-going population spike (Lømo, 1971; Sloviter, 1991). The threshold for action potential initiation is determined by the intrinsic excitability of the granule cells, but also by the strength of GABAergic inhibition onto the granule cells (Jedlicka, Muellerleile, and Schwarzacher, 2018). Since the perforant path also innervates molecular layer interneurons, the granule cell output in response to perforant path stimulation serves as a proxy for the overall E-I balance in the dentate gyrus (Jedlicka, Muellerleile, and Schwarzacher, 2018).

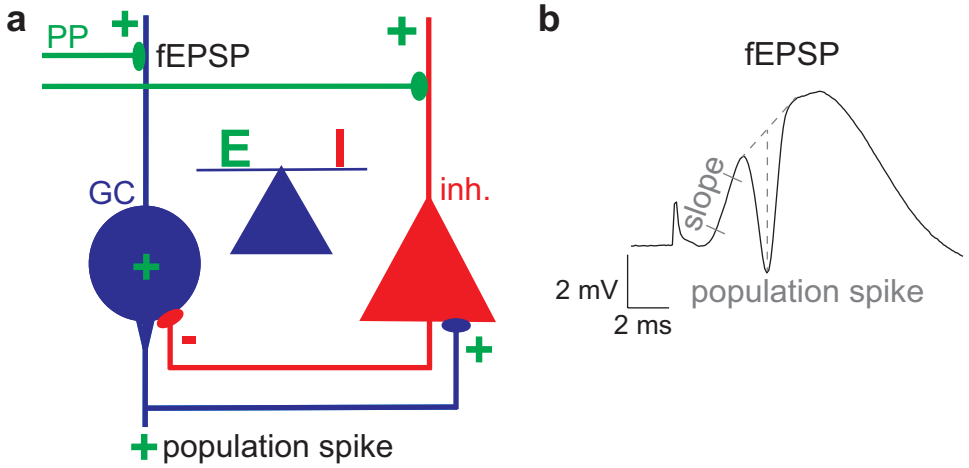


FIGURE 1.1: (a) Circuit diagram of the dentate gyrus depicting the most important excitatory and inhibitory connections. The perforant path (PP) forms excitatory synapses with dentate granule cells (GC) as well as inhibitory interneurons (inh.). The action potential output of the granule cells (measured by the population spike) is determined by the interplay of the excitatory input strength, the intrinsic neuronal excitability, and the strength of the feedforward and feedback inhibition. Under normal conditions, excitation and inhibition are carefully balanced to preserve the action potential output of the granule cells. (b) Representative trace of an evoked field excitatory postsynaptic potential (fEPSP) recorded in the granule cell layer of the dentate gyrus in response to a 700 µA, 0.1 ms current pulse (see stimulus artefact). The fEPSP slope is used as a measure of the synaptic input strength, and the superimposed population spike represents the action potential output of the granule cell population. The diagram in panel (a) is inspired by Figure 6d in Jedlicka et al., 2011

Previous research in the laboratory has shown that the amplitude of the population spike is sensitive to changes in the action potential-generating capabilities of the granule cells (Winkels et al., 2009) as well as the strength of inhibitory synaptic transmission onto granule cells (Jedlicka

et al., 2009). When stimulating the perforant path with increasing current intensities, the resulting response curve of the population spike amplitude reveals differences in the onset and synchrony of action potential firing. In order to quantify the degree of inhibitory synaptic transmission, the perforant path is stimulated with two spike-eliciting pulses in short succession. The perforant path also activates inhibitory interneurons, which in turn inhibit the granule cells. Thus, the second population spike is smaller than the first population spike at short interpulse intervals, a phenomenon referred to as paired-pulse inhibition (PPI). At longer interpulse intervals, metabotropic $GABA_B$ autoreceptors on the interneurons are activated and inhibit their activity, resulting in the disinhibition of the population spike (Foster et al., 2013). While the granule cells also form excitatory connections onto interneurons, resulting in feedback inhibition, computer simulations of the dentate network have shown that feedforward inhibition mediated by perforant-path-activated interneurons targeting the perisomatic region of the granule cells is the major contributor to PPI (Jedlicka, Deller, and Schwarzacher, 2010). Therefore, a reduction in the interpulse interval at which the inhibition turns into disinhibition indicates that perisomatic inhibition is weakened, which can explain an increase in the granule cell population spike output (Jedlicka et al., 2011). In contrast, an increase in the duration of PPI is more difficult to interpret, since it can indicate either an increase in the relative strength of inhibitory synaptic transmission or a decrease in the intrinsic excitability (i.e., the efficiency with which increases in synaptic input are translated into action potentials) of the granule cells (Winkels et al., 2009).

Most research into the mechanisms that maintain E-I balance focus on the synaptic contributions (Okun and Lampl, 2009), but changes in the intrinsic excitability can also lead to disruptions of the network E-I balance (He and Cline, 2019). Dentate granule cells can fire action potentials across a wide range of frequencies, making them efficient integrators of afferent inputs (Mishra and Narayanan, 2020). Thus, even small changes in the intrinsic excitability can have a strong impact on information processing in the dentate gyrus. Dentate granule cells are less excitable than many other types of principal neurons due to a combination of intrinsic properties, such as a hyperpolarized resting potential (RMP), prominent spike frequency adaptation, and strong feedback and feedforward inhibition from GABAergic interneurons (Coulter and Carlson, 2007). These features maintain sparse coding in the dentate gyrus, which is important for one proposed function of the dentate gyrus, i.e. pattern separation or the differentiation between similar inputs (Cayco-Gajic and Silver, 2019). Intriguingly, one study has identified an impairment in pattern separation ability in autistic adults, but the number of participants was low (South et al., 2015). In addition to affecting information processing, changes in the dentate E-I balance can lead to hyperexcitability and the development of temporal lobe epilepsy (TLE). It has been proposed that the dentate gyrus may serve as a ”gate” that limits the propagation of epileptiform activity to the more vulnerable downstream regions of the hippocampus. In support of this hypothesis, the normally sparse firing of granule cells is shifted to a sustained and rhythmic mode in a rodent model of TLE (pilocarpine injection) (Artinian et al., 2011), and the optogenetic activation of dentate granule cells can induce seizures in non-epileptic mice (Krook-Magnuson et al., 2015). Many TLE patients exhibit a reorganization of the dentate network, with a dispersion of the granule cell layer and the loss of granule cells, commonly referred to as hippocamal sclerosis (Blümcke et al., 2009). Interestingly, dentate granule cells from epileptic patients with severe hippocampal sclerosis exhibited an increased membrane conductivity that was primarily mediated by an increase of inward-rectifier potassium and hyperpolarization-activated cyclic nucleotide-gated (HCN) channel conductances, thus decreasing the granule cell intrinsic excitability in response to the elevated excitatory synaptic input (Stegen et al., 2012). These findings illustrate the importance of the granule cell excitability for the maintenance of dentate E-I balance.

## 1.5 Aims and Objectives

As detailed above, the physiological roles of the autism candidate genes Nbea, Nlgn3 and Nlgn4 suggest that deficits in synaptic function might underlie some of the behavioral symptoms in the mouse models and in autistic individuals. The aim of this thesis was to evaluate each of these proteins in the context of the E-I imbalance theory of ASD. To this end, *in vivo* electrophysiological recordings of the excitatory and inhibitory network activity in the hippocampal dentate gyrus were performed while electrically stimulating the perforant path using established protocols (Jedlicka et al., 2009; Jedlicka et al., 2011; Jedlicka et al., 2015).

The primary objective was to analyze the contribution of Nbea, Nlgn3 and Nlgn4 to E-I balance in the dentate gyrus. The function of excitatory perforant path-granule cell synapses was interrogated with input-output (I-O) and paired-pulse facilitation protocols while inhibitory synaptic transmission was investigated by measuring the inhibition of the granule cell population spike in response to paired-pulse stimulation. Changes in the network E-I balance were determined from the amplitude of the population spike, which is influenced by the excitatory and inhibitory synaptic inputs as well as the intrinsic excitability of the granule cells. In order to determine the contribution of the intrinsic excitability to the network E-I balance, the *in vivo* electrophysiological recordings were supplemented with whole-cell patch-clamp recordings of granule cells in organotypic entorhino-hippocampal slice cultures (OTCs) from Nlgn4 KO and WT mice (Manuscript 3).

As a secondary objective, the involvement of Nbea, Nlgn3 and Nlgn4 in LTP, a form of synaptic plasticity which has been reported to be altered in several ASD mouse models, e.g. in Fmr1-KO mice (Yun and Trommer, 2011) and in mice haploinsufficient for SET-domain-containing 5 gene (Deliu et al., 2018), was investigated using different theta-burst stimulation (TBS) LTP induction protocols *in vivo*. Both Nbea and Nlgn3 had previously been implicated in the regulation of Hebbian synaptic plasticity in hippocampal subregion CA1 (Nuytens et al., 2013) and the cerebellum (Baudouin et al., 2012), respectively, but it was unknown whether Nlgn4 also played a role in synaptic plasticity. In addition to Hebbian synaptic plasticity, the involvement of Nlgn4 in homeostatic synaptic plasticity was investigated in OTCs using an activity blockade protocol.

For the fulfillment of this dissertation, three manuscripts were written. **Manuscript 1** describes the experiments in Nbea$^{+/-}$ mice, **Manuscript 2** details the experiments in Nlgn3 KO mice, and **Manuscript 3** is based on the experiments in Nlgn4 KO mice. The findings related to the dentate E-I balance and granule cell intrinsic excitability and synaptic plasticity are discussed in the following section.

# Chapter 2

# Discussion

The individual contributions of Nbea, Nlgn3 and Nlgn4 to E-I balance in the dentate gyrus of adult mice were assessed using established stimulation protocols (cf. Jedlicka et al., 2011; Jedlicka et al., 2015). Based on their haploinsufficient or KO phenotypes, it can be concluded that Nbea, Nlgn3 and Nlgn4 have distinct functions in the dentate granule cells *in vivo*. The overall ratio of excitation to inhibition, as assessed by the action potential output of the granule cells, was slightly decreased in mice haploinsufficient for Nbea ($Nbea^{+/-}$) and in Nlgn4 KO mice, but unchanged in Nlgn3 KO mice. These results are consistent with the finding that both increases and decreases in E-I balance are associated with ASD, and that homeostatic mechanisms may be able to compensate for the primary deficits in excitation or inhibition in certain brain regions (Nelson and Valakh, 2015). Interestingly, the differences in dentate E-I balance observed in the Nbea and Nlgn4 mutants appear to be mediated by differences in the intrinsic excitability of the granule cells, rather than differences in the synaptic input. Furthermore, the apparent lack of change in the E-I balance observed in Nlgn3 KO mice despite a decrease in excitatory synaptic strength can be explained by a compensatory increase in the intrinsic excitability of the granule cells. These results indicate that alterations in the intrinsic excitability of granule cells play an important role in regulating the dentate E-I balance, and may be a common mechanism disrupted in ASD.

## Nbea, Nlgn3 and Nlgn4 Differentially Affect Dentate E-I Balance and Granule Cell Excitability

In order to compare the the impact of different autism-related mutations on E-I balance in the intact dentate gyrus, current pulses at increasing intensities (from 30 to 800 µA) were delivered to the angular bundle of the perforant path. The slope of the evoked fEPSPs represents the synaptic input strength (Lømo, 1971; Bronzino et al., 1994), and the population spike amplitude represents the summed action potential firing of the granule cell population (Lømo, 1971; Sloviter, 1991), which is controlled by the balance of excitatory and inhibitory inputs to the granule cells as well as the intrinsic excitability of the granule cells (Figure 1.1). PPI experiments provide information about the relative strength of the (mostly feedforward) $GABA_A$-receptor-mediated inhibition of the granule cells, which is predominantly mediated by perisomatically targeting interneurons (Jedlicka, Deller, and Schwarzacher, 2010). Measuring the intrinsic excitability of the granule cells is not possible using field potential recordings. However, a change in intrinsic excitability can be inferred if (1) the E-I balance is altered but both the synaptic input strength and the degree of PPI are unchanged, or if (2) the synaptic input strength is altered but both the action potential output and the degree of PPI are unchanged.

In **Manuscript 1**, the effect of Nbea on E-I balance in the dentate gyrus was investigated in $Nbea^{+/-}$ mice, which exhibit an approximately 30% reduction in Nbea protein levels (Niesmann et al., 2011) and are used as a mouse model for autism-related Nbea haploinsufficiency. Synaptic

transmission at perforant path-granule cell synapses was unchanged in Nbea$^{+/-}$ mice, but the population spike amplitude was slightly reduced compared to WT littermates. EPSP-spike (E-S) coupling was weaker in Nbea$^{+/-}$ mice, evidenced by a rightward shift of the Nbea$^{+/-}$ curve when plotting the population spike amplitude against the fEPSP slope for each stimulation intensity. The top parameter of the Boltzmann-fitted E-S curves was significantly reduced in the Nbea$^{+/-}$ group, indicating that Nbea$^{+/-}$ mice achieved lower maximal spike amplitudes. While the PPI analysis revealed a significant interaction effect when the maximal stimulation intensity was used, the genotype effect was not significant. Therefore, we could rule out a slight difference in inhibitory synaptic function, but the effects on the duration of PPI were minimal. We concluded that Nbea haploinsufficiency leads to a reduction in the dentate E-I ratio, most likely by decreasing the intrinsic excitability of granule cells.

In contrast to the Nbea$^{+/-}$ mice, Nlgn3 KO mice exhibited no change in the population spike output (**Manuscript 2**). However, E-S coupling was increased in Nlgn3 KO mice due to a significant reduction in excitatory transmission at perforant path-granule cell synapses. The PPI analysis revealed a tendency towards increased network inhibition in Nlgn3 KO mice, seemingly in opposition to a greater granule cell excitability. However, the effect was very slight and could be explained by a decrease in the endocannabinoid-mediated disinhibition of CCK interneurons, as reported in hippocampal subregion CA1 (Földy, Malenka, and Südhof, 2013). In the absence of a significant reduction in the duration of PPI, these findings suggest that the intrinsic excitability was increased in Nlgn3-deficient granule cells. We hypothesized that the decreased synaptic input to granule cells might have triggered homeostatic mechanisms to increase the excitability and thereby preserve the action potential output and dentate E-I balance. The first evidence for a homeostatic regulation of intrinsic excitability in vertebrate neurons came from experiments in cortical cultures that had been treated with the sodium channel antagonist tetrodotoxin (TTX) to block spontaneous activity. After two days of treatment, the conductance of voltage-gated sodium channels had increased while the conductance of persistent outward and hyperpolarizing currents had decreased, resulting in an increase in the intrinsic excitability of cortical pyramidal cells (Desai, Rutherford, and Turrigiano, 1999). Since then, several different mechanisms for the plasticity of intrinsic excitability have been identified, such as the downregulation of BK-type calcium-activated potassium currents in brainstem neurons (Nelson, Gittis, and Du Lac, 2005), the downregulation of dendritic HCN channels in activity-deprived sensory cortical pyramidal neurons (Breton and Stuart, 2009), or the relocation of the axon initial segment in dissociated hippocampal neurons subject to global depolarization (Grubb and Burrone, 2010). While our experiments could not identify the exact molecular mechanisms of the excitability changes in Nbea haploinsufficient and Nlgn3 KO granule cells, it is noteworthy that the decrease in the granule cell intrinsic excitability in Nbea$^{+/-}$ mice appears to be a primary deficit (i.e., there are no apparent differences in the synaptic input strengths which could trigger homeostatic mechanisms), while the increase in the intrinsic excitability in Nlgn3 KO mice appears to be a secondary deficit caused by the decrease in synaptic transmission.

The Nlgn4 KO mice exhibited no differences in excitatory synaptic transmission compared to WT littermates, but showed tendencies towards a later onset (in terms of the stimulation intensity) and a reduced amplitude of the granule cell population spike (**Manuscript 3**). PPI was slightly increased in Nlgn4 KO mice, evidenced by a rightward shift of the PPI curve, which could indicate either an increase in GABAergic inhibition onto granule cells or a decrease in the intrinsic excitability of the granule cells (Winkels et al., 2009). In order to distinguish between these hypotheses, we performed whole-cell patch clamp recordings of granule cells in OTCs prepared from Nlgn4 KO mouse pups and WT littermates. These experiments revealed slight differences in the intrinsic excitability of granule cells, specifically regarding the spike frequency adaptation and the tendency to enter depolarization block at high current intensities. Interestingly, there were no differences in the amplitude and frequency of spontaneous EPSCs and inhibitory postsynaptic currents (IPSCs) in Nlgn4-deficient granule cells, and the relative

balance of excitatory to inhibitory synaptic transmission was similar in both groups, further supporting a decrease in the intrinsic excitability of the granule cells as an explanation for the E-I imbalance observed *in vivo*. Previous results from the laboratory had shown that GABAergic interneurons exert stronger control over the granule cell excitability when the generation of action potentials is impaired (Winkels et al., 2009). While the *in vitro* data did not indicate any differences in the properties of individual action potentials, the Nlgn4-deficient granule cells exhibited weaker spike frequency adaptation, but also tended to enter depolarization block at lower current intensities. These contradictory findings could be explained by the opposing effects of extrasynaptic NMDA receptors: while NMDA receptors are generally regarded as increasing the neuronal excitability, a recent modeling study showed that the coupling of NMDA receptors, which are voltage-gated and calcium-permeable, to calcium-activated potassium channels during spike generation leads to a decrease in neuronal excitability (Gall and Dupont, 2020). Thus, a lower spike threshold and increased spike frequency can co-occur with an earlier entry into depolarization block, as seen in the Nlgn4-deficient granule cells.

In conclusion, our experiments show that the three autism candidate genes Nbea, Nlgn3 and Nlgn4 affect the intrinsic excitability of granule cells with different effects on the network E-I balance: Nbea haploinsufficiency and Nlgn4 deletion lead to a reduction in the intrinsic excitability and the E-I ratio, while the loss of Nlgn3 results in an increase in the intrinsic excitability and no apparent difference in the E-I ratio. Furthermore, the two neuroligins that have been implicated in ASD, Nlgn3 and Nlgn4, each lead to an increase in network inhibition in the dentate gyrus when deleted, despite having different effects on the synaptic and intrinsic excitability. These findings lend support to the hypothesis that different autism-related mutations lead to common disruptions in the neuronal and network E-I balance.

## Nbea Regulates E-S Potentiation in Dentate Granule Cells, While Nlgn3 and Nlgn4 Are Not Involved in Synaptic Plasticity

$Nbea^{+/-}$ mice exhibited a stronger potentiation of the population spike amplitude in response to a TBS LTP induction protocol. The potentiation of the fEPSP slope was similar in WT and $Nbea^{+/-}$ mice, which suggests that the Nbea haploinsufficiency led to an increase in the intrinsic excitability of the granule cells, resulting in greater E-S potentiation (**Manuscript 1**). E-S potentiation refers to the potentiation of the population spike that cannot be explained by the potentiation of the fEPSP (Andersen et al., 1980). While the potentiation of the fEPSP always co-occurs with the potentiation of the population spike, population spike potentiation is independent of fEPSP potentiation and therefore caused by a different underlying mechanism (Taube and Schwartzkroin, 1988). In the rat dentate gyrus, weak stimulation of the medial perforant path results in E-S potentiation of the granule cell population spike if accompanied by simultaneous strong stimulation of the ipsilateral supramammillary nucleus, which the authors attributed to the depression of inhibitory synaptic transmission by coactivation of perforant path and supramammillary inputs to inhibitory interneurons in the dentate network (Nakanishi, Saito, and Abe, 2001). The lack of a pronounced deficit in PPI effectively rules out that a decrease in inhibitory input strength is responsible for the enhanced E-S potentiation in the dentate gyrus of $Nbea^{+/-}$ mice, so a difference in the TBS-induced upregulation of the intrinsic excitability of the haploinsufficient granule cells is the likeliest explanation for the observed phenotype.

The intrinsic excitability of granule cells is influenced by several different mechanisms: the degree of EPSP amplification, the action potential threshold, and the RMP (Debanne, Inglebert, and Russier, 2019). EPSP amplification is a local mechanism which only affects nearby synaptic inputs, whereas the latter two mechanisms are global because they affect all synaptic inputs. The HCN channel and the Kv4.2 voltage-gated potassium channel are the primary mediators of

EPSP attenuation in dendrites (Debanne, Inglebert, and Russier, 2019), and their expression is downregulated following LTP induction in CA1 pyramidal neurons (Frick, Magee, and Johnston, 2004; Losonczy, Makara, and Magee, 2008; Campanac et al., 2008). Since Nbea acts as an AKAP, it is possible that it binds Kv4.2 channels to mediate their interaction with potassium channel interacting proteins, resulting in an increased surface expression, as was demonstrated for a different AKAP (Lin et al., 2010). Thus, the enhanced E-S potentiation could be explained by a reduction in Nbea-mediated expression of Kv4.2 channels in haploinsufficient mice. However, Nbea haploinsufficiency may also indirectly affect the neuronal excitability by regulating the activity of phosphorylated cAMP response element binding protein (pCREB), a crucial mediator of synaptic plasticity and neuronal excitability (Lisman et al., 2018). In support of this proposed interaction, the knockdown of Nbea in neuroendocrine cells led to increased levels of pCREB *in vitro*, and the pCREB target brain-derived neurotrophic factor was upregulated in hippocampi of $Nbea^{+/-}$ mice (Nuytens et al., 2013). Importantly, our results indicate that Nbea may differentially influence the intrinsic excitability based on the synaptic activity: while we reported an increase in EPSP amplification following TBS, the intrinsic excitability was reduced in $Nbea^{+/-}$ granule cells during baseline synaptic activation. Different mechanisms, such as an increase in the action potential threshold or a decrease in the RMP, might explain the reduction in pre-TBS E-S coupling in the $Nbea^{+/-}$ mice. The action potential threshold is determined by voltage-gated sodium and potassium channels (Debanne, Inglebert, and Russier, 2019), while HCN channels influence the RMP in granule cells (Mellor, Nicoll, and Schmitz, 2002). It was previously shown that Nbea mediates the surface expression of AMPA receptors via its pleckstrin homology (PH)-BEACH domain (Repetto et al., 2018), so it is conceivable that Nbea might traffic other ion channels to the membrane.

The increase in E-S potentiation in the $Nbea^{+/-}$ mice could have important functional implications. Enhanced LTP has been associated with less specific hippocampal place fields (Taverna et al., 2005), which could explain the observed learning deficits in the Morris water maze (Nuytens et al., 2013), a test of hippocampal-dependent spatial memory in rodents (Vorhees and Williams, 2014). Previous research had shown that the potentiation of the population spike, but not the potentiation of the fEPSP, in hippocampal subregion CA1 correlated with performance in the Morris water maze, which suggests that the population spike is a better physiological correlate of spatial memory (Kleschevnikov and Marchbanks, 1993). Therefore, our findings of an increased E-S potentiation in dentate granule cells might be highly relevant to the impairments in spatial memory in Nbea haploinsufficient mice.

While the I-O and PPI experiments suggested an increase in the intrinsic excitability of Nlgn3-deficient granule cells, the LTP experiments revealed no significant differences in the relative levels of synaptic and E-S potentiation (**Manuscript 2**), further supporting the hypothesis that the loss of Nlgn3 indirectly affects the intrinsic excitability whereas the loss of Nbea has a direct effect on the intrinsic excitability. The same LTP induction protocol consisting of an initial weak TBS followed by a strong TBS was used in both studies. The Nlgn3 KO mice exhibited a slight tendency towards weaker population spike potentiation following the strong TBS, but this difference was not statistically significant. Importantly, the increased E-S coupling in Nlgn3 KO mice was preserved following TBS, as evidenced by the decreased absolute fEPSP slope values in the KO mice. In contrast to the $Nbea^{+/-}$ mice, the absolute values of the population spike amplitude were not significantly different between WT and Nlgn3 KO mice. During the training phase and in the probe trial of the Morris water maze, Nlgn3 KO mice performed similarly to WT littermates, indicating that spatial learning was not impaired by the loss of Nlgn3 (Radyushkin et al., 2009). In a contextual fear conditioning task, Nlgn3 KO mice exhibited a decrease in freezing behavior compared to their WT littermates, however, the authors attributed this behavior to their hyperactivity, rather than a memory impairment (Radyushkin et al., 2009). Thus, our findings of unimpaired LTP induction in the dentate gyrus corroborate the findings of unimpaired spatial learning in Nlgn3-deficient mice.

Similarly to Nlgn3 KO mice, Nlgn4 KO mice showed no differences in the potentiation of the fEPSP slope induced by strong TBS (**Manuscript 3**). The population spike was also potentiated to a similar degree in KO mice, indicating that the decrease in the intrinsic excitability during baseline stimulation did not translate into a difference in E-S potentiation. The use of OTCs in our *in vitro* experiments allowed us to investigate synaptic scaling, a form of homeostatic synaptic plasticity that develops in response to prolonged blockade of activity (Turrigiano et al., 1998). TTX-induced upscaling of the miniature EPSC (mEPSC) amplitude was similar in Nlgn4-deficient and WT granule cells, suggesting that the trafficking of AMPARs to the postsynaptic membrane was not affected by the loss of Nlgn4. These results are consistent with reports of unchanged spatial learning tested with the Morris water maze and unimpaired contextual fear conditioning in Nlgn4 KO mice (Jamain et al., 2008).

In summary, the *in vivo* experiments revealed unimpaired synaptic potentiation but an increase in E-S potentiation in $Nbea^{+/-}$ mice, which could lead to a decrease in the specificity of hippocampal place fields and thus, impaired spatial learning. In contrast, Nlgn3 and Nlgn4 KO mice exhibited no differences in Hebbian or homeostatic synaptic plasticity and no spatial learning deficits. Thus, the increased severity of the Nbea haploinsufficiency phenotype correlates with its autism risk gene ranking, which is higher than that of Nlgn3 and Nlgn4 (Krishnan et al., 2016).

## Limitations

In order to accurately assess the E-I balance of a neural circuit, it is essential that all excitatory and inhibitory connections remain intact. While the *in vivo* experiments are better than *ex vivo* and *in vitro* approaches in maintaining the connectivity, their behavioral relevance is limited by the use of anesthesia. Many commonly used anesthetics, such as propofol, act as selective agonists of $GABA_A$ receptors (Sanna et al., 1995), while others, such as ketamine, are selective antagonists of NMDA receptors (Yamakura et al., 1993). If only a single transmitter receptor is targeted, the degree of enhancement or reduction must be very high to achieve proper anesthestic depth. In contrast, urethane enhances GABAergic and glycinergic transmission and reduces glutamatergic synaptic transmission to a similar extent (Hara and Harris, 2002). Therefore, the E-I balance should be less affected by urethane anesthesia compared to other anesthetics, though we cannot rule out a confounding effect.

The fEPSP arising from the stimulation of the perforant path has long been established as a "stable and easily recorded" potential that correlates with the sum of the EPSPs in the individual granule cells (Lømo, 1971). The unique cytoarchitecture of the dentate gyrus, which is characterized by the curved arrangement of tightly packed neurons with polarized dendritic trees, promotes the convergence of currents from distal sources in the hilus, where the largest fEPSPs can be recorded; however, the granule cells in both blades must be activated to achieve the maximal fEPSP (Fernández-Ruiz et al., 2013). In these experiments, the angular bundle of the perforant path, which contains axons projecting to both supra- and infrapyramidal granule cells, was stimulated. Thus, the fEPSP represents a large population of granule cells from both blades, and not just the cells in the immediate vicinity of the recording electrode. In contrast, only suprapyramidal granule cells were recorded *in vitro* (**Manuscript 3**) because the upper (suprapyramidal) blade is better developed in OTCs. The lower (infrapyramidal) blade requires intact meninges, which are removed during the OTC preparation, for proper postnatal development (Heimrich and Frotscher, 1991). Besides the developmental aspects, there are other important functional, morphological, and electrophysiological differences between granule cells of the upper and lower blades. Suprapyramidal granule cells are preferentially activated by spatial experience (Chawla et al., 2005) and other hippocampal-dependent tasks (Erwin et al., 2020) and have larger dendrites than infrapyramidal granule cells (Gallitano et al., 2016).

However, in response to molecular layer stimulation, infrapyramidal granule cells were shown to be more excitable than suprapyramidal granule cells (Scharfman et al., 2002). Therefore, the excitability of the dentate gyrus as a whole, measured *in vivo*, might be higher than the excitability of the suprapyramidal granule cells measured *in vitro*.

Another unique feature of the dentate gyrus is the presence of predominantly unidirectional connections (Amaral, Scharfman, and Lavenex, 2007) (but see Figure 1 in Xu et al., 2016 for an overview of reciprocal connections within the hippocampal formation). The entorhino-dentate projection to the granule cells is not reciprocated, so there is no danger of suppressing the perforant path input via feedback inhibition. The perforant path consists of two pathways, the medial and the lateral, which target the middle and outer molecular layer, respectively (Hjorth-Simonsen, 1972). The medial perforant path (MPP) primarily consists of axons from spiny stellate neurons in layer II of the medial entorhinal cortex, while the lateral perforant path (LPP) includes projections from horizontal tripolar neurons in addition to stellate neurons in the lateral entorhinal cortex (Schwartz and Coleman, 1981). The cytoarchitecture and connectivity of the medial and lateral entorhinal cortex differ considerably (Knierim, Neunuebel, and Deshmukh, 2014), as do the membrane properties of their projection neurons: LPP neurons have a higher input resistance and exhibit a different pattern of action potential firing than MPP neurons (Wang and Lambert, 2003). Even after accounting for differences in electrotonic decay along the granule cell dendritic tree, the waveforms of the EPSPs evoked by MPP and LPP stimulation still differ, confirming the differences in their synaptic properties (Abraham and McNaughton, 1984). The MPP and LPP also differ in terms of the type of information they carry to the dentate gyrus: in simple terms, the MPP encodes the context while the LPP encodes the content of an experience (Knierim, Neunuebel, and Deshmukh, 2014). Furthermore, the LPP preferentially targets newly integrated adult-born granule cells (Woods et al., 2018). To reduce possible confounding influences resulting from the stimulation of both pathways, such as nonlinear interactions (Dimoka et al., 2008), it is preferred to stimulate either the MPP or the LPP. While most *in vivo* studies in rats stimulate the MPP and LPP separately, it is impossible to target just one pathway in the much smaller mouse brain (Cooke et al., 2006). However, every effort was made to predominantly target the medial perforant path *in vivo*. To measure the E-I ratio *in vitro*, the stimulation electrode was placed in the middle of the molecular layer where the presumptive MPP axons terminate. Thus, the contribution of the lateral perforant path to the dentate E-I balance is underestimated by our measurements.

Other projections to the dentate gyrus which were not investigated in our experiments also play an important role in controlling the activity of the granule cells (Leranth and Hajszan, 2007). The commissural projection, which consists of mossy cell axons from the hilus of the dentate gyrus, targets granule cells and GABAergic interneurons in the inner molecular layer of the contralateral dentate gyrus and suppresses the granule cell population spike in a feedforward manner (Buzsáki and Eidelberg, 1981; Buzsáki and Czéh, 1981). In fact, the commissural fibers activate a greater variety of dentate interneurons, resulting in a greater level of inhibition in granule cells compared to MPP stimulation, which primarily activates basket cell-like interneurons and only transiently activates dendritically-targeting interneurons (Hsu et al., 2016). In contrast, extrahippocampal afferents from the medial septum and the supramammillary nucleus facilitate the granule cell population spike (Fantie and Goddard, 1982; Mizumori, McNaughton, and Barnes, 1989). The cholinergic afferents of the septo-hippocampal projection target the axon initial segment of the granule cells and activate muscarinic acetylcholine receptors, which in turn increase the activity of T-type calcium channels, resulting in a prolonged increase in the local calcium concentration which inhibits the function of Kv7 voltage-gated potassium channels that regulate the spike threshold (Martinello et al., 2015). The afferents from the supramammillary nucleus target the granule cell dendrites of the inner molecular layer, where they form predominantly asymmetric synapses and co-release glutamate and GABA (Hashimotodani et al., 2018). However, the net effect of this innervation is excitatory, so the EPSP elicited by stimulation of the

supramammillary afferents sums with the perforant path-evoked EPSP, leading to an increase in the granule cell population spike (Hashimotodani et al., 2018). These results indicate that the regulation of dentate E-I balance depends on a delicate interplay of excitatory and inhibitory inputs from several different brain regions. Therefore, the E-I imbalances we detected in our experiments using perforant path stimulation should ideally be validated in behaving mice in which all inputs to the dentate gyrus are active.

While the use of constitutive KO mice limits the conclusions that can be drawn regarding the direct contribution of the protein in question to the observed phenotype due to possible developmental compensation, these concerns are mitigated by the use of validated mouse models which exhibit characteristic autistic traits. These pronounced behavioral phenotypes indicate it is unlikely that the function of Nlgn3 and Nlgn4 is fully compensated by other neuronal adhesion proteins. These concerns also do not apply to the Nbea haploinsufficient mice, which are expected to express functional Nbea protein during all developmental stages, albeit at lower levels. Immunoblot analysis of hippocampal synaptosomes revealed that Nlgn3 KO mice exhibited a reduction in Nlgn1 protein levels, which could partially explain the defects in synaptic transmission (**Manuscript 2**). However, Nlgn1 and Nlgn3 appear to regulate different synaptic proteins: the presynaptic VGlut1 is downregulated in Nlgn3, but not in Nlgn1, KO synaptosomes whereas the AMPA receptor subunits GluR1 and GluR2 are downregulated in Nlgn1, but not Nlgn3, KO synaptosomes (Jedlicka et al., 2015). Thus, the deficits in synaptic transmission appear to be mediated by different molecular mechanisms in Nlgn1 and Nlgn3 KO mice, though a partial overlap of function cannot be excluded.

## Conclusions and Outlook

The presented findings indicate that the reduction or deletion of Nbea, Nlgn3 and Nlgn4, three different autism-associated proteins, leads to changes in the intrinsic excitability of dentate granule cells with differing effects on the dentate E-I balance *in vivo*. While the E-I balance is shifted towards inhibition in the $Nbea^{+/-}$ (**Manuscript 1**) and Nlgn4 KO (**Manuscript 3**) mice, the E-I balance is preserved due to a compensatory increase in the intrinsic granule cell excitability in Nlgn3 KO mice (**Manuscript 2**). Synaptic plasticity is not impaired in the mutant mice, but E-S potentiation is increased in $Nbea^{+/-}$ mice, which also exhibit deficits in hippocampal-dependent learning (Nuytens et al., 2013). Taken together, these results support the E-I imbalance theory of ASD, but they also raise several questions that could be addressed in future experiments.

To address the above-mentioned limitations of the constitutive KO mice, it would be necessary to repeat the experiments in conditional KO mice in which the gene in question is knocked out after neuronal development is complete. However, recent work in Nlgn2 conditional knockout mice using a tamoxifen-inducible cre-lox system showed that the knockdown efficacy is much lower than in a constitutive KO, with approximately 40% protein remaining in the hippocampus and no discernible phenotype (Frank, 2021). Thus, more effective knockout or knockdown strategies must be used to circumvent developmental compensation while fully abolishing protein function.

Cell-type-specific conditional KO mice could be used to test the hypothesis that a relative increase in inhibitory transmission from perisomatically targeting CCK interneurons and a relative decrease in inhibitory transmission from dendritically targeting SOM interneurons leads to an increase in network inhibition while also increasing the intrinsic excitability of Nlgn3 KO mice, as suggested in **Manuscript 2**.

In order to reconcile our finding of a lack of an IPSC deficit in the Nlgn4-deficient OTCs with the previous finding of an IPSC deficit in acute slices from Nlgn4 KO mice (Hammer et al., 2015), it would be necessary to measure IPSCs in CA3 pyramidal cells in OTCs. Corroborating

the findings from the acute slices would indicate that the lack of an impairment in inhibitory transmission in granule cells is due to a region-specific difference in Nlgn4 function, rather than an artefact caused by the experimental preparations.

Finally, it would be of particular interest to test the hypothesis that restoring E-I balance, for instance with selective sodium channel agonists (Osteen et al., 2017), in Nbea$^{+/-}$ and Nlgn4 KO mice might alleviate the behavioral abnormalities in these ASD models.

# Bibliography


Abraham, W. C. and McNaughton, N. (1984). "Differences in Synaptic Transmission Between Medial and Lateral Components of the Perforant Path". *Brain Research*, 303: 251–260.

Abrahams, B. S. et al. (2013). "SFARI Gene 2.0: A community-driven knowledgebase for the autism spectrum disorders (ASDs)". *Molecular Autism*, 4 (36).

Alvares, G. A., Quintana, D. S., and Whitehouse, A. J. (2017). "Beyond the hype and hope: Critical considerations for intranasal oxytocin research in autism spectrum disorder". *Autism Research*, 10: 25–41.

Amaral, D. and Lavenex, P. (2007). "Hippocampal Neuroanatomy". In: *The Hippocampus Book*. Ed. by P. Andersen, R. Morris, D. Amaral, T. Bliss, and J. O'Keefe. 1st ed. New York: Oxford University Press, pp. 37–110.

Amaral, D. G., Scharfman, H. E., and Lavenex, P. (2007). "The dentate gyrus: fundamental neuroanatomical organization (dentate gyrus for dummies)". *Progress in Brain Research*, 163: 3–22.

American Psychiatric Association (2013). Diagnostic and Statistical Manual of Mental Disorders. 5th ed. Washington, DC: American Psychiatric Association.

Andersen, P., Sundberg, S. H., Sveen, O., Swann, J. W., and Wigström, H. (1980). "Possible mechanisms for long-lasting potentiation of synaptic transmission in hippocampal slices from guinea-pigs". *The Journal of Physiology*, 302: 463–482.

Antshel, K. M. and Russo, N. (2019). "Autism Spectrum Disorders and ADHD: Overlapping Phenomenology, Diagnostic Issues, and Treatment Considerations". *Current Psychiatry Reports*, 21: 34.

Artinian, J., Peret, A., Marti, G., Epsztein, J., and Crépel, V. (2011). "Synaptic kainate receptors in interplay with INaP shift the sparse firing of dentate granule cells to a sustained rhythmic mode in temporal lobe epilepsy". *The Journal of Neuroscience*, 31 (30): 10811–10818.

Aylward, E. H. et al. (1999). "MRI volumes of amygdala and hippocampus in non-mentally retarded autistic adolescents and adults". *Neurology*, 53: 2145–2150.

Bader, P. L. et al. (2011). "Mouse model of Timothy syndrome recapitulates triad of autistic traits". *Proceedings of the National Academy of Sciences of the United States of America*, 108 (37): 15432–15437.

Banerjee-Basu, S. and Packer, A. (2010). "SFARI Gene: an evolving database for the autism research community". *DMM Disease Models and Mechanisms*, 3: 133–135.

Bariselli, S. et al. (2018). "Role of VTA dopamine neurons and neuroligin 3 in sociability traits related to nonfamiliar conspecific interaction". *Nature Communications*, 9 (3173).

Baudouin, S. J. et al. (2012). "Shared Synaptic Pathophysiology in Syndromic and Nonsyndromic Rodent Models of Autism". *Science*, 338 (6103): 128–132.

Bauman, M. D. and Schumann, C. M. (2018). "Advances in nonhuman primate models of autism: Integrating neuroscience and behavior". *Experimental Neurology*, 299: 252–265.

Bemben, M. A. et al. (2019). "Isoform-specific cleavage of neuroligin-3 reduces synapse strength". *Molecular Psychiatry*, 24: 145–160.

Bernaerts, S., Boets, B., Steyaert, J., Wenderoth, N., and Alaerts, K. (2020). "Oxytocin treatment attenuates amygdala activity in autism: a treatment-mechanism study with long-term follow-up". *Translational Psychiatry*, 10: 383.

Blümcke, I. et al. (2009). "Towards a clinico-pathological classification of granule cell dispersion in human mesial temporal lobe epilepsies". *Acta Neuropathologica*, 117: 535–544.

Bohm, H. V., Stewart, M. G., and Healy, A. M. (2013). "On the Autistic Spectrum Disorder concordance rates of twins and non-twin siblings". *Medical Hypotheses*, 81: 789–791.

Bolliger, M. F. et al. (2008). "Unusually rapid evolution of Neuroligin-4 in mice". *Proceedings of the National Academy of Sciences of the United States of America*, 105 (17): 6421–6426.

Bölte, S., Girdler, S., and Marschik, P. B. (2019). "The contribution of environmental exposure to the etiology of autism spectrum disorder". *Cellular and Molecular Life Sciences*, 76: 1275–1297.

Boucard, A. A., Chubykin, A. A., Comoletti, D., Taylor, P., and Südhof, T. C. (2005). "A splice code for trans-synaptic cell adhesion mediated by binding of neuroligin 1 to $\alpha$- and $\beta$-neurexins". *Neuron*, 48: 229–236.

Boulin, T. et al. (2021). "Functional analysis of a de novo variant in the neurodevelopment and generalized epilepsy disease gene NBEA". *Molecular Genetics and Metabolism*, 134: 195–202.

Bourgeron, T. (2009). "A synaptic trek to autism". *Current Opinion in Neurobiology*, 19: 231–234.

Bourgeron, T. (2015). "From the genetic architecture to synaptic plasticity in autism spectrum disorder". *Nature Reviews Neuroscience*, 16: 551–563.

Bowling, K. M. et al. (2017). "Genomic diagnosis for children with intellectual disability and/or developmental delay". *Genome Medicine*, 9: 43.

Braver, T. S. (2012). "The variable nature of cognitive control: A dual mechanisms framework". *Trends in Cognitive Sciences*, 16 (2): 106–113.

Breton, J. D. and Stuart, G. J. (2009). "Loss of sensory input increases the intrinsic excitability of layer 5 pyramidal neurons in rat barrel cortex". *The Journal of Physiology*, 587: 5107–5119.

Bromley, R. L. et al. (2013). "The prevalence of neurodevelopmental disorders in children prenatally exposed to antiepileptic drugs". *Journal of Neurology, Neurosurgery and Psychiatry*, 84: 637–643.

Bronzino, J. D., Abu-Hasaballah, K., Austin-LaFrance, R. J., and Morgane, P. J. (1994). "Maturation of long-term potentiation in the hippocampal dentate gyrus of the freely moving rat". *Hippocampus*, 4 (4): 439–446.

Buckmaster, P. S. and Schwartzkroin, P. A. (1995). "Interneurons and inhibition in the dentate gyrus of the rat in vivo". *The Journal of Neuroscience*, 15 (1): 774–789.

Budreck, E. C. and Scheiffele, P. (2007). "Neuroligin-3 is a neuronal adhesion protein at GABAergic and glutamatergic synapses". *European Journal of Neuroscience*, 26: 1738–1748.

Buzsáki, G. and Czéh, G. (1981). "Commissural and perforant path interactions in the rat hippocampus - Field potentials and unitary activity". *Experimental Brain Research*, 43: 429–438.

Buzsáki, G. and Eidelberg, E. (1981). "Commissural projection to the dentate gyrus of the rat: evidence for feed-forward inhibition". *Brain Research*, 230: 346–350.

Buzsáki, G. and Moser, E. I. (2013). "Memory, navigation and theta rhythm in the hippocampal-entorhinal system". *Nature Neuroscience*, 16 (2): 130–138.

Campanac, E., Daoudal, G., Ankri, N., and Debanne, D. (2008). "Downregulation of dendritic Ih in CA1 pyramidal neurons after LTP". *The Journal of Neuroscience*, 28 (34): 8635–8643.

Campisi, L., Imran, N., Nazeer, A., Skokauskas, N., and Azeem, M. W. (2018). "Autism spectrum disorder". *British Medical Bulletin*, 127: 91–100.

Castermans, D. et al. (2003). "The neurobeachin gene is disrupted by a translocation in a patient with idiopathic autism". *Journal of Medical Genetics*, 40: 352–356.

Castermans, D. et al. (2010). "SCAMP5, NBEA and AMISYN: Three candidate genes for autism involved in secretion of large dense-core vesicles". *Human Molecular Genetics*, 19 (7): 1368–1378.

Cayco-Gajic, N. A. and Silver, R. A. (2019). "Re-evaluating Circuit Mechanisms Underlying Pattern Separation". *Neuron*, 101: 584–602.

Chadman, K. K., Fernandes, S., DiLiberto, E., and Feingold, R. (2019). "Do animal models hold value in Autism spectrum disorder (ASD) drug discovery?" *Expert Opinion on Drug Discovery*, 14 (8): 727–734.

Chadman, K. K., Yang, M., and Crawley, J. N. (2009). "Criteria for validating mouse models of psychiatric diseases". *American Journal of Medical Genetics, Part B: Neuropsychiatric Genetics*, 150B: 1–11.

Chadman, K. K. et al. (2008). "Minimal aberrant behavioral phenotypes of neuroligin-3 R451C knockin mice". *Autism Research*, 1: 147–158.

Chanda, S., Aoto, J., Lee, S. J., Wernig, M., and Südhof, T. C. (2016). "Pathogenic mechanism of an autism-associated neuroligin mutation involves altered AMPA-receptor trafficking". *Molecular Psychiatry*, 21: 169–177.

Chawla, M. K. et al. (2005). "Sparse, environmentally selective expression of Arc RNA in the upper blade of the rodent fascia dentata by brief spatial experience". *Hippocampus*, 15: 579–586.

Cheng, C. H., Chan, P. Y. S., Hsu, S. C., and Liu, C. Y. (2018). "Meta-analysis of sensorimotor gating in patients with autism spectrum disorders". *Psychiatry Research*, 262: 413–419.

Chez, M. G. et al. (2006). "Frequency of epileptiform EEG abnormalities in a sequential screening of autistic patients with no known clinical epilepsy from 1996 to 2005". *Epilepsy and Behavior*, 8: 267–271.

Chih, B., Engelman, H., and Scheiffele, P. (2005). "Control of Excitatory and Inhibitory Synapse Formation by Neuroligins". *Science*, 307 (5713): 1324–1328.

Chisholm, K., Lin, A., Abu-Akel, A., and Wood, S. J. (2015). "The association between autism and schizophrenia spectrum disorders: A review of eight alternate models of co-occurrence". *Neuroscience and Biobehavioral Reviews*, 55: 173–183.

Cooke, S. F. et al. (2006). "Autophosphorylation of $\alpha$CaMKII is not a general requirement for NMDA receptor-dependent LTP in the adult mouse." *The Journal of Physiology*, 574: 805–818.

Coulter, D. A. and Carlson, G. C. (2007). "Functional regulation of the dentate gyrus by GABA-mediated inhibition". *Progress in Brain Research*, 163: 235–244.

Courchesne, E., Campbell, K., and Solso, S. (2011). "Brain growth across the life span in autism: Age-specific changes in anatomical pathology". *Brain Research*, 1380: 138–145.

Crusio, W. E. (2015). "Key issues in contemporary behavioral genetics". *Current Opinion in Behavioral Sciences*, 2: 89–95.

Cullinane, A. R., Schäffer, A. A., and Huizing, M. (2013). "The BEACH Is Hot: A LYST of Emerging Roles for BEACH-Domain Containing Proteins in Human Disease". *Traffic*, 14: 749–766.

De Rubeis, S. et al. (2014). "Synaptic, transcriptional and chromatin genes disrupted in autism". *Nature*, 515: 209–215.

De Smet, H. J., Paquier, P., Verhoeven, J., and Mariën, P. (2013). "The cerebellum: Its role in language and related cognitive and affective functions". *Brain and Language*, 127 (3): 334–342.

Debanne, D., Inglebert, Y., and Russier, M. (2019). "Plasticity of intrinsic neuronal excitability". *Current Opinion in Neurobiology*, 54: 73–82.

Degroote, S., Hunting, D., and Takser, L. (2017). "Improved assessment of sensorimotor gating in animal models relevant to ASD: A data modelling approach to quantify PrePulse Inhibition of the acoustic startle reflex". *Journal of Neuroscience Methods*, 276: 13–22.

Delattre, V., La Mendola, D., Meystre, J., Markram, H., and Markram, K. (2013). "Nlgn4 knockout induces network hypo-excitability in juvenile mouse somatosensory cortex in vitro". *Scientific Reports*, 3: 2897.

Deliu, E. et al. (2018). "Haploinsufficiency of the intellectual disability gene SETD5 disturbs developmental gene expression and cognition". *Nature Neuroscience*, 21: 1717–1727.

Desai, N. S., Rutherford, L. C., and Turrigiano, G. G. (1999). "Plasticity in the intrinsic excitability of cortical pyramidal neurons". *Nature Neuroscience*, 2 (6): 515–520.

Dimoka, A., Courellis, S. H., Marmarelis, V. Z., and Berger, T. W. (2008). "Modeling the nonlinear dynamic interactions of afferent pathways in the dentate gyrus of the hippocampus". *Annals of Biomedical Engineering*, 36 (5): 852–864.

Elsabbagh, M. et al. (2012). "Global Prevalence of Autism and Other Pervasive Developmental Disorders". *Autism Research*, 5: 160–179.

Erwin, S. R. et al. (2020). "A Sparse, Spatially Biased Subtype of Mature Granule Cell Dominates Recruitment in Hippocampal-Associated Behaviors". *Cell Reports*, 31: 107551.

Etherton, M. R. et al. (2011). "Autism-linked neuroligin-3 R451C mutation differentially alters hippocampal and cortical synaptic function". *Proceedings of the National Academy of Sciences of the United States of America*, 108 (33): 13764–13769.

Ey, E. et al. (2012). "Absence of deficits in social behaviors and ultrasonic vocalizations in later generations of mice lacking neuroligin4". *Genes, Brain and Behavior*, 11: 928–941.

Fantie, B. D. and Goddard, G. V. (1982). "Septal modulation of the population spike in the fascia dentata produced by perforant path stimulation in the rat". *Brain Research*, 252: 227–237.

Farzana, F. et al. (2016). "Neurobeachin Regulates Glutamate- and GABA-Receptor Targeting to Synapses via Distinct Pathways". *Molecular Neurobiology*, 53: 2112–2123.

Fatemi, S. H. et al. (2012). "Consensus paper: Pathological role of the cerebellum in Autism". *Cerebellum*, 11: 777–807.

Fernández-Ruiz, A. et al. (2013). "Cytoarchitectonic and dynamic origins of giant positive local field potentials in the dentate gyrus." *The Journal of Neuroscience*, 33 (39): 15518–32.

Földy, C., Malenka, R. C., and Südhof, T. C. (2013). "Autism-associated neuroligin-3 mutations commonly disrupt tonic endocannabinoid signaling". *Neuron*, 78: 498–509.

Foster, J. D., Kitchen, I., Bettler, B., and Chen, Y. (2013). "GABAB receptor subtypes differentially modulate synaptic inhibition in the dentate gyrus to enhance granule cell output". *British Journal of Pharmacology*, 168: 1808–1819.

Frank, F. (2021). Die Konsequenzen der zeitspezifischen Deletion von Neuroligin 2 für die synaptische Übertragung, Plastizität und neuronale Exzitabilität im Gyrus Dentatus von adulten Mäusen. Doctoral thesis. Johann Wolfgang Goethe-Universität.

Frick, A., Magee, J., and Johnston, D. (2004). "LTP is accompanied by an enhanced local excitability of pyramidal neuron dendrites". *Nature Neuroscience*, 7 (2): 126–135.

Futai, K., Doty, C. D., Baek, B., Ryu, J., and Sheng, M. (2013). "Specific Trans-synaptic interaction with inhibitory interneuronal neurexin underlies differential ability of neuroligins to induce functional inhibitory synapses". *The Journal of Neuroscience*, 33 (8): 3612–3623.

Gall, D. and Dupont, G. (2020). "Tonic activation of extrasynaptic NMDA receptors decreases intrinsic excitability and promotes bistability in a model of neuronal activity". *International Journal of Molecular Sciences*, 21: 206.

Gallitano, A. L., Satvat, E., Gil, M., and Marrone, D. F. (2016). "Distinct dendritic morphology across the blades of the rodent dentate gyrus". *Synapse*, 70 (7): 277–282.

Gatford, N. J. F. et al. (2021). "Neuroligin-3 and Neuroligin-4X form Nanoscopic clusters and regulate growth cone organization and size". *Human Molecular Genetics*, ddab277.

Gaugler, T. et al. (2014). "Most genetic risk for autism resides with common variation". *Nature Genetics*, 46 (8): 881–885.

Gilman, S. R. et al. (2011). "Rare De Novo Variants Associated with Autism Implicate a Large Functional Network of Genes Involved in Formation and Function of Synapses". *Neuron*, 70: 898–907.

Goubau, C., Buyse, G. M., Di Michele, M., Van Geet, C., and Freson, K. (2013). "Regulated granule trafficking in platelets and neurons: A common molecular machinery". *European Journal of Paediatric Neurology*, 17: 117–125.

Gromova, K. V. et al. (2018). "Neurobeachin and the Kinesin KIF21B Are Critical for Endocytic Recycling of NMDA Receptors and Regulate Social Behavior". *Cell Reports*, 23 (9): 2705–2717.

Grubb, M. S. and Burrone, J. (2010). "Activity-dependent relocation of the axon initial segment fine-tunes neuronal excitability". *Nature*, 465: 1070–1074.

Grzadzinski, R., Huerta, M., and Lord, C. (2013). "DSM-5 and autism spectrum disorders (ASDs): an opportunity for identifying ASD subtypes". *Molecular Autism*, 4: 12.

Hamilton, S. M. et al. (2014). "Fmr1 and Nlgn3 knockout rats: Novel tools for investigating autism spectrum disorders". *Behavioral Neuroscience*, 128 (2): 103–109.

Hammer, M. et al. (2015). "Perturbed Hippocampal Synaptic Inhibition and $\gamma$-Oscillations in a Neuroligin-4 Knockout Mouse Model of Autism". *Cell Reports*, 13: 516–523.

Hara, K. and Harris, R. (2002). "The anesthetic mechanism of urethane: the effects on neurotransmitter-gated ion channels". *Anesthesia and Analgesia*, 94: 313–318.

Hashimotodani, Y., Karube, F., Yanagawa, Y., Fujiyama, F., and Kano, M. (2018). "Supramammillary Nucleus Afferents to the Dentate Gyrus Co-release Glutamate and GABA and Potentiate Granule Cell Output". *Cell Reports*, 25: 2704–2715.

He, H. Y. and Cline, H. T. (2019). "What Is Excitation/Inhibition and How Is It Regulated? A Case of the Elephant and the Wisemen". *Journal of Experimental Neuroscience*, 13: 10–12.

Heimrich, B. and Frotscher, M. (1991). "Differentiation of dentate granule cells in slice cultures of rat hippocampus: a Golgi/electron microscopic study". *Brain Research*, 538: 263–268.

Hjorth-Simonsen, A. (1972). "Projection of the lateral part of the entorhinal area to the hippocampus and fascia dentata". *Journal of Comparative Neurology*, 146: 219–231.

Holingue, C., Newill, C., Lee, L. C., Pasricha, P. J., and Daniele Fallin, M. (2018). "Gastrointestinal symptoms in autism spectrum disorder: A review of the literature on ascertainment and prevalence". *Autism Research*, 11: 24–36.

Hoon, M. et al. (2011). "Neuroligin-4 is localized to glycinergic postsynapses and regulates inhibition in the retina". *Proceedings of the National Academy of Sciences of the United States of America*, 108 (7): 3053–3058.

Hoon, M., Krishnamoorthy, V., Gollisch, T., Falkenburger, B., and Varoqueaux, F. (2017). "Loss of Neuroligin3 specifically downregulates retinal GABAA$\alpha$2 receptors without abolishing direction selectivity". *PLoS ONE*, 12 (7): e0181011.

Horn, M. E. and Nicoll, R. A. (2018). "Somatostatin and parvalbumin inhibitory synapses onto hippocampal pyramidal neurons are regulated by distinct mechanisms". *Proceedings of the National Academy of Sciences of the United States of America*, 115 (3): 589–594.

Hörnberg, H. et al. (2020). "Rescue of oxytocin response and social behaviour in a mouse model of autism". *Nature*, 584: 252–256.

Howes, O. D. et al. (2018). "Autism spectrum disorder: Consensus guidelines on assessment, treatment and research from the British Association for Psychopharmacology". *Journal of Psychopharmacology*, 32 (1): 3–29.

Hsu, T. T., Lee, C. T., Tai, M. H., and Lien, C. C. (2016). "Differential Recruitment of Dentate Gyrus Interneuron Types by Commissural Versus Perforant Pathways". *Cerebral Cortex*, 26: 2715–2727.

Hultman, C. M., Sandin, S., Levine, S. Z., Lichtenstein, P., and Reichenberg, A. (2011). "Advancing paternal age and risk of autism: New evidence from a population-based study and a meta-analysis of epidemiological studies". *Molecular Psychiatry*, 16: 1203–1212.

Iossifov, I. et al. (2014). "The contribution of de novo coding mutations to autism spectrum disorder". *Nature*, 515: 216–221.

Iossifov, I. et al. (2015). "Low load for disruptive mutations in autism genes and their biased transmission". *Proceedings of the National Academy of Sciences of the United States of America*, 112 (41): E5600–E5607.

Izquierdo, A., Brigman, J. L., Radke, A. K., Rudebeck, P. H., and Holmes, A. (2017). "The neural basis of reversal learning: An updated perspective". *Neuroscience*, 345: 12–26.

Jamain, S. et al. (2003). "Mutations of the X-linked genes encoding neuroligins NLGN3 and NLGN4 are associated with autism". *Nature Genetics*, 34: 27–29.

Jamain, S. et al. (2008). "Reduced social interaction and ultrasonic communication in a mouse model of monogenic heritable autism". *Proceedings of the National Academy of Sciences of the United States of America*, 105 (5): 1710–1715.

Jaramillo, T. C., Liu, S., Pettersen, A., Birnbaum, S. G., and Powell, C. M. (2014). "Autism-Related Neuroligin-3 Mutation Alters Social Behavior and Spatial Learning". *Autism Research*, 7: 264–272.

Jaramillo, T. C. et al. (2018). "Genetic background effects in Neuroligin-3 mutant mice: Minimal behavioral abnormalities on C57 background". *Autism Research*, 11: 234–244.

Jedlicka, P., Deller, T., and Schwarzacher, S. W. (2010). "Computational modeling of GABAA receptor-mediated paired-pulse inhibition in the dentate gyrus". *Journal of Computational Neuroscience*, 29: 509–519.

Jedlicka, P., Muellerleile, J., and Schwarzacher, S. W. (2018). "Synaptic Plasticity and Excitation-Inhibition Balance in the Dentate Gyrus: Insights from in Vivo Recordings in Neuroligin-1, Neuroligin-2, and Collybistin Knockouts". *Neural Plasticity*, 2018: Article ID 6015753.

Jedlicka, P. et al. (2009). "Impairment of in vivo theta-burst long-term potentiation and network excitability in the dentate gyrus of synaptopodin-deficient mice lacking the spine apparatus and the cisternal organelle". *Hippocampus*, 19: 130–140.

Jedlicka, P. et al. (2011). "Increased dentate gyrus excitability in neuroligin-2-deficient mice in vivo". *Cerebral Cortex*, 21: 357–367.

Jedlicka, P. et al. (2015). "Neuroligin-1 regulates excitatory synaptic transmission, LTP and EPSP-spike coupling in the dentate gyrus in vivo". *Brain Structure and Function*, 220: 47–58.

Ju, A. et al. (2014). "Juvenile manifestation of ultrasound communication deficits in the neuroligin-4 null mutant mouse model of autism". *Behavioural Brain Research*, 270: 159–164.

Kafkafi, N. et al. (2018). "Reproducibility and replicability of rodent phenotyping in preclinical studies". *Neuroscience and Biobehavioral Reviews*, 87: 218–232.

Kanner, L. (1943). "Autistic Disturbances of Affective Contact". *Nervous Child*, 2: 217–250.

Kazdoba, T. M. et al. (2016). "Translational Mouse Models of Autism: Advancing Toward Pharmacological Therapeutics". *Current Topics in Behavioral Neuroscience*, 28: 1–52.

Keller, R., Basta, R., Salerno, L., and Elia, M. (2017). "Autism, epilepsy, and synaptopathies: a not rare association". *Neurological Sciences*, 38: 1353–1361.

Kleschevnikov, A. M. and Marchbanks, R. M. (1993). "Behavioral parameters of the spatial memory correlate with the potentiation of the population spike, but not with the population excitatory postsynaptic potential, of the CA1 region in rat hippocampal slices". *Neuroscience Letters*, 152: 125–128.

Knierim, J. J., Neunuebel, J. P., and Deshmukh, S. S. (2014). "Functional correlates of the lateral and medial entorhinal cortex: Objects, path integration and local - Global reference frames". *Philosophical Transactions of the Royal Society B: Biological Sciences*, 369: 20130369.

Koehnke, J. et al. (2010). "Splice form dependence of $\beta$-neurexin/neuroligin binding interactions". *Neuron*, 67: 61–74.

El-Kordi, A. et al. (2013). "Development of an autism severity score for mice using Nlgn4 null mutants as a construct-valid model of heritable monogenic autism". *Behavioural Brain Research*, 251: 41–49.

Krishnan, A. et al. (2016). "Genome-wide prediction and functional characterization of the genetic basis of autism spectrum disorder". *Nature Neuroscience*, 19 (11): 1454–1462.

Krook-Magnuson, E. et al. (2015). "In vivo evaluation of the dentate gate theory in epilepsy". *The Journal of Physiology*, 593: 2379–2388.

Krueger-Burg, D. et al. (2016). "The sociobox: A novel paradigm to assess complex social recognition in male mice". *Frontiers in Behavioral Neuroscience*, 10: 151.

Lai, E. S. K. et al. (2021). "An Autism-Associated Neuroligin-3 Mutation Affects Developmental Synapse Elimination in the Cerebellum". *Frontiers in Neural Circuits*, 15: 676891.

Lai, M. C. et al. (2019). "Prevalence of co-occurring mental health diagnoses in the autism population: a systematic review and meta-analysis". *The Lancet Psychiatry*, 6 (10): 819–829.

Langeberg, L. K. and Scott, J. D. (2005). "A-kinase-anchoring proteins". *Journal of Cell Science*, 118: 3217–3220.

Laumonnier, F. et al. (2004). "X-Linked Mental Retardation and Autism Are Associated with a Mutation in the NLGN4 Gene, a Member of the Neuroligin Family". *American Journal of Human Genetics*, 74: 552–557.

Lee, B. et al. (2018). "The Possible Role of Neurobeachin in Extinction of Contextual Fear Memory". *Scientific Reports*, 8: 13752.

Lee, E., Lee, J., and Kim, E. (2017). "Excitation/Inhibition Imbalance in Animal Models of Autism Spectrum Disorders". *Biological Psychiatry*, 81: 838–847.

Leembruggen, A. J. et al. (2020). "Colonic dilation and altered ex vivo gastrointestinal motility in the neuroligin-3 knockout mouse". *Autism Research*, 13: 691–701.

Leranth, C. and Hajszan, T. (2007). "Extrinsic afferent systems to the dentate gyrus". *Progress in Brain Research*, 163: 63–85.

Lin, L., Sun, W., Wikenheiser, A. M., Kung, F., and Hoffman, D. A. (2010). "KChIP4a regulates Kv4.2 channel trafficking through PKA phosphorylation". *Molecular and Cellular Neuroscience*, 43: 315–325.

Lisman, J., Cooper, K., Sehgal, M., and Silva, A. J. (2018). "Memory formation depends on both synapse-specific modifications of synaptic strength and cell-specific increases in excitability". *Nature Neuroscience*, 21: 309–314.

Lømo, T. (1971). "Patterns of activation in a monosynaptic cortical pathway: the perforant path input to the dentate area of the hippocampal formation." *Experimental Brain Research*, 12: 18–45.

Loomes, R., Hull, L., and Mandy, W. P. L. (2017). "What Is the Male-to-Female Ratio in Autism Spectrum Disorder? A Systematic Review and Meta-Analysis". *Journal of the American Academy of Child and Adolescent Psychiatry*, 56 (6): 466–474.

Lord, C., Elsabbagh, M., Baird, G., and Veenstra-Vanderweele, J. (2018). "Autism spectrum disorder". *The Lancet*, 392: 508–520.

Losonczy, A., Makara, J. K., and Magee, J. C. (2008). "Compartmentalized dendritic plasticity and input feature storage in neurons". *Nature*, 452: 436–441.

Mahfouz, A., Ziats, M. N., Rennert, O. M., Lelieveldt, B. P., and Reinders, M. J. (2015). "Shared Pathways Among Autism Candidate Genes Determined by Co-expression Network Analysis of the Developing Human Brain Transcriptome". *Journal of Molecular Neuroscience*, 57: 580–594.

Maier, S. et al. (2015). "Increased hippocampal volumes in adults with high functioning autism spectrum disorder and an IQ greater than 100: A manual morphometric study". *Psychiatry Research - Neuroimaging*, 234: 152–155.

Marro, S. G. et al. (2019). "Neuroligin-4 Regulates Excitatory Synaptic Transmission in Human Neurons". *Neuron*, 103: 617–626.

Martinello, K. et al. (2015). "Cholinergic afferent stimulation induces axonal function plasticity in adult hippocampal granule cells". *Neuron*, 85: 346–363.

Mastrovito, D., Hanson, C., and Hanson, S. J. (2018). "Differences in atypical resting-state effective connectivity distinguish autism from schizophrenia". *NeuroImage: Clinical*, 18: 367–376.

Maxeiner, S. et al. (2020). "Evolution of the Autism-Associated Neuroligin-4 Gene Reveals Broad Erosion of Pseudoautosomal Regions in Rodents". *Molecular Biology and Evolution*, 37 (5): 1243–1258.

McElhanon, B. O., McCracken, C., Karpen, S., and Sharp, W. G. (2014). "Gastrointestinal symptoms in autism spectrum disorder: A meta-analysis". *Pediatrics*, 133: 872–883.

McKavanagh, R., Buckley, E., and Chance, S. A. (2015). "Wider minicolumns in autism: A neural basis for altered processing?" *Brain*, 138: 2034–2045.

Medrihan, L. et al. (2009). "Neurobeachin, a protein implicated in membrane protein traffic and autism, is required for the formation and functioning of central synapses". *The Journal of Physiology*, 587: 5095–5106.

Mellor, J., Nicoll, R. A., and Schmitz, D. (2002). "Mediation of hippocampal mossy fiber long-term potentiation by presynaptic Ih channels". *Science*, 295: 143–147.

Mishra, P. and Narayanan, R. (2020). "Heterogeneities in intrinsic excitability and frequency-dependent response properties of granule cells across the blades of the rat dentate gyrus". *Journal of Neurophysiology*, 123: 755–772.

Mizumori, S. J., McNaughton, B. L., and Barnes, C. A. (1989). "A comparison of supramammillary and medial septal influences on hippocampal field potentials and single-unit activity". *Journal of Neurophysiology*, 61 (1): 15–31.

Modabbernia, A., Velthorst, E., and Reichenberg, A. (2017). "Environmental risk factors for autism: an evidence-based review of systematic reviews and meta-analyses". *Molecular Autism*, 8: 13.

Modi, B. et al. (2019). "Possible Implication of the CA2 Hippocampal Circuit in Social Cognition Deficits Observed in the Neuroligin 3 Knock-Out Mouse, a Non-Syndromic Animal Model of Autism". *Frontiers in Psychiatry*, 10: 513.

Möhrle, D. et al. (2020). "What we can learn from a genetic rodent model about autism". *Neuroscience and Biobehavioral Reviews*, 109: 29–53.

Mosconi, M. W. et al. (2009). "Longitudinal study of amygdala volume and joint attention in 2- to 4-year-old children with autism". *Archives of General Psychiatry*, 66 (5): 509–516.

Moy, S. S. et al. (2004). "Sociability and preference for social novelty in five inbred strains: An approach to assess autistic-like behavior in mice". *Genes, Brain and Behavior*, 3: 287–302.

Mulhern, M. S. et al. (2018). "NBEA: Developmental disease gene with early generalized epilepsy phenotypes". *Annals of Neurology*, 84: 788–795.

Nair, R. et al. (2013). "Neurobeachin regulates neurotransmitter receptor trafficking to synapses". *Journal of Cell Biology*, 200 (1): 61–80.

Nakanishi, K., Saito, H., and Abe, K. (2001). "The supramammillary nucleus contributes to associative EPSP-spike potentiation in the rat dentate gyrus in vivo". *European Journal of Neuroscience*, 13: 793–800.

Nakanishi, M., Anderson, M. P., and Takumi, T. (2019). "Recent genetic and functional insights in autism spectrum disorder". *Current Opinion in Neurology*, 32: 627–634.

Nardello, R. et al. (2021). "A paradigmatic autistic phenotype associated with loss of PCDH11Y and NLGN4Y genes". *BMC Medical Genomics*, 14: 198.

Nelson, A. B., Gittis, A. H., and Du Lac, S. (2005). "Decreases in CaMKII activity trigger persistent potentiation of intrinsic excitability in spontaneously firing vestibular nucleus neurons". *Neuron*, 46: 623–631.

Nelson, S. B. and Valakh, V. (2015). "Excitatory/Inhibitory Balance and Circuit Homeostasis in Autism Spectrum Disorders". *Neuron*, 87: 684–698.

Nguyen, T. A., Lehr, A. W., and Roche, K. W. (2020). "Neuroligins and Neurodevelopmental Disorders: X-Linked Genetics". *Frontiers in Synaptic Neuroscience*, 12: 33.

Nguyen, T. A. et al. (2020). "A Cluster of Autism-Associated Variants on X-Linked NLGN4X Functionally Resemble NLGN4Y". *Neuron*, 106: 759–768.

Niesmann, K. et al. (2011). "Dendritic spine formation and synaptic function require neurobeachin". *Nature Communications*, 2: 510–557.

Norris, R. H., Churilov, L., Hannan, A. J., and Nithianantharajah, J. (2019). "Mutations in neuroligin-3 in male mice impact behavioral flexibility but not relational memory in a touchscreen test of visual transitive inference". *Molecular Autism*, 10: 42.

Nuytens, K. et al. (2013). "Haploinsufficiency of the autism candidate gene Neurobeachin induces autism-like behaviors and affects cellular and molecular processes of synaptic plasticity in mice". *Neurobiology of Disease*, 51: 144–151.

Nygaard, K. R., Maloney, S. E., and Dougherty, J. D. (2019). "Erroneous inference based on a lack of preference within one group: Autism, mice, and the social approach task". *Autism Research*, 12: 1171–1183.

Odent, P., Creemers, J. W., Bosmans, G., and D'Hooge, R. (2021). "Spectrum of social alterations in the Neurobeachin haploinsufficiency mouse model of autism". *Brain Research Bulletin*, 167: 11–21.

Oku, S. et al. (2020). "Alternative splicing at neuroligin site A regulates glycan interaction and synaptogenic activity". *eLife*, 9: 1–26.

Okun, M. and Lampl, I. (2009). "Balance of excitation and inhibition". *Scholarpedia*, 4 (8): 7467.

Osteen, J. D., Sampson, K., Iyer, V., Julius, D., and Bosmans, F. (2017). "Pharmacology of the Nav1.1 domain IV voltage sensor reveals coupling between inactivation gating processes". *Proceedings of the National Academy of Sciences of the United States of America*, 114 (26): 6836–6841.

Pan, P. Y., Bölte, S., Kaur, P., Jamil, S., and Jonsson, U. (2021). "Neurological disorders in autism: A systematic review and meta-analysis". *Autism*, 25 (3): 812–830.

Polepalli, J. S. et al. (2017). "Modulation of excitation on parvalbumin interneurons by neuroligin-3 regulates the hippocampal network". *Nature Neuroscience*, 20 (2): 219–229.

Port, R. G., Oberman, L. M., and Roberts, T. P. (2019). "Revisiting the excitation / inhibition imbalance hypothesis of ASD through a clinical lens". *The British Journal of Radiology*, 92: 20180944.

Posar, A. and Visconti, P. (2018). "Sensory abnormalities in children with autism spectrum disorder". *Jornal de Pediatria*, 94 (4): 342–350.

Poulopoulos, A. et al. (2012). "Homodimerization and isoform-specific heterodimerization of neuroligins". *Biochemical Journal*, 446: 321–330.

Prelich, G. (2012). "Gene overexpression: Uses, mechanisms, and interpretation". *Genetics*, 190: 841–854.

Premoli, M. et al. (2021). "Automatic classification of mice vocalizations using Machine Learning techniques and Convolutional Neural Networks". *PLoS ONE*, 16 (1): e0244636.

Puleo, C. M., Reichenberg, A., Smith, C. J., Kryzak, L. A., and Silverman, J. M. (2008). "Do autism-related personality traits explain higher paternal age in autism?" *Molecular Psychiatry*, 13: 243–244.

Radyushkin, K. et al. (2009). "Neuroligin-3-deficient mice: Model of a monogenic heritable form of autism with an olfactory deficit". *Genes, Brain and Behavior*, 8: 416–425.

Reddy, K. S. (2005). "Cytogenetic abnormalities and fragile-x syndrome in Autism Spectrum Disorder". *BMC Medical Genetics*, 6: 1–16.

Rein, B., Ma, K., and Yan, Z. (2020). "A standardized social preference protocol for measuring social deficits in mouse models of autism". *Nature Protocols*, 15: 3464–3477.

Reissner, C., Klose, M., Fairless, R., and Missler, M. (2008). "Mutational analysis of the neurexin/neuroligin complex reveals essential and regulatory components". *Proceedings of the National Academy of Sciences of the United States of America*, 105 (39): 15124–15129.

Repetto, D. et al. (2018). "Molecular dissection of neurobeachin function at excitatory synapses". *Frontiers in Synaptic Neuroscience*, 10: 28.

Ritvo, E. R., Mason-Brothers, A., Menkes, J. H., and Sparkes, R. S. (June 1988). "Association of autism, retinoblastoma, and reduced esterase D activity". *Archives of General Psychiatry*, 45 (6): 600.

Robertson, C. E. and Baron-Cohen, S. (2017). "Sensory perception in autism". *Nature Reviews Neuroscience*, 18: 671–684.

Robertson, C. E., Ratai, E. M., and Kanwisher, N. (2016). "Reduced GABAergic Action in the Autistic Brain". *Current Biology*, 26: 80–85.

Rojas, D. C. et al. (2006). "Regional gray matter volumetric changes in autism associated with social and repetitive behavior symptoms". *BMC Psychiatry*, 6: 56.

Rosen, N. E., Lord, C., and Volkmar, F. R. (2021). "The Diagnosis of Autism: From Kanner to DSM-III to DSM-5 and Beyond". *Journal of Autism and Developmental Disorders*, 51: 4253–4270.

Rothwell, P. E. et al. (2014). "Autism-associated neuroligin-3 mutations commonly impair striatal circuits to boost repetitive behaviors". *Cell*, 158: 198–212.

Rubenstein, J. L. and Merzenich, M. M. (2003). "Model of autism: Increased ratio of excitation/inhibition in key neural systems". *Genes, Brain and Behavior*, 2: 255–267.

Russell, G. et al. (2019). "Selection bias on intellectual ability in autism research: A cross-sectional review and meta-analysis". *Molecular Autism*, 10: 9.

Rydzewska, E. et al. (2019). "Prevalence of sensory impairments, physical and intellectual disabilities, and mental health in children and young people with self/proxy-reported autism: Observational study of a whole country population". *Autism*, 23 (5): 1201–1209.

Sanna, E. et al. (1995). "Actions of the general anesthetic propofol on recombinant human GABA(A) receptors: Influence of receptor subunits". *Journal of Pharmacology and Experimental Therapeutics*, 274 (1): 353–360.

Savelyeva, L., Sagulenko, E., Schmitt, J. G., and Schwab, M. (2006). "The neurobeachin gene spans the common fragile site FRA13A". *Human Genetics*, 118: 551–558.

Scattoni, M. L., Gandhy, S. U., Ricceri, L., and Crawley, J. N. (2008). "Unusual repertoire of vocalizations in the BTBR T+tf/J mouse model of autism". *PLoS ONE*, 3 (8): e3067.

Scharfman, H. E., Sollas, A. L., Smith, K. L., Jackson, M. B., and Goodman, J. H. (2002). "Structural and functional asymmetry in the normal and epileptic rat dentate gyrus". *The Journal of Comparative Neurology*, 454: 424–439.

Schumann, C. M. et al. (2004). "The amygdala is enlarged in children but not adolescents with autism; the hippocampus is enlarged at all ages". *The Journal of Neuroscience*, 24 (28): 6392–6401.

Schwartz, S. P. and Coleman, P. D. (1981). "Neurons of origin of the perforant path". *Experimental Neurology*, 74: 305–312.

Servadio, M., Vanderschuren, L. J., and Trezza, V. (2015). "Modeling autism-relevant behavioral phenotypes in rats and mice: Do 'autistic' rodents exist?" *Behavioural Pharmacology*, 26: 522–540.

Silverman, J. L., Gastrell, P. T., Karras, M. N., Solomon, M., and Crawley, J. N. (2015). "Cognitive abilities on transitive inference using a novel touchscreen technology for mice". *Cerebral Cortex*, 25: 1133–1142.

Silverman, J. L., Yang, M., Lord, C., and Crawley, J. N. (2010). "Behavioural phenotyping assays for mouse models of autism". *Nature Reviews Neuroscience*, 11 (7): 490–502.

Skuse, D. H. (2007). "Rethinking the nature of genetic vulnerability to autistic spectrum disorders". *Trends in Genetics*, 23 (8): 387–395.

Sloviter, R. S. (1991). "Feedforward and feedback inhibition of hippocampal principal cell activity evoked by perforant path stimulation: GABA-mediated mechanisms that regulate excitability In Vivo". *Hippocampus*, 1 (1): 31–40.

Smith, M. et al. (2002). "Molecular genetic delineation of a deletion of chromosome 13q12→q13 in a patient with autism and auditory processing deficits". *Cytogenetic and Genome Research*, 98: 233–239.

Smith, V. and Brown, N. (2014). "Prenatal valproate exposure and risk of autism spectrum disorders and childhood autism". *Archives of Disease in Childhood: Education and Practice Edition*, 99: 198.

Sohal, V. S. and Rubenstein, J. L. (2019). "Excitation-inhibition balance as a framework for investigating mechanisms in neuropsychiatric disorders". *Molecular Psychiatry*, 24: 1248–1257.

Soler-Llavina, G. J., Fuccillo, M. V., Ko, J., Südhof, T. C., and Malenka, R. C. (2011). "The neurexin ligands, neuroligins and leucine-rich repeat transmembrane proteins, perform convergent and divergent synaptic functions in vivo". *Proceedings of the National Academy of Sciences of the United States of America*, 108 (40): 16502–16509.

Solomon, M., Frank, M. J., Smith, A. C., Ly, S., and Carter, C. S. (2011). "Transitive inference in adults with autism spectrum disorders". *Cognitive, Affective and Behavioral Neuroscience*, 11: 437–449.

Solomon, M. et al. (2015). "Atypical Learning in Autism Spectrum Disorders: A Functional Magnetic Resonance Imaging Study of Transitive Inference". *Journal of the American Academy of Child and Adolescent Psychiatry*, 54 (11): 947–955.

South, M. et al. (2015). "Overactive Pattern Separation Memory Associated with Negative Emotionality in Adults Diagnosed with Autism Spectrum Disorder". *Journal of Autism and Developmental Disorders*, 45: 3458–3467.

Stegen, M. et al. (2012). "Adaptive intrinsic plasticity in human dentate gyrus granule cells during temporal lobe epilepsy". *Cerebral Cortex*, 22: 2087–2101.

Su, Y. et al. (2004). "Neurobeachin Is Essential for Neuromuscular Synaptic Transmission". *The Journal of Neuroscience*, 24 (14): 3627–3636.

Südhof, T. C. (2017). "Synaptic Neurexin Complexes: A Molecular Code for the Logic of Neural Circuits". *Cell*, 171: 745–769.

Sussman, D. et al. (2015). "The autism puzzle: Diffuse but not pervasive neuroanatomical abnormalities in children with ASD". *NeuroImage: Clinical*, 8: 170–179.

Tabuchi, K. et al. (Oct. 2007). "A Neuroligin-3 Mutation Implicated in Autism Increases Inhibitory Synaptic Transmission in Mice". *Science*, 318 (5847): 71–76.

Taube, J. S. and Schwartzkroin, P. A. (1988). "Mechanisms of long-term potentiation: EPSP/spike dissociation, intradendritic recordings, and glutamate sensitivity". *The Journal of Neuroscience*, 8 (5): 1632–1644.

Taurines, R. et al. (2012). "ADHD and autism: Differential diagnosis or overlapping traits? A selective review". *ADHD Attention Deficit and Hyperactivity Disorders*, 4: 115–139.

Taverna, F. A. et al. (2005). "Defective place cell activity in nociceptin receptor knockout mice with elevated NMDA receptor-dependent long-term potentiation". *The Journal of Physiology*, 565: 579–591.

Thomas, A. M., Schwartz, M. D., Saxe, M. D., and Kilduff, T. S. (2017). "Sleep/wake physiology and quantitative electroencephalogram analysis of the neuroligin-3 knockout rat model of autism spectrum disorder". *Sleep*, 40 (10).

Tick, B., Bolton, P., Happé, F., Rutter, M., and Rijsdijk, F. (2016). "Heritability of autism spectrum disorders: A meta-analysis of twin studies". *Journal of Child Psychology and Psychiatry and Allied Disciplines*, 57 (5): 585–595.

Top, D. N. et al. (2016). "Atypical Amygdala Response to Fear Conditioning in Autism Spectrum Disorder". *Biological Psychiatry: Cognitive Neuroscience and Neuroimaging*, 1: 308–315.

Topál, J., Román, V., and Turcsán, B. (2019). "The dog (Canis familiaris) as a translational model of autism: It is high time we move from promise to reality". *Wiley Interdisciplinary Reviews: Cognitive Science*, 10: e1495.

Tordjman, S. et al. (2014). "Gene × environment interactions in autism spectrum disorders: Role of epigenetic mechanisms". *Frontiers in Psychiatry*, 5: 53.

Turrigiano, G. G., Leslie, K. R., Desai, N. S., Rutherford, L. C., and Nelson, S. B. (1998). "Activity-dependent scaling of quantal amplitude in neocortical neurons." *Nature*, 391: 892–896.

Uchigashima, M. et al. (2020a). "Neuroligin3 splice isoforms shape inhibitory synaptic function in the mouse hippocampus". *The Journal of Biological Chemistry*, 295 (25): 8589–8595.

Uchigashima, M. et al. (2020b). "Specific Neuroligin3-$\alpha$Neurexin1 signaling regulates GABAergic synaptic function in mouse hippocampus". *eLife*, 9: 1–31.

Unichenko, P. et al. (2017). "Autism Related Neuroligin-4 Knockout Impairs Intracortical Processing but not Sensory Inputs in Mouse Barrel Cortex". *Cerebral Cortex*: 1–14.

Varoqueaux, F. et al. (2006). "Neuroligins Determine Synapse Maturation and Function". *Neuron*, 51: 741–754.

Venkatesh, H. S. et al. (2015). "Neuronal activity promotes glioma growth through neuroligin-3 secretion". *Cell*, 161: 803–816.

Veroniki, A. A. et al. (2017). "Comparative safety of antiepileptic drugs for neurological development in children exposed during pregnancy and breast feeding: A systematic review and network meta-analysis". *BMJ Open*, 7: e017248.

Vivanti, G. and Messinger, D. S. (2021). "Theories of Autism and Autism Treatment from the DSM III Through the Present and Beyond: Impact on Research and Practice". *Journal of Autism and Developmental Disorders*, 51: 4309–4320.

Volders, K., Nuytens, K., and Creemers, J. W. M. (2011). "The Autism Candidate Gene Neurobeachin Encodes a Scaffolding Protein Implicated in Membrane Trafficking and Signaling". *Current Molecular Medicine*, 11: 204–217.

Vorhees, C. V. and Williams, M. T. (2014). "Assessing spatial learning and memory in rodents". *ILAR Journal*, 55 (2): 310–332.

Vorstman, J. A. et al. (2017). "Autism genetics: Opportunities and challenges for clinical translation". *Nature Reviews Genetics*, 18: 362–376.

Wang, X. et al. (2000). "Neurobeachin: A protein kinase A-anchoring, beige/Chediak-higashi protein homolog implicated in neuronal membrane traffic." *The Journal of Neuroscience*, 20 (23): 8551–65.

Wang, X. and Lambert, N. A. (2003). "Membrane properties of identified lateral and medial perforant pathway projection neurons". *Neuroscience*, 117: 485–492.

Williams, N. M. et al. (2012). "Genome-wide analysis of copy number variants in attention deficit hyperactivity disorder: The role of rare variants and duplications at 15q13.3". *American Journal of Psychiatry*, 169: 195–204.

Willner, P. (1984). "The validity of animal models of depression". *Psychopharmacology*, 83: 1–16.

Winkels, R. et al. (2009). "Reduced excitability in the dentate gyrus network of $\beta$IV-spectrin mutant mice in vivo". *Hippocampus*, 19: 677–686.

Woods, N. I. et al. (2018). "Preferential targeting of lateral entorhinal inputs onto newly integrated granule cells". *The Journal of Neuroscience*, 38 (26): 5843–5853.

World Health Organization (2021). "6A02 Autism spectrum disorder". In: *International Classification of Diseases-11th revision*. World Health Organization.

Wu, S. et al. (2017). "Advanced parental age and autism risk in children: a systematic review and meta-analysis". *Acta Psychiatrica Scandinavica*, 135: 29–41.

Xu, J. et al. (2019). "Neuroligin 3 Regulates Dendritic Outgrowth by Modulating Akt/mTOR Signaling". *Frontiers in Cellular Neuroscience*, 13: 518.

Xu, Q., Zuo, C., Liao, S., Long, Y., and Wang, Y. (2020). "Abnormal development pattern of the amygdala and hippocampus from childhood to adulthood with autism". *Journal of Clinical Neuroscience*, 78: 327–332.

Xu, X., Sun, Y., Holmes, T. C., and López, A. J. (2016). "Noncanonical connections between the subiculum and hippocampal CA1". *The Journal of Comparative Neurology*, 524: 3666–3673.

Yamakura, T., Mori, H., Masaki, H., Shimoji, K., and Mishina, M. (1993). "Different sensitivities of NMDA receptor channel subtypes to non-competitive antagonists". *NeuroReport*, 4: 687–690.

Yan, J. et al. (2008). "Analysis of the neuroligin 4Y gene in patients with autism". *Psychiatric Genetics*, 18: 204–207.

Yang, M., Silverman, J. L., and Crawley, J. N. (2011). "Automated three-chambered social approach task for mice". *Current Protocols in Neuroscience*, 56: 1–8.

Yang, M. et al. (2012). "Reduced excitatory neurotransmission and mild Autism-Relevant phenotypes in adolescent shank3 null mutant mice". *The Journal of Neuroscience*, 32 (19): 6525–6541.

Yoshida, T. et al. (2021). "Canonical versus non-canonical transsynaptic signaling of neuroligin 3 tunes development of sociality in mice". *Nature Communications*, 12: 1848.

Yun, S. H. and Trommer, B. L. (2011). "Fragile X mice: Reduced long-term potentiation and N-Methyl-D-Aspartate receptor-mediated neurotransmission in dentate gyrus". *Journal of Neuroscience Research*, 89: 176–182.

Zhang, B. et al. (2017). "Developmental plasticity shapes synaptic phenotypes of autism-associated neuroligin-3 mutations in the calyx of held". *Molecular Psychiatry*, 22: 1483–1491.

Zhang, C. et al. (2009). "A neuroligin-4 missense mutation associated with autism impairs neuroligin-4 folding and endoplasmic reticulum export". *The Journal of Neuroscience*, 29 (35): 10843–10854.

Zhao, H., Jiang, Y. H., and Zhang, Y. Q. (2018). "Modeling autism in non-human primates: Opportunities and challenges". *Autism Research*, 11: 686–694.

## Chapter 3

# Manuscript 1

## Enhanced LTP of population spikes in the dentate gyrus of mice haploinsufficient for neurobeachin

*published in*
Scientific Reports

**Declaration of author contributions to the manuscript: "Enhanced LTP of population spikes in the dentate gyrus of mice haploinsufficient for neurobeachin"**

Status: *accepted*

name of journal: *Scientific Reports*

Contributing authors: Julia Muellerleile, Aline Blistein, Astrid Rohlmann, Frederieke Scheiwe, Markus Missler, Stephan W. Schwarzacher, Peter Jedlička

**What are the contributions of the doctoral candidate and her co-authors?**

**(1) Concept and design**
Doctoral candidate: 0%
Co-author Aline Blistein: 0%
Co-author Astrid Rohlmann: 20%
Co-author Frederieke Scheiwe: 0%
Co-author Markus Missler: 20%
Co-author Stephan W. Schwarzacher: 30%
Co-author Peter Jedlička: 30%

**(2) Conducting tests and experiments**
Doctoral candidate: 20% (electrophysiological experiments in Figure 1f-j, histology)
Co-author Aline Blistein: 70% (all other electrophysiological experiments)
Co-author Astrid Rohlmann: 10% (electron microscopy)
Co-author Frederieke Scheiwe: 0%
Co-author Markus Missler: 0%
Co-author Stephan W. Schwarzacher: 0%
Co-author Peter Jedlička: 0%

**(3) Compilation of data sets and figures**
Doctoral candidate: 70% (compilation of Figures 1-4 and S1)
Co-author Aline Blistein: 20% (compilation of data sets for Figures 1-4)
Co-author Astrid Rohlmann: 5% (compilation of data set for Figure 2a+b)
Co-author Frederieke Scheiwe: 5% (compilation of data set for Figure 2a+b)
Co-author Markus Missler: 0%
Co-author Stephan W. Schwarzacher: 0%
Co-author Peter Jedlička: 0%

**(4) Analysis and interpretation of data**
Doctoral candidate: 40% (analysis and interpretation of electrophysiological data)
Co-author Aline Blistein: 30% (analysis and interpretation of electrophysiological data)
Co-author Astrid Rohlmann: 5% (interpretation)
Co-author Frederieke Scheiwe: 10% (analysis of EM data)
Co-author Markus Missler: 5% (interpretation)
Co-author Stephan W. Schwarzacher: 5% (interpretation)
Co-author Peter Jedlička: 5% (interpretation)

**(5) Drafting of manuscript**
Doctoral candidate: 60% (original draft, editing)
Co-author Aline Blistein: 20% (original draft)
Co-author Astrid Rohlmann: 5% (editing)
Co-author Frederieke Scheiwe: 0%
Co-author Markus Missler: 5% (editing)
Co-author Stephan W. Schwarzacher: 5% (editing)
Co-author Peter Jedlička: 5% (editing)

# Enhanced LTP of population spikes in the dentate gyrus of mice haploinsufficient for neurobeachin

**Julia Muellerleile[1,2,5*], Aline Blistein[1,5*], Astrid Rohlmann[3], Frederieke Scheiwe[3], Markus Missler[3], Stephan W. Schwarzacher[1,6] & Peter Jedlicka[1,4,6]**

[1]Institute of Clinical Neuroanatomy, Neuroscience Center, Goethe University Frankfurt am Main, Frankfurt, Germany

[2]Faculty of Biosciences, Goethe University Frankfurt am Main, Frankfurt, Germany

[3]Institute of Anatomy and Molecular Neurobiology, University of Münster, Münster, Germany

[4]Faculty of Medicine, Justus-Liebig-University Giessen, Giessen, Germany

[5]These authors contributed equally: Julia Muellerleile and Aline Blistein

[6]These authors jointly supervised this work: Stephan W. Schwarzacher and Peter Jedlicka

[*] Correspondence and requests for materials should be addressed to J.M. (muellerleile@med.uni-frankfurt.de) or A.B. (aline_blistein@web.de)

## Abstract

Deletion of the autism candidate molecule neurobeachin (Nbea), a large PH-BEACH-domain containing neuronal protein, has been shown to affect synaptic function by interfering with neurotransmitter receptor targeting and dendritic spine formation. Previous analysis of mice lacking one allele of the Nbea gene identified impaired spatial learning and memory in addition to altered autism-related behaviours. However, no functional data from living heterozygous Nbea mice ($Nbea^{+/-}$) are available to corroborate the behavioural phenotype. Here, we explored the consequences of Nbea haploinsufficiency on excitation/inhibition balance and synaptic plasticity in the intact hippocampal dentate gyrus of $Nbea^{+/-}$ animals in vivo by electrophysiological recordings. Based on field potential recordings, we show that $Nbea^{+/-}$ mice display enhanced LTP of the granule cell population spike, but no differences in basal synaptic transmission, synapse numbers, short-term plasticity, or network inhibition. These data indicate that Nbea haploinsufficiency causes remarkably specific alterations to granule cell excitability in vivo, which may contribute to the behavioural abnormalities in $Nbea^{+/-}$ mice and to related symptoms in patients.

## Introduction

Neurobeachin (Nbea) belongs to the BEACH (beige and Chediak-Higashi) domain-containing protein family whose members are involved in the trafficking of membrane proteins (for review, see[1]). Nbea is highly expressed in endocrine cells and neurons where it is enriched at tubulovesicular endomembranes and in the postsynaptic compartment, and plays a role in vesicle secretion, presumably via regulation of protein kinase A (PKA)[2-4]. Previous research established Nbea as an essential molecule in synapse function because homozygous Nbea knockout mice ($Nbea^{-/-}$) die immediately after birth from breathing paralysis due to a dramatic reduction of evoked synaptic transmission at the neuromuscular junction and in respiratory neurons in the brainstem[5,6]. Despite this dramatic phenotype, the exact role of Nbea is still incompletely understood as its effects are pleiotropic and not all phenotypic observations could be repeated in independent models and assays. While it is widely agreed that complete deletion of Nbea in mice leads to defects of spontaneous and evoked synaptic transmission at excitatory and inhibitory synapses[4-7], only some of the defects can be attributed to reduced surface levels of postsynaptic AMPA, NMDA and $GABA_A$ receptor subunits[4,7-10]. Moreover, while the overall density of asymmetric, presumably excitatory synaptic contacts and synaptic vesicle protein levels are diminished in acute slices from Nbea-deficient embryonic mice[5], these parameters appear normal in primary neuronal cultures[4,8]. In contrast, the number of excitatory synapses on spines, small protrusions arising from dendritic shafts where most excitatory synapses reside, is reduced in both knockout cultures and brain tissue[8,9]. Additional research identified roles of Nbea in dense-core vesicle function in mouse pancreatic cells and platelets[3,11] and, possibly, in transcriptional regulation[12]. Collectively, these findings indicate that Nbea is a fascinating but elusive molecule that mandates the use of highly specific techniques to uncover its functions.

Nbea was identified as a candidate gene for autism spectrum disorder (ASD) based on a translocation of the Nbea gene found in a patient with ASD[13]. Deletions of the chromosomal regions on which Nbea resides have also been discovered in other patients with ASDs[14-16] and developmental/intellectual disability[17]. The Nbea gene is located across a common fragile site, making it more vulnerable to breakage during metaphase[18]. Compared to other genes, the human Nbea gene has a lower tolerance for disruptive mutations, which indicates that it is under purifying selection and thus a likely candidate gene for ASD[19]. To address this important aspect, several groups investigated heterozygous $Nbea^{+/-}$ mice, which exhibit a 30% reduction in forebrain Nbea protein levels[8], for construct and face validity. In fact, autism-related abnormalities are present in $Nbea^{+/-}$ mice including altered social behaviours, increased self-grooming, delayed spatial learning and memory, increased conditioned fear responses, and impaired fear memory extinction[20,21]. Along with these findings, long-term potentiation (LTP) was enhanced in acute slices of the CA1 region of the hippocampus, an important site for spatial learning[20]. These intriguing results indicate that Nbea might play an important role in the regulation of synaptic plasticity in the hippocampus, but this finding has not been confirmed by in vivo experiments.

Here, we performed electrophysiological recordings in the hippocampus of $Nbea^{+/-}$ mice in vivo to study the potentially important role of Nbea in synaptic transmission and plasticity in the intact brain. Field potentials evoked by stimulation of the perforant path were recorded in the granule cell layer of the dentate gyrus in anaesthetised mice. We found that $Nbea^{+/-}$ mice displayed enhanced LTP of the granule cell population spike, which shows that Nbea has a functional role in vivo that could help explain the behavioural phenotypes observed in haploinsufficient mice.

## Results

**The granule cell population spike is enhanced following LTP induction in Nbea$^{+/-}$ mice.** Nbea deficiency is known to improve the induction and maintenance of long-term potentiation (LTP) at Schaffer collateral synapses in acute slices of the hippocampus in vitro[20]. Here, we tested whether LTP is also altered in intact animals, a prerequisite for drawing firm conclusions about the pathomechanism in human patients with Nbea haploinsufficiency[13]. LTP at perforant path-to-granule cell (PP-GC) synapses in Nbea$^{+/-}$ and wild-type littermate control mice was induced by theta-burst stimulation (TBS) protocols. Since Nbea$^{+/-}$ mutant mice lack only about about 30% of Nbea protein[8], we decided to use a previously established stimulation protocol[22] consisting of a weak TBS followed by strong TBS 30 min after the weak TBS to uncover even subtle differences between both groups (Fig. 1a–e). The stimulation intensities were set to elicit a stable population spike and were similar between groups (Fig. 1b, 4 wild-type and 7 Nbea$^{+/-}$ mice, 227.5±45.71 µA vs. 227.4±43.35 µA, unpaired Welch's *t* test, P=0.9991). The pre-TBS population spike amplitude was also quite similar between groups (Figure 1c, 5 wild-type and 7 Nbea$^{+/-}$ mice, 4.861±0.9791 mV vs. 4.292±0.3686 mV, unpaired Welch's *t* test, P=0.5517). During the 30 minutes following the weak TBS, we observed an almost 40% higher potentiation of the population spike relative to the pre-TBS baseline in Nbea$^{+/-}$ compared to control mice (Fig. 1e, 135.6±5.692% for wild-type and 173.8±8.459% for Nbea$^{+/-}$ mice, unpaired Welch's *t* test, P=0.0046). The strong TBS further increased the spike amplitude in wild-type mice, thus substantiating the efficacy of LTP induction by TBS in control mice. In contrast, the population spike amplitude was not further enhanced by the second TBS in Nbea$^{+/-}$ mice, revealing that a weak TBS is sufficient to induce maximal potentiation in Nbea$^{+/-}$ mice (Fig. 1d). There was no significant difference between groups in the spike amplitude potentiation following the strong TBS, neither in the first 30 minutes (171.2±12.02% for Nbea$^{+/-}$, 145.2±9.004% for wild-type, unpaired Welch's *t* test, P=0.1405, Fig. 1e) nor the last 30 minutes (162.8±9.152% for Nbea$^{+/-}$, 137.7±9.792% for wild-type, unpaired Welch's *t* test, P=0.0929, Fig. 1e).

In a separate set of experiments, we induced LTP using only the weak TBS protocol in order to determine whether the Nbea$^{+/-}$ mice also displayed an enhancement in synaptic efficacy as measured by the fEPSP slope (Fig. 1f-j). The population spike was minimised to allow for accurate assessment of the initial fEPSP slope. Both the stimulation intensities (Fig. 1g, 3 wild-type and 4 Nbea$^{+/-}$ mice, 275.0±43.30 µA vs. 323.8±44.60 µA, unpaired Welch's *t* test, P=0.4767) and the pre-TBS slopes (Fig. 1h, 0.5564±0.07608 mv/ms for wild-type and 0.5433±0.1521 mV/ms for Nbea$^{+/-}$ mice, unpaired Welch's *t* test, 0.9421) were similar between groups; however, the population spike amplitudes were highly variable and therefore not included in the analysis. Interestingly, there were no significant differences in the potentiation of the fEPSP slope in the first 30 min after wTBS (Fig. 1j, 4 Nbea$^{+/-}$ and 3 wild-type mice, 144.1±12.57% vs. 157.1±14.08%, unpaired Welch's *t* test, P=0.5302). Together, these data demonstrate that (1) even a moderate reduction in Nbea protein levels is sufficient to alter long-term potentiation of population spikes in the dentate gyrus of living mice, but that (2) potentiation fEPSP slope is apparently not affected by Nbea.

**Excitatory transmission at PP-GC synapses is unchanged in Nbea$^{+/-}$ mice.** Previous studies revealed a strong reduction of evoked glutamatergic postsynaptic responses in the complete absence of Nbea protein in acute slices and primary neuronal cultures of homozygous mice[4,5] establishing that Nbea is essential for basic synaptic transmission. However, slice recordings of fEPSP slopes from heterozygous neurons were remarkably normal[20] and spontaneous glutamatergic postsynaptic responses only showed a slight reduction in frequency and rise time but not in amplitude[8]. In order to explore the pre- and postsynaptic properties of haploinsufficient Nbea$^{+/-}$ mice in vivo, we probed the function of excitatory medial PP-GC synapses with different stimulation protocols.

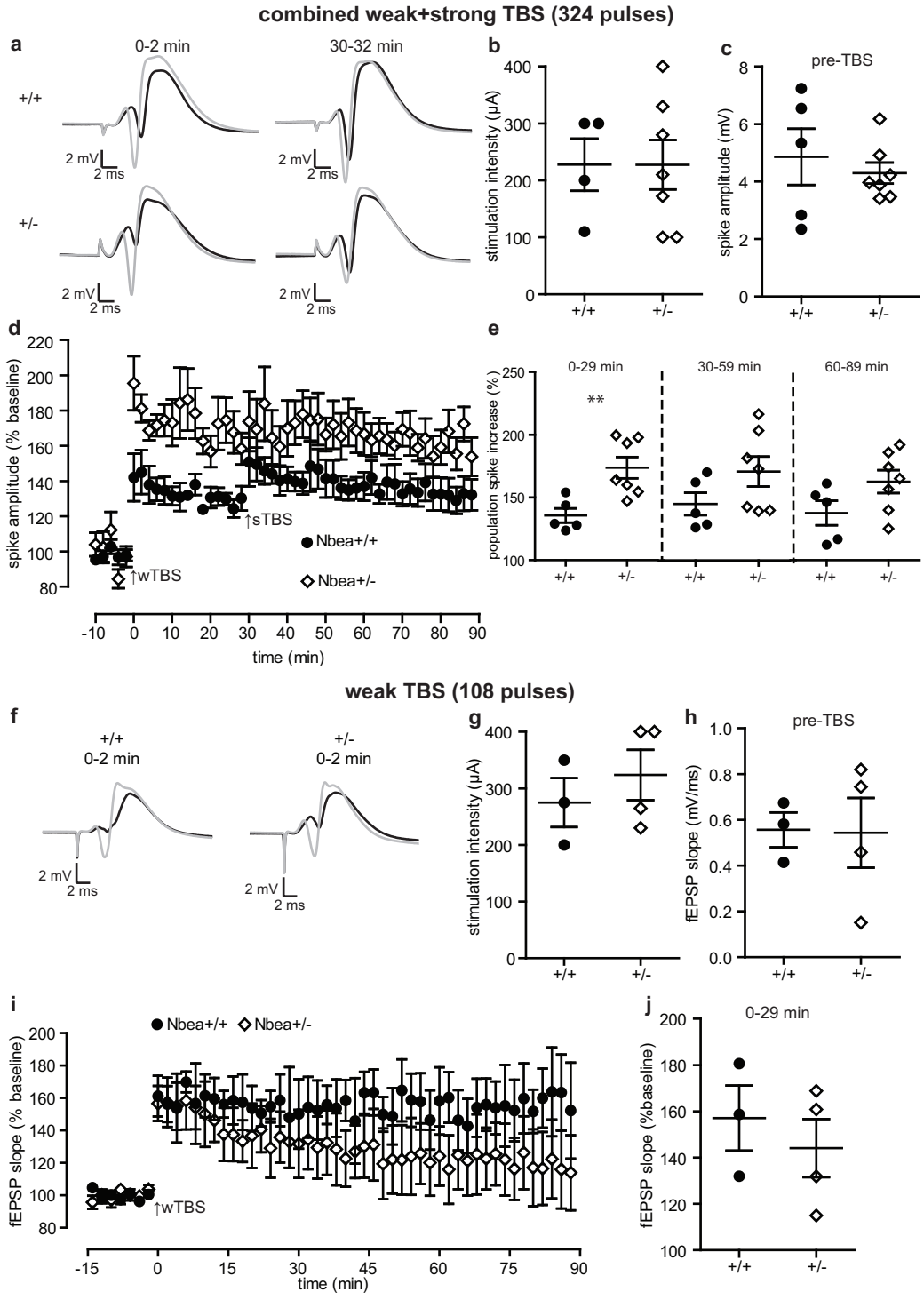


FIGURE 1: Enhanced long-term potentiation of the population spike at perforant path-to-granule cell synapses in Nbea$^{+/-}$ mice. (**a-e**) Long-term potentiation (LTP) of the population spike amplitude induced by weak theta-burst stimulation (wTBS, 3 series of 6 trains of 6 stimuli at 400 Hz, 200 ms between trains and 20 s between series) at 0 min followed by strong TBS (sTBS, 6 series of 6 trains of 6 stimuli at 400 Hz, 200 ms between trains and 20 s between series) at 30 min. (**a**) Representative traces showing the averaged responses during the 2 min preceding (black trace) and the 2 min immediately following (grey trace) wTBS and sTBS for a wild-type and Nbea$^{+/-}$ mouse. (**b**) No difference in the stimulation intensity (P=0.9991) or the (**c**) pre-TBS population spike amplitude (P=0.5517) between Nbea$^{+/-}$ mice as compared to wild-type littermate controls. (**d**) Time course of the spike LTP experiments.

(*continued on next page*)

FIGURE 1: (*continued from last page*) (**e**) Comparison of the mean increase in the population spike in Nbea$^{+/-}$ and wild-type mice during the 30 min following wTBS (**P=0.0046), the first 30 min following sTBS (P=0.1405), and the last 30 min of recording (P=0.0929). (**f-j**) LTP of the fEPSP slope induced by wTBS alone. (**f**) Representative traces showing the averaged responses during the 2 min preceding (black trace) and the 2 min immediately following (grey trace) wTBS for a wild-type and Nbea$^{+/-}$ mouse.**g**) No difference in the stimulation intensity (P=0.4767) or the (**h**) pre-TBS fEPSP slope (P=0.9421) between Nbea+/- mice and wild-type littermate controls. (**i**) Time course of the slope LTP experiments. (**j**) Comparison of the increase in the fEPSP slope following wTBS in wild-type and Nbea$^{+/-}$ mice (P=0.5302). Unpaired Welch's *t* test used for all comparisons. All values reported as means ± SEM.

To exclude the possibility that morphological changes such as a reduction in the number of synaptic contacts interfered with our analysis of functional plasticity, we examined the relevant ultrastructure of these synapses. Samples of the middle molecular layer of the hippocampal dentate gyrus, the very location of medial PP-GC synapses, were imaged in wild-type littermate control and Nbea$^{+/-}$ mice by transmission electron microscopy. No apparent structural alterations were detected concerning the shape of asymmetric (type 1) synapses (representative image in Fig. 2a) or their position on dendritic spine heads and dendritic shafts. Moreover, quantification of the area density of the number of asymmetric synapses in the middle molecular layer revealed no significant differences between control and mutant mice (Fig. 2b, n=7 sections from 2 mice per genotype, 49.71±6.221 for Nbea$^{+/-}$ and 55.71±3.790 for wild-type mice, unpaired Welch's *t* test, P=0.4295).

Next, we measured paired-pulse facilitation (PPF), a form of presynaptic short-term plasticity which depends mostly on the condition of presynaptic terminals[23]. To elicit PPF, we stimulated the perforant path axons at increasing interpulse intervals (IPIs). To avoid activation of the postsynaptic membranes by the firing of granule cells, we used intensities that were subthreshold for population spike evocation. We then measured the augmentation of the fEPSP amplitude (PPF) as the ratio of the two fEPSP amplitudes induced by two successive stimuli at IPIs from 15 to 100 ms (Fig. 2c). As shown previously, PP-GC synapses express PPF at low IPIs which declines with increasing IPI[22,24]. The stimulation intensities (in µA) used to elicit PPF were not significantly different between groups (52.28±5.526 for Nbea$^{+/-}$ and 68.30±8.561 for wild-type, unpaired Welch's *t* test, P=0.1354). The variation observed in the degree of PPF was not due to genotype (n=19 Nbea$^{+/-}$ and 10 wild-type mice, P=0.2876 determined by two-way ANOVA with Bonferroni's multiple-comparison tests) or the interaction between IPI and genotype (P=0.2434), suggesting that properties of short-term plasticity are not altered by the reduction in Nbea protein levels.

Furthermore, to exclude the possibility that input-output (I-O) relations were changed in Nbea$^{+/-}$ neurons, I-O curves were measured to probe differences in basal excitatory transmission of PP-GC synapses. We stimulated the perforant path across a range of stimulation intensities (30-800 µA, Fig. 2d) and analysed the slope of the resulting fEPSPs, since the slope is an indicator of synaptic strength[25]. We found that the variation in the I-O relationship was not caused by the genotype (n=14 Nbea$^{+/-}$ and 10 wild-type mice, two-way ANOVA with Bonferroni's multiple-comparison tests, P=0.6143), or the interaction between stimulation intensity and genotype (P=0.7891), confirming results obtained from slice recordings at the Schaffer collateral terminals[20]. Together, these results indicate that a moderate reduction in Nbea protein levels by about 30% in haploinsufficient mice[8] does not affect properties of basal excitatory transmission at hippocampal synapses in vivo.

**EPSP-spike coupling is slightly reduced in Nbea$^{+/-}$ mice.** One advantage of our recording method is that the synaptic strength and the excitability of the granule cell population can be assessed separately. The population spike is superimposed on the fEPSP and represents the summed firing activity of the granule cells[26]. Therefore, we studied the excitability of granule

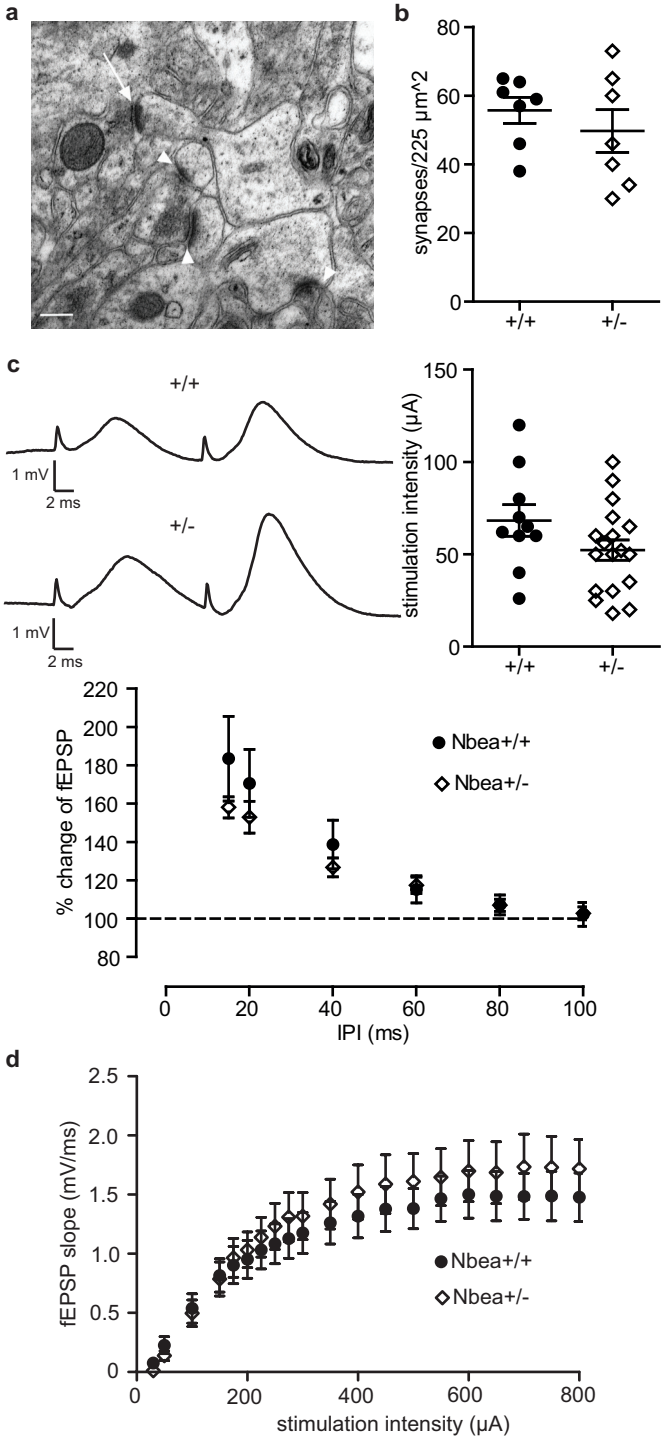


FIGURE 2: Normal synaptic ultrastructure and basal synaptic transmission at perforant path-to-granule cell synapses in Nbea$^{+/-}$ mice. (**a**) Representative electron micrograph of the middle molecular layer of the dentate gyrus from a Nbea$^{+/-}$ mouse, showing four asymmetric (type 1) synapses terminating on dendritic profiles (arrowheads). One bouton forms a spinous synapse on an unequivocal dendritic spine (arrow). Scale bar, 200 nm. (**b**) Quantitative comparison of the area density of asymmetric synapses in the middle molecular layer of the dentate gyrus from wild-type and Nbea$^{+/-}$ mice (unpaired Welch's *t* test, P=0.4295). (**c**) Paired-pulse facilitation of the fEPSP amplitude elicited at stimulus intensities subthreshold for spike generation was not different in wild-type and Nbea$^{+/-}$ mice (two-way ANOVA with Bonferroni's multiple-comparison tests, P=0.2876 for genotype, P=0.2434 for interaction). Example traces show the response to PPF stimulation at an interpulse interval (IPI) of 15 ms.

(*continued on next page*)

FIGURE 2: (*continued from last page*) Inset: stimulation intensities used to elicit PPF were not significantly different between groups (unpaired Welch's *t* test, P=0.1354). (**d**) The response of the fEPSP slope to perforant path stimulation at increasing stimulus intensities shows no difference between wild-type and Nbea$^{+/-}$ mice (two-way ANOVA with Bonferroni's multiple-comparison post-tests, P=0.6143 for genotype, P=0.7891 for interaction). All values reported as means ± SEM.

cells in control versus Nbea$^{+/-}$ mice by measuring the population spike amplitudes across a range of stimulus intensities from 30 to 800 µA. Comparing the results from both groups (Fig. 3a), there were no significant differences in the ability of Nbea haploinsufficient granule cells to produce action potentials compared to their wild-type littermates (n=14 Nbea$^{+/-}$ and 10 wild-type mice, two-way ANOVA with Bonferroni's multiple-comparison tests, P=0.0676). The interaction between stimulation intensity and genotype was also not a significant factor in explaining the variation (P=0.4168). These data suggest that the action-potential-generating capability of GCs is not altered by deletion of one allele of the Nbea gene.

To further examine the relationship between the synaptic input strength and firing ability of granule cells, we performed a fEPSP-population spike (E-S) coupling analysis by plotting fEPSP

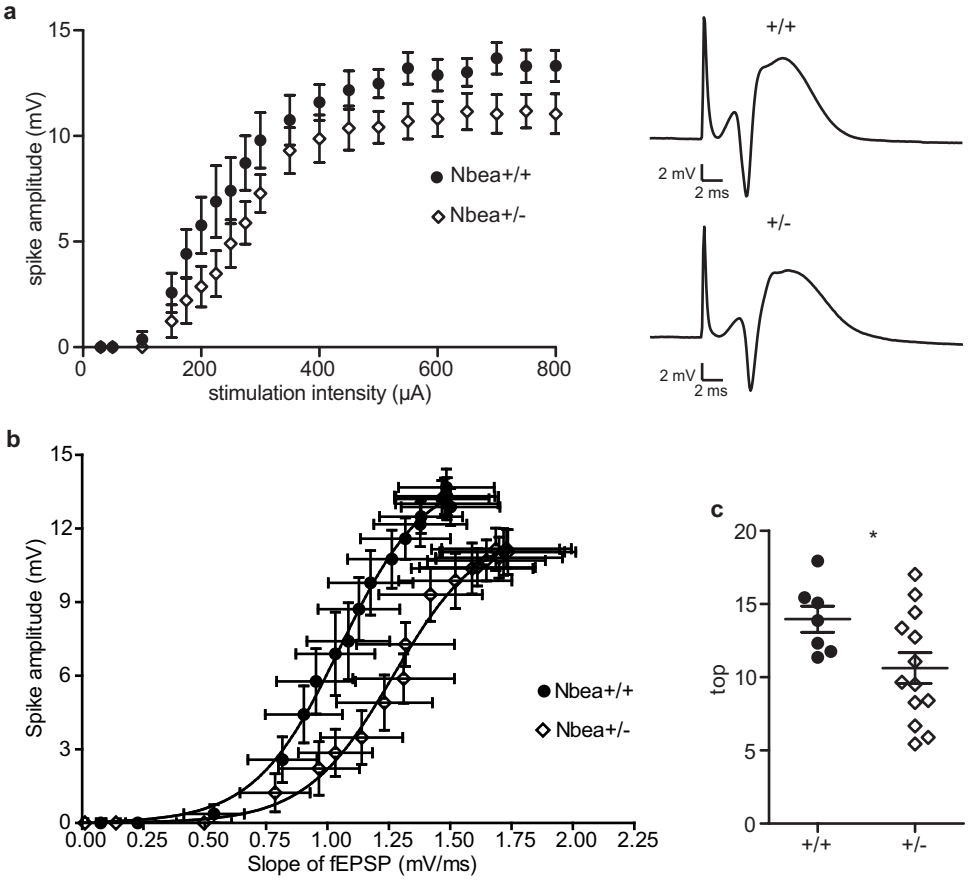


FIGURE 3: Lower excitability and impairment of EPSP-population spike (E-S) coupling in Nbea$^{+/-}$ mice. (**a**) The input-output curve for the population spike amplitude in response to increasing stimulation intensities was not significantly different when comparing wild-type and Nbea$^{+/-}$ mice (two-way ANOVA with Bonferroni's multiple-comparison post-tests, P=0.0676 for genotype, P=0.4168 for interaction). Representative traces show the responses to 800 µA stimulation. (**b**) EPSP-spike (E-S) coupling fitted with a Boltzmann function. (**c**) At higher stimulus intensities, the coupling between fEPSP slope and population spike values as measured by the top fit parameter is significantly reduced in Nbea$^{+/-}$ mice (unpaired Welch's *t* test, *P=0.0261). All values reported as means ± SEM.

slopes against population spike amplitudes (Fig. 3b). The coupling between synaptic drive and the action potential firing ability reflects the intrinsic excitability of the neurons[27] as well as the excitation/inhibition balance of the local circuits[28]. This analysis revealed a rightward shift and a lower top parameter of the Boltzmann-fitted Nbea$^{+/-}$ E-S curve (Fig. 3c, n=7 wild-type and 13 Nbea+/- mice, 13.96±0.8924 vs.10.62±1.044, unpaired Welch's *t* test, P=0.0261) with respect to the wild-type curve. The rightward shift indicates that heterozygous mice require a stronger synaptic input than their wild-type littermates to produce a similar spike response, i.e. reduced E-S coupling. The reduction in the top parameter reflects the lower maximal spike amplitude in heterozygotes. Thus, our in vivo recordings revealed a reduced tendency of Nbea$^{+/-}$ neurons to translate changes in synaptic input into changes in firing. We therefore tested whether this reduced E-S coupling was due to differences in the balance of excitation and inhibition in the dentate gyrus of Nbea$^{+/-}$ mice by examining network inhibition.

**Network inhibition is unaltered in Nbea$^{+/-}$ mice.** Recordings in intact mice allow the assessment of distinct properties of neuronal network behaviour that are often difficult to replicate in acute slices or cultures, such as the influence of inhibition on firing activity[29]. Earlier studies have reported that inhibitory synapse function was severely compromised in both acute slices and primary neuronal cultures of null-mutant Nbea neurons[4,5,7,8]. We assessed network inhibition in the dentate gyrus of Nbea$^{+/-}$ mice in vivo by measuring paired-pulse inhibition (PPI) at short IPIs. In addition, we determined disinhibition (PPDI) at longer IPIs. PPI reflects the recruitment of GABAergic interneurons mediating granule cell inhibition by both feedforward and feedback mechanisms[26,30,31], and PPDI reflects the inhibition of these interneurons[32]. We first applied stimulation intensities triggering population spikes of approximately 1 mV but could not detect significant differences in PPI between Nbea+/- and wild-type mice. PPI/PPDI curves were nearly congruent (Fig. 4a, n=15 Nbea$^{+/-}$ and 12 wild-type mice, two-way ANOVA with Bonferroni's multiple-comparison tests, P=0.6760 for genotype, P=0.3239 for interaction) and the IPI at which PPI switched to PPDI was similar in both groups (37.09±1.937 ms for Nbea$^{+/-}$ and 34.27±2.453 ms for wild-type mice, Welch's *t* test, P=0.3766). To determine whether there was a difference between wild-type and Nbea$^{+/-}$ mice at a higher stimulus intensity, we applied 800 µA/0.2 ms stimuli to recruit as much feedback inhibition as possible. The genotype effect was not significant (Fig. 4b, n=15 Nbea$^{+/-}$ and 12 wild-type mice, two-way ANOVA with Bonferroni's multiple-comparison tests, P=0.4264), but the interaction between genotype and IPI was significant (P=0.0057). This indicates that there might have been an effect of the genotype at some IPIs, but there were no major functional consequences to this discrepancy since the PPI/PPDI shift was not significantly different between groups (40.30±1.995 ms for Nbea$^{+/-}$ and 39.11±2.241 ms for wild-type mice, unpaired Welch's *t* test, P=0.6948). These results suggest that the haploinsufficiency of Nbea does not primarily manifest itself at inhibitory synapses, although more subtle changes or effects at distinct types of inhibitory neurons cannot be excluded based on our finding of decreased E-S coupling.

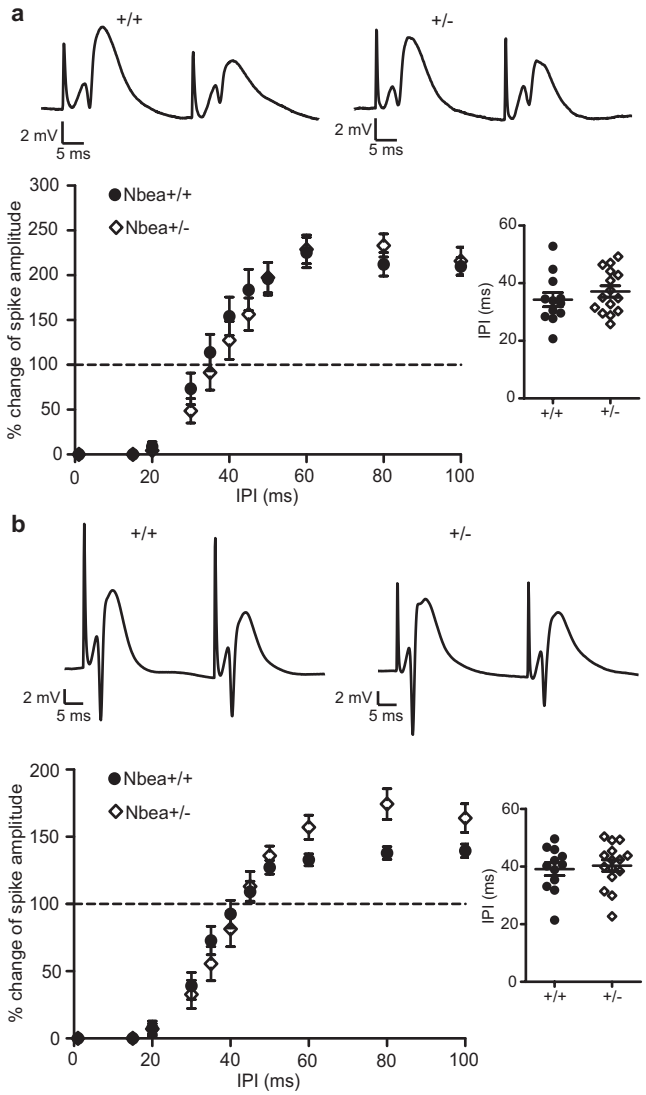


FIGURE 4: Unaltered network inhibition in Nbea$^{+/-}$ mice. (**a**) Paired-pulse inhibition and disinhibition of the population spike amplitude (PPI/PPDI) at the minimum stimulus intensity for eliciting a spike was not significantly different in wild-type and Nbea$^{+/-}$ mice (two-way ANOVA with Bonferroni's multiple-comparison post-tests, P=0.6760 for genotype, P=0.3239 for interaction). The interpulse interval (IPI) at which PPI switched to PPDI was also not significantly different (inset, unpaired Welch's *t* test, P=0.1073). Representative traces show the response to stimulation at 30 ms IPI. (**b**) Paired-pulse inhibition and disinhibition of the population spike amplitude (PPI/PPDI) at the maximal stimulus intensity of 800 µA was not impaired in Nbea$^{+/-}$ compared to wild-type mice (two-way ANOVA with Bonferroni's multiple-comparison post-tests, P=0.4264 for genotype, P=0.0057 for interaction). The IPI at which PPI switched to PPDI was not significantly different (inset, unpaired Welch's *t* test, P=0.6948). Representative traces show the response to stimulation at 35 ms IPI. All values reported as means ± SEM.

## Discussion

Using in vivo field potential recordings from the mouse hippocampus, we provide evidence for an involvement of the neuronal BEACH-domain containing protein Nbea in granule cell excitability in the intact brain. While LTP of the population spike was enhanced in the dentate gyrus of Nbea$^{+/-}$ mice, LTP of the fEPSP slope as well as basal synaptic transmission, short-term presynaptic plasticity, and network inhibition were unaffected. These are important findings because they demonstrate that even a moderate reduction of Nbea protein level[8] can cause functional abnormalities in distinct neural circuitry.

Our results indicate an enhanced response to LTP stimulation in Nbea$^{+/-}$ mice. Following LTP induction with a weak TBS protocol in vivo, we found a comparable increase in synaptic potentiation and a significantly larger increase in the granule cell spike response to perforant path stimulation in Nbea$^{+/-}$ mice. A previous study reported enhanced LTP in the CA1 region in acute slices from female Nbea$^{+/-}$ mice following a similar TBS protocol[20], indicating that Nbea plays a functional role in different hippocampal subregions and in different aspects of LTP. What is the behavioural relevance of enhanced LTP? Although LTP is widely believed to be essential for synaptic modifications underlying memory formation, enhanced LTP does not necessarily lead to improved memory formation. In fact, multiple studies have reported an association between impairments in learning and memory and augmented LTP[33–38]. In line with the inverse correlation between spatial memory and LTP, Nbea$^{+/-}$ mice showed impaired learning and memory in behavioural tests[20]. The learning deficits were most pronounced in delayed spatial learning tested in the Morris water maze task, which is highly sensitive to hippocampal lesions[39]. However, Nuytens et al. (2013) only reported one measure of LTP, namely, the EPSP slope. A previous study found a correlation between LTP of the CA1 population spike and the performance of rats in the Morris water maze, whereas LTP of the EPSP was not correlated[40]. This suggests that potentiation of the population spike, and not the EPSP, forms the physiological basis for delayed spatial learning. Furthermore, while both CA1 and the dentate gyrus are important sites for spatial learning[41,42], the dentate gyrus is also important for the discrimination of similar environments (pattern separation)[43]. In line with this, an increase in LTP has been shown to coincide with less specific hippocampal place fields[44]. During spatial exploration, the capability for enhanced LTP of the population spike may lead to overactivation of the granule cells and hence to a seemingly paradoxical decrease of information content in the hippocampal neuronal network, which may be associated with learning deficits[33]. Therefore, our finding that Nbea$^{+/-}$ mice displayed enhanced population spike LTP in the dentate gyrus can help explain their impairments in spatial memory. From this we predict that future behavioural tests might be successful in revealing deficits in pattern separation tasks in Nbea$^{+/-}$ mice.

Despite the difference in spike LTP, we found that basal synaptic function was unaffected by Nbea deficiency. There were no significant changes in the input-output relationship of fEPSP slopes to the stimulation intensity in Nbea$^{+/-}$ mice as compared to their wild-type littermates. Therefore, the basal glutamate-mediated synaptic transmission is likely not affected by the haploinsufficiency of Nbea. These results are consistent with previous work comparing input-output curves in acute hippocampal slices between wild-type and Nbea$^{+/-}$ mice where no differences were detected at low stimulation intensities[20]. However, previous experiments using Nbea$^{-/-}$ neurons found that in contrast to spontaneous release events, the amplitudes of action-potential induced excitatory postsynaptic currents were significantly affected by the complete lack of Nbea[9]. This can be explained directly by the impaired AMPA receptor subunit trafficking to postsynaptic membranes[9] which limits the number of glutamate receptors. While the amount of receptors in Nbea$^{-/-}$ neurons might suffice to respond to the neurotransmitter release by single vesicles, they are more than saturated by an action potential induced glutamate release[9]. Unaltered evoked glutamatergic responses in Nbea$^{+/-}$ mice indicate that either AMPAR-subunit trafficking is less impaired in haploinsufficient animals or they have compensatory mechanisms

to generate equally strong responses as wild-type mice.

Presynaptic short-term plasticity at perforant path-granule cell synapses was not affected by a reduction in Nbea levels as revealed by unchanged paired-pulse facilitation (PPF). This finding is in line with in vitro experiments using both heterozygous[20] as well as knockout[4] neurons. In acute hippocampal slices, PPF at CA1 synapses was not affected[20]. In recordings from synaptically connected pairs of neurons in culture, it was found that the synaptic phenotype of Nbea knockout was only observed if the responding postsynaptic neuron was Nbea-deficient, indicating that presynaptic short-term plasticity mechanisms are unaltered[4]. While these results are seemingly in opposition to the earlier results indicating a strong presynaptic role for Nbea[5,6], this discrepancy might reflect a difference in Nbea function between hippocampal and cortical neurons where Nbea acts mostly postsynaptically[4,20] and brainstem neurons[5] and neuromuscular junctions[6] where Nbea also has an important presynaptic function.

In contrast to the measures of synaptic transmission, action potential generation (measured by the population spike amplitude) in the granule cells was slightly, but non-significantly, reduced in $Nbea^{+/-}$ mice. The E-S analysis, in which the population spike amplitudes are plotted against the fEPSP slopes for each stimulation intensity, revealed diminished granule cell firing in response to an EPSP of a given size in $Nbea^{+/-}$ mice as compared to wild-type mice, suggesting that Nbea might regulate the intrinsic excitability of granule cells (albeit at very high stimulation intensities that may not reflect physiological levels of synaptic activity). A decrease in E-S coupling could reflect a higher level of feed-forward inhibition in $Nbea^{+/-}$ mice, which is mediated by basket cells[45] or it could be due to changes in voltage-gated conductances that increase the intrinsic excitability of the granule cells. Further investigations using paired recordings are necessary to answer this question definitively.

To our surprise, we were unable to observe any differences in network inhibition between $Nbea^{+/-}$ and wild-type mice as assessed by PPI/PPDI measurements. This was unexpected since Nbea was shown to have a greater effect on inhibitory than excitatory synaptic transmission in brainstem acute slices, which may result in an increased excitation-inhibition (E/I) ratio[5]. In line with this, other studies implicated Nbea in the trafficking of glycine and $GABA_A$ receptors to postsynaptic membranes[4,7,46] and it was shown that $Nbea^{-/-}$ cells had a 40% reduction in cell surface levels of $GABA_A$ receptors[4]. Therefore, we expected PPI to be impaired by a reduction in Nbea. However, most of these previous studies were performed using dissociated neuronal cultures[4,7,46], where the ratio of GABAergic to glutamatergic cells and the connectivity can differ from the in vivo conditions[47]. Another reason for unchanged network inhibition might be that the loss of one allele in $Nbea^{+/-}$ mice is insufficient to reduce $GABA_A$ receptor levels.

Based on our data, we conclude that the increased potentiation of the population spike we observed in $Nbea^{+/-}$ mice is due to changes in the intrinsic excitability of granule cells, rather than synaptic mechanisms. This is suggested by our finding that the increase in the population spike of $Nbea^{+/-}$ mice is greater than the fEPSP slope increase, which was comparable to that of wild-type mice following the single weak TBS protocol. The potentiation of the population spike that cannot be accounted for by the potentiation of the EPSP is known as E-S potentiation[48,49]. Since network inhibition measured by PPI was unchanged in $Nbea^{+/-}$ mice, differences in the intrinsic excitability of granule cells are the likeliest cause for the difference in E-S potentiation. Several mechanisms, such as an increase in the conductance of voltage-gated sodium channels[50] or a reduction in A-type potassium current[51] have been proposed to underlie E-S potentiation, though calcium influx appears to be essential[49]. Importantly, the action potential threshold does not necessarily correlate with E-S potentiation[49], so the difference we observed in (pre-TBS) E-S coupling (which is a reflection of the firing threshold and synchrony) is not an indication of the degree of (post-TBS) E-S potentiation in the same cells. The exact mechanism by which Nbea might affect intrinsic excitability is unknown, but it is conceivable that Nbea might regulate the membrane trafficking of A-type potassium channels via its PH(pleckstrin homology)-BEACH domain in a similar manner to its trafficking of GluA2 AMPAR subunits[9]. Another possibility

lies in the function of Nbea as an A-kinase anchoring protein[2]. It was previously shown that A-kinase anchoring proteins interact with Kv4.2 channels, which mediate the backpropagation of action potentials, in order to enhance their surface expression[52] and that the turnover of Kv4.2 channels is regulated by PKA in distal dendrites of CA1 pyramidal cells[53]. The downregulation of Kv4.2 channels has also been proposed as a potential mechanism for the changes in intrinsic excitability observed after LTP induction in the dentate gyrus in vitro[54]. Thus, Nbea might influence the intrinsic excitability of granule cells by trafficking and/or regulating the turnover of voltage-gated ion channels in dendrites.

ASD is often described as a synaptopathy due to many animal models exhibiting changes in synaptic function[55,56]. However, changes in intrinsic neuronal excitability might have stronger impact on the firing activity of neurons that exhibit high levels of dendritic voltage attenuation such as dentate granule cells[57]. Therefore, our finding that the autism candidate gene Nbea affects the intrinsic plasticity of granule cells highlights the importance of studying non-synaptic mechanisms of plasticity. Further research will be necessary to unravel the precise molecular mechanisms of this proposed function, but the difference in population spike LTP we observed suggests that there are important functional consequences to this difference in excitability.

## Methods

**Animals.** Animal experiments were performed with every effort to minimise animal suffering and in accordance with local institutional and governmental regulations regarding the use of laboratory animals both at the University of Münster as approved by the Landesamt für Natur, Umwelt und Verbraucherschutz (LANUV, NRW, Germany) under license numbers 84-02.05.20.11.209 and 84-02.04.2015.A423 and at the University of Frankfurt as approved by the Regierungspräsidium Darmstadt and the animal welfare officer responsible for the institution. All experiments were performed on 2- to 5-month-old male heterozygous Neurobeachin ($Nbea^{+/-}$) mice and wild-type littermate controls. Genotyping and characterisation of this mouse line was carried out as reported previously[5,8]. Electrophysiological measurements and all data analyses were carried out by investigators blind to the genotype.

**Anaesthesia and surgery.** Urethane (Sigma-Aldrich, Munich, Germany) solution (1.25 g of urethane in 10 ml 0.9% NaCl solution) was used to anaesthetise the animals with an initial injection (1.2 g/kg body weight) applied intraperitoneally. Supplemental doses (0.2-0.5 g/kg) were injected subcutaneously until the interdigital reflex could no longer be triggered. The body temperature of the animal was constantly controlled through a rectal probe and maintained at 36.5–37.5°C using a heating pad. For local anaesthesia of the scalp prilocainhydrochloride with adrenalin 1:200,000 (Xylonest 1%, AstraZeneca, Wedel, Germany) was injected subcutaneously at the site of incision. The head of the anaesthetised mouse was placed into a stereotactic frame for accurate insertion of electrodes. The ideal electrode positions were based on a mouse brain atlas[58] and adjusted according to our previous experience of perforant path stimulation in mice in vivo[22,24]. After drilling the stimulation and recording holes into the skull and removing the dura mater, a bipolar stimulation electrode (NE-200, 0.5 mm tip separation, Rhodes Medical Instruments, Summerland, CA, USA or PBSC1075, 1.0 mm tip separation, FHC, Bowdoin, ME, USA) was lowered into the angular bundle of the perforant path (coordinates: 2.5 mm lateral and 3.7 mm posterior to bregma, 1.8 mm below the brain surface). A glass or tungsten recording electrode was positioned above the suprapyramidal granule cell layer (GCL) of the dentate gyrus (coordinates: 1.0 mm lateral and 1.7 mm posterior to bregma). Borosilicate glass capillaries were pulled using a horizontal puller (DMZ-Universal-Electrode-Puller, Zeitz Instrumente, Martinsried, Germany) and filled with physiological saline solution. The tungsten microlectrodes (TM33B01KT, World Precision Instruments, Sarasota, FL) had an impedance of 0.1 MΩ. The recording electrode was lowered into the tissue in 0.05-0.1 mm increments while monitoring the laminar profile of the response evoked by a 500 µA/0.1 ms stimulus. A positive-going EPSP with a superimposed population spike at a latency of approximately 4 ms indicated that the recording electrode had reached the granule cell layer or hilus of the dentate gyrus and that the stimulation electrode had been correctly positioned in the more medial aspect of the perforant path[59].

**Stimulation protocols and data analysis.** Current pulses (20-800 µA, 0.1-0.2 ms duration) were generated by a stimulus generator (STG1004, Multichannel Systems, Reutlingen, Germany). The recorded field excitatory post-synaptic potentials (fEPSPs) were first amplified (P55 preamplifier, Grass Technologies, West Warwick, RI, USA) and then digitized at 10 kHz for visualisation and offline analysis (Digidata 1440A, Molecular Devices, Union City, CA, USA). The analysis of electrophysiological data was executed using Clampfit 10.2 software (Molecular Devices, Union City, MA, USA) as well as custom Matlab scripts (Mathworks, Natick, MA, USA).

Input-output recordings determine granule cell responses to different stimulation intensities and allow insight into properties of basal excitatory transmission in the dentate gyrus. Three responses were collected and averaged for each stimulus intensity ranging from 30 to 800 µA (0.1 ms stimulus duration). The amplitude of the population spike was defined as the average of the amplitude from the first positive peak to the antipeak and the amplitude from the antipeak

to the second positive peak. Only those mice that exhibited a population spike at a stimulation intensity of 300 µA or less were included in the analysis to avoid including mice in which the stimulation electrode was not optimally placed. For the analysis of the slope of the fEPSP, only the early component of the waveform, which is less affected by the population spike, was used. In the analysis relating the fEPSP slope to spike amplitude (E-S plot) each curve was fitted using a Boltzmann function.

In order to investigate the conditions of the presynaptic membrane at perforant path-granule cell synapses, paired-pulse facilitation (PPF) of the fEPSP was measured. To achieve PPF of the fEPSP, two subsequent pulses at an intensity below the population spike threshold (between 20 and 120 µA/0.2 ms), with interpulse intervals (IPIs) varying from 15 to 100 ms were applied. Six paired-pulse responses at each IPI were collected and averaged, and the percentage of facilitation was calculated as relative potentiation of the second fEPSP to the first fEPSP.

Paired-pulse inhibition (PPI) and disinhibition (PPDI) of the population spike were examined to assess the efficacy of inhibition in the hippocampal network. Two pulses at weak stimulation intensities (evoking approximately 1 mV population spikes) were delivered with an IPI ranging from 20 ms to 100 ms. A total of six paired-pulse responses were recorded at each IPI and averaged. The percentage of change of the population spike amplitude was calculated as the relative change of the spike amplitude following the second pulse in comparison to the spike amplitude following the first one. A Boltzmann equation was used to fit PPI/PPDI curves, hereby obtaining the mean IPI at which the amplitudes of both population spikes are expected to be equal.

As a measure of synaptic plasticity and long-term potentiation (LTP), we compared responses with baseline stimulation prior to theta-burst stimulation (TBS) with responses subsequent to TBS. TBS is an effective LTP induction protocol, as the optimal repetition rate corresponds to the frequency of the hippocampal theta rhythm, an EEG pattern previously related indirectly to memory storage processes[60]. LTP was induced using weak TBS (i.e. three series of six trains of six pulses at 400 Hz, with 0.2 s between trains and 20 s between series) alone or a combination of weak TBS followed by strong TBS (i.e. six series of six trains of six pulses at 400 Hz, with 0.2 s between trains and 20 s between series) 30 min later[22]. Both the pulse width and the stimulus intensity during TBS were doubled in comparison to baseline recordings. The intensity of the baseline stimulus was set to generate a reliable population spike in order to examine the differences in LTP of the population spike. Since the potentiated population spike was often so large as to obscure the initial slope of the fEPSP, we performed another set of experiments in which the baseline stimulation intensity was set to elicit a minimal population spike. The maximum allowable baseline stimulus intensity was 400 µA. The potentiation of the population spike/fEPSP slope was expressed as a percentage change relative to the pre-TBS baseline.

**Histology.** Following the electrophysiological recordings, some mice were transcardially perfused in deep anaesthesia with 4% paraformaldehyde (PFA) in 0.1 M PBS. Brains were removed and post-fixed overnight in 4% PFA/0.1 M PBS at 4 °C. After embedding in Agar, 50 µm thick coronal sections were cut with a vibratome (Leica VT 1000 s, Wetzlar, Germany) and stored in cryoprotection solution (30% ethylene glycol, 20% glycerin in PBS) at – 20 °C until further use. Hippocampal sections were stained with 0.1% toluidine blue aqueous solution, differentiated in ethanol, and mounted on glass slides with DPX (all chemicals from Merck, Darmstadt, Germany). Finally, the sections were viewed under a microscope (Olympus BX40, Tokyo, Japan) to verify the correct placement of the stimulation and recording electrodes (Supplementary Figure S1).

**Electron microscopy.** Brain tissue from wild-type and Nbea$^{+/-}$ mice was embedded in epon resin (Electron Microscopy Science, EMS, Hatfield, USA). For embedding, anaesthetised adult male mice were transcardially perfused with 25 ml of 2% glutaraldehyde (Roth, Karlsruhe,

Germany) and 2% PFA (Merck, Darmstadt, Germany) in 0.1 M PB at 37 °C, and postfixed at 4 °C overnight. Blocks of hippocampal tissue were contrasted in 1% osmium tetroxide for 2 h at room temperature. Following washes with distilled water and dehydrating, tissue was incubated with propylene oxide (EMS) for 45 min, infiltrated with propylene oxide/epon (1:1) for 1 h, in pure epon overnight, and hardened at 60 °C for 24 h. Additional contrasting of thin sections from brains was done on Formvar-coated copper grids with a saturated solution of 12% uranyl acetate and lead citrate.

For direct comparison with electrophysiological analysis, coronal samples containing the middle molecular layer (MML) of the dorsal hippocampal dentate gyrus 1.9 mm posterior to bregma, representing the major termination area of the perforant pathway, were investigated. Ultrastructural analysis was done with a transmission electron microscope (Libra 120, Zeiss) at 80 kV, and images taken with a CCD camera (Tröndle, Moorenweis, Germany). For quantifying the density of asymmetric synapses, tissue areas of 225 µm² were reconstructed from 9 individual images and 7 of these reconstructions (total area of 1575 µm²) analysed per genotype (n=7 reconstructions from 2 animals per genotype). Asymmetric (type 1) synapses were defined as contacts with a visible synaptic cleft, a distinct postsynaptic density and at least three synaptic vesicles.

**Statistical analysis.** All statistical analyses were performed using the software Prism 7 for Windows or Mac (GraphPad Software, La Jolla, CA, USA). Electrophysiological and ultrastructural data were tested for statistical significance using an unpaired Student's *t* test (with Welch's correction if the variance or group sizes differed) or a two-way analysis of variance (ANOVA) with Bonferroni's multiple-comparison post-tests. The Shapiro-Wilk test was used to determine whether the samples were drawn from a normal distribution. A two-tailed P-value lower than 0.05 was considered to be significant. Group values are reported as means ± standard error of the mean (SEM).

## Data availability

All data will be made available upon request.

Received: 29 October 2019; Accepted: 7 September 2020; Published online: 29 September 2020

## References


1. Cullinane, A. R., Schäffer, A. A. & Huizing, M. The BEACH Is Hot: A LYST of Emerging Roles for BEACH-Domain Containing Proteins in Human Disease. *Traffic* **14**, 749–766 (2013).

2. Wang, X. et al. Neurobeachin: A protein kinase A-anchoring, beige/Chediak-higashi protein homolog implicated in neuronal membrane traffic. *J. Neurosci.* **20**, 8551–8565 (2000).

3. Castermans, D. et al. SCAMP5, NBEA and AMISYN: Three candidate genes for autism involved in secretion of large dense-core vesicles. *Hum. Mol. Genet.* **19**, 1368–1378 (2010).

4. Nair, R. et al. Neurobeachin regulates neurotransmitter receptor trafficking to synapses. *J. Cell Biol.* **200**, 61–80 (2013).

5. Medrihan, L. et al. Neurobeachin, a protein implicated in membrane protein traffic and autism, is required for the formation and functioning of central synapses. *J. Physiol.* **587**, 5095–5106 (2009).

6. Su, Y. et al. Neurobeachin is essential for neuromuscular synaptic transmission. *J. Neurosci.* **24**, 3627–3636 (2004).

7. Farzana, F. et al. Neurobeachin regulates glutamate- and GABA-receptor targeting to synapses via distinct pathways. *Mol. Neurobiol.* **53**, 2112–2123 (2016).

8. Niesmann, K. et al. Dendritic spine formation and synaptic function require neurobeachin. *Nat. Commun.* **2**, 510–557 (2011).

9. Repetto, D. et al. Molecular dissection of neurobeachin function at excitatory synapses. *Front. Synaptic Neurosci.* **10**, 1–17 (2018).

10. Gromova, K. V. et al. Neurobeachin and the kinesin KIF21B are critical for endocytic recycling of NMDA receptors and regulate social behavior. *Cell Rep.* **23**, 2705–2717 (2018).

11. Nuytens, K. et al. Platelets of mice heterozygous for neurobeachin, a candidate gene for autism spectrum disorder, display protein changes related to aberrant protein kinase A activity. *Mol. Autism* **4**(1), 43 (2013).

12. Tuand, K. et al. Nuclear localization of the autism candidate gene neurobeachin and functional interaction with the NOTCH1 intracellular domain indicate a role in regulating transcription. *PLoS One* **11**, 1–23 (2016).

13. Castermans, D. et al. The neurobeachin gene is disrupted by a translocation in a patient with idiopathic autism. *J. Med. Genet.* **40**, 352–356 (2003).

14. Ritvo, E. R., Mason-Brothers, A., Menkes, J. H. & Sparkes, R. S. Association of autism, retinoblastoma, and reduced esterase D activity. *Arch. Gen. Psychiatry* **45**, 600 (1988).

15. Smith, M. et al. Molecular genetic delineation of a deletion of chromosome 13q12→q13 in a patient with autism and auditory processing deficits. *Cytogenet. Genome Res.* **98**, 233–239 (2002).

16. Reddy, K. S. Cytogenetic abnormalities and fragile-x syndrome in Autism Spectrum Disorder. *BMC Med. Genet.* **6**, 1–16 (2005).

17. Bowling, K. M. et al. Genomic diagnosis for children with intellectual disability and/or developmental delay. *Genome Med.* **9**, 1–11 (2017).

18. Savelyeva, L., Sagulenko, E., Schmitt, J. G. & Schwab, M. The neurobeachin gene spans the common fragile site FRA13A. *Hum. Genet.* **118**, 551–558 (2006).

19. Iossifov, I. et al. Low load for disruptive mutations in autism genes and their biased transmission. *Proc. Natl. Acad. Sci.* **112**, E5600–E5607 (2015).

20. Nuytens, K. et al. Haploinsufficiency of the autism candidate gene Neurobeachin induces autism-like behaviors and affects cellular and molecular processes of synaptic plasticity in mice. *Neurobiol. Dis.* **51**, 144–151 (2013).

21. Lee, B. et al. The Possible Role of Neurobeachin in Extinction of Contextual Fear Memory. *Sci. Rep.* **8**, 1–14 (2018).

22. Jedlicka, P. et al. Neuroligin-1 regulates excitatory synaptic transmission, LTP and EPSP-spike coupling in the dentate gyrus in vivo. *Brain Struct. Funct.* **220**, 47–58 (2015).

23. Zucker, R. S. & Regehr, W. G. Short-term synaptic plasticity. *Annu. Rev. Physiol.* **64**, 355–405 (2002).

24. Jedlicka, P. et al. Impairment of in vivo theta-burst long-term potentiation and network excitability in the dentate gyrus of synaptopodin-deficient mice lacking the spine apparatus and the cisternal organelle. *Hippocampus* **19**, 130–140 (2009).

25. Bronzino, J. D., Abu-Hasaballah, K., Austin-LaFrance, R. J. & Morgane, P. J. Maturation of long-term potentiation in the hippocampal dentate gyrus of the freely moving rat. *Hippocampus* **4**, 439–446 (1994).

26. Sloviter, R. S. Feedforward and feedback inhibition of hippocampal principal cell activity evoked by perforant path stimulation: GABA-mediated mechanisms that regulate excitability in vivo. *Hippocampus* **1**, 31–40 (1991).

27. Andersen, P., Sundberg, S. H., Sveen, O., Swann, J. W. & Wigström, H. Possible mechanisms for long-lasting potentiation of synaptic transmission in hippocampal slices from guinea pigs. *J. Physiol.* **302**, 463–482 (1980).

28. Marder, C. P. & Buonomano, D. V. Timing and balance of inhibition enhance the effect of long-term potentiation on cell firing. *J. Neurosci.* **24**, 8873–8884 (2004).

29. Jedlicka, P., Muellerleile, J. & Schwarzacher, S. W. Synaptic plasticity and excitation-inhibition balance in the dentate gyrus: insights from in vivo recordings in neuroligin-1, neuroligin-2, and collybistin Knockouts. *Neural Plasticity* https://doi.org/10.1155/2018/6015753 (2018).

30. Bronzino, J. D., Blaise, J. H. & Morgane, P. J. The paired-pulse index: A measure of hippocampal dentate granule cell modulation. *Ann. Biomed. Eng.* **25**, 870–873 (1997).

31. Jedlicka, P., Deller, T. & Schwarzacher, S. W. Computational modeling of GABAA receptor-mediated paired-pulse inhibition in the dentate gyrus. *J. Comput. Neurosci.* **29**, 509–519 (2010).

32. Brucato, F. H., Mott, D. D., Lewis, D. V. & Swartzwelder, H. S. GABAB receptors modulate synaptically-evoked responses in the rat dentate gyrus, in vivo. *Brain Res.* **677**, 326–332 (1995).

33. Migaud, M. et al. Enhanced long-term potentiation and impaired learning in mice with mutant postsynaptic density-95 protein. *Nature* **396**, 433–439 (1998).

34. Uetani, N. et al. Impaired learning with enhanced hippocampal long-term potentiation in PTP$\delta$-deficient mice. *EMBO J.* **19**, 2775–2785 (2000).

35. Gu, Y. et al. Impaired conditioned fear and enhanced long-term potentiation in Fmr2 knockout mice. *J. Neurosci.* **22**, 2753–2763 (2002).

36. Meng, Y. et al. Abnormal spine morphology and enhanced LTP in LIMK-1 knockout mice. *Neuron* **35**, 121–133 (2002).

37. Rutten, K. et al. Enhanced long-term potentiation and impaired learning in phosphodiesterase 4D-knockout (PDE4D$^{-/-}$) mice. *Eur. J. Neurosci.* **28**, 625–632 (2008).

38. Kim, M. H. et al. Enhanced NMDA receptor-mediated synaptic transmission, enhanced long-term potentiation, and impaired learning and memory in mice lacking IRSp53. *J. Neurosci.* **29**, 1586–1595 (2009).

39. Morris, R. G. M., Garrud, P., Rawlins, J. N. P. & O'Keefe, J. Place navigation impaired in rats with hippocampal lesions. *Nature* **297**, 681–683 (1982).

40. Kleschevnikov, A. M. & Marchbanks, R. M. Behavioral parameters of the spatial memory correlate with the potentiation of the population spike, but not with the population excitatory postsynaptic potential, of the CA1 region in rat hippocampal slices. *Neurosci. Lett.* **152**, 125–128 (1993).

41. Beer, Z. et al. The memory for time and space differentially engages the proximal and distal parts of the hippocampal subfields CA1 and CA3. *PLoS Biol.* **16**, 1–21 (2018).

42. Sasaki, T. et al. Dentate network activity is necessary for spatial working memory by supporting CA3 sharp-wave ripple generation and prospective firing of CA3 neurons. *Nat. Neurosci.* **21**, 258–269 (2018).

43. McHugh, T. J. et al. Dentate gyrus NMDA receptors mediate rapid pattern separation in the hippocampal network. *Science* **317**, 94–99 (2007).

44. Taverna, F. A. et al. Defective place cell activity in nociceptin receptor knockout mice with elevated NMDA receptor-dependent long-term potentiation. *J. Physiol.* **565**, 579–591 (2005).

45. Han, Z. -S, Buhl, E. H., Lörinczi, Z. & Somogyi, P. A High Degree of Spatial Selectivity in the Axonal and Dendritic Domains of Physiologically Identified Local-circuit Neurons in the Dentate Gyrus of the Rat Hippocampus. *Eur. J. Neurosci.* **5**, 395–410 (1993).

46. del Pino, I., Paarmann, I., Karas, M., Kilimann, M. W. & Betz, H. The trafficking proteins Vacuolar Protein Sorting 35 and Neurobeachin interact with the glycine receptor $\beta$-subunit. *Biochem. Biophys. Res. Commun.* **412**, 435–440 (2011).

47. Belle, A. M. et al. Evaluation of in vitro neuronal platforms as surrogates for in vivo whole brain systems. *Sci. Rep.* **8**, 1–9 (2018).

48. Taube, J. S. & Schwartzkroin, P. A. Mechanisms of long-term potentiation: EPSP/spike dissociation, intradendritic recordings, and glutamate sensitivity. *J. Neurosci.* **8**, 1632–1644 (1988).

49. Carpenter-Hyland, E., Bichler, E. K., Smith, M., Sloviter, R. S. & Benveniste, M. Epileptic pilocarpine-treated rats exhibit aberrant hippocampal EPSP-spike potentiation but retain long-term potentiation. *Physiol. Rep.* **5**, 1–19 (2017).

50. Xu, J., Kang, N., Jiang, L., Nedergaard, M. & Kang, J. Activity-dependent long-term potentiation of intrinsic excitability in hippocampal CA1 pyramidal neurons. *J. Neurosci* **25**, 1750–1760 (2005).

51. Frick, A., Magee, J. & Johnston, D. LTP is accompanied by an enhanced local excitability of pyramidal neuron dendrites. *Nat. Neurosci.* **7**, 126–135 (2004).

52. Lin, L., Sun, W., Wikenheiser, A. M., Kung, F. & Hoffman, D. A. KChIP4a regulates Kv4.2 channel trafficking through PKA phosphorylation. *Mol. Cell. Neurosci.* **43**, 315–325 (2010).

53. Nestor, M. W. & Hoffman, D. A. Differential cycling rates of Kv4.2 channels in proximal and distal dendrites of hippocampal CA1 pyramidal neurons. *Hippocampus* **22**, 969–980 (2012).

54. Lopez-Rojas, J., Heine, M. & Kreutz, M. R. Plasticity of intrinsic excitability in mature granule cells of the dentate gyrus. *Sci. Rep.* **6**, 21615 (2016).

55. Bourgeron, T. A synaptic trek to autism. *Curr. Opin. Neurobiol.* **19**, 231-234 https://doi.org/10.1016/j.conb.2009.06.003 (2009)

56. Wang, X., Kery, R. & Xiong, Q. Synaptopathology in autism spectrum disorders: complex effects of synaptic genes on neural circuits. *Prog. Neuro-Psychopharmacol. Biol. Psychiatry* **84**, 398–415 (2018).

57. Krueppel, R., Remy, S. & Beck, H. Dendritic integration in hippocampal dentate granule cells. *Neuron* **71**, 512–528 (2011).

58. Franklin, K. B. J. & Paxinos, G. *The Mouse Brain in Stereotaxic Coordinates* (Academic Press London, 1997).

59. Cooke, S. F. et al. Autophosphorylation of $\alpha$CaMKII is not a general requirement for NMDA receptor-dependent LTP in the adult mouse. *J. Physiol.* **574**, 805–818. https://doi.org/10.1113/jphysiol.2006.111559 (2006)

60. Larson, J. & Lynch, G. Role of N-methyl-D-aspartate receptors in the induction of synaptic potentiation by burst stimulation patterned after the hippocampal theta-rhythm. *Brain Res.* **441**, 111–118 (1988).

## Acknowledgments

The authors' work was supported by grants from the Deutsche Forschungsgemeinschaft (DFG) to P.J. (JE 528/6-1) and M.M. (Mi479/6-1) and by a LOEWE Grant from the State of Hesse for the "Center for Personalized Translational Epilepsy Research" (CePTER), Goethe-University Frankfurt to S.W.S.

## Author contributions

A.B. and J.M. performed the electrophysiological experiments, analysed data, and wrote the paper. A.R. and F.S. performed electron microscopy experiments and analysed data. M.M. designed experiments, supervised the research, provided essential mouse strains, and wrote the paper. P.J. and S.W.S. designed experiments, supervised the research, and wrote the paper.

## Funding

Open Access funding enabled and organized by Projekt DEAL.

## Competing interests

The authors declare no competing interests.

## Additional Information

**Supplementary Information** is available for this paper at https://doi.org/10.1038/s41598-020-72925-4.

**Correspondence** and requests for materials should be addressed to J.M. or A.B.

**Reprints and permissions information** is available at www.nature.com/reprints.

**Publisher's note** Springer Nature remains neutral with regard to jurisdictional claims in published maps and institutional affiliations.

## Supplementary Information

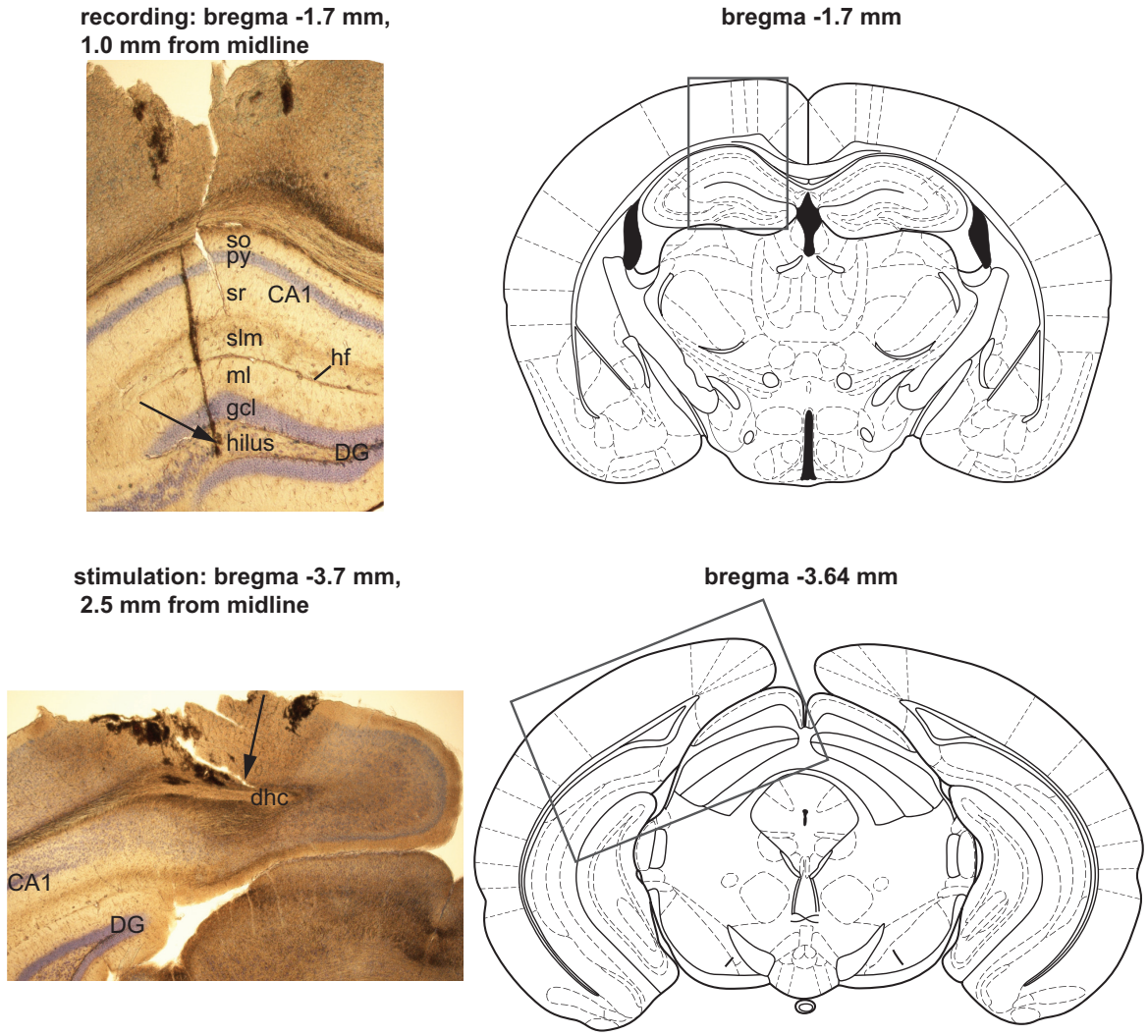


FIGURE S1: Histological verification of stimulation and recording sites. Nissl-stained sections showing the recording electrode position in the hilus of the dentate gyrus (DG) (top left) and the stimulation electrode placement in the angular bundle of the perforant path (bottom left) in one mouse. Arrows indicate the electrode tracks. Anatomical regions were labeled using a mouse brain atlas (reprinted with permission from *The mouse brain in stereotaxic coordinates*, K. B. J. Franklin & G. Paxinos, Figures 45 and 61, Academic Press, 2001). Abbreviations: CA1=cornu ammonis 1, DG=dentate gyrus, gcl=granule cell layer, hf=hippocampal fissure, dhc=dorsal hippocampal commissure, ml=molecular layer, py=pyramidal cell layer, slm=stratum lacunosum moleculare, so=stratum oriens, sr=stratum radiatum.

## Chapter 4

# Manuscript 2

## Neuroligin-3 Regulates Excitatory Synaptic Transmission and EPSP-Spike Coupling in the Dentate Gyrus In Vivo

*published in*
Molecular Neurobiology

**Declaration of author contributions to the manuscript: "Neuroligin-3 Regulates Excitatory Synaptic Transmission and EPSP-Spike Coupling in the Dentate Gyrus In Vivo"**

Status: *accepted*

name of journal: *Molecular Neurobiology*

Contributing authors: Julia Muellerleile, Matej Vnencak, Angelo Ippolito, Dilja Krueger-Burg, Tassilo Jungenitz, Stephan W. Schwarzacher, Peter Jedlička

**What are the contributions of the doctoral candidate and her co-authors?**

**(1) Concept and design**
Doctoral candidate: 0%
Co-author Matej Vnencak: 0%
Co-author Angelo Ippolito: 0%
Co-author Dilja Krueger-Burg: 30%
Co-author Tassilo Jungenitz: 0%
Co-author Stephan W. Schwarzacher: 35%
Co-author Peter Jedlička: 35%

**(2) Conducting tests and experiments**
Doctoral candidate: 0%
Co-author Matej Vnencak: 60% (electrophysiological experiments, histology)
Co-author Angelo Ippolito: 20% (electrophysiological experiments)
Co-author Dilja Krueger-Burg: 20% (synaptosome preparation)
Co-author Tassilo Jungenitz: 0%
Co-author Stephan W. Schwarzacher: 0%
Co-author Peter Jedlička: 0%

**(3) Compilation of data sets and figures**
Doctoral candidate: 80% (compilation of Figures 1-4 and S1
Co-author Matej Vnencak: 0%
Co-author Angelo Ippolito: 0%
Co-author Dilja Krueger-Burg: 20% (compilation of Figure 5 and Table1)
Co-author Tassilo Jungenitz: 0%
Co-author Stephan W. Schwarzacher: 0%
Co-author Peter Jedlička: 0%

**(4) Analysis and interpretation of data**
Doctoral candidate: 50% (analysis of electrophysiological data and interpretation)
Co-author Matej Vnencak: 10% (analysis of electrophysiological data)
Co-author Angelo Ippolito: 0%
Co-author Dilja Krueger-Burg: 15% (analysis of synaptosome data, interpretation)
Co-author Tassilo Jungenitz: 15% (analysis of electrophysiological data and interpretation)
Co-author Stephan W. Schwarzacher: 5% (interpretation)
Co-author Peter Jedlička: 5% (interpretation)

**(5) Drafting of manuscript**
Doctoral candidate: 80% (original draft, editing)
Co-author Matej Vnencak: 0%
Co-author Angelo Ippolito: 0%
Co-author Dilja Krueger-Burg: 5% (editing)
Co-author Tassilo Jungenitz: 5% (editing)
Co-author Stephan W. Schwarzacher: 5% (editing)
Co-author Peter Jedlička: 5% (editing)

# Neuroligin-3 Regulates Excitatory Synaptic Transmission and EPSP-Spike Coupling in the Dentate Gyrus In Vivo

**Julia Muellerleile[1,2], Matej Vnencak[1], Angelo Ippolito[1,3], Dilja Krueger-Burg[4,5], Tassilo Jungenitz[1], Stephan W. Schwarzacher[1], Peter Jedlicka [1,6]**

[1] Institute of Clinical Neuroanatomy, Neuroscience Center, Goethe University Frankfurt, 60590 Frankfurt/Main, Germany

[2] Faculty of Biosciences, Goethe University Frankfurt, 60438 Frankfurt/Main, Germany

[3] Department of Anesthesia, Intensive Care Medicine and Pain Therapy, University Hospital Frankfurt, Goethe University, 60590 Frankfurt/Main, Germany

[4] Department of Molecular Neurobiology, Max Planck Institute of Experimental Medicine, 37075 Göttingen, Germany

[5] Department of Psychiatry and Psychotherapy, University Medical Center, Georg-August-University Göttingen, 37075 Göttingen, Germany

[6] Faculty of Medicine, Justus-Liebig-University Giessen, 35392 Giessen, Germany

Stephan W. Schwarzacher and Peter Jedlicka contributed equally to this work

correspondence to: Julia Muellerleile
muellerleile@med.uni-frankfurt.de

Received: 8 June 2021/ Accepted: 22 November 2021/ Published online: 29 November 2021

# Abstract

Neuroligin-3 (Nlgn3), a neuronal adhesion protein implicated in autism spectrum disorder (ASD), is expressed at excitatory and inhibitory postsynapses and hence may regulate neuronal excitation/inhibition balance. To test this hypothesis, we recorded field excitatory postsynaptic potentials (fEPSPs) in the dentate gyrus of Nlgn3-knockout (KO) and wildtype mice. Synaptic transmission evoked by perforant-path stimulation was reduced in KO mice, but coupling of the fEPSP to the population spike was increased, suggesting a compensatory change in granule cell excitability. These findings closely resemble those in neuroligin-1 (Nlgn1) KO mice and could be partially explained by the reduction in Nlgn1 levels we observed in hippocampal synaptosomes from Nlgn3 KO mice. However, unlike Nlgn1, Nlgn3 is not necessary for long-term potentiation. We conclude that while Nlgn1 and Nlgn3 have distinct functions, both are required for intact synaptic transmission in the mouse dentate gyrus. Our results indicate that interactions between neuroligins may play an important role in regulating synaptic transmission, and that ASD-related neuroligin mutations may also affect the synaptic availability of other neuroligins.

**Keywords:** Neuroligins, Autism Spectrum disorder, Synaptic transmission, In vivo electrophysiology, Synaptosomal preparation

## Introduction

Neuroligins are transmembrane cell adhesion proteins which are localized to the postsynaptic membrane and stabilize synapses by binding to presynaptic neurexin proteins [1]. There are several neuroligin genes in vertebrates, of which three—neuroligin-1 (Nlgn1), neuroligin-2 (Nlgn2), and neuroligin-3 (Nlgn3)—are highly conserved between rodents and humans [1]. Neuroligins have been implicated in synapse formation and maturation as well as neurotransmitter receptor trafficking via their interactions with scaffolding proteins such as PSD95 at excitatory postsynapses and gephyrin at inhibitory postsynapses [1]. Experiments in rodents have revealed that Nlgn1 is expressed only at excitatory synapses [2] and Nlgn2 is found mainly at inhibitory synapses [3]. In contrast, Nlgn3 is expressed at both types of synapses [4] and forms heterodimers with Nlgn1 [5]. Intriguingly, Nlgn3 has been implicated in autism spectrum disorder (ASD) in mutation screenings [6, 7]. Therefore, understanding the synaptic function of Nlgn3 and how it might relate to the cognitive and behavioral symptoms of ASD is a longstanding goal in neuroligin research.

There is compelling evidence for the involvement of Nlgn3 in the etiology of ASD. Mutations in Nlgn3 have been identified in several cases of ASD and intellectual disability [8]. Furthermore, Nlgn3 knockout (KO) rats and mice, as well as mice with an autism-associated Nlgn3 mutation, exhibit ASD-related behavioral abnormalities such as reduced sociability [9–11], impaired social memory [10, 12, 13], decreased vocalization [12, 14], increased repetitive behaviors [13, 15, 16] and hyperactivity [9, 12, 13, 16]. While there are various genetic, environmental, and epigenetic risk factors for ASD [17], several studies have found that many ASD-related genes are involved in synaptogenesis or synaptic function, which suggests that synaptic dysfunction is a common pathomechanism [18–20]. It has been proposed that changes in the expression of neuroligins might alter the balance of excitation to inhibition in single neurons [21], which could lead to secondary changes in network activity that give rise to the neurobehavioral symptoms of ASD [22].

Since Nlgn3 is expressed at both excitatory and inhibitory synapses, it is ideally positioned to regulate the neuronal excitation/inhibition (E/I) balance, which could include the functional control of Nlgn1 and Nlgn2. It was recently shown that the extracellular domains of Nlgn1 and Nlgn2 can be proteolytically cleaved in response to activity only if heterodimerized with Nlgn3 [23], representing one mechanism by which Nlgn3 could regulate the levels of functional Nlgn1 and Nlgn2. However, Nlgn3 appears to have additional, both synapse- and region-specific functions that differ from those of the other neuroligins. For instance, in contrast to Nlgn1, Nlgn3 mainly regulates AMPA-receptor-mediated transmission (but see [24]), whereas Nlgn1 is important for both AMPA- and NMDA-receptor-mediated transmission at hippocampal synapses [25–27]. Nlgn3 also appears to have a different selectivity for specific interneuron types in hippocampal area CA1 than Nlgn2 [28]. However, most studies of Nlgn3 function have relied on dissociated cultures or acute slice preparations, which cannot replicate all features of the intact brain. Therefore, we sought to analyze the contribution of Nlgn3 to E/I balance in vivo in the hippocampal dentate gyrus, which has been implicated in social recognition memory [29] in addition to other forms of learning and memory [30].

To this end, we recorded local field potentials evoked by stimulation of the perforant path, the main cortical projection to the dentate gyrus, in Nlgn3 KO and wildtype (WT) mice. Previous experiments in acute slices showed that Nlgn3 regulates AMPAR-mediated synaptic transmission at perforant path-granule cell (PP-GC) synapses [26]. Here, we show that the deletion of Nlgn3 leads to a reduction in excitatory synaptic transmission, similarly to what we observed in Nlgn1 KO mice [31]. In support of a stronger role at excitatory, as opposed to inhibitory, synapses, the expression of Nlgn1, but not Nlgn2, was reduced in hippocampal synaptosomes from Nlgn3 KO mice, indicating that Nlgn3 may partially exert its effects on synaptic function by regulating the synaptic availability of Nlgn1. Network inhibition in the dentate gyrus was

not impaired by the loss of Nlgn3, yet we observed an increase in the excitability of granule cells, a possible compensatory response to the reduced synaptic strength. We also found evidence for a functional segregation of Nlgn1 and Nlgn3 at PP-GC synapses regarding the regulation of long-term potentiation (LTP), in accordance with previous reports that Nlgn3 is not necessary for LTP at hippocampal synapses [26, 32]. Together, these results provide important insights into the physiological role of Nlgn3 at PP-GC synapses and can help explain the ASD-related social memory impairments in Nlgn3-deficient mice.

# Methods

## Animals

Animal experiments were performed in accordance with the German law regarding the use of laboratory animals (Tierschutz-Versuchstierverordnung) and were approved by the Regierungspräsidium Darmstadt and the animal welfare officer responsible for the institute. Male Nlgn3 KO mice (RRID: MGI:4353654) and WT littermate controls on a C57BL/6JRj background aged 8-12 weeks were used in all experiments. The generation of this mouse line was described previously [33]. Mice were housed in polycarbonate cages (Tecniplast) with woodchip bedding in a ventilated cabinet (Scantainer) at a 12-h light/dark cycle with access to food and water ad libitum. All experiments and analyses were carried out by investigators blind to the genotype.

## Surgery and Electrophysiology

The surgical and electrophysiological procedures were carried out as described previously [31] (see Supplementary Information for details). Briefly, urethane-anesthetized mice were placed into a stereotactic frame for the accurate insertion of electrodes at previously determined locations. A bipolar stimulation electrode (NE-200, 0.5 mm tip separation, Rhodes Medical Instruments, Summerland, CA, USA) was lowered into the angular bundle of the perforant path (coordinates: 3.7 mm posterior to bregma, 2.5 mm lateral to the midline, 1.8 mm below the brain surface). Then, a tungsten recording electrode (TM33A10KT, World Precision Instruments, Sarasota, FL, USA) was positioned above suprapyramidal granule cell layer of the dentate gyrus (coordinates: 1.7 mm posterior to bregma, 1.0 mm lateral to the midline) and lowered in 0.05-0.1 mm increments while monitoring the laminar profile of the response waveform elicited by a 500 µA/0.1 ms stimulus. The turn of the potential from negative to positive indicated that the recording electrode had reached the hilus of the dentate gyrus, the optimal recording site [34], and a population spike latency of approximately 4 ms indicated that the stimulation electrode had been correctly positioned in the more medial portion of the perforant path [35]. The stimulation protocols were applied in the following order: input-output (30-800 µA, 0.1 ms pulse duration), paired-pulse facilitation (20-120 µA double-pulse stimulation at intervals from 15 to 100 ms, 0.2 ms pulse duration), paired-pulse (dis)inhibition (minimal or maximal stimulation intensity, interpulse intervals from 15 to 1,000 ms, 0.2 ms pulse duration), and theta-burst stimulation (TBS) for the induction of LTP. The strong TBS protocol consisted of six series of six trains of six pulses at 400 Hz, with 0.2 s between trains and 20 s between series. The weak TBS protocol consisted of three series of TBS. For the baseline recordings, 0.1 ms pulses were repeated at 0.1 Hz with a stimulation intensity set to elicit a population spike in the range of 1-3 mV before LTP induction.

## Preparation of Hippocampal Synaptosomal Fractions and Immunoblot Analysis

The preparation of synaptosomal fractions was carried out as previously described [31] (see Supplementary Information for details). The following primary antibodies were used: Nlgn1 (RRID: AB_887747, Synaptic Systems, Göttingen, Germany), PSD-95 (RRID: AB_2877189, NeuroMAB, Davis, CA, USA), AMPA receptor subunit 1 (GluR1, RRID: AB_2113602, Chemicon, Temecula, CA, USA), AMPA receptor subunit 2 (GluR2, RRID: AB_2113732, Synaptic Systems, Göttingen, Germany), NMDA receptor subunit 1 (NR1, RRID: AB_887750, Synaptic Systems, Göttingen, Germany), vesicular glutamate transporter 1 (VGlut1, RRID: AB_887878, Synaptic Systems, Göttingen, Germany), vesicular inhibitory amino acid transporter (VIAAT, RRID: AB_2189938, Synaptic Systems, Göttingen, Germany), gephyrin (RRID: AB_887719, Synaptic Systems, Göttingen, Germany), actin (RRID: AB_258912, Sigma-Aldrich, St. Louis, MO, USA)

and Nlgn2 (antibody 799, Nils Brose). After washing and incubation with the secondary antibodies (Gt anti-M-IRDye800 and Gt anti Rb-IRDye680, LiCor Biosciences, Lincoln, NE, USA, and Gt-anti-GP-IRDye700, Rockland Immunochemicals, Gilbertsville, PA, USA), blots were scanned on an Odyssey Infrared Imager (LiCor Biosciences, Lincoln, NE, USA), and the signal intensity for each sample was quantified using the Odyssey 2.1 software. Each sample value was divided by the total protein loading value for the corresponding lane, and then normalized to the average sample value of all lanes on the same blot to correct for blot-to-blot variance. Data are expressed relative to the WT values.

### Statistical Analysis

To ensure comparable levels of anesthesia throughout the experiment, only those mice that exhibited a population spike by the 400 µA stimulation intensity and showed a successful induction of LTP ($>$ 10% increase in the pre-TBS fEPSP slope) were included in the statistical analysis.

Data were analyzed using GraphPad Prism 7 for Windows (GraphPad Software, San Diego, CA, USA) and figures were prepared using Adobe Illustrator CS6 (Adobe, San Jose, CA, USA). The normality of the distributions was first assessed using the Shapiro-Wilk test, and parametric data sets were compared using an unpaired two-tailed Student's *t*-test (with Welch's correction to account for different variances). If the data were non-normally distributed, a Wilcoxon signed-rank test was used instead. Data which differed in two variables were analyzed using a two-way repeated measures analysis of variance (ANOVA) followed by Bonferroni multiple-comparison tests, and normality was assessed by examining the quantile-quantile plots. A two-tailed *p*-value lower than 0.05 was considered significant. Group values are expressed as the means ± the standard error (SEM).

## Results

### Reduced Excitatory Synaptic Transmission at Perforant Path-Granule Cell Synapses in Nlgn3 Knockout Mice

We first investigated whether Nlgn3 affects excitatory transmission in the dentate gyrus by recording fEPSPs evoked by perforant path stimulation in anesthetized WT and Nlgn3 KO mice. Input-output curves of the fEPSP slope in response to increasing stimulation intensities revealed that on average, Nlgn3 KO mice ($n = 16$) responded with lower slopes compared to their WT littermates ($n = 20$) (Fig. 1a). Analyzing these results by two-way repeated measures ANOVA revealed a significant effect of the genotype ($p = 0.0033$) as well as the interaction between genotype and stimulation intensity ($p < 0.0001$). Subsequent Bonferroni multiple-comparison post-tests revealed that the fEPSP slopes in KO mice were significantly reduced at stimulation intensities ranging from 300-800 µA (300-450, 650-800 µA: $p < 0.05$; 500-600 µA: $p < 0.01$), but not at the lower stimulation intensities. This variable response to the different stimulation intensities might account for the significant interaction effect. However, since the mean fEPSP slope was reduced in Nlgn3 KO mice at nearly every stimulation intensity, we concluded that excitatory synaptic transmission from the perforant path to granule cells is impaired in Nlgn3 KO mice.

At low interpulse intervals, PP-GC synapses undergo facilitation of the fEPSP [36, 37], which is generally attributed to presynaptic calcium signaling and reflects a low initial vesicle release probability [38]. We used a paired-pulse stimulation protocol to test whether differences in the vesicle release probability could explain the reduction in synaptic transmission in Nlgn3 KO mice. When comparing the degree of facilitation across a range of interpulse intervals from 15 ms to 100 ms in 20 WT and 16 Nlgn3 KO mice, we observed a trend towards decreased PPF in the KO mice, but this difference did not reach statistical significance (two-way repeated measures ANOVA with Bonferroni post-tests, genotype: $p = 0.087$, interaction: $p = 0.272$, Fig. 1b).

### Altered Granule Cell Excitability and Increased EPSP-Spike Coupling in Nlgn3 Knockout Mice

Next, we examined whether the reduction in synaptic transmission in Nlgn3 KO mice led to a reduction in granule cell excitability measured by the amplitude of the population spike, which represents the firing activity of the granule cell population [39]. The main effect of the genotype on the population spike amplitude measured across the same range of stimulation intensities used for the input-output curve of the fEPSP slope was not significant (two-way repeated measures ANOVA with Bonferroni post-tests, genotype: $p = 0.33$, Fig. 2a). However, the effect of the interaction between genotype and stimulation intensity was significant ($p = 0.0074$), which might reflect a variable effect of the genotype at different stimulation intensities. Indeed, the Nlgn3 KO mice exhibited slightly higher spike amplitudes at lower stimulation intensities, but lower spike amplitudes at higher stimulation intensities, and approximately equal amplitudes at the highest stimulation intensities. Therefore, the effect of the Nlgn3 deletion on the excitability of granule cells appears to be stimulation-dependent.

To further study the interplay between synaptic transmission and excitability, we plotted the population spike amplitude against the fEPSP slope for each stimulation intensity of the input-output protocol, yielding the EPSP-spike plot (Fig. 2b). The curves for the WT and Nlgn3 KO mice diverged significantly along the x-axis, which we quantified by comparing the v50 values of the Boltzmann-fitted EPSP-spike plots for each individual (unpaired Welch's $t$-test, $p = 0.025$). As expected from the reduction in fEPSP slopes, the Nlgn3 KO mice had lower v50 values (KO: $0.80 \pm 0.05$, $n = 15$; WT: $1.0 \pm 0.07$, $n = 16$, Fig. 2b, inset). The maximum population

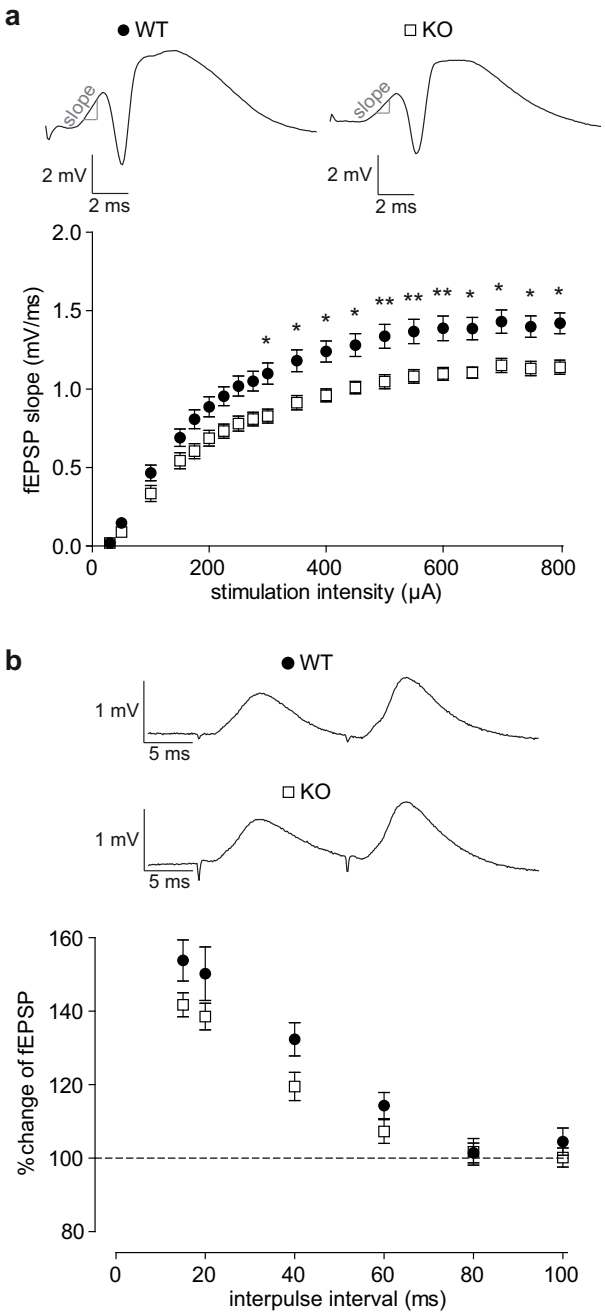


FIGURE 1: Impaired transmission at excitatory perforant path synapses in the dentate gyrus of Nlgn3-deficient mice is not caused by differences in the presynaptic vesicle release probability. (a) The input-output curves of the fEPSP slope elicited by increasing stimulation intensities from 30 to 800 µA reveal a decrease in the strength of PP-GC synapses in Nlgn3 KO ($n = 16$) mice compared to WT littermates ($n = 20$). Asterisks denote statistical significance determined by Bonferroni multiple comparison tests (*$p < 0.05$, **$p < 0.01$). *Top* Representative responses to 500 µA stimulation for one WT and one Nlgn3 KO mouse. (b) Facilitation of the PP-GC fEPSP elicited by double-pulse stimulation at interpulse intervals (IPI) from 15 to 100 ms is only slightly lower in Nlgn3 KO ($n = 16$) mice compared to WT littermates ($n = 20$). *Top* Representative responses to two pulses with a 15 ms IPI for one WT and one Nlgn3 KO mouse. Data are represented as $mean \pm SEM$

spike measured by the top parameter of the Boltzmann fit was not significantly different between groups (unpaired Welch's *t*-test, $p = 0.79$; WT: $4.03 \pm 0.23$; KO: $3.95 \pm 0.19$, data not shown), indicating that the Nlgn3 KO mice achieved similar population spike amplitudes with lower levels of synaptic transmission, i.e., enhanced EPSP-spike coupling.

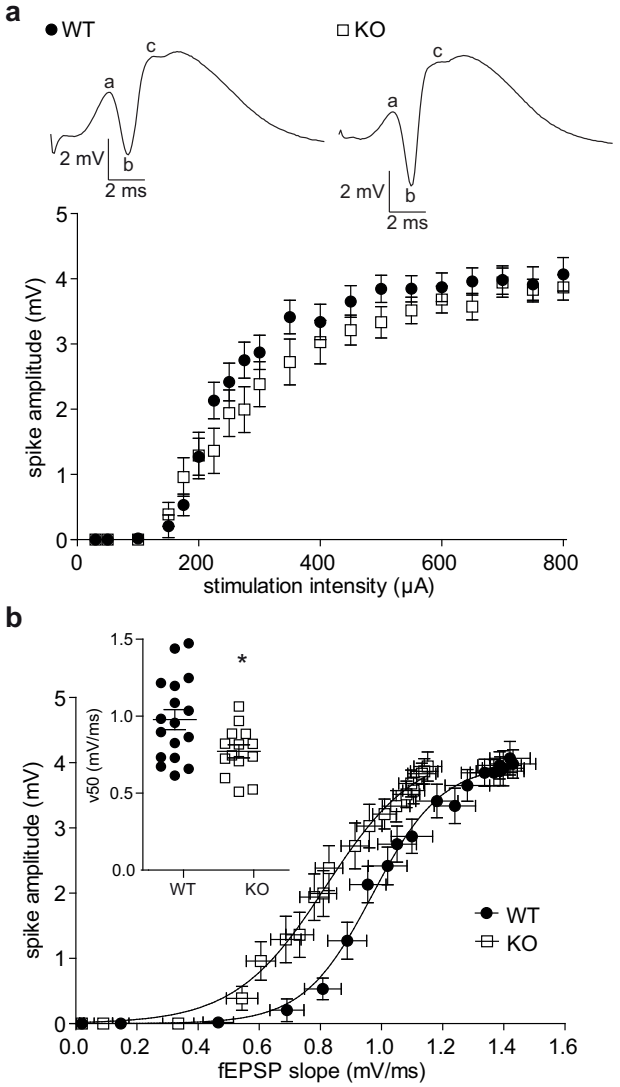


FIGURE 2: EPSP-spike coupling in dentate granule cells is increased in Nlgn3-deficient mice. (a) The input-output curve of the population spike elicited by perforant path stimulation at intensities from 30 to 800 µA reveals no significant difference between WT ($n = 20$) and Nlgn3 KO ($n = 16$) mice. *Top* Representative responses to 800 µA stimulation for one WT and one Nlgn3 KO mouse. The population spike amplitude was calculated from the difference between the first positive peak (a) and the antipeak (b) and the difference from the antipeak to the second positive peak (c) as follows: $((a - b) + (b - c))/2$ (b) Plotting the population spike amplitude against the fEPSP slope reveals a leftward shift in the EPSP-spike curve of Nlgn3 KO ($n = 16$) relative to WT ($n = 20$) mice. *Inset* shows the v50 values of the Boltzmann-fitted EPSP-spike curves, which differed significantly between WT ($n = 16$) and Nlgn3 KO ($n = 15$) mice (unpaired Welch's t-test, $^*p < 0.05$). Data are represented as $mean \pm SEM$

## Slight Alterations in the Level of Network Inhibition Experienced by Granule Cells in Nlgn3 KO Mice

An increase in EPSP-spike coupling could be caused by an increase in the intrinsic neuronal excitability, a decrease in the level of inhibition, or both. Granule cells experience both feedback

and feedforward inhibition from different classes of interneurons. Paired-pulse stimulation protocols can provide insight into the level of (primarily perisomatic) feedforward (and, to a lesser extent, feedback) inhibition by quantifying the inhibition of the second population spike [40]. To test for paired-pulse inhibition, we stimulated the perforant path at maximum intensity (800 µA) to recruit as many inhibitory interneurons as possible at interpulse intervals ranging from 15 ms to 1,000 ms and measured the degree of inhibition of the second population spike (Fig. 3). There was no significant main effect of the genotype on paired-pulse inhibition (two-way repeated measures ANOVA, $n = 20$ WT and 16 KO, $p = 0.89$), but the interaction between interpulse interval and genotype was significant ($p = 0.0047$). The suppression of the second population spike is mediated via the activation of $GABA_A$ receptors on granule cells [40]. However, at higher interpulse intervals, the inhibition turns into disinhibition due to the activation of metabotropic $GABA_B$ autoreceptors on interneuron terminals [41–43]. We interpolated the interpulse interval at which the amplitude of the second spike equaled that of the first spike with a Boltzmann fit of the curve to estimate the shift from PPI to PPDI in each animal. While the ANOVA results support an interaction between the genotype and the interpulse interval, the interpulse interval at which the PPI-PPDI shift occurred was not significantly different in Nlgn3 KO mice, ($44.90 \pm 0.85$ ms for WT vs. $47.04 \pm 1.20$ ms for KO, unpaired Welch's *t*-test, $p = 0.16$, Fig. 3a, inset). We repeated the same protocol using the minimum stimulation intensity needed to elicit a population spike and likewise found a significant interaction effect ($n = 19$ WT and 16 KO, two-way repeated measures ANOVA, $p = 0.022$), but no difference in the PPI-PPDI shift ($44.15 \pm 1.14$ ms for WT vs. $47.00 \pm 1.49$ ms for KO, unpaired Welch's *t*-test, $p = 0.16$, Fig. 3b, inset). Taken together, these results do not rule out a slight difference in the level of network inhibition in the dentate gyrus of Nlgn3 KO mice.

## No Evidence of Impaired Long-Term Potentiation at Perforant Path-Granule Cell Synapses in Nlgn3 Knockout Mice

Next, we investigated whether the reduction in the slopes of the fEPSPs we observed in Nlgn3 KO mice might manifest in reduced levels of synaptic plasticity. LTP induced by high frequency bursts repeated at the theta frequency is an effective experimental paradigm to investigate changes in plasticity of excitatory synapses [44]. We induced LTP using a previously established strong TBS protocol consisting of six series of six bursts of six pulses, the bursts were repeated at 5 Hz and the pulses within a burst were repeated at 400 Hz [35]. Both the Nlgn3 KO mice ($n = 10$) and their WT littermates ($n = 8$) showed a strong initial potentiation of the fEPSP slope which did not differ between groups (0-10 min, $137.7 \pm 4.7\%$ for WT vs. $137.3 \pm 4.1\%$ for Nlgn3 KO mice, unpaired Welch's *t*-test, $p = 0.95$, Fig. 4a). The potentiation remained similar between groups also towards the end of the recording period (50-60 min, $122.7 \pm 3.9\%$ for WT vs. $124.7 \pm 4.0\%$ for Nlgn3 KO, unpaired Welch's *t*-test, $p = 0.73$, Fig. 4a). The population spike also showed a similar initial degree of potentiation between groups ($156.4 \pm 10.6\%$ for WT vs. $165.3 \pm 12.8\%$ for Nlgn3 KO mice, unpaired Welch's *t*-test, $p = 0.60$, Fig. 4b). The groups also did not differ in the degree of potentiation towards the end of the recording period ($149.1 \pm 6.4\%$ for WT vs. $155.8 \pm 12.2\%$ for Nlgn3 KO, unpaired Welch's *t*-test, $p = 0.63$, Fig. 4b).

We reasoned that using a weaker TBS protocol to "prime" the synapses followed by a strong TBS protocol might amplify differences between groups, a strategy which had been successful in Nlgn1 KO mice [31]. Therefore, we first stimulated the perforant path with three series of TBS, followed by the strong TBS protocol 30 minutes later. This experimental manipulation revealed no differences between WT ($n = 10$) and Nlgn3 KO mice ($n = 5$) regarding the relative increase in the fEPSP slopes after the weak TBS (0-10 min, $134.7 \pm 3.4\%$ for WT vs. $147.2 \pm 7.5\%$ for Nlgn3 KO mice, unpaired Welch's *t*-test, $p = 0.18$, Fig. 4c) and after the strong TBS (30-40 min, $144.4 \pm 4.0\%$ for WT vs. $158.2 \pm 8.8\%$ for Nlgn3 KO mice, unpaired Welch's *t*-test, $p = 0.20$, Fig. 4c). There were also no significant differences between WT and Nlgn3 KO mice regarding

the relative increase in the population spike after the weak TBS (0-10 min, $170.5 \pm 12.8\%$ for WT vs. $146.7 \pm 14.2\%$ for Nlgn3 KO mice, unpaired Welch's *t*-test, $p = 0.24$, Fig. 4d) and after the strong TBS (30-40 min, $173.2 \pm 16.3\%$ for WT vs. $138.9 \pm 9.2\%$ for Nlgn3 KO mice, unpaired Welch's *t*-test, $p = 0.091$, Fig. 4d).

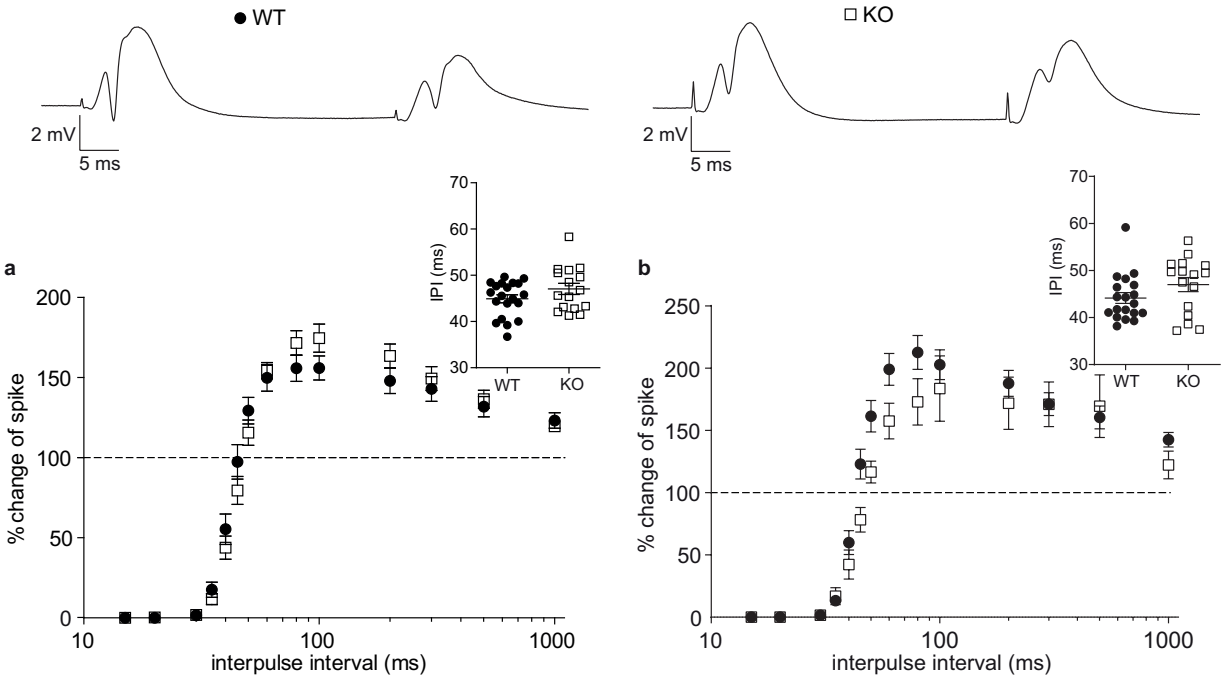


FIGURE 3: Paired-pulse experiments reveal a tendency towards increased network inhibition in the dentate gyrus of Nlgn3 KO mice. (a) Paired-pulse inhibition (PPI) of the granule cell population spike elicited by maximal intensity (800 µA) double-pulse stimulation at interpulse intervals from 15 to 1000 ms is similar between WT ($n = 20$) and Nlgn3 KO mice ($n = 16$). *Top* Representative responses to two pulses with a 40 ms IPI for one WT and one Nlgn3 KO mouse. *Inset* shows the interpulse interval at which the amplitude of the second spike equaled that of the first spike determined by a Boltzmann fit of the PPI curve, which was not significantly different between WT and Nlgn3 KO mice. (b) PPI of the granule cell population spike elicited by minimal intensity double-pulse stimulation at interpulse intervals from 15 to 1000 ms reveals a slight rightward shift in Nlgn3 KO ($n = 16$) compared to WT mice ($n = 19$). The minimum stimulation intensity that elicited a population spike was set for each mouse individually. *Inset* shows that the interpulse interval at which the amplitude of the second spike equaled that of the first spike determined by a Boltzmann fit of the PPI curve is similar in WT and Nlgn3 KO mice. Data are represented as $mean \pm SEM$

While there were no significant differences in the relative magnitude of LTP, comparing the absolute values of the fEPSP slopes revealed that Nlgn3 KO mice generally had lower slopes compared to the WT controls, as would be expected from the reduction in synaptic transmission observed in the input-output curves. The fEPSP slopes were not significantly different (determined by Welch's *t*-test) during the three time periods we measured in the single strong TBS experiments (pre-TBS baseline: $0.88 \pm 0.14$ mV/ms for WT vs. $0.68 \pm 0.04$ mV/ms for Nlgn3 KO mice, $p = 0.20$; 0-10 minutes: $1.25 \pm 0.22$ mV/ms for WT vs. $0.94 \pm 0.06$ mV/ms for Nlgn3 KO mice, $p = 0.22$; 50-60 minutes: $1.11 \pm 0.20$ mV/ms for WT vs. $0.86 \pm 0.08$ mV/ms for Nlgn3 KO, $p = 0.28$, Supplementary Fig. 1a). In the combined weak and strong TBS experiments, the slopes differed significantly during the pre-TBS baseline ($0.62 \pm 0.04$ mV/ms for WT vs. $0.46 \pm 0.04$ mV/ms for Nlgn3 KO mice, unpaired Welch's *t*-test, $p = 0.013$, Supplementary Fig. 1c), following the weak TBS ($0.83 \pm 0.05$ mV/ms for WT vs. $0.67 \pm 0.03$ mV/ms for Nlgn3 KO mice, unpaired Welch's *t*-test, $p = 0.012$, Supplementary Fig. 1c), and after the strong TBS

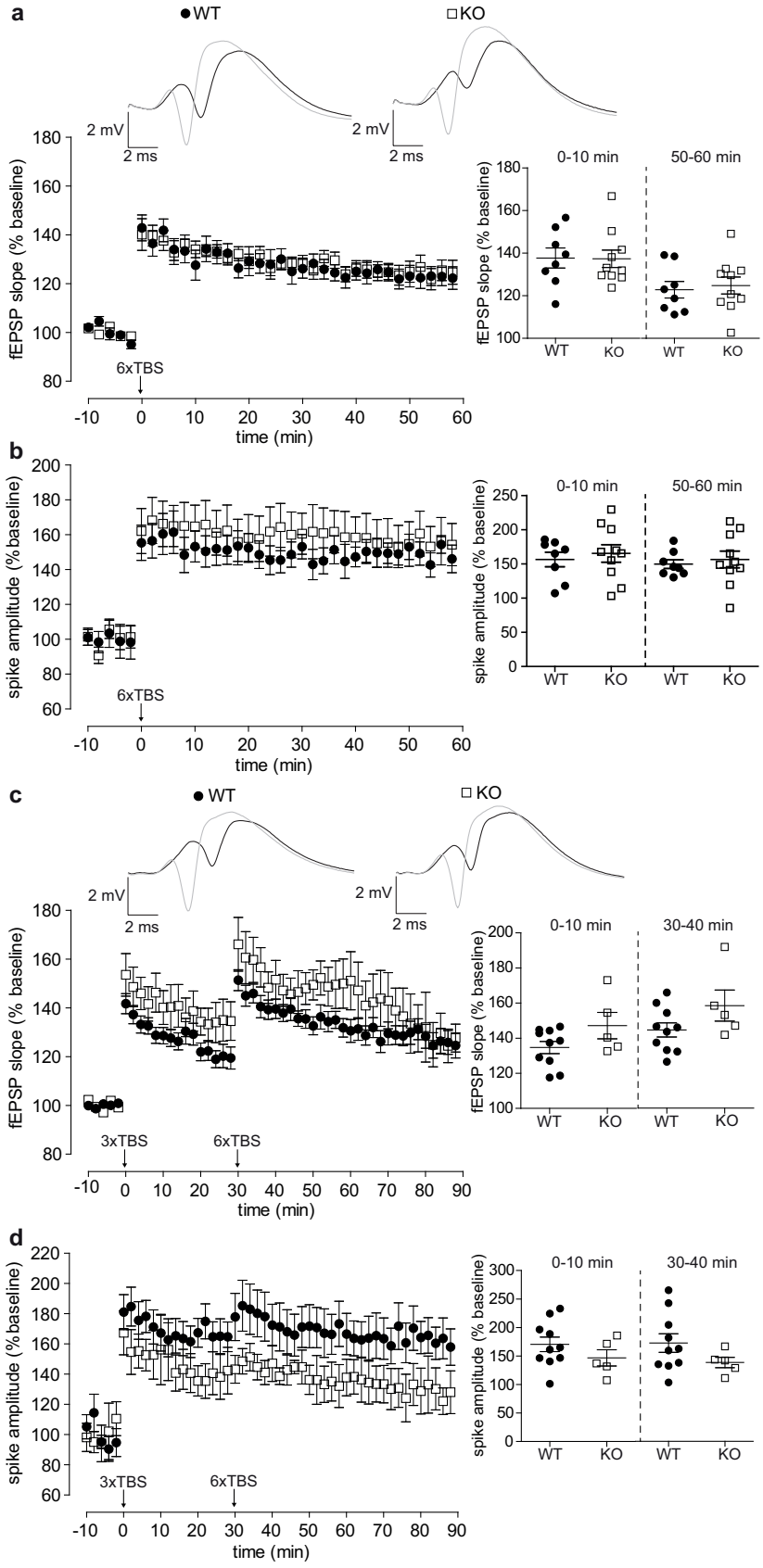


FIGURE 4: Nlgn3 KO mice exhibit no impairments of LTP at PP-GC synapses. (a) LTP induced by strong TBS (see Methods) is similar in WT ($n = 8$) and Nlgn3 KO ($n = 10$) mice. *Top* Representative traces of the averaged evoked responses of one WT and one Nlgn3 KO mouse to 0.1 Hz test pulses during the two minutes preceding (black) and the two minutes following (gray) TBS. *Diagrams* show the mean change in the fEPSP slope relative to the pre-TBS baseline from 0-10 min and 50-60 min following TBS.

(*continued on next page*)

FIGURE 4: (*continued from last page*) (b) The increase in the population spike amplitude following strong TBS is also similar in WT and Nlgn3 KO mice. *Diagrams* show the mean increase in the population spike relative to the pre-TBS baseline from 0-10 minutes and 50-60 min following TBS. (c) LTP induced by weak TBS (see Methods) followed by strong TBS of PP-GC synapses in WT ($n = 10$) and Nlgn3 KO ($n = 5$) mice. *Top* Representative traces of the averaged evoked responses of one WT and one Nlgn3 KO mouse to 0.1 Hz test pulses during the two minutes preceding (black) and the two minutes following (gray) the weak TBS. *Diagrams* show the mean increase in the fEPSP slopes relative to the pre-TBS baseline after weak TBS (0-10 min) and after strong TBS (30-40 min). (d) The increase in the population spike amplitude following the combined weak and strong TBS shows a trend towards greater potentiation in WT mice. *Diagrams* show the mean change in the population spike relative to the pre-TBS baseline after weak TBS and after strong TBS. Data are represented as $mean \pm SEM$. See also Fig. S1

($0.89 \pm 0.06$ mV/ms for WT vs. $0.72 \pm 0.04$ mV/ms for Nlgn3 KO mice, unpaired Welch's *t*-test, $p = 0.036$, Supplementary Fig. 1c). These data indicate that Nlgn3-deficient mice exhibited equally strong relative LTP despite a reduction in the absolute synaptic strength, which could be caused by a reduction in the number of functional synapses in these mice. At the same time, the absolute population spike amplitudes were not different between groups during the pre-TBS baseline (Supplementary Fig. 1b+d), as the stimulation intensity was adjusted to elicit an approximately 2 mV population spike during the pre-TBS baseline. Even after LTP induction, the population spike amplitudes did not differ significantly between groups. Therefore, the increased EPSP-spike coupling was maintained in Nlgn3 KO mice after LTP induction, even though the absolute levels of synaptic transmission were reduced.

## Reduced Nlgn1 and VGlut1 Protein Levels in Hippocampal Synaptosomes from Nlgn3 KO Mice

We asked whether the functional differences in synaptic transmission we had observed could be explained by changes in the expression levels of certain synaptic proteins. To this end, we analyzed the levels of several presynaptic (VGlut1, VIAAT) and postsynaptic (PSD95, GluR1, GluR2, NR1, gephyrin, Nlgn1, Nlgn2) proteins as well as actin using quantitative immunoblots from hippocampal synaptosomes (Fig. 5). Interestingly, we found that Nlgn1 was downregulated in Nlgn3 KO synaptosomes ($71.8 \pm 5.4\%$ compared to WT levels, $n = 17$ pairs, unpaired Student's t-test, $p < 0.001$, Table 1). VGlut1 was also significantly reduced in Nlgn3 KO synaptosomes ($81.1 \pm 7.3\%$ compared to WT levels, $n = 17$ pairs, Wilcoxon signed rank test, $p = 0.035$, Table 1). No other synaptic proteins were significantly up- or downregulated in Nlgn3 KO mice.

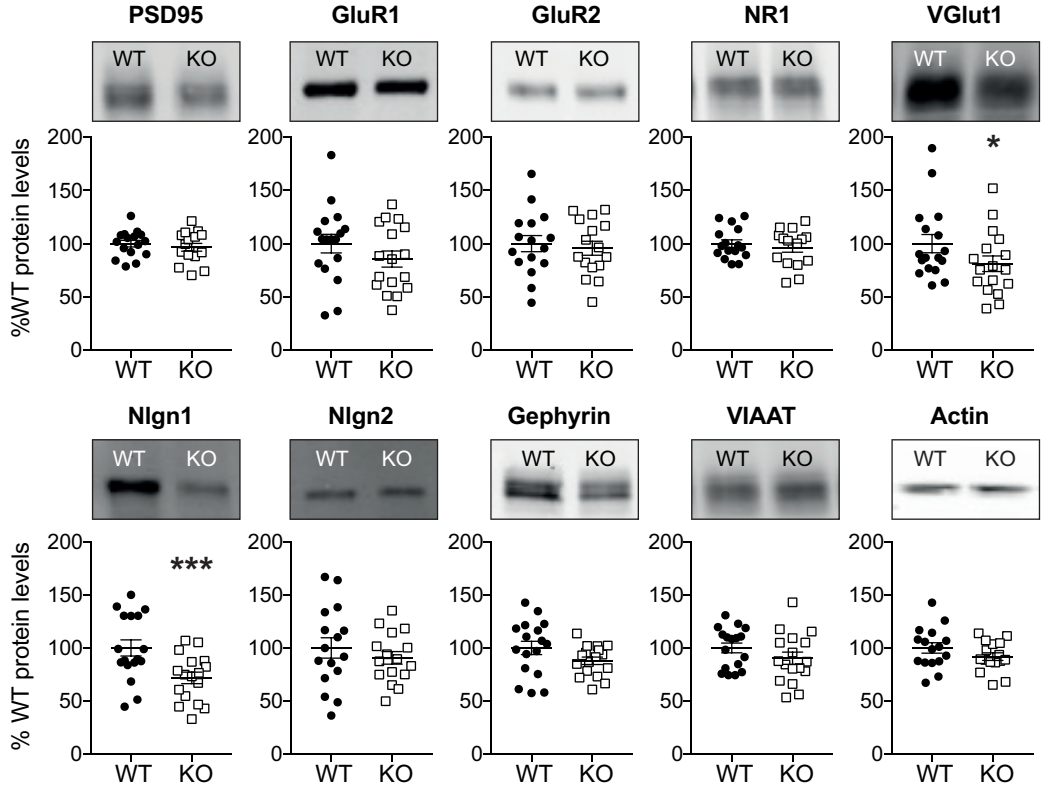


FIGURE 5: Nlgn3 deletion decreases VGlut1 and Nlgn1 expression levels in hippocampal synaptosomes. Representative immunoblots of hippocampal synaptosomes for each of the proteins and the quantification of the relative expression levels as a percentage of the WT protein level. Levels of VGlut1 and Nlgn1 were reduced in hippocampal synaptosomal preparations from Nlgn3 KO mice (8-12 weeks, $n = 16 - 17$ pairs, see Table 1). Asterisks denote statistical significance by Student's t-test or Wilcoxon signed-rank test ($^{*}p < 0.05$, $^{***}p < 0.001$). Data are represented as $mean \pm SEM$

TABLE 1: Immunoblot data from hippocampal synaptosomes (males, 8-12 weeks, $n$ = number of pairs).

| | WT | | KO | | | |
|---|---|---|---|---|---|---|
| | **Mean** | **SEM** | **Mean** | **SEM** | ***p*-value** | ***n*** |
| **PSD95** | 100.0 | 3.1 | 96.6 | 3.6 | 0.395 | 16 |
| **GluR1** | 100.0 | 8.8 | 85.5 | 7.5 | 0.125 | 17 |
| **GluR2** | 100.0 | 7.6 | 95.7 | 6.6 | 0.365 | 16 |
| **NR1** | 100.0 | 3.7 | 96.2 | 4.3 | 0.422 | 16 |
| **VGlut1** | 100.0 | 8.5 | 81.1 | 7.3 | 0.035 | 17 |
| **VIAAT** | 100.0 | 4.6 | 90.3 | 5.7 | 0.138 | 17 |
| **Gephyrin** | 100.0 | 6.3 | 87.9 | 3.5 | 0.062 | 17 |
| **Nlgn1** | 100.0 | 7.5 | 71.8 | 5.4 | $< 0.001$ | 17 |
| **Nlgn2** | 100.0 | 9.6 | 90.7 | 5.9 | 0.333 | 16 |
| **Actin** | 100.0 | 4.9 | 91.9 | 3.6 | 0.136 | 16 |

## Discussion

Using in vivo field potential recordings, we show that the loss of Nlgn3 leads to a reduction in excitatory synaptic transmission at PP-GC synapses, supporting a role for Nlgn3 at these synapses. On the other hand, the coupling of the EPSP to the population spike is enhanced in Nlgn3-deficient mice, which could indicate a reduction of perisomatic inhibition and/or a compensatory increase in the intrinsic excitability of granule cells to maintain the normal action potential output despite the decreased synaptic input. These results resemble previous findings in Nlgn1 KO mice [31], and the observed reduction in Nlgn1 levels in hippocampal synaptosomes suggests that Nlgn3 may affect the availability of Nlgn1 at PP-GC synapses. However, in contrast to our findings in Nlgn1 KO mice, LTP experiments revealed no significant differences at these synapses in Nlgn3 KO mice, confirming previous studies proposing distinct functions for Nlgn1 and Nlgn3 at excitatory synapses [26].

Excitatory synaptic transmission from the perforant path to granule cells was significantly reduced in Nlgn3 KO mice (Fig. 1a), indicating that Nlgn3 plays a role in the formation and/or function of these synapses in vivo. Given the importance of the entorhino-dentate projection for social recognition memory [29], a reduction in the strength of these synapses could help explain the observed social memory impairments in Nlgn3 KO mice [10, 12, 13]. Our finding is consistent with previous reports of decreased AMPA-receptor-mediated currents in granule cells that had been virally transfected with microRNAs targeting Nlgn3 [26]. Furthermore, CA1 pyramidal cells in acute slices prepared from KO mice and from mice with an ASD-related point mutation that affects AMPA-receptor binding (R704C) exhibited decreased miniature excitatory postsynaptic current (EPSC) frequencies [32, 45]. Introducing the R704C mutation in cultured hippocampal neurons also produced deficits in AMPA-receptor-mediated synaptic transmission [46]. However, the conditional KO of Nlgn3 in cultured hippocampal neurons produced no discernible defect in AMPA-receptor-mediated transmission [25], which could be the result of developmental compensation by other neuroligins or synaptic adhesion molecules in the neurons in which Nlgn3 was deleted. The cultures used in these experiments were prepared from newborn mice, the neurons were transfected with the cKO construct at day 3 in vitro (DIV), and the experiments were performed around DIV 14, a time of ongoing synaptogenesis during which the function of Nlgn3 can still be compensated by the fellow neurexin-binding protein leucine-rich repeat transmembrane protein (LRRTM) 2 in hippocampal subregion CA1 [47]. It was recently shown that LRRTM4 specifically controls synaptogenesis in the dentate gyrus [48], so compensation of the developmental role of Nlgn3 is highly likely. Developmental compensation of the early postnatal function of Nlgn3 was also reported at excitatory synapses in the brainstem [49], but the pronounced synaptic deficits we (and others) observe in adult Nlgn3 KO mice indicate that the function of Nlgn3 during synaptogenesis differs from its function at mature synapses.

Since a reduction in synaptic transmission could be caused by a decrease in the vesicle release probability at the presynaptic boutons, we compared presynaptic function in Nlgn3 KO and WT mice using a paired-pulse protocol (Fig. 1b). A previous study had shown that the PSD95-Nlgn1-neurexin transsynaptic interaction mediates the presynaptic vesicle release probability by increasing the calcium sensitivity of the presynaptic terminal [50]. Nlgn1 overexpression decreased the paired pulse ratio (PPR), but the RNA interference-mediated knockdown of Nlgn1 had no effect on the PPR, which the authors attributed to compensation by other neuroligins [50]. We observed no difference in the degree of PPF, a form of short-term presynaptic plasticity which depends on the calcium levels and calcium buffering capability of the presynaptic terminals [38], at PP-GC synapses in Nlgn1 KO mice [31], and PPF was also unaltered in Nlgn3 KO mice. However, it is important to note that PPF only reflects the dynamics of presynaptic vesicle release, so differences in the number of vesicles or the amounts of neurotransmitter per vesicle are not detectable using this protocol.

To further differentiate between pre- and postsynaptic deficits, we quantified the relative abundance of different proteins in hippocampal synaptosomes from Nlgn3-deficient mice (Fig. 5). Intriguingly, we observed a significant decrease in the relative abundance of VGlut1, a presynaptic marker of excitatory synapses, in the Nlgn3-deficient synaptosomes, which might imply a reduction in the number of synapses or synaptic vesicles. This reduction may be specific to hippocampal synapses, since a previous study investigating whole-brain lysates from Nlgn3 KO mice reported no differences in the levels of VGlut1 [11]. Importantly, the relative abundance of the postsynaptic scaffolding protein PSD95 was not reduced in Nlgn3-deficient synaptosomes, suggesting that Nlgn3 KO and WT mice have a comparable number of excitatory synapses. We previously showed that the expression of glutamate receptors was reduced in hippocampal synaptosomes from Nlgn1 KO mice [31]. However, the AMPA receptor subunits GluR1 and GluR2 were not reduced in the Nlgn3-deficient synaptosomes. Similarly, the abundance of NMDA-receptor subunit NR1 was also unchanged in Nlgn3 KO synaptosomes, in accordance with previous results showing that Nlgn3 is not involved in the regulation of NMDA-receptor-mediated transmission [25, 26]. Taken together, the synaptosomal data support a reduction in presynaptic release, as opposed to postsynaptic strength, in Nlgn3 KO mice. However, it should be noted that our synaptosomal preparation is not specific for PP-GC synapses but includes all hippocampal synapses. An immunohistochemical analysis of these proteins could potentially uncover region- or layer-specific differences in their distribution in Nlgn3 KO mice.

Interestingly, Nlgn1 was also reduced by almost 30% in Nlgn3-deficient synaptosomes, in keeping with previous findings from whole brain lysates of Nlgn3 KO mice [11]. The mechanism by which deletion of Nlgn3 results in a partial loss of Nlgn1 remains unknown. The most parsimonious explanation for this observation is that in the absence of Nlgn3, Nlgn1-Nlgn3 heterodimers can no longer be formed [5] and the corresponding Nlgn1 is no longer trafficked to the synapse. Alternatively, it is conceivable that Nlgn3 has a direct regulatory influence on Nlgn1 levels, e.g. due to regulation of Nlgn1 cleavage as previously reported [23]. In the latter case, the phenotypes observed in the Nlgn3 KO may indirectly result from the loss of Nlgn1 rather than from direct synaptic effects of Nlgn3. However, the small magnitude of the Nlgn1 reduction makes it unlikely for this to be the only mechanism by which loss of Nlgn3 results in the observed synaptic effects. Furthermore, it is clear that deletion of Nlgn1 or Nlgn3 cause distinct consequences for other synaptic markers. In particular, VGlut1 was specifically downregulated in synaptosomes from Nlgn3 KO but not Nlgn1 KO mice, whereas the AMPA receptor subunits GluR1 and GluR2 were specifically reduced in Nlgn1 KO but not Nlgn3 KO synaptosomes. These observations effectively rule out that the changes observed in the Nlgn3 KO mice result exclusively indirectly from loss of synaptic Nlgn1. Future studies will be necessary to differentiate the extent to which the effects of Nlgn3 deletion on synaptic transmission are mediated by direct molecular functions of Nlgn3, by the loss of Nlgn1/Nlgn3 heterodimers, by indirect consequences of the Nlgn1 reduction, or by a combination of all of these mechanisms. Moreover, investigations of conditional KO mice would help to rule out developmental compensation and might yield interesting mechanistic insights into the function of Nlgn3. Importantly, however, the precise mechanism by which loss of Nlgn3 affects synaptic transmission has little bearing on the consequences of our findings for the use of the constitutive Nlgn3 KO mice as a face- and construct-valid model of ASD. Regardless of direct vs. indirect molecular effects, our data indicate that abnormalities in transmission at PP-GC synapses may contribute to the consequences of loss-of-function variants of Nlgn3 on autism-related behavioral phenotypes.

In contrast to the reduction in excitatory synaptic transmission, the excitability of the granule cells was enhanced in Nlgn3 KO mice. EPSP-spike coupling, i.e., the responsiveness (in terms of the population spike amplitude) of the granule cells to an EPSP of a given size, was significantly increased in KO mice (Fig. 2b), which could have important functional implications. Increased EPSP-spike coupling might decrease the filtering capability of granule cells and lead to deficits

in pattern separation. To our knowledge, pattern separation has not been assessed in Nlgn3 KO mice, but in other forms of hippocampal-dependent learning (contextual fear conditioning), these mice showed only mild defects (impaired freezing) which could have been caused by their hyperactivity [12]. Thus, the increased EPSP-spike coupling might instead serve a homeostatic function in the dentate network by maintaining the granule cell firing rate despite the reduced synaptic input, thereby preserving hippocampal-dependent learning.

EPSP-spike coupling can be influenced by intrinsic cellular properties, such as the resting membrane potential or the distribution of ion channels [51], but also by the level of synaptic inhibition [52]. We therefore examined PPI of the granule cell population spike as a partial readout of the inhibitory network activity in the dentate gyrus (Fig. 3). PPI is mediated by feedback inhibition from granule cells onto local interneurons and feedforward inhibition from direct perforant path activation of interneurons (mostly parvalbuminergic basket cells) [40]. Both Nlgn1 and Nlgn2 KO mice exhibited a strong reduction in the duration of PPI, which could be explained by a reduction in feedforward interneuron activation [31] or a reduction in perisomatic inhibition [53]. While the duration of PPI in Nlgn3 KO mice did not differ significantly from that in WT mice, we found a statistically significant effect of the interaction between the genotype and the interpulse interval using two different stimulation protocols, which could indicate that Nlgn3 might only affect feedback or feedforward inhibition, or only certain interneuron populations. For instance, in hippocampal area CA1, the deletion of Nlgn3 led to an increase in synaptic transmission from cholecystokinin (CCK) expressing basket cells, but had no effect on the function of parvalbuminergic basket cells, a difference which could be traced to the Nlgn3-dependent regulation of endocannabinoid signaling in CCK basket cells [54]. Since PPI is mainly mediated by perisomatic inhibition [40], the contribution of dendrite-targeting interneurons to the granule cell excitability may not be reflected in our measurements. Nlgn3 was shown to regulate inhibitory synaptic transmission from dendrite-targeting somatostatin (SOM) expressing interneurons in hippocampal subregion CA1 [28]. Feedforward inhibition from molecular layer interneurons decreases the granule cell excitability during entorhinal input integration [55], so changes in dendritic inhibition might alter the granule cell excitability without affecting PPI (cf. [56]). Thus, the seemingly opposing results of increased granule cell excitability and possibly increased PPI could be explained by a decrease in SOM-mediated dendritic inhibition and an increase in CCK-mediated perisomatic inhibition, respectively. Whole-cell recordings to determine the intrinsic membrane properties of Nlgn3-deficient granule cells, accompanied by paired recordings from granule cells and interneurons, could address these hypotheses in future experiments.

Lastly, we investigated the effects of Nlgn3 KO on LTP induction at PP-GC synapses. If the trafficking of postsynaptic receptors is not impaired by the loss of Nlgn3, the relative increase in the synaptic strength following LTP induction would not be affected, even if the absolute synaptic strength is diminished in the KO. Indeed, we observed similar relative levels of LTP induced by TBS protocols in Nlgn3 KO mice and their WT littermates (Fig. 4a and c). These findings differ from our previous results comparing TBS-induced LTP in Nlgn1 KO and WT mice, which revealed deficits in LTP at PP-GC synapses in the KO mice [31]. In contrast to WT mice, the GluA2 glutamate receptor subunit was not upregulated in the stimulated Nlgn1 KO mice compared to naïve controls, partially explaining the LTP impairments [31]. However, despite the reduction of Nlgn1 protein levels in the Nlgn3-deficient synaptosomes, LTP was unimpaired in Nlgn3 KO mice, suggesting that the remaining Nlgn1 is sufficient for the recruitment of postsynaptic receptors following TBS. Previous experiments in a different species (rat) using a different method of manipulating Nlgn3 expression (microRNA-mediated knockdown), a different experimental system (acute slices), and a different LTP-induction protocol (pairing) also showed that Nlgn3, unlike Nlgn1, is not involved in LTP at PP-GC synapses [26]. Therefore, the functional separation of Nlgn1 and Nlgn3 at the PP-GC synapse appears to be a robust phenomenon that is evolutionarily conserved between rats and mice. This functional difference

can partially be explained by alternative splicing of the different neuroligin isoforms. Unlike Nlgn3, Nlgn1 contains an alternative splice site (B) which determines its neurexin binding specificity [57]. Nlgn1 containing this splice site insertion (Nlgn1B) binds only $\beta$-neurexin, while Nlgn1 lacking this insertion binds both $\alpha$- and $\beta$-neurexin [57]. Nlgn1B is the dominant Nlgn1 variant in dissociated rat hippocampal neurons [58] and was shown to be crucial for the expression of LTP in CA1 pyramidal neurons, whereas Nlgn3 lacks this insertion and is not required for hippocampal LTP [26]. It is tempting to speculate that the insertion-lacking Nlgn1 variant might be preferentially reduced in Nlgn3 KO mice while the levels of the Nlgn1B variant remain unaffected, thus explaining the reduction in synaptic transmission and unaltered relative magnitude of LTP at PP-GC synapses. It is conceivable that the Nlgn1-Nlgn3 heterodimer selectively regulates synaptic transmission at these synapses while the Nlgn1B homodimer regulates LTP.

In summary, our study shows that Nlgn3 plays a specific role at excitatory postsynapses in the dentate gyrus in vivo. Given the importance of Nlgn3 as an ASD candidate gene [6, 7], the dissection of its function at identified synapses and networks is mandatory for understanding its role in the pathomechanisms leading to ASD. We also confirmed the functional segregation of Nlgn1 and Nlgn3 at excitatory synapses in the dentate gyrus: Nlgn1 regulates excitatory synaptic transmission, plays a role in the trafficking of glutamate receptors to the synapse, and affects LTP and network inhibition [31] whereas Nlgn3 primarily regulates synaptic transmission. However, the reduction of Nlgn1 protein expression levels in Nlgn3 KO synaptosomes indicates that both neuroligins are required for intact excitatory transmission at PP-GC synapses. Therefore, interactions between neuroligins might play an important role in determining synaptic strength. Our results underscore the advantages of in vivo recordings of field potentials in studying the synaptic function of neuroligins and show that this method can be used not only to confirm findings from in vitro and ex vivo experiments, but also to generate new hypotheses that will lead to a better understanding of the neural underpinnings of ASD.

**Supplementary Information** The online version contains supplementary material available at https://doi.org/10.1007/s12035-021-02663-9.

**Acknowledgements** We thank Nils Brose (MPI of Experimental Medicine, Göttingen, Germany) for providing the Nlgn3 KO mouse line and Thomas Deller (Institute of Clinical Neuroanatomy, Frankfurt, Germany) for his continuous support.

**Author Contribution** Conceptualization, P.J. and S.W.S.; methodology, P.J.; software, M.V. and T.J.; formal analysis, D.K.-B, J.M., M.V., and T.J.; investigation, A.I., D.K.-B, J.M., M.V., and T.J.; writing (original draft preparation), J.M.; writing (review and editing), D.K.-B., J.M., M.V., P.J., S.W.S., and T.J.; visualization, D.K.-B. and J.M.; supervision, P.J.; project administration, P.J. and S.W.S.; funding acquisition, D.K.-B., P.J., and S.W.S.

**Funding** Open Access funding enabled and organized by Projekt DEAL. This research was supported by the German Research Foundation (Deutsche Forschungsgemeinschaft), grant numbers JE 528/6–1 (to P.J.) and SCHW 534/6–1 (to S.W.S.) as well as by an International Reintegration Grant, European Commission (grant number PIRG7-GA-2010–268358 to D.K.-B.).

**Availability of Data and Material** All data are available upon request from the corresponding author.

**Code Availability** Custom code is available upon request from the corresponding author.

## Declarations

**Ethics Approval** Animal experiments were conducted in accordance with the German law regarding the use of laboratory animals (Tierschutz-Versuchstierverordnung) and approved by the Regierungspräsidium Darmstadt and the animal welfare officer responsible for the institute.

**Consent to Participate** Not applicable.

**Consent for Publication** Not applicable.

**Conflict of Interest** The authors declare no competing interests.

## References


1. Südhof TC (2017) Synaptic Neurexin Complexes: A Molecular Code for the Logic of Neural Circuits. Cell 171:745–769. https://doi.org/10.1016/j.cell.2017.10.024

2. Song JY, Ichtchenko K, Südhof TC, Brose N (1999) Neuroligin 1 is a postsynaptic cell-adhesion molecule of excitatory synapses. Proc Natl Acad Sci U S A 96:1100–1105. https://doi.org/10.1073/pnas.96.3.1100

3. Varoqueaux F, Jamain S, Brose N (2004) Neuroligin 2 is exclusively localized to inhibitory synapses. Eur J Cell Biol 83:449–456. https://doi.org/10.1078/0171-9335-00410

4. Budreck EC, Scheiffele P (2007) Neuroligin-3 is a neuronal adhesion protein at GABAergic and glutamatergic synapses. Eur J Neurosci 26:1738–1748. https://doi.org/10.1111/j.1460-9568.2007.05842.x

5. Poulopoulos A, Soykan T, Tuffy LP, et al (2012) Homodimerization and isoform-specific heterodimerization of neuroligins. Biochem J 446:321–330. https://doi.org/10.1042/BJ20120808

6. Jamain S, Quach H, Betancur C, et al (2003) Mutations of the X-linked genes encoding neuroligins NLGN3 and NLGN4 are associated with autism. Nat Genet 34:27–29. https://doi.org/10.1038/ng1136

7. Quartier A, Courraud J, Thi Ha T, et al (2019) Novel mutations in NLGN3 causing autism spectrum disorder and cognitive impairment. Hum Mutat 40:2021–2032. https://doi.org/10.1002/humu.23836

8. Nguyen TA, Lehr AW, Roche KW (2020) Neuroligins and Neurodevelopmental Disorders: X-Linked Genetics. Front Synaptic Neurosci 12:1–10. https://doi.org/10.3389/fnsyn.2020.00033

9. Hamilton SM, Green JR, Veeraragavan S, et al (2014) Fmr1 and Nlgn3 knockout rats: Novel tools for investigating autism spectrum disorders. Behav Neurosci 128:103–109. https://doi.org/10.1037/a0035988

10. Modi B, Pimpinella D, Pazienti A, et al (2019) Possible Implication of the CA2 Hippocampal Circuit in Social Cognition Deficits Observed in the Neuroligin 3 Knock-Out Mouse, a Non-Syndromic Animal Model of Autism. Front Psychiatry 10:1–16. https://doi.org/10.3389/fpsyt.2019.00513

11. Tabuchi K, Blundell J, Etherton MR, et al (2007) A neuroligin-3 mutation implicated in autism increases inhibitory synaptic transmission in mice. Science 318:71–76. https://doi.org/10.1126/science.1146221

12. Radyushkin K, Hammerschmidt K, Boretius S, et al (2009) Neuroligin-3-deficient mice: Model of a monogenic heritable form of autism with an olfactory deficit. Genes, Brain Behav 8:416–425. https://doi.org/10.1111/j.1601-183X.2009.00487.x

13. Bariselli S, Hörnberg H, Prévost-Solié C, et al (2018) Role of VTA dopamine neurons and neuroligin 3 in sociability traits related to nonfamiliar conspecific interaction. Nat Commun 9:3173. https://doi.org/10.1038/s41467-018-05382-3

14. Kalbassi S, Bachmann SO, Cross E, et al (2017) Male and female mice lacking neuroligin-3 modify the behavior of their wild-type littermates. eNeuro 4:1–14. https://doi.org/10.1523/ENEURO.0145-17.2017

15. Rothwell PE, Fuccillo M V., Maxeiner S, et al (2014) Autism-associated neuroligin-3 mutations commonly impair striatal circuits to boost repetitive behaviors. Cell 158:198–212. https://doi.org/10.1016/j.cell.2014.04.045

16. Thomas AM, Schwartz MD, Saxe MD, Kilduff TS (2017) Sleep/wake physiology and quantitative electroencephalogram analysis of the neuroligin-3 knockout rat model of autism spectrum disorder. Sleep 40(10). https://doi.org/10.1093/sleep/zsx138

17. Masini E, Loi E, Vega-Benedetti AF, et al (2020) An overview of the main genetic, epigenetic and environmental factors involved in autism spectrum disorder focusing on synaptic activity. Int J Mol Sci 21:1–22. https://doi.org/10.3390/ijms21218290

18. De Rubeis S, He X, Goldberg AP, et al (2014) Synaptic, transcriptional and chromatin genes disrupted in autism. Nature 515:209–215. https://doi.org/10.1038/nature13772

19. Gilman SR, Iossifov I, Levy D, et al (2011) Rare De Novo Variants Associated with Autism Implicate a Large Functional Network of Genes Involved in Formation and Function of Synapses. Neuron 70:898–907. https://doi.org/10.1016/j.neuron.2011.05.021

20. Mahfouz A, Ziats MN, Rennert OM, et al (2015) Shared Pathways Among Autism Candidate Genes Determined by Co-expression Network Analysis of the Developing Human Brain Transcriptome. J Mol Neurosci 57:580–594. https://doi.org/10.1007/s12031-015-0641-3

21. Levinson JN, El-Husseini A (2005) Building excitatory and inhibitory synapses: Balancing neuroligin partnerships. Neuron 48:171–174. https://doi.org/10.1016/j.neuron.2005.09.017

22. Nelson SB, Valakh V (2015) Excitatory/Inhibitory Balance and Circuit Homeostasis in Autism Spectrum Disorders. Neuron 87:684–698. https://doi.org/10.1016/j.neuron.2015.07.033

23. Bemben MA, Nguyen TA, Li Y, et al (2019) Isoform-specific cleavage of neuroligin-3 reduces synapse strength. Mol Psychiatry 24:145–160. https://doi.org/10.1038/s41380-018-0242-y

24. Polepalli JS, Wu H, Goswami D, et al (2017) Modulation of excitation on parvalbumin interneurons by neuroligin-3 regulates the hippocampal network. Nat Neurosci 20:219–229. https://doi.org/10.1038/nn.4471

25. Chanda S, Hale WD, Zhang B, et al (2017) Unique versus Redundant Functions of Neuroligin Genes in Shaping Excitatory and Inhibitory Synapse Properties. J Neurosci 37:6816–6836. https://doi.org/10.1523/JNEUROSCI.0125-17.2017

26. Shipman SL, Nicoll RA (2012) A Subtype-Specific Function for the Extracellular Domain of Neuroligin 1 in Hippocampal LTP. Neuron 76:309–316. https://doi.org/10.1016/j.neuron.2012.07.024

27. Shipman SL, Schnell E, Hirai T, et al (2011) Functional dependence of neuroligin on a new non-PDZ intracellular domain. Nat Neurosci 14:718–726. https://doi.org/10.1038/nn.2825

28. Horn ME, Nicoll RA (2018) Somatostatin and parvalbumin inhibitory synapses onto hippocampal pyramidal neurons are regulated by distinct mechanisms. Proc Natl Acad Sci U S A 115:589–594. https://doi.org/10.1073/pnas.1719523115

29. Leung C, Cao F, Nguyen R, et al (2018) Activation of Entorhinal Cortical Projections to the Dentate Gyrus Underlies Social Memory Retrieval. Cell Rep 23:2379–2391. https://doi.org/10.1016/j.celrep.2018.04.073

30. Kesner RP (2018) An analysis of dentate gyrus function (an update). Behav Brain Res 354:84–91. https://doi.org/10.1016/j.bbr.2017.07.033

31. Jedlicka P, Vnencak M, Krueger DD, et al (2015) Neuroligin-1 regulates excitatory synaptic transmission, LTP and EPSP-spike coupling in the dentate gyrus in vivo. Brain Struct Funct 220:47–58. https://doi.org/10.1007/s00429-013-0636-1

32. Etherton MR, Földy C, Sharma M, et al (2011) Autism-linked neuroligin-3 R451C mutation differentially alters hippocampal and cortical synaptic function. Proc Natl Acad Sci U S A 108:13764–13769. https://doi.org/10.1073/pnas.1111093108

33. Varoqueaux F, Aramuni G, Rawson RL, et al (2006) Neuroligins Determine Synapse Maturation and Function. Neuron 51:741–754. https://doi.org/10.1016/j.neuron.2006.09.003

34. Fernández-Ruiz A, Muñoz S, Sancho M, et al (2013) Cytoarchitectonic and dynamic origins of giant positive local field potentials in the dentate gyrus. J Neurosci 33:15518–32. https://doi.org/10.1523/JNEUROSCI.0338-13.2013

35. Cooke SF, Wu J, Plattner F, et al (2006) Autophosphorylation of $\alpha$CaMKII is not a general requirement for NMDA receptor-dependent LTP in the adult mouse. J Physiol 805–818. https://doi.org/10.1113/jphysiol.2006.111559

36. Chen PE, Errington ML, Kneussel M, et al (2009) Behavioral deficits and subregion-specific suppression of LTP in mice expressing a population of mutant NMDA receptors throughout the hippocampus. Learn Mem 16:635–644. https://doi.org/10.1101/lm.1316909

37. Khuu MA, Pagan CM, Nallamothu T, et al (2019) Intermittent hypoxia disrupts adult neurogenesis and synaptic plasticity in the dentate gyrus. J Neurosci 39:1320–1331. https://doi.org/10.1523/JNEUROSCI.1359-18.2018

38. Regehr WG (2012) Short-term presynaptic plasticity. Cold Spring Harb Perspect Biol 4:1–19. https://doi.org/10.1101/cshperspect.a005702

39. Sloviter RS (1991) Feedforward and feedback inhibition of hippocampal principal cell activity evoked by perforant path stimulation: GABA-mediated mechanisms that regulate excitability In Vivo. Hippocampus 1:31–40. https://doi.org/10.1002/hipo.450010105

40. Jedlicka P, Deller T, Schwarzacher SW (2010) Computational modeling of $GABA_A$ receptor-mediated paired-pulse inhibition in the dentate gyrus. J Comput Neurosci 29:509–519. https://doi.org/10.1007/s10827-010-0214-y

41. Steffensen SC, Henriksen SJ (1991) Effects of baclofen and bicuculline on inhibition in the fascia dentata and hippocampus regio superior. Brain Res 538:46–53. https://doi.org/10.1016/0006-8993(91)90374-5

42. Brucato FH, Mott DD, Lewis D V., Swartzwelder HS (1995) $GABA_B$ receptors modulate synaptically-evoked responses in the rat dentate gyrus, in vivo. Brain Res 677:326–332. https://doi.org/10.1016/0006-8993(95)00180-X

43. Foster JD, Kitchen I, Bettler B, Chen Y (2013) $GABA_B$ receptor subtypes differentially modulate synaptic inhibition in the dentate gyrus to enhance granule cell output. Br J Pharmacol 168:1808–1819. https://doi.org/10.1111/bph.12073

44. Larson J, Munkácsy E (2015) Theta-burst LTP. Brain Res 1621:38–50. https://doi.org/10.1016/j.brainres.2014.10.034

45. Etherton MR, Tabuchi K, Sharma M, et al (2011) An autism-associated point mutation in the neuroligin cytoplasmic tail selectively impairs AMPA receptor-mediated synaptic transmission in hippocampus. EMBO J 30:2908–2919. https://doi.org/10.1038/emboj.2011.182

46. Chanda S, Aoto J, Lee SJ, et al (2016) Pathogenic mechanism of an autism-associated neuroligin mutation involves altered AMPA-receptor trafficking. Mol Psychiatry 21:169–177. https://doi.org/10.1038/mp.2015.20

47. Soler-Llavina GJ, Fuccillo M V, Ko J, et al (2011) The neurexin ligands, neuroligins and leucine-rich repeat transmembrane proteins, perform convergent and divergent synaptic functions in vivo. Proc Natl Acad Sci U S A 108:16502–16509. https://doi.org/10.1073/pnas.1114028108

48. Siddiqui TJ, Tari PK, Connor SA, et al (2013) An LRRTM4-HSPG complex mediates excitatory synapse development on dentate gyrus granule cells. Neuron 79:680–695. https://doi.org/10.1016/j.neuron.2013.06.029

49. Zhang B, Seigneur E, Wei P, et al (2017) Developmental plasticity shapes synaptic phenotypes of autism-associated neuroligin-3 mutations in the calyx of held. Mol Psychiatry 22:1483–1491. https://doi.org/10.1038/mp.2016.157

50. Futai K, Kim MJ, Hashikawa T, et al (2007) Retrograde modulation of presynaptic release probability through signaling mediated by PSD-95-neuroligin. Nat Neurosci 10:186–195. https://doi.org/10.1038/nn1837

51. Debanne D, Inglebert Y, Russier M (2019) Plasticity of intrinsic neuronal excitability. Curr Opin Neurobiol 54:73–82. https://doi.org/10.1016/j.conb.2018.09.001

52. Carvalho TP, Buonomano D V. (2009) Differential Effects of Excitatory and Inhibitory Plasticity on Synaptically Driven Neuronal Input-Output Functions. Neuron 61:774–785. https://doi.org/10.1016/j.neuron.2009.01.013

53. Jedlicka P, Hoon M, Papadopoulos T, et al (2011) Increased Dentate Gyrus Excitability in Neuroligin-2-Deficient Mice in Vivo. Cereb Cortex 21:357–367. https://doi.org/10.1093/cercor/bhq100

54. Földy C, Malenka RC, Südhof TC (2013) Autism-associated neuroligin-3 mutations commonly disrupt tonic endocannabinoid signaling. Neuron 78:498–509. https://doi.org/10.1016/j.neuron.2013.02.036

55. Mircheva Y, Peralta MR, Tóth K (2019) Interplay of entorhinal input and local inhibitory network in the hippocampus at the origin of slow inhibition in granule cells. J Neurosci 39:6399–6413. https://doi.org/10.1523/JNEUROSCI.2976-18.2019

56. Moser EI (1996) Altered inhibition of dentate granule cells during spatial learning in an exploration task. J Neurosci 16:1247–1259. https://doi.org/10.1523/jneurosci.16-03-01247.1996

57. Boucard AA, Chubykin AA, Comoletti D, et al (2005) A splice code for trans-synaptic cell adhesion mediated by binding of neuroligin 1 to $\alpha$- and $\beta$-neurexins. Neuron 48:229–236. https://doi.org/10.1016/j.neuron.2005.08.026

58. Chih B, Gollan L, Scheiffele P (2006) Alternative Splicing Controls Selective Trans-Synaptic Interactions of the Neuroligin-Neurexin Complex. Neuron 51:171–178. https://doi.org/10.1016/j.neuron.2006.06.005

# Supplementary Information

## Extended Methods

*Anesthesia and Surgery*
Urethane (Sigma-Aldrich, Munich, Germany) solution (1.25 g of urethane in 10 ml 0.9% NaCl solution) was used to anesthetize the mice with an initial injection (1.2 g/kg body weight) applied intraperitoneally. Supplemental doses (totalling 0.3-1 g/kg) were injected subcutaneously until the proper anesthetic depth was attained. This anesthetic protocol has been previously published [1] and urethane has been shown to affect inhibitory, excitatory, and modulatory neurotransmitter receptors to similar degrees [2]. The body temperature of the animal was constantly monitored through a rectal probe and maintained at 36.5–37.5°C using a heating pad. Additional local anesthesia was provided by a subcutaneous injection of prilocaine hydrochloride with adrenaline 1:200,000 (Xylonest 1%, AstraZeneca, Wedel, Germany) into the scalp. The mouse was then placed into a stereotactic frame (David Kopf Instruments) for the accurate determination of the recording and stimulation locations. After exposing the skull, the location of bregma was determined from the intersection of the sagittal and the coronal sutures. The holes for the stimulation (coordinates: 3.7 mm posterior to bregma, 2.5 mm lateral to the midline) and recording (coordinates: 1.7 mm posterior to bregma, 1.0 mm lateral to the midline) electrodes were made with a dental drill (Dremel), and the dura mater was carefully removed before inserting the electrodes. The ground electrode was inserted into the neck musculature.

*Stimulation protocols and data analysis*
Current pulses were generated by a stimulus generator (STG1004, Multichannel Systems, Reutlingen, Germany). The recorded field excitatory post-synaptic potentials (fEPSPs) were first amplified (P55 preamplifier, Grass Technologies, West Warwick, RI, USA) and then digitized at 10 kHz for visualization and offline analysis (Digidata 1440A, Molecular Devices, Union City, CA, USA). The Clampfit 10.2 software (Molecular Devices, Union City, MA, USA) and custom Matlab scripts (Mathworks, Natick, MA, USA) were used for the analysis of the field excitatory postsynaptic potentials (fEPSPs).

First, the granule cell responses to different stimulation intensities (i.e., the input-output relationship) was determined by applying a series of stimuli ranging from 30 to 800 µA (0.1 ms stimulus duration) and collecting the evoked fEPSP. Three responses were collected and averaged for each stimulus intensity. The amplitude of the population spike (defined as the average of the amplitude from the first positive peak to the antipeak and the amplitude from the antipeak to the second positive peak, see Fig. 2a) was used to determine the excitability of the granule cell population. The slope of the fEPSP, which was measured during the early component of the waveform to avoid contamination by the population spike (see Fig. 1a), was used as an indicator of synaptic efficacy. In the analysis relating the fEPSP slope to the spike amplitude (EPSP-spike plot) each curve was fitted using a Boltzmann function. Only curves with a goodness of fit value ($R^2$) greater than 0.80 were used for the analysis of the v50 values.

Next, paired-pulse facilitation (PPF) of the fEPSP was elicited by two subsequent pulses at an intensity below the population spike threshold (between 20 and 120 µA/0.2 ms), with interpulse intervals (IPIs) varying from 15 to 100 ms. A total of three paired-pulse responses at each IPI were collected and averaged, and the facilitation factor for each IPI was calculated by dividing the amplitude of the second fEPSP by that of the first fEPSP.

In order to examine feedback and feedforward inhibition in the dentate network, paired-pulse inhibition (PPI) and disinhibition (PPDI) of the population spike were elicited at weak stimulation intensities (evoking approximately 1 mV population spikes) and at maximal stimulation intensities for IPIs ranging from 15 to 1,000 ms (0.2 ms pulse duration/three repetitions per IPI). The relative inhibition of the population spike amplitude was calculated by dividing

the spike amplitude following the second pulse by the spike amplitude following the first pulse. After fitting the PPI/PPDI curves with a Boltzmann function, the IPI at which both responses would be equal was determined.

Finally, LTP was induced by theta-burst stimulation (TBS), a stimulation protocol patterned after the hippocampal theta rhythm [3]. In some mice, a strong TBS protocol (i.e. six series of six trains of six pulses at 400 Hz, with 0.2 s between trains and 20 s between series) was applied [4]. In other mice, an initial weak TBS protocol (i.e., only three series of six trains of six pulses at 400 Hz, 0.2 s between trains and 20 s between series) was followed by the strong TBS protocol 30 min later [1]. In both groups, the perforant path was stimulated with 0.1 ms pulses at 0.1 Hz with a stimulation intensity set to elicit a population spike in the range of 1-3 mV before LTP induction. Both the pulse width and the stimulus intensity during TBS were doubled in comparison to the baseline. The maximum allowable baseline stimulus intensity was 400 µA. The potentiation of the fEPSP and the population spike following TBS were expressed as percentages relative to the pre-TBS mean values.

*Preparation of hippocampal synaptosomal fractions and immunoblot analysis*

Mice aged 8-12 weeks were sacrificed by rapid decapitation and the brains were removed. The hippocampi were dissected out on ice, and all subsequent steps were carried out at 4 °C. Hippocampi were homogenized in solution A (0.32 M sucrose, 1 mM $MgCl_2$, 0.5 mM $CaCl_2$, 1 mM HEPES, pH 7.4, containing freshly added protease inhibitor cocktail) with 12 strokes at 900 rpm using a motor-operated Teflon/glass homogenizer (Potter S, Sartorius, Göttingen, Germany). The homogenates were centrifuged for 10 min at approximately 1,000x*g* (supernatants were saved) and the pellets were resuspended in solution A, re-homogenized with 3 strokes at 900 rpm, and re-centrifuged for 10 min at 1,000x*g*. The supernatants from the two centrifugation steps were pooled and centrifuged for 10 min at approximately 10,000x*g*. The resulting pellets were resuspended in solution B (0.32 M sucrose, 1 mM HEPES, pH 7.4 containing freshly added protease inhibitor cocktail, EMD Biosciences, Darmstadt, Germany), homogenized with 4-5 strokes at 900 rpm and layered on top of a sucrose gradient consisting of 0.85 M, 1.0 M, and 1.2 M sucrose layers (each containing 1 mM HEPES and protease inhibitor cocktail). Gradients were centrifuged for 2 h at 21,600 rpm (approximately 82,500xg) in a swinging bucket rotor (SW 40 Ti rotor, Beckman Coulter, Krefeld, Germany). The band at the interface between 1.0 and 1.2 M sucrose layers containing the synaptosomes was collected. Sodium dodecyl sulfate (SDS) was added until reaching a final concentration of 1%, and the lysed synaptosomes were stored at -80 °C until immunoblotting.

Prior to immunoblot analysis, the protein concentration was assessed using a BCA assay (Thermo Scientific, Waltham, MA, USA). Samples containing 1–5 µg protein were boiled in 1x loading buffer (2% SDS, 62.5 mM Tris, 10% glycerol, 1% $\beta$-mercaptoethanol, 0.01% bromophenol blue, pH 6.8) for 5 min, resolved on 10% SDS-PAGE gels, transferred onto nitrocellulose membranes, and stained for total protein using a MemCode assay (Thermo Scientific, Waltham, MA, USA) to determine transfer efficiency. Membranes were blocked in 50% LiCor blocking buffer (LiCor Biosciences, Lincoln, NE, USA) in phosphate-buffered saline (PBS) for 1 h and then incubated in primary antibody dilution buffer (50% LiCor blocking buffer and 0.1% Tween-20 in PBS) at 4°C overnight. The following primary antibodies were used: Nlgn1 (RRID: 887747, Synaptic Systems, Göttingen, Germany), PSD-95 (RRID: AB_2877189, NeuroMAB, Davis, CA, USA), AMPA receptor subunit 1 (GluR1, RRID: AB_2113602, Chemicon, Temecula, CA, USA), AMPA receptor subunit 2 (GluR2, RRID: AB_2113732, Synaptic Systems, Göttingen, Germany), NMDA receptor subunit 1 (NR1, RRID: AB_887750, Synaptic Systems, Göttingen, Germany), vesicular glutamate transporter 1 (VGlut1, RRID: AB_887878, Synaptic Systems, Göttingen, Germany), vesicular inhibitory amino acid transporter (VIAAT, RRID: AB_2189938, Synaptic Systems, Göttingen, Germany), gephyrin (RRID: AB_887719, Synaptic Systems, Göttingen, Germany), actin (RRID: AB_258912, Sigma-Aldrich, St. Louis, MO, USA) and Nlgn2 (antibody

799, Nils Brose). Membranes were washed 4x in PBS with 0.1% Tween-20, then incubated with secondary antibody (Gt anti-M-IRDye800 and Gt anti Rb-IRDye680, LiCor Biosciences, Lincoln, NE, USA, and Gt-anti-GP-IRDye700, Rockland Immunochemicals, Gilbertsville, PA, USA) in secondary antibody dilution buffer (50% LiCor blocking buffer, 0.1% Tween-20 and 0.01% SDS in PBS) for 1 h at 4°C. Blots were washed as above, scanned on an Odyssey Infrared Imager (LiCor Biosciences, Lincoln, NE, USA), and the signal intensity for each sample was quantified using the Odyssey 2.1 software. Each sample value was divided by the total protein loading value for the corresponding lane, and then normalized to the average sample value of all lanes on the same blot to correct for blot-to-blot variance. Data are expressed relative to the WT values.

## References

1. Jedlicka P, Vnencak M, Krueger DD, et al (2015) Neuroligin-1 regulates excitatory synaptic transmission, LTP and EPSP-spike coupling in the dentate gyrus in vivo. Brain Struct Funct 220:47–58. https://doi.org/10.1007/s00429-013-0636-1

2. Hara K, Harris R (2002) The anesthetic mechanism of urethane: the effects on neurotransmitter-gated ion channels. Anesth Analg 94:313–318. https://doi.org/10.1213/00000539-200202000-00015

3. Larson J, Lynch G (1988) Role of N-methyl-D-aspartate receptors in the induction of synaptic potentiation by burst stimulation patterned after the hippocampal $\theta$-rhythm. Brain Res 441:111–118. https://doi.org/10.1016/0006-8993(88)91388-1

4. Cooke SF, Wu J, Plattner F, et al (2006) Autophosphorylation of $\alpha$CaMKII is not a general requirement for NMDA receptor-dependent LTP in the adult mouse. J Physiol 805–818. https://doi.org/10.1113/jphysiol.2006.111559

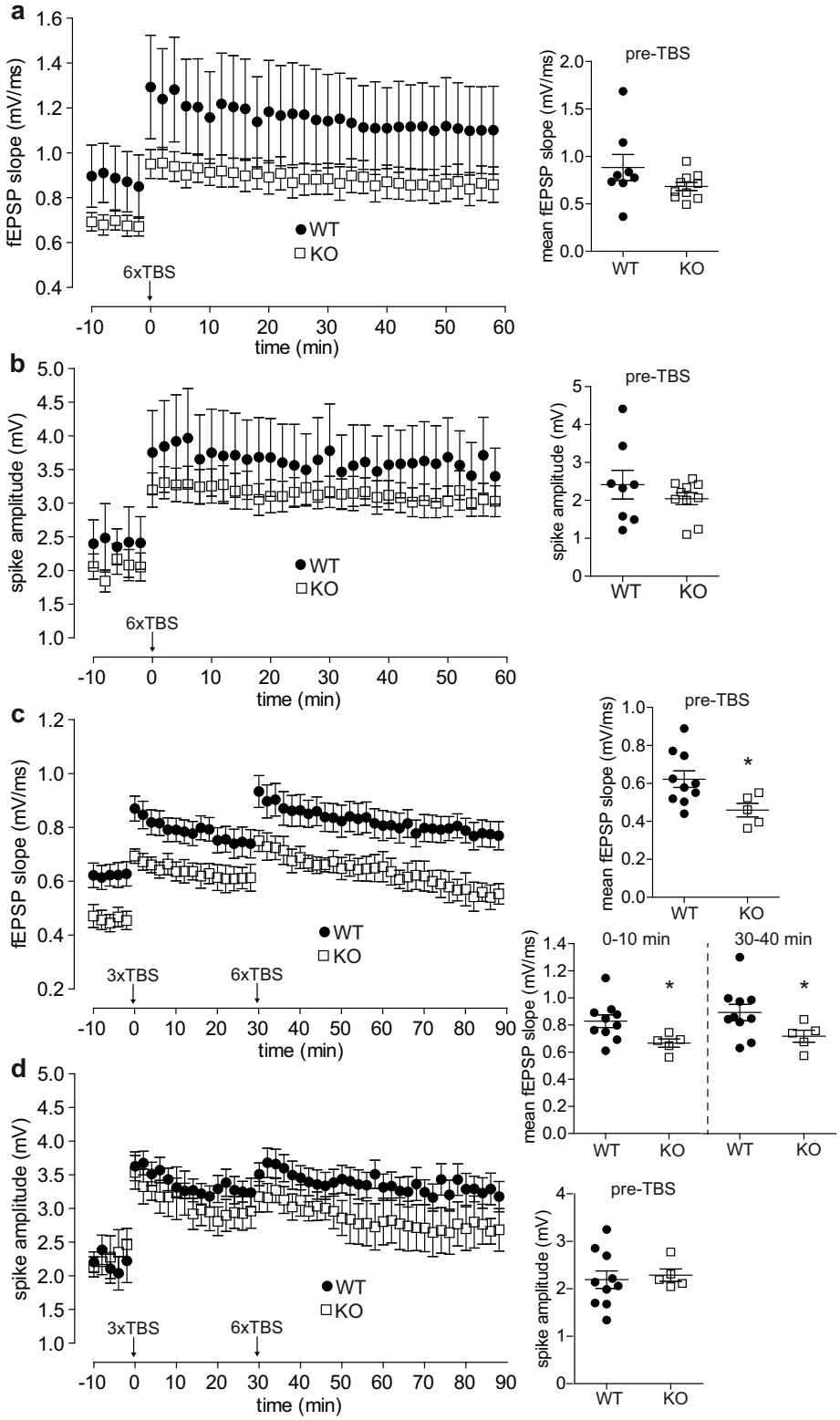


FIGURE S1: Absolute values of the fEPSP slope, but not the population spike amplitude, during LTP measurements were lower in Nlgn3-deficient mice. (a) During the pre-TBS baseline and following strong TBS, (see Methods) Nlgn3 KO ($n = 10$) mice had lower fEPSP slopes than WT ($n = 8$) mice. *Diagram* shows the mean fEPSP slope during the pre-TBS baseline. (b) The population spike amplitudes during the pre-TBS baseline and following strong TBS were similar in both groups. *Diagrams* shows that the mean population spike amplitude during the pre-TBS baseline did not differ significantly between WT and Nlgn3 KO mice.

(*continued on next page*)

FIGURE S1: (*continued from last page*) (c) During the pre-TBS baseline and following the combined weak and strong TBS, Nlgn3 KO ($n = 5$) had lower slopes compared to WT ($n = 10$) mice. *Diagrams* show the mean fEPSP slopes during the pre-TBS baseline, after the weak TBS (0-10 min), and after the strong TBS (30-40 min). (d) The population spike amplitudes during the pre-TBS baseline and following the combined weak and strong TBS were similar in WT and Nlgn3 KO mice. *Diagram* shows that the mean population spike amplitude during the pre-TBS baseline. Asterisks denote statistical significance by unpaired Welch's *t*-test (*$p < 0.05$). Data are represented as $mean \pm SEM$

## Chapter 5

# Manuscript 3

## Altered granule cell excitability and increased network inhibition, but preserved Hebbian and homeostatic synaptic plasticity, in the dentate gyrus of Neuroligin-4 knockout mice *in vivo* and *in vitro*

*submitted*

**Declaration of author contributions to the manuscript: "Altered granule cell excitability and increased network inhibition, but preserved Hebbian and homeostatic synaptic plasticity, in the dentate gyrus of Neuroligin-4 knockout mice *in vivo* and *in vitro*"**

Status: *submitted*

name of journal: *n. a.*

Contributing authors: Julia Muellerleile, Matej Vnencak, Valeed Sethi, Tassilo Jungenitz, Stephan W. Schwarzacher, Peter Jedlička

**What are the contributions of the doctoral candidate and her co-authors?**

**(1) Concept and design**
Doctoral candidate: 0%
Co-author Matej Vnencak: 0%
Co-author Valeed Sethi: 0%
Co-author Tassilo Jungenitz: 0%
Co-author Stephan W. Schwarzacher: 40%
Co-author Peter Jedlička: 60%

**(2) Conducting tests and experiments**
Doctoral candidate: 60% (*in vitro* electrophysiological experiments, histology)
Co-author Matej Vnencak: 20% (*in vivo* electrophysiological experiments, histology)
Co-author Valeed Sethi: 5% (*in vivo* electrophysiological experiments)
Co-author Tassilo Jungenitz: 0%
Co-author Stephan W. Schwarzacher: 0%
Co-author Peter Jedlička: 15% (*in vivo* electrophysiological experiments)

**(3) Compilation of data sets and figures**
Doctoral candidate: 100% (compilation of Figures 1-9 and S1
Co-author Matej Vnencak: 0%
Co-author Valeed Sethi: 0%
Co-author Tassilo Jungenitz: 0%
Co-author Stephan W. Schwarzacher: 0%
Co-author Peter Jedlička: 0%

**(4) Analysis and interpretation of data**
Doctoral candidate: 55% (analysis of electrophysiological data and interpretation)
Co-author Matej Vnencak: 20% (analysis of *in vivo* electrophysiological data)
Co-author Valeed Sethi: 0%
Co-author Tassilo Jungenitz: 15% (analysis of *in vivo* electrophysiological data and interpretation)
Co-author Stephan W. Schwarzacher: 5% (interpretation)
Co-author Peter Jedlička: 5% (interpretation)

**(5) Drafting of manuscript**
Doctoral candidate: 85% (original draft, editing)
Co-author Matej Vnencak: 0%
Co-author Valeed Sethi: 0%
Co-author Tassilo Jungenitz: 5% (editing)
Co-author Stephan W. Schwarzacher: 5% (editing)
Co-author Peter Jedlička: 5% (editing)

# Altered granule cell excitability and increased network inhibition, but preserved Hebbian and homeostatic synaptic plasticity, in the dentate gyrus of Neuroligin-4 knockout mice *in vivo* and *in vitro*

**Julia Muellerleile[1,2], Matej Vnencak[1], Valeed Sethi[1], Tassilo Jungenitz[1], Stephan W. Schwarzacher[1*], Peter Jedlicka [1,3*]**

[1] Institute of Clinical Neuroanatomy, Neuroscience Center, Goethe University Frankfurt, 60590 Frankfurt/Main, Germany

[2] Faculty of Biological Sciences, Goethe University Frankfurt, 60438 Frankfurt/Main, Germany

[3] Faculty of Medicine, Justus-Liebig-University Giessen, 35392 Giessen, Germany

[*] Stephan W. Schwarzacher and Peter Jedlicka contributed equally to this work

correspondence to: Julia Muellerleile, Institute of Clinical Neuroanatomy, Neuroscience Center, Goethe University Frankfurt, Theodor-Stern-Kai 7, 60590 Frankfurt/Main, Germany
muellerleile@med.uni-frankfurt.de

## Abstract

Loss-of-function mutations in Neuroligin-4 (Nlgn4), a member of the Neuroligin family of postsynaptic adhesion proteins, cause autism spectrum disorder (ASD) in humans. Nlgn4 knockout (KO) in mice leads to social behavior deficits and complex alterations of synaptic inhibition or excitation, depending on the brain region, with altered excitation-inhibition (E-I) balance as a common consequence. In the present study, we comprehensively analyzed synaptic function and plasticity at the cellular and network levels in hippocampal dentate gyrus of Nlgn4 KO mice. Compared to wildtype littermates, Nlgn4 KOs exhibited increased paired-pulse inhibition of dentate granule cell population spikes, but no impairments of synaptic transmission or plasticity *in vivo*. *In vitro* patch-clamp recordings in organotypic entorhino-hippocampal slice cultures confirmed that synaptic transmission and homeostatic synaptic scaling are unimpaired in Nlgn4 KO granule cells, but revealed subtle defects in their intrinsic excitability. Thus, the loss of Nlgn4 alters dentate granule cell excitability and increases network inhibition in the dentate gyrus without impairing synaptic function. These results underscore the importance of non-synaptic mechanisms in determining E-I balance.

**Keywords:** neuroligins; synaptic transmission; *in vivo* electrophysiology; organotypic entorhino-hippocampal slice culture; whole-cell patch clamp recording; dentate granule cell

## Introduction

Neuroligins (Nlgn1-4) are transmembrane cell adhesion proteins that physically link the pre- and postsynapse by binding to presynaptic Neurexins [1] and regulate synapse assembly and maturation via interactions with multiple postsynaptic scaffold and signaling proteins, such as PSD95 [2, 3], gephyrin, or collybistin [4]. Nlgn4, arguably the most enigmatic of the four family members is expressed at lower levels than the other Neuroligins in mice [5], but plays an important role in the regulation of synaptic transmission in different brain regions [6–10]. Strikingly, loss-of-function mutations in the human Nlgn4 ortholog NLGN4X cause autism spectrum disorder (ASD) in humans [11–13], and Nlgn4 knockout (KO) mice exhibit ASD-like traits [14–16], establishing Nlgn4 KO mice as construct- and face-valid ASD models that can yield important insights into the pathomechanisms of ASD.

The synaptic localization and function of Nlgn4 in mice differs between brain regions. In retina and brainstem, Nlgn4 controls the assembly and function of glycinergic synapses [6, 7], whereas it predominantly operates at GABAergic synapses in hippocampal area CA3 [9] and at both excitatory and inhibitory synapses in the cortex [8, 10]. Analyses of the human ortholog indicated a function of NLGN4X at excitatory synapses [17–21]. However, all corresponding studies involved conditions of NLGN4X overexpression, under which Neuroligins are well known to lose any synapse type specificity they may have *in vivo*.

The KO mouse model offers the key advantage of studying Nlgn4 function *in vivo* in defined brain regions that are involved in the cognitive and behavioral symptoms of ASD. One such region is the hippocampal dentate gyrus, which has been implicated in different forms of learning and memory, including social memory [22], and serves an important function by controlling the excitability of the hippocampus proper [23]. The principal neurons of the dentate gyrus, the granule cells, are characterized by a low resting membrane potential and sparse firing activity, which is controlled by strong GABAergic inhibition. As Nlgn4 regulates perisomatic inhibition of CA3 pyramidal cells [9], we hypothesized that it might serve a similar function in granule cells. Therefore, we analyzed the consequences of Nlgn4 KO on synaptic transmission, excitability, and network inhibition in the dentate gyrus using *in vivo* field potential recordings. Unexpectedly, we found that network inhibition is increased in the Nlgn4 KO dentate gyrus. Patch clamp recordings in hippocampal slice cultures revealed that the increased excitability is not due to altered inhibitory synaptic input to granule cells, but rather to subtle alterations in the frequency-current relationship that reflect a reduction of the intrinsic excitability of Nlgn4-deficient granule cells. Taken together, these results are consistent with the E-I imbalance theory of ASD and underscore the importance of non-synaptic mechanisms in determining E-I balance.

# Methods

## Animals

Animal experiments were performed in accordance with the German law regarding the use of laboratory animals (Tierschutz-Versuchstierverordnung) and all procedures were approved by the Regierungspräsidium Darmstadt and the animal welfare officer responsible for the institute (Faculty of Medicine, Goethe University Frankfurt). Mice were housed in individually ventilated cages or in filter-top cages within a ventilated cabinet (Scantainer) at a constant temperature and a 12-hour light/dark cycle with food and water available *ad libitum*. Nlgn4 KO (RRID: MGI:3775814, [14]) and wildtype (WT) littermates from heterozygote interbreedings were used in all experiments. Genotyping was carried out as previously described [15].

## Surgery and *in vivo* electrophysiology

The surgical procedure and electrophysiological measurements were performed as described previously [24]. Briefly, adult male mice (aged 8-12 weeks) were anesthetized with urethane (1.2 g/kg body weight in the initial dose, then 0.2-0.5 g/kg doses for maintenance) and placed in a stereotactic frame (Kopf instruments) for the insertion of the stimulation and recording electrodes according to the coordinates from a mouse brain atlas [25]. Prilocaine hydrochloride with adrenaline (Xylonest 1%, AstraZeneca) was used for local anesthesia of the scalp. A bipolar stimulation electrode (NE-200, 0.5 mm tip separation, Rhodes Medical Instruments) was inserted into the angular bundle of the perforant path (coordinates: 3.7 mm posterior to bregma, 2.5 mm lateral to the midline, 1.8 mm below the brain surface), and a tungsten recording electrode (TM33A10KT, World Precision Instruments) was positioned above the ipsilateral dentate gyrus (coordinates: 1.7 mm posterior to bregma, 1.0 mm lateral to the midline) and lowered in 0.05-0.1 mm increments until the suprapyramidal granule cell layer was reached, determined by the waveform in response to 500 µA/0.1 ms current pulses provided by a stimulus generator (STG1004, Multichannel Systems). The field excitatory postsynaptic potentials (fEPSPs) were pre-amplified (P55 preamplifier, Grass Technologies) and digitized at 10 kHz (Digidata 1440A, Molecular Devices) for visualization and offline analysis. The stimulation protocols were applied in the following order: increasing stimulation intensities from 30 to 800 µA for input-output measurements, low intensity paired-pulse stimulation to elicit paired-pulse facilitation (PPF) of the fEPSP, maximal intensity paired-pulse stimulation to elicit paired-pulse inhibition (PPI) of the population spike, and theta-burst stimulation (TBS) for the induction of long-term potentiation (LTP). Prior to LTP induction, a 10-minute baseline was recorded at a stimulation intensity set to elicit a 1-2 mV population spike. The stimulation intensity and duration were doubled during the TBS, which consisted of six series (separated by 20 seconds) of six trains (separated by 0.2 seconds) of six 400 Hz pulses. After TBS, evoked field potentials using the pre-TBS stimulation intensity were recorded for 1 hour. At the end of the experiment, the deeply anesthetized mice were transcardially perfused with 4% (w/v) paraformaldehyde and the brains were stored at -20°C until histological analysis.

## Preparation of organotypic entorhino-hippocampal slice cultures

Slice cultures were prepared from mice of either sex at postnatal day 4 or 5 as previously described [26]. Brains were rapidly removed, attached to a vibratome base plate with tissue glue (Histoacryl, B. Braun), and placed in preparation medium containing HEPES-buffered minimum essential medium (MEM, Gibco/Thermo Fisher) containing Earle's salts, 0.65% glucose, 0.1 mg/mL streptomycin, 100 U/mL penicillin (all from Merck/Sigma-Aldrich), and 2mM Glutamax (Gibco/ThermoFisher); adjusted to a pH between 7.3 and 7.4 with HCl (VWR Chemicals) and NaOH. 300 µm thick horizontal sections were cut with the vibratome (Leica

VT1000S) set to a low speed (0.13 mm/s) and high frequency (80-90 Hz). The hippocampus and the attached entorhinal cortex were dissected with sterile scalpels and carefully placed on a membrane filter insert (Millicell-CM, Millipore, 0.4 µm pore size, 30 mm diameter) in a six-well plate containing pre-warmed incubation medium (1 ml per well). The incubation medium was identical to the preparation medium but was supplemented with 25% (v/v) heat-inactivated normal horse serum (Gibco/ThermoFisher) and buffered with 0.15% (v/v) sodium bicarbonate to maintain a pH of 7.3 in the presence of $CO_2$. Cultures were maintained at 35°C a humidified incubator (95% air, 5% $CO_2$, Heraeus) for a minimum of 18 days before experimental manipulation, and the incubation medium was exchanged fully every 2-3 days. The day of preparation was considered day 0 *in vitro* (0 DIV).

### Tetrodotoxin treatment of mature organotypic entorhino-hippocampal slice cultures

Mature ($\geq$ 18 DIV) slice cultures were treated with 2 µM tetrodotoxin (TTX, Alomone Labs) dissolved in water or pure water by pipetting 1 µl of the solution into the well. After 48 hours, the cultures were used for patch-clamp recordings. TTX-treated cultures were placed in TTX-containing ACSF when they were cut out of the filter insert, whereas vehicle-treated cultures were cut in normal ACSF.

### Electrophysiological recording of granule cells in organotypic entorhino-hippocampal slice cultures

Whole-cell patch-clamp recordings were obtained from dentate granule cells (GCs) at 20-25 DIV. The bath solution consisted of artificial cerebrospinal fluid (ACSF) made up of (in mM) 126 NaCl, 2.5 KCl, 26 $NaHCO_3$, 1.25 $NaH_2PO_4$, 2 $CaCl_2$, 2 $MgCl_2$ (all from Merck/Sigma-Aldrich), 10 glucose (AppliChem). The pH was maintained with a mixture of 95% $O_2$/5% $CO_2$, and the bath temperature was set to 28-30°C. In most experiments, we used an intracellular solution consisting of (in mM) 126 potassium gluconate, 10 HEPES, 4 KCl, 4 ATP-Mg (all from Merck/Sigma-Aldrich), 0.3 GTP-$Na_2$ (Carl Roth), 10 PO-Creatine (Merck/Sigma-Aldrich) and 0.3% (w/v) biocytin (Cayman Chemical) adjusted to pH 7.25 with KOH. The osmolality was adjusted to 285 mOsm/kg with glucose. During miniature excitatory postsynaptic current (mEPSC) recording, 0.5 µM TTX, 10 µM D-APV, and 10 µM gabazine (all from Alomone Labs) were added to the bath solution. For recording spontaneous and evoked EPSCs and inhibitory postsynaptic currents (IPSCs) from the same cell, we used a modified version of a previously published cesium-gluconate-based intracellular solution [27]; our solution consisted of (in mM) 130 cesium gluconate (Hellobio), 10 HEPES, 10 EGTA, 2 $MgCl_2$, 2 ATP-$Na_2$ (all from Merck/Sigma-Aldrich), 0.4 GTP-$Na_2$ (Carl Roth), 5 QX314-Cl (Alomone labs), and 0.3% (w/v) biocytin (Cayman Chemical) adjusted to a pH of 7.25 and an osmolality of 285 mOsm/kg with CsOH and glucose, respectively. In these experiments, 10 µM D-APV was added to the bath solution to block N-methyl-D-aspartate (NMDA) receptors.

Patch pipettes were prepared from borosilicate glass capillaries (GC150TF-10, 1.5 mm outer diameter, Warner Instruments/Harvard Apparatus) pulled to a tip resistance of 3-5 MΩ using a horizontal puller (DMZ-Universal Electrode Puller, Zeitz Instrumente). The dentate gyrus was identified by infrared-differential interference contrast videomicroscopy using an upright microscope (Axioscope 2FS) equipped with a 40x water-immersion objective (Achroplan 0.8 numerical aperture, both from Zeiss) coupled to an infrared-sensitive CCD camera (Hamamatsu). Whole-cell patch clamp recordings of granule cells of the suprapyramidal blade of the dentate gyrus were made with a Multiclamp 700B amplifier and a CV-7B headstage (Molecular Devices) at a holding potential of -70 mV except during experiments in which the cesium-based intracellular solution was used, in which sEPSCs and sIPSCs were recorded at -60 mV and 10 mV, respectively. Data were digitized at 10 kHz (Digidata 1440A, Molecular Devices). The

resting membrane potential was measured immediately after break-in. Series resistance was monitored every 1-2 minutes, and recordings were discarded if the series resistance and leak current reached $\geq$ 30 MΩ or $\geq$ 100 pA, respectively.

The frequency-current relationship was measured in current-clamp configuration. Square current pulses (1 second duration) were applied in 10 pA increments from -100 pA to 490 pA, with 1 second interpulse intervals. The input resistance was calculated from the linear fit of the voltage difference plotted against the current injection during the negative current steps (-100 to -10 pA). After the protocol had completed, the series resistance was measured and only those cells in which the series resistance remained below 30 MΩ were included in the final analysis.

Evoked EPSCs and IPSCs were obtained by stimulating the middle and outer molecular layer with a concentric bipolar electrode (#CBAPC75, FHC) with a stimulus generator (STG1004, Multichannel Systems). The minimum stimulation intensity that elicited an EPSC was used to record evoked EPSCs and IPSCs. Per cell, 5-6 responses were recorded consecutively with 15 second interstimulus intervals at -60 mV and 10 mV holding potential. The series resistance was measured after completion of the stimulation protocol and only those cells in which the series resistance remained below 30 MΩ were included in the analysis.

### Staining and *post hoc* identification of granule cells

Following electrophysiological recording, cultures were fixed in solution containing 4% (w/v) paraformaldehyde (PFA, Honeywell/Fluka) and 4% (w/v) sucrose in phosphate-buffered saline (PBS, 0.1 M, pH 7.4, Dulbecco's, Life Technologies) for 1 hour and 2% (w/v) PFA/30% (w/v) sucrose in PBS overnight. After washing in PBS, membranes were permeabilized and nonspecific binding was blocked using a solution of Triton X-100 (VWR) and normal goat serum (NGS, Invitrogen) in PBS. Biocytin-filled neurons were stained by incubation with Alexa488-conjugated streptavidin (Invitrogen, 1:500 in PBS, 1% NGS, 0.2% Triton X-100) for 1 hour, and nuclei were subsequently stained with TO-PRO Iodide (Invitrogen, 1:5000 in PBS) for 15 minutes. Cultures were mounted on glass slides with anti-fade mounting medium (Dako Fluorescence Mounting Medium, Agilent) and observed under a confocal microscope (Eclipse C1si laser-scanning microscope, Nikon). Stained neurons were *post hoc* identified as granule cells of the suprapyramidal blade of the dentate gyrus based on morphological and anatomical criteria (identification of dendrites and/or axonal projections within the dentate gyrus).

### Data analysis and statistics

Data were analyzed with Clampfit 10.7 software (Molecular Devices), Excel 2016 (Microsoft), MATLAB version R2018b (Mathworks), and Python version 3.9 (Python Software Foundation, https://www.python.org/). The MiniAnalysis software (Version 6.0.7, Synaptosoft) was used to quantify the s/mEPSCs and sIPSCs. Traces were low-pass filtered using an Elliptic filter with a cutoff frequency of 1000 Hz. The threshold for event detection was set to 3 pA for EPSCs and 10 pA for IPSCs. A minimum of 100 events per recorded neuron were selected by an investigator blind to the genotype and experimental treatment. Frequency-current and action potential analyses were performed with custom MATLAB scripts. Spike frequency adaptation was quantified by the ratio of the first interspike interval to the last interspike interval in a spike train.

All statistical analyses were performed with Prism 8.0 software (GraphPad Software). Mean values were tested for normality using the D'Agostino & Pearson test. If the data were normally distributed, parametric statistical tests were used to compare group values. A two-way (repeated measures) analysis of variance (ANOVA) or a mixed model (if there were missing values) was used to test for significant differences between groups that differed in more than one variable, and the Bonferroni correction for multiple comparisons was applied to all post-tests. The

mixed model implemented in GraphPad Prism 8.0 uses a compound symmetry covariance matrix and is fit using Restricted Maximum Likelihood. The results can be interpreted like a repeated measures ANOVA (Motulsky, GraphPad Statistics Guide). Normality was assessed with quantile-quantile plots. The alpha level was set to 0.05, and only two-tailed *p*-values were computed. A Boltzmann sigmoidal equation was used to fit the EPSP-spike and PPI data. The bottom was set to zero, and only fits with a goodness-of-fit ($R^2$) value greater than 0.8 were included in the final analysis. All group values are given as the mean $\pm$ the standard error of the mean (SEM) along with the 95% confidence interval (CI).

## Results

### Unchanged excitatory synaptic transmission in the dentate gyrus of Nlgn4 KO mice

We first tested whether Nlgn4 plays a role at excitatory synapses in the dentate gyrus of adult mice, as we had previously observed for Nlgn1 [24] and Nlgn3 [28]. Immunostaining for Nlgn4 in the hippocampus has been unsuccessful, possibly due to posttranslational modifications of the protein, so its synaptic localization has been deduced from electrophysiological measurements in KO mice [9]. Therefore, we stimulated the perforant path and measured evoked field potentials in the dentate gyrus of WT and Nlgn4 KO mice to probe excitatory synaptic transmission from the excitatory perforant path to granule cells. We analyzed presynaptic short-term plasticity by applying a double-pulse stimulation protocol with increasing interpulse intervals to elicit paired-pulse facilitation of the fEPSP. This analysis revealed no significant differences between the WT and KO mice (Figure 1a, $n = 17$ WT and 16 KO mice, two-way repeated measures ANOVA, $p = 0.18$ for genotype, $p = 0.29$ for interaction). To examine postsynaptic function, we measured the slope of the fEPSP in response to different stimulation intensities and likewise found no differences between groups (Figure 1b, two-way repeated measures ANOVA, $p = 0.46$ for genotype, $p = 0.96$ for interaction). Therefore, it appears that Nlgn4 is not required for basal excitatory synaptic transmission onto granule cells in adult mice.

### Unaltered induction of long-term potentiation at perforant path-granule cell synapses in Nlgn4 KO mice

We had previously shown that Nlgn1 co-regulates long-term potentiation (LTP) at perforant path-granule cell synapses, most likely by promoting the trafficking of glutamate receptors to the postsynapse [24]. To test whether Nlgn4 also plays a role in synaptic plasticity, we induced LTP using a strong theta-burst stimulation (TBS) protocol and compared the potentiation of the fEPSP slope in WT and Nlgn4 KO mice (see examples in Figure 2a). There were no differences in the increase of the fEPSP slope during the induction period (Figure 2b+c, WT: $146.5 \pm 3.5\%$, 95% CI [139.1, 154.0], $n = 16$; KO: $145.3 \pm 3.6\%$, 95% CI [137.6, 153.1], $n = 13$; unpaired $t$-test with Welch's correction, $p = 0.81$) or during the final 10 minutes of recording (WT: $123.7 \pm 3.0\%$, 95% CI [117.2, 130.1], $n = 16$; KO: $120.1 \pm 3.4\%$, 95% CI [112.6, 127.6], $n = 12$; unpaired $t$-test with Welch's correction, $p = 0.44$); indicating that Hebbian synaptic plasticity is not affected by the loss of Nlgn4.

We also analyzed the potentiation of the population spike, a second component of LTP that is not dependent on the degree of synaptic potentiation [29]. Approximately 50% of the increase in the population spike amplitude induced by TBS are due to non-synaptic changes, i.e., changes in the intrinsic excitability of granule cells [30]. Therefore, a reduction in the spike potentiation could reflect a decrease in the intrinsic excitability. However, the increase in the population spike following TBS was very similar in both groups during the initial phase (Figure 2d+e, WT: $162.7 \pm 12.3\%$, 95% CI [136.4, 188.9], $n = 16$; KO: $166.0 \pm 9.4\%$, 95% CI [145.4, 186.5], $n = 13$; unpaired $t$-test with Welch's correction, $p = 0.83$), and was only slightly lower in the Nlgn4 KO mice during the final phase (WT: $151.4 \pm 12.0\%$, 95% CI [125.8, 177.1], $n = 16$; KO: $133.6 \pm 12.8\%$, 95% CI [105.4, 161.7], $n = 12$; unpaired $t$-test with Welch's correction, $p = 0.32$). Thus, the TBS-induced potentiation of the population spike is not severely affected by the loss of Nlgn4.

### Slightly altered population spike threshold in the dentate gyrus of Nlgn4 KO mice

As a measure of the basal granule cell excitability, we compared the amplitude of the population spike in response to different stimulation intensities between WT and KO mice. The population spikes were slightly reduced in the Nlgn4 KO mice, but this difference was not significant (Figure 3a, $n = 17$ WT and 16 KO mice, two-way repeated measures ANOVA, $p = 0.15$ for geno-

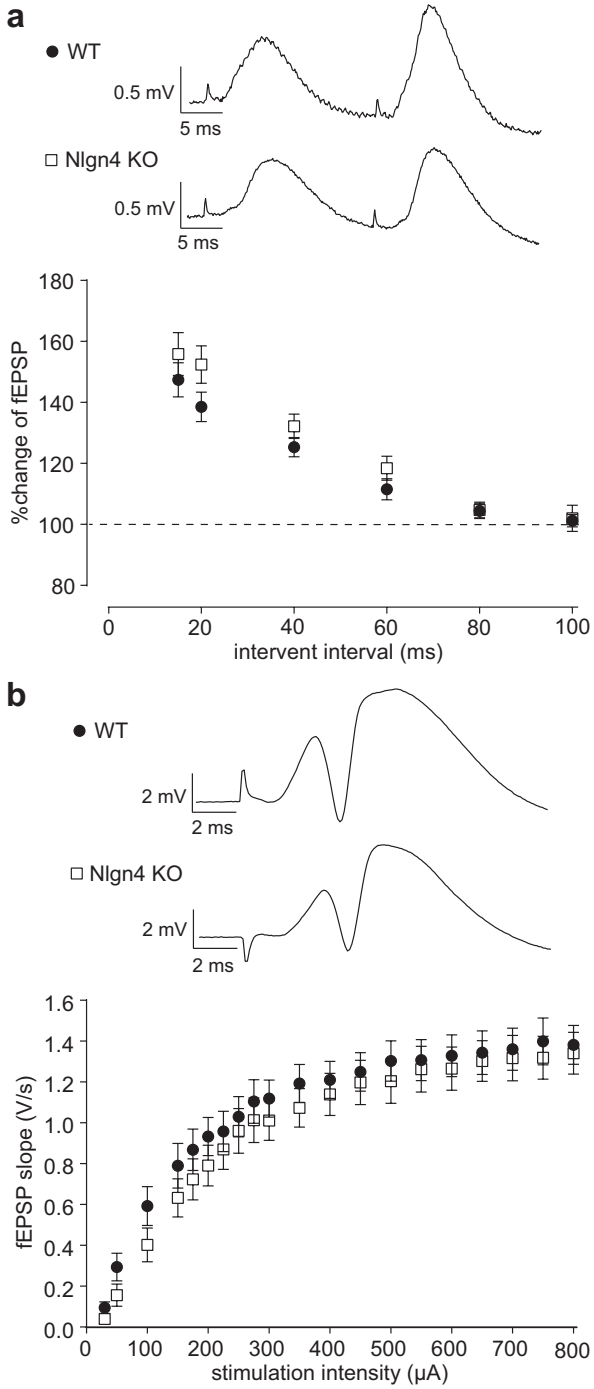


FIGURE 1: Unchanged excitatory synaptic transmission in the dentate gyrus of Nlgn4 KO mice *in vivo*. (a) Paired-pulse facilitation of the granule cell fEPSP at different interpulse intervals was not significantly different in KO mice ($n = 17$ WT and 16 KO mice, two-way repeated measures ANOVA, $p = 0.18$ for genotype, $p = 0.29$ for interaction) as illustrated by representative traces from one WT and one KO mouse at 20 ms interpulse intervals (top). (b) No significant differences in the postsynaptic strength measured by the fEPSP slope ($n = 17$ WT and 16 KO mice, two-way repeated measures ANOVA, $p = 0.46$ for genotype, $p = 0.96$ for interaction), traces show the evoked fEPSP in response to 700 µA stimulation from one WT and one KO mouse (top)

type, $p = 0.68$ for interaction). The stimulation intensity at which the first population spike appeared was slightly increased in the Nlgn4 KO mice ($206.3 \pm 19.16$ µA, 95% CI [165.4, 247.1]) compared to their WT littermates ($164.7 \pm 13.40$, 95% CI [136.3, 193.1]), approaching statistical

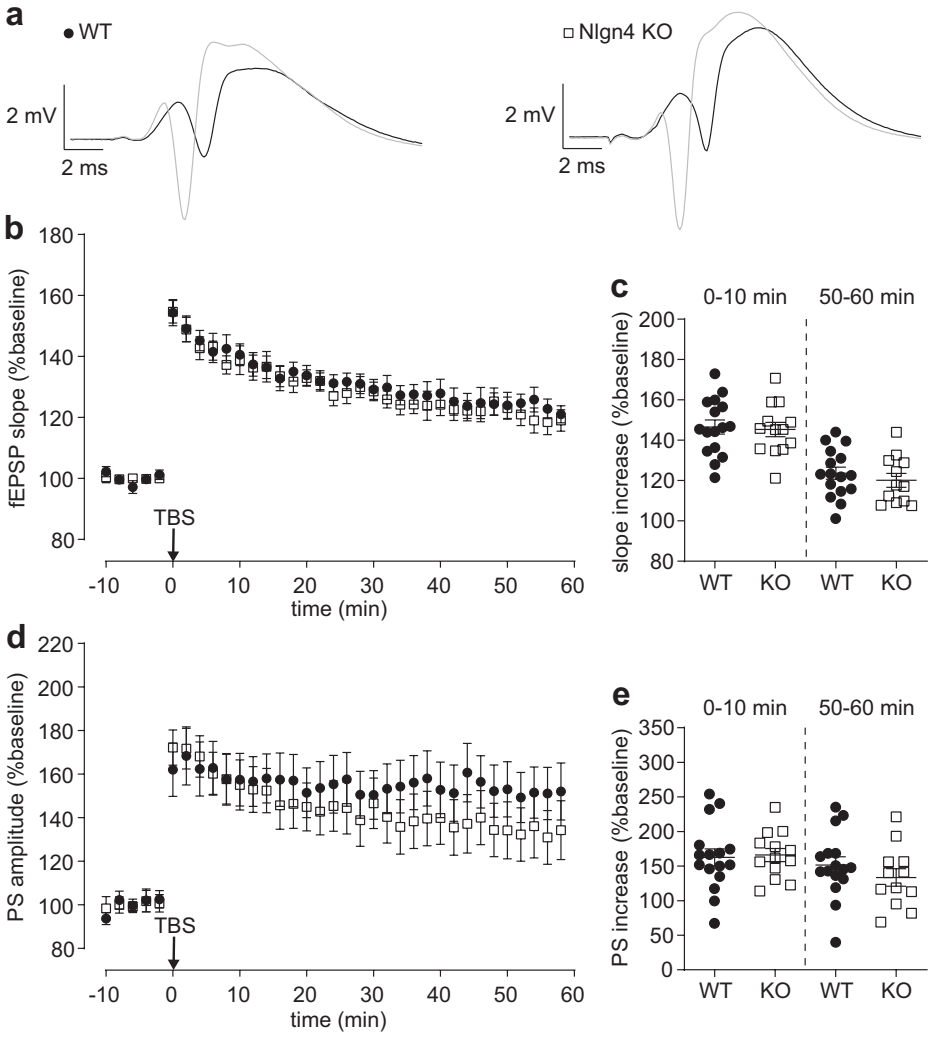


FIGURE 2: Unaltered long-term potentiation at perforant path-granule cell synapses in Nlgn4 KO mice. (a) Averaged traces showing the evoked fEPSP during the last two minutes of the baseline (black) and during the first two minutes following TBS (gray) from one WT and one KO mouse. (b) The time course of the fEPSP slope expressed relative to the pre-TBS baseline and (c) the quantification of the slope increase (unpaired $t$-test with Welch's correction, 0-10 min: $n = 16$ WT and 13 KO mice, $p = 0.81$, 50-60 min: $n = 16$ WT and 12 KO mice, $p = 0.44$) revealed a similar degree of potentiation in WT and KO mice. (d) The time course of the population spike amplitude expressed relative to the pre-TBS baseline and (e) the quantification of the spike increase (unpaired $t$-test with Welch's correction, 0-10 min: $n = 16$ WT and 13 KO mice, $p = 0.83$, 50-60 min: $n = 16$ WT and 12 KO mice, $p = 0.32$) also showed no significant differences between WT and KO mice

significance (Figure 3a inset, unpaired $t$-test with Welch's correction, $p = 0.087$). We also examined the EPSP-spike curves (i.e., the relationship between fEPSP slope and population spike amplitude at each stimulation intensity) and fitted these with a Boltzmann sigmoidal function. The mean EPSP-spike curves could be fitted using the same parameters (Figure 3b, extra sum-of-squares F test, $p = 0.14$), and the comparison of the v50 parameter of the individual fits yielded no significant difference between WT and Nlgn4 KO (Figure 3b inset, $n = 13$ WT and 13 KO mice, unpaired $t$-test with Welch's correction, $p = 0.50$). Given the known involvement of Nlgn4 in inhibitory synaptic transmission in area CA3 of the hippocampus [9], we speculated that the slightly altered granule cell excitability is due to a difference in the level of inhibition.

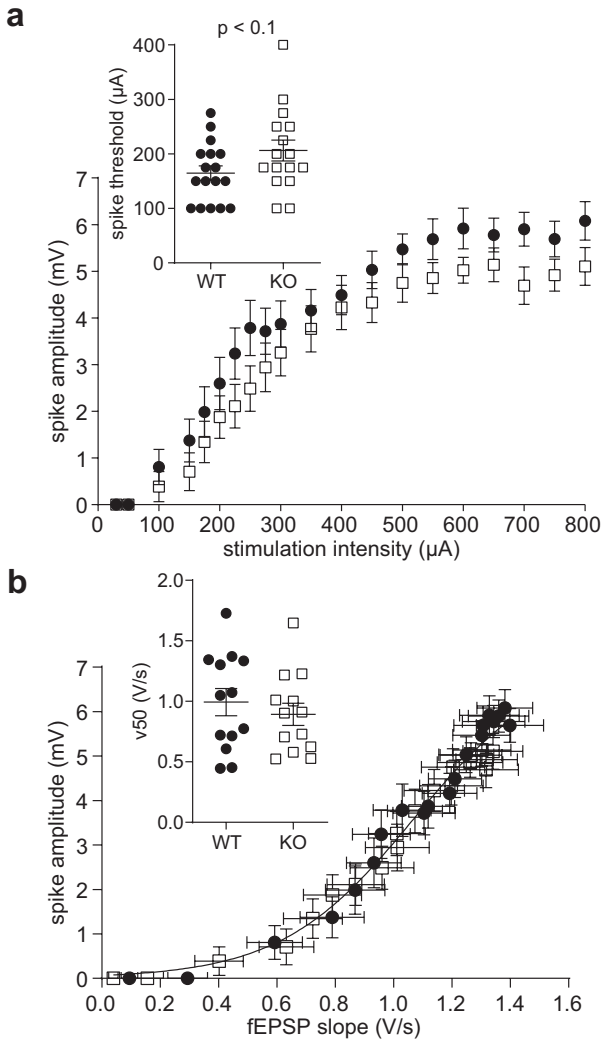


FIGURE 3: Slight differences in granule cell excitability, but unaltered EPSP-spike coupling, in Nlgn4 KO mice. (a) Granule cell excitability was assessed by the amplitude of the population spike ($n = 17$ WT and 16 KO mice, two-way repeated measures ANOVA, $p = 0.15$ for genotype, $p = 0.68$ for interaction) at increasing stimulation intensities, and the onset of the population spike occurred at slightly higher stimulation intensities in Nlgn4 KO compared to WT mice (inset, unpaired $t$-test with Welch's correction, $p = 0.087$). (b) The EPSP-spike relationship fitted by a Boltzmann sigmoidal function revealed no differences as quantified by the v50 parameter of the fit function (inset, $n = 13$ for both groups, unpaired $t$-test with Welch's correction, $p = 0.50$)

## Altered network inhibition in the dentate gyrus of Nlgn4 KO mice

To test whether Nlgn4 regulates inhibition in the dentate gyrus, we used a paired-pulse protocol to examine feedback and feed-forward inhibition of the granule cell population spike (Figure 4a), which is mediated by local interneurons [31]. Surprisingly,we observed an increase in network inhibition in Nlgn4 KO mice, indicated by a slight rightward shift of the PPI curve when using the maximal stimulation intensity of 800 µA (Figure 4b, two-way repeated measures ANOVA, $n = 17$ WT and 16 KO, $p = 0.53$ for genotype, $p = 0.017$ for interaction). To quantify the degree of inhibition, the early portion of the PPI curves (until 100 ms inter-pulse interval) was fitted by a Boltzmann sigmoidal function and the corresponding inter-pulse interval at which the amplitude of the second population spike reached 50% (WT: $38.71 \pm 1.42$ ms, 95% CI [35.70, 41.72], $n = 17$; KO: $42.75 \pm 1.55$ ms, 95% CI [39.45, 46.05], $n = 16$; unpaired $t$-test with Welch's correction, $p = 0.064$), 75% (WT: $41.14 \pm 1.48$ ms, 95% CI [38.01, 44.28], $n = 17$; KO: $45.32 \pm 1.59$

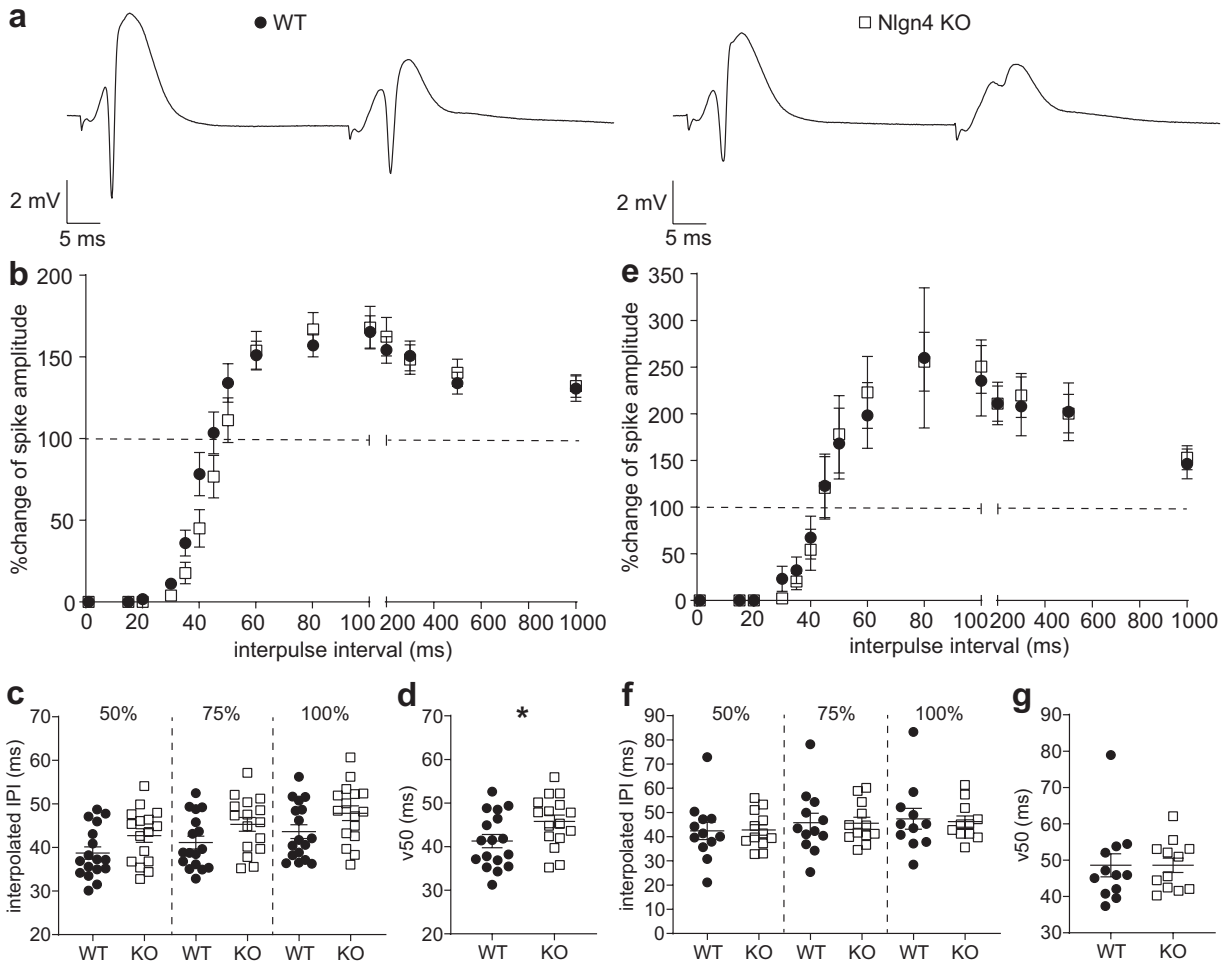


FIGURE 4: Altered network inhibition in the dentate gyrus of Nlgn4 KO mice. (a) Evoked fEPSPs from a WT and a KO mouse in response to 800 µA stimulation at 40 ms interpulse intervals. Paired-pulse (dis)inhibition of the granule cell population spike was measured in response to (b) 800 µA stimulation at different interpulse intervals revealed slight differences in network inhibition ($n = 17$ WT and 16 KO mice, two-way repeated measures ANOVA, $p = 0.53$ for genotype, $p = 0.017$ for interaction). (c) The PPI/PPDI curve was fit by a Boltzmann sigmoidal function to interpolate the interpulse intervals at different levels of inhibition; i.e., the interpulse interval at which the amplitude of the second spike reached 50% ($n = 17$ WT and 16 KO mice, $p = 0.064$), 75% ($n = 17$ WT and 16 KO mice, $p = 0.064$), and 100% ($n = 17$ WT and 16 KO mice, $p = 0.076$, unpaired $t$-test with Welch's correction) of the first spike amplitude. (d) The v50 fit parameter was significantly higher in KO mice for the maximal stimulation intensity ($n = 17$ WT and 16 KO mice, unpaired $t$-test with Welch's correction, $p = 0.040$). (e) The PPI/PPDI curve in response to minimal stimulation intensity revealed no significant differences between genotypes ($n = 12$ per group, mixed-effects model, $p = 0.94$ for genotype, $p > 0.99$ for interaction). (f) Interpolated interpulse intervals for different levels of inhibition were not significantly different (50%: $n = 12$ per group, $p = 0.84$, 75%: $n = 12$ per group, $p = 0.93$, 100%: $n = 11$ per group, $p > 0.99$, Mann-Whitney test). (g) The v50 fit parameter for the minimal stimulation intensity did not differ between WT and KO mice ($n = 12$ per group, $p = 0.71$, Mann-Whitney test)

ms, 95% CI [41.93, 48.70], $n = 16$; unpaired $t$-test with Welch's correction, $p = 0.064$) and 100% (WT: $43.64 \pm 1.57$ ms, 95% CI [40.32, 46.97], $n = 17$; KO: $47.87 \pm 1.69$ ms, 95% CI [44.27, 51.46], $n = 16$; unpaired $t$-test with Welch's correction, $p = 0.076$) of the first population spike amplitude was interpolated (Figure 4c). The v50 parameter of the Boltzmann-fitted PPI/PPDI curve was significantly higher in KO mice (Figure 4d, WT: $41.28 \pm 1.50$ ms, 95% CI [38.08, 44.48]; KO: $45.79 \pm 1.46$ ms, 95% CI [42.68, 48.91]; unpaired $t$-test with Welch's correction, $p = 0.040$), indicating a difference in the curves. Using the minimal stimulation intensity that elicited a

spike, there were no significant differences in the PPI/PPDI curve (Figure 4e, mixed-effects model, $n = 12$ per group, $p = 0.94$ for genotype, $p > 0.99$ for interaction). The quantification of the interpulse interval at different degrees of inhibition revealed no significant differences at 50% (Figure 4f, WT: $42.38 \pm 3.60$ ms, 95% CI [34.46, 50.31], $n = 12$; KO: $42.78 \pm 2.20$ ms, 95% CI [37.94, 47.62], $n = 12$; Mann-Whitney test, $p = 0.84$), 75% (WT: $45.81 \pm 3.85$ ms, 95% CI [37.33, 54.28], $n = 12$; KO: $45.58 \pm 2.43$ ms, 95% CI [40.23, 50.93], $n = 12$; Mann-Whitney test, $p = 0.93$) or 100% (WT: $47.38 \pm 4.33$ ms, 95% CI [37.74, 57.02], $n = 11$; KO: $46.25 \pm 2.35$ ms, 95% CI [41.01, 51.48], $n = 11$; Mann-Whitney test, $p > 0.99$) of the first population spike amplitude. The v50 parameter also did not differ significantly (Figure 4g, WT: $48.59 \pm 3.18$ ms, 95% CI [41.60, 55.59], $n = 12$; KO: $48.61 \pm 1.97$ ms, 95% CI [44.27, 52.95], $n = 12$; Mann-Whitney test, $p = 0.71$) between WT and KO mice, indicating that differences in the level of network inhibition only occurred when the granule cells were maximally stimulated. While these results are in accord with the slightly reduced excitability we observed (Figure 3a), we could not determine whether the increased PPI was caused by an increase in GABAergic inhibition or by a decrease in the intrinsic granule cell excitability, which would be expected to increase the relative efficacy of GABAergic inhibition in controlling the granule cell excitability [32].

## Unaltered passive electrotonic properties and subtle alterations in excitability in dentate granule cells Nlgn4 KO slice cultures

To better interpret our *in vivo* findings regarding the decreased granule cell excitability and altered network inhibition, we performed patch-clamp recordings of individual granule cells in organotypic entorhino-hippocampal slice cultures prepared from WT and Nlgn4 KO mice (Figure 5a). We examined the passive and active electrotonic properties of single granule cells using current-clamp recordings of the membrane voltage in combination with somatic current injections of increasing intensity (Figure 5b). In these experiments, we used a potassium-gluconate-based intracellular solution without calcium buffers to avoid influencing the frequency of action potential discharge [33].

The input resistance, as determined by the linear fit of the voltage differences during hyperpolarizing current injections, was higher in Nlgn4 KO granule cells compared to WT cells (Figure 5c, $223.0 \pm 25.6$ MΩ, 95% CI [165.1, 280.9] vs. $167.5 \pm 14.9$ MΩ, 95% CI [133.1, 201.9]), potentially leading to a higher excitability of these neurons, but this difference did not reach statistical significance (unpaired *t*-test with Welch's correction, $p = 0.082$). The resting membrane potential was similar in Nlgn4 KO ($-78.1 \pm 1.7$ mV, 95% CI [-74.3, -81.9], $n = 10$) and WT ($-80.1 \pm 1.4$ mV, 95% CI [-76.8, -83.4], $n = 9$; unpaired *t*-test with Welch's correction, $p = 0.37$) granule cells (Figure 5d). Based on these findings, we conclude that passive electrotonic properties of granule cells are not strongly affected by the Nlgn4 KO.

Next, we examined the frequency-current (F-I) relationship in individual granule cells by measuring the number of action potentials fired during depolarizing current injections (Figure 5e). Analyzing the resulting F-I curves with a mixed-effects model revealed a significant interaction effect of the current intensity and the genotype ($p = 0.0031$), meaning that the difference between Nlgn4-deficient and WT granule cells was dependent on the current intensity. However, the overall effect of the genotype was not significant ($p = 0.28$). We noticed that the Nlgn4-deficient granule cells appeared to start firing action potentials at a lower current intensity, so we compared the current intensity at which the first action potential was elicited (rheobase). The rheobase was slightly lower in Nlgn4-deficient granule cells (Figure 5f, $80.0 \pm 14.1$ pA vs. $100.0 \pm 10.4$ pA for WT), but the 95% confidence intervals overlapped considerably ([48.0, 112.0] for KO vs. [76.0, 124.0] for WT), and the *t*-test indicated no significant changes ($p = 0.27$). At higher current intensities, the WT granule cells exhibited a higher firing frequency, but neither the maximum firing frequency (Figure 5g, $31.89 \pm 2.07$ Hz for WT, 95% CI [27.13, 36.65] vs. $29.60 \pm 1.69$ Hz for WT, 95% CI [25.78, 33.42]; unpaired *t*-test with Welch's correction, $p = 0.40$)

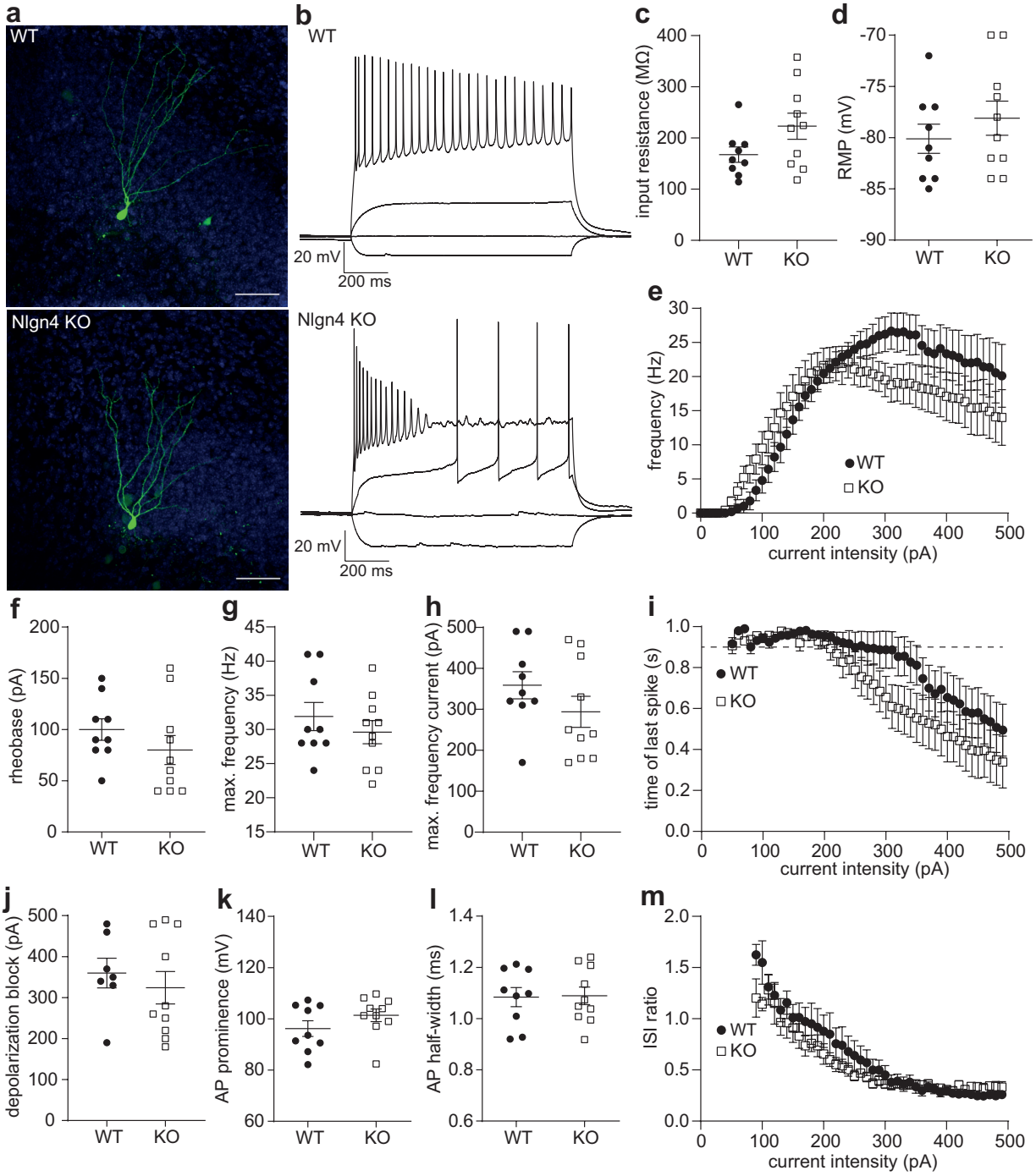


FIGURE 5: Unaltered passive electrotonic properties and subtle alterations in excitability in dentate granule cells from Nlgn4-deficient slice cultures. (a) *Post-hoc* identified recorded granule cells from a WT and a Nlgn4-deficient slice culture (maximum intensity z-projection, scale bar = 50 µm) (b) Voltage traces from one WT and one KO granule cell during -50, 0, 50, and 300 pA current injections. Note that the Nlgn4-deficient granule cell commenced spiking and entered depolarization block at lower current intensities compared to the WT cell. (c) The input resistance (unpaired $t$-test with Welch's correction, $p = 0.082$) and (d) the resting membrane potential (unpaired $t$-test with Welch's correction, $p = 0.37$) did not differ significantly between WT ($n = 9$) and KO ($n = 10$) granule cells. (e) The spike frequency plotted against the current intensity (F-I curve) reveals a significant interaction effect ($n = 9$ WT and 10 KO granule cells, mixed-effects model, $p = 0.0031$), but no effect of genotype ($p = 0.28$) on firing frequency. Comparison of (f) the rheobase (unpaired $t$-test with Welch's correction, $p = 0.27$), (g) the maximum firing frequency (unpaired $t$-test with Welch's correction, $p = 0.40$), and (h) the current at

(*continued on next page*)

FIGURE 5: (*continued from last page*) which the maximum firing frequency was attained (unpaired *t*-test with Welch's correction, $p = 0.21$) reveal no significant differences between WT ($n = 9$) and KO ($n = 10$) granule cells. (i) The time of the last spike during the 1-second current injection as a function of the current intensity showed that WT granule cells ($n = 9$) appeared to enter depolarization block (represented by the dashed line at 0.9 s) at higher intensities than Nlgn4-deficient granule cells ($n = 10$). (j) The mean current intensity during which cells entered depolarization block was not significantly different ($n = 7$ WT and 10 KO granule cells, Mann-Whitney test, $p = 0.67$). Neither (k) the action potential prominence (unpaired *t*-test with Welch's correction, $p = 0.28$) or (l) the width at half-maximal prominence (unpaired *t*-test with Welch's correction, $p = 0.92$) differed significantly between WT ($n = 9$) and KO ($n = 10$) granule cells. (m) Spike frequency adaptation was quantified by the ratio of the first interspike interval to the last interspike interval (ISI ratio) at each current intensity

nor the current intensity to reach the maximum firing frequency (Figure 5h, $294.0 \pm 37.8$ pA for KO, 95% CI [208.5, 379.5] vs. $358.9 \pm 33.1$ for WT, 95% CI [282.6, 435.2]; unpaired *t*-test with Welch's correction, $p = 0.21$) differed significantly between genotypes. Since the reduced firing frequencies in the KO group could be caused by the cells entering depolarization block at a lower current intensity, we also examined the time the last action potential was fired as a function of the current intensity (Figure 5i, mixed-effects model, $p = 0.13$ for genotype, $p = 0.50$ for interaction). The current at which the cell entered depolarization block also revealed no significant differences between genotypes (Figure 5j, $324.0 \pm 40.0$ pA for KO, 95% CI [234.6, 413.4] vs. $360.0 \pm 36.1$ for WT, 95% CI [271.6, 448.4]; Mann-Whitney test, $p = 0.67$). However, it should be noted that all Nlgn4-deficient granule cells entered depolarization block eventually, while two WT granule cells fired continuously without entering depolarization block during any of the tested current intensities. Therefore, we also analyzed the probability to enter depolarization block in the range of stimulation intensities tested (chi-squared test of independence, $\chi^2 = 2.53$, $p = 0.12$, Table 1). Taken together, these results indicate the Nlgn4-deficient granule cells are slightly more excitable, which could be related to their higher input resistance, but also tend to enter depolarization block at lower stimulation intensities compared to WT granule cells.

Action potentials are initiated at the axon initial segment, a specialized region containing a wide variety of ion channels that regulate different aspects of action potential firing. For instance, the action potential amplitude is dependent on the density of voltage-gated sodium channels in the axon initial segment, whereas the action potential half-width is regulated by $K_v1$ voltage-gated potassium channels, and $K_v7$ potassium channels impact spike frequency adaptation [34]. We therefore compared the properties of individual action potentials at the rheobase current to detect possible defects in action potential generation in the Nlgn4-deficient granule cells. The action potential prominence was slightly higher in the KO (Figure 5k, prominence: $101.4 \pm 2.5$ mV, 95% CI [95.8, 107.0] for KO, $96.2 \pm 3.1$ mV, 95% CI [89.2,103.3] for WT, Mann-Whitney test, $p = 0.28$). The action potential width at half-prominence was extremely similar (Figure 5l, $1.09 \pm 0.03$ ms, 95% CI [1.01, 1.17] for KO, $1.08 \pm 0.04$ ms, 95% CI [1.00, 1.17] for WT, unpaired *t*-test with Welch's correction, $p = 0.92$). Based on these two results, we concluded that the generation of action potentials was not affected by the deletion of Nlgn4. Both Nlgn4-deficient and WT granule cells exhibited spike frequency adaptation, which was quantified by the ratio of the first interspike interval (ISI) to the last ISI (Figure 5m). The results of the mixed model were inconclusive because the quantile-quantile plots revealed a strong deviation from normality. We therefore chose to compare the ISI ratios at the maximum firing frequency. This value was slightly higher in Nlgn4-deficient granule cells ($0.38 \pm 0.03$, 95% CI [0.30, 0.46]) compared to WT granule cells ($0.29 \pm 0.02$, 95% CI [0.24, 0.35]), and approached significance (unpaired *t*-test with Welch's correction, $p = 0.062$). This slight difference suggests that at lower current intensities, the spike train dynamics might be affected by the loss of Nlgn4.

TABLE 1: $\chi^2$ contingency table for entry into depolarization block, degrees of freedom = 1.

| | entered depolarization block? | | |
|---|---|---|---|
| | yes | no | total |
| WT | 7 | 2 | 9 |
| KO | 10 | 0 | 10 |
| total | 17 | 2 | 19 |

## Excitatory and inhibitory synaptic transmission is unaltered in Nlgn4-deficient dentate granule cells

To corroborate our *in vivo* findings of unaltered excitatory synaptic transmission in the dentate gyrus, we measured spontaneous EPSCs from granule cells in organotypic entorhino-hippocampal slice cultures (Figure 6a). In somatic patch clamp, the AMPAR currents are more strongly attenuated if distal synapses are insufficiently voltage clamped [35], so it is likely that the slower NMDAR currents and the proximal synaptic currents are overrepresented in these samples. Therefore, we used a cesium-gluconate-based intracellular solution in these experiments, which improves the space clamp by blocking potassium channels and thereby allows for a more accurate measurement of distal synaptic currents. We recorded sEPSCs at a holding potential of -60 mV in the presence of D-APV to isolate the AMPAR currents. There was no significant difference in the amplitude (Figure 6b, WT: $17.22 \pm 1.04$ pA, 95% CI [14.97, 19.47], $n = 14$; KO: $18.97 \pm 0.94$ pA, 95% CI [16.93, 21.01], $n = 13$; Mann-Whitney test, $p = 0.14$) or frequency (Figure 6c, WT: $10.99 \pm 2.01$ Hz, 95% CI [6.65, 15.32]; KO: $11.09 \pm 2.00$ Hz, 95% CI [6.73, 15.44]; Mann-Whitney test, $p = 0.94$) of the sEPSCs, and we also found no difference in the rise time (Figure 6d, WT: $2.69 \pm 0.09$ ms, 95% CI [2.49, 2.88]; KO: $2.68 \pm 0.07$ ms, 95% CI [2.53, 2.83], unpaired *t*-test with Welch's correction, $p = 0.97$) or decay time (Figure 6e, WT: $10.73 \pm 0.42$ ms, 95% CI [9.81, 11.64]; KO: $11.36 \pm 0.29$ ms, 95% CI [10.73, 11.98]; unpaired *t*-test with Welch's correction, $p = 0.23$).

Besides a decrease in the granule cell excitability, the difference in paired-pulse inhibition we observed *in vivo* could be caused by an increase in inhibitory synaptic strength in Nlgn4-deficient mice. To test this hypothesis, we recorded sIPSCs from the same granule cells we used for the sEPSC recordings at a holding potential of 10 mV (Figure 6f). The distribution of the sIPSC amplitudes and interevent intervals was similar in WT and Nlgn4-deficient granule cells (Figure 6g+h). We found no significant difference in the mean amplitude (Figure 6g, WT: $56.97 \pm 8.35$ pA, 95% CI [38.93, 75.00], $n = 14$; KO: $55.05 \pm 4.44$ pA, 95% CI [45.37, 64.73], $n = 13$; Mann-Whitney test, $p = 0.58$), frequency (Figure 6h, WT: $18.07 \pm 2.56$ Hz, 95% CI [12.54, 23.59]; KO: $17.24 \pm 1.88$ Hz, 95% CI [13.15, 21.32]; unpaired *t*-test with Welch's correction, $p = 0.80$), rise time (Figure 6i, WT: $3.73 \pm 0.08$ ms, 95% CI [3.55, 3.91]; KO: $3.83 \pm 0.13$ ms, 95% CI [3.55, 4.12]; unpaired *t*-test with Welch's correction, $p = 0.50$), or decay time (Figure 6j, WT: $34.00 \pm 0.90$ ms, 95% CI [32.06, 35.94]; KO: $34.37 \pm 0.95$ ms, 95% CI [32.31, 36.43]; Mann-Whitney test, $p = 0.33$) of the sIPSCs. Based on these results, we concluded that both excitatory and inhibitory transmission in granule cells is not affected by the loss of Nlgn4 in organotypic slice cultures.

## Excitation-inhibition balance is preserved in Nlgn4-deficient dentate granule cells

Previous studies reported a reduced cortical E-I ratio in Nlgn4 KO mice [8, 10], which fits to the increased network inhibition we observed *in vivo*; however, these studies had not determined

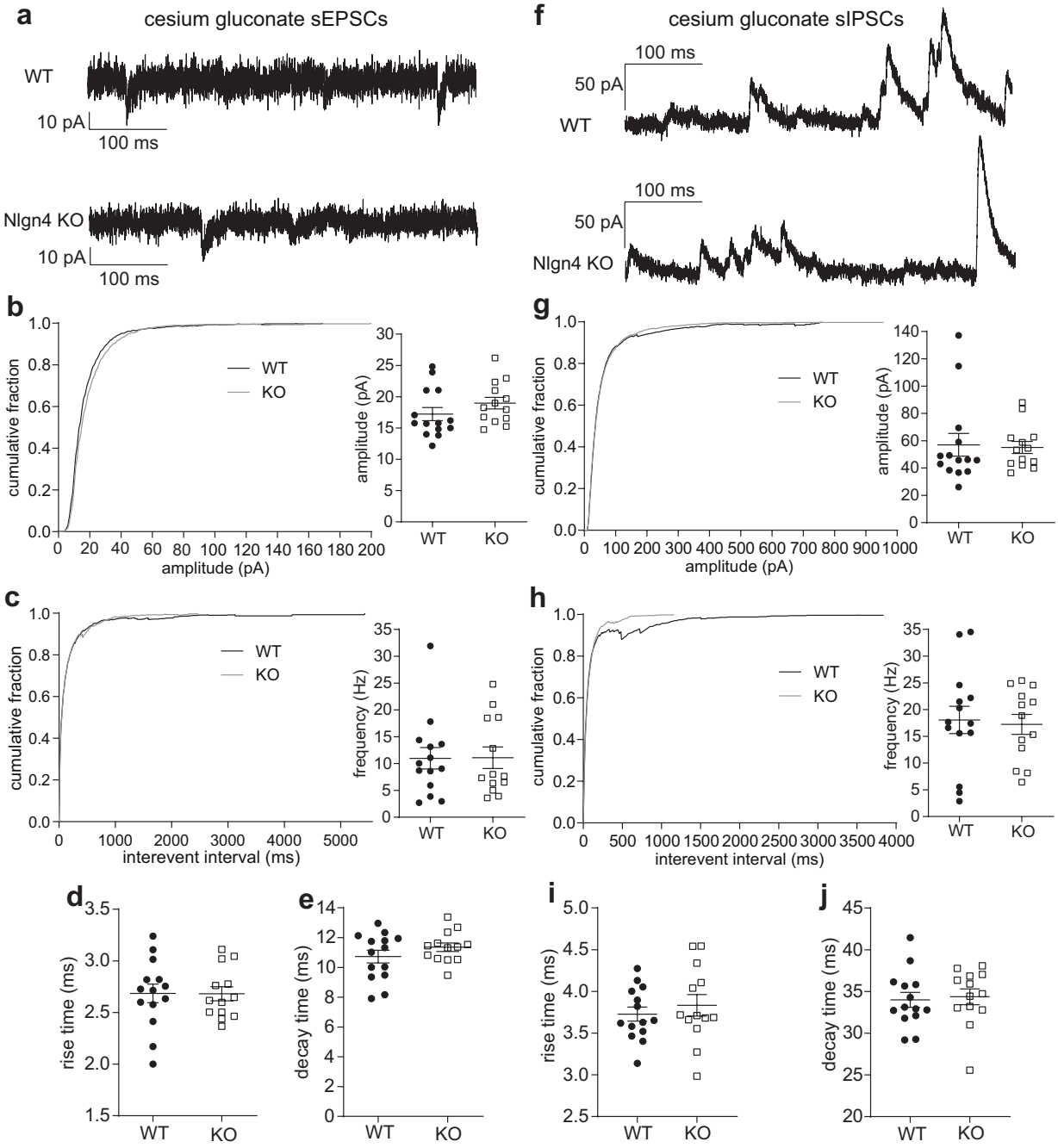


FIGURE 6: Comparable excitatory and inhibitory synaptic transmission in dentate granule cells from Nlgn4-deficient and wild-type slice cultures. (a) Representative sEPSC traces from one WT and one Nlgn4-deficient granule cell recorded using a cesium-gluconate-based intracellular solution at a holding potential of -60 mV. (b) Cumulative plots and mean-error plots reveal a similar distribution and mean of the sEPSC amplitude in WT ($n = 14$) and Nlgn4-deficient ($n = 13$) granule cells (Mann-Whitney test, $p = 0.14$). (c) Cumulative plots reveal a similar distribution of the sEPSC inter-event-interval and mean-error plots show a similar mean sEPSC frequency in WT ($n = 14$) and Nlgn4-deficient ($n = 13$) granule cells (Mann-Whitney test, $p = 0.94$). Comparison of (d) sEPSC rise times (unpaired $t$-test with Welch's correction, $p = 0.97$) and (e) sEPSC decay times (unpaired $t$-test with Welch's correction, $p = 0.23$) in WT ($n = 14$) and Nlgn4-deficient ($n = 13$) granule cells revealed no significant differences. (f) Representative granule cell sIPSC traces from organotypic cultures prepared from WT and Nlgn4 KO mice recorded with a cesium-gluconate-based intracellular solution at a holding potential of 10 mV. (g) Cumulative plots and mean-error plots reveal a similar distribution and mean of the sIPSC amplitudes in WT ($n = 14$) and Nlgn4-deficient ($n = 13$) granule cells (Mann-Whitney test, $p = 0.58$). (h) Cumulative plots reveal a

(*continued on next page*)

FIGURE 6: (*continued from last page*) similar distribution of the inter-event-intervals and mean-error plots show a similar sIPSC frequency in WT ($n = 14$) and Nlgn4-deficient ($n = 13$) granule cells (unpaired $t$-test with Welch's correction, $p = 0.80$). There were no significant differences in the (i) rise time (unpaired $t$-test with Welch's correction, $p = 0.50$) or (j) decay time (Mann-Whitney test, $p = 0.33$) between WT ($n = 14$) and Nlgn4-deficient ($n = 13$) granule cells

the E-I ratio of individual neurons. Using the cesium-gluconate-based intracellular solution, we adjusted the holding potential to record EPSCs (at -60 mV) or IPSCs (at 10 mV) in response to the same stimulation intensity and compute the excitation-inhibition (E-I) ratio of individual granule cells. We observed a slightly lower mean E-I ratio in Nlgn4 KO granule cells (Figure 7, $0.27 \pm 0.07$, 95% CI [0.13, 0.43], $n = 10$) compared to WT cells ($0.36 \pm 0.06$, 95% CI [0.23, 0.48], $n = 11$), but this difference was not significant (Mann-Whitney test, $p = 0.13$).

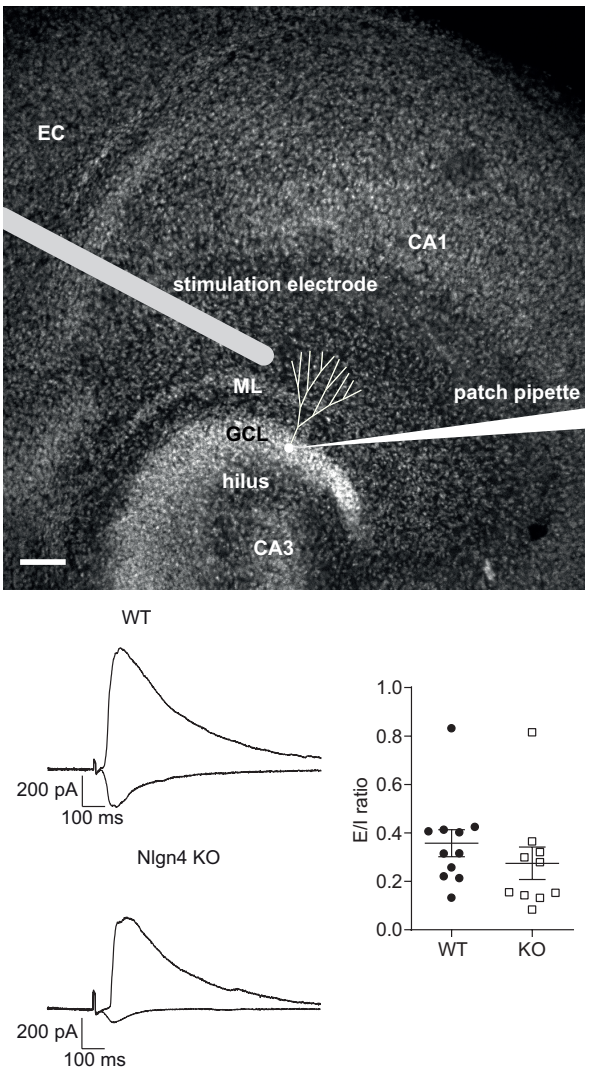


FIGURE 7: Excitation-inhibition balance is preserved in Nlgn4-deficient dentate granule cells. (top) relative location of the stimulation electrode in the molecular layer of an organotypic entorhino-hippocampal slice culture. CA1 = cornu ammonis 1, CA3 = cornu ammonis 3, EC = entorhinal cortex, GCL = granule cell layer, ML = molecular layer. Scale bar = 100 µm. (bottom left) Representative EPSCs and IPSCs evoked by molecular layer stimulation recorded in the same granule cell in slice cultures prepared from WT and Nlgn4 KO mice. (bottom right) The excitation-inhibition ratios did not differ significantly between WT and Nlgn4-deficient granule cells (Mann-Whitney test, $p = 0.13$)

### Homeostatic synaptic plasticity in dentate granule cells is not affected by the loss of Nlgn4

Our *in vivo* data had shown that Hebbian synaptic plasticity was largely unaffected by the deletion of Nlgn4, but it was unclear whether this finding generalized to other forms of synaptic plasticity operating with different molecular mechanisms. Homeostatic synaptic plasticity is a compensatory mechanism to normalize synaptic activity in response to a reduction in synaptic input [36]. Interestingly, impairments of homeostatic plasticity have been reported in several ASD mouse models [37], so we hypothesized that Nlgn4 might be involved in synaptic upscaling. We induced homeostatic synaptic upscaling using previously established synaptic scaling protocol [38]. Synaptic activity was blocked for two days by adding TTX to the culture medium. Control cultures were treated with the same volume of water for the same duration of time. Miniature EPSCs were recorded with a potassium-gluconate-based intracellular solution in the presence of TTX, D-APV and gabazine (Figure 8a). The activity blockade led to an increase in mEPSC amplitude compared to controls for both WT ($n = 11$ control and 11 TTX) and KO ($n = 14$ control and 11 TTX) granule cells (Figure 8b and Table 2, two-way ANOVA with Bonferroni's multiple comparison tests). The treatment accounted for most of the difference in amplitudes (two-way ANOVA, $p = 0.0008$), while the genotype ($p = 0.53$) and interaction ($p = 0.88$) effects were not significant. This increase in the mean amplitude was also reflected in the cumulative probability plots, which we quantified with the mean of the Gaussian function used to fit the individual curves (Figure 8c, unpaired *t*-test with Welch's correction, $p = 0.031$ for WT, $p = 0.0037$ for KO). We observed a significant effect of the genotype on the mEPSC frequency (Figure 8d, two-way ANOVA, $p = 0.031$), but the Bonferroni-corrected post-tests revealed no significant differences between WT and Nlgn4 KO granule cells (Table 3). The treatment effect approached significance ($p = 0.066$), but the interaction effect was not significant ($p = 0.39$). Neither the mEPSC rise time (Figure 8e, two-way ANOVA with Bonferroni's multiple-comparison post-tests, $p = 0.42$ for treatment, $p = 0.57$ for genotype, $p = 0.20$ for interaction) nor the mEPSC decay time (Figure 8f, two-way ANOVA with Bonferroni's multiple-comparison post-tests, $p = 0.18$ for treatment, $p = 0.81$ for genotype, $p = 0.13$ for interaction) differed based on the treatment or the genotype. Therefore, we concluded that homeostatic synaptic plasticity is preserved in granule cells from Nlgn4-deficient cultures.

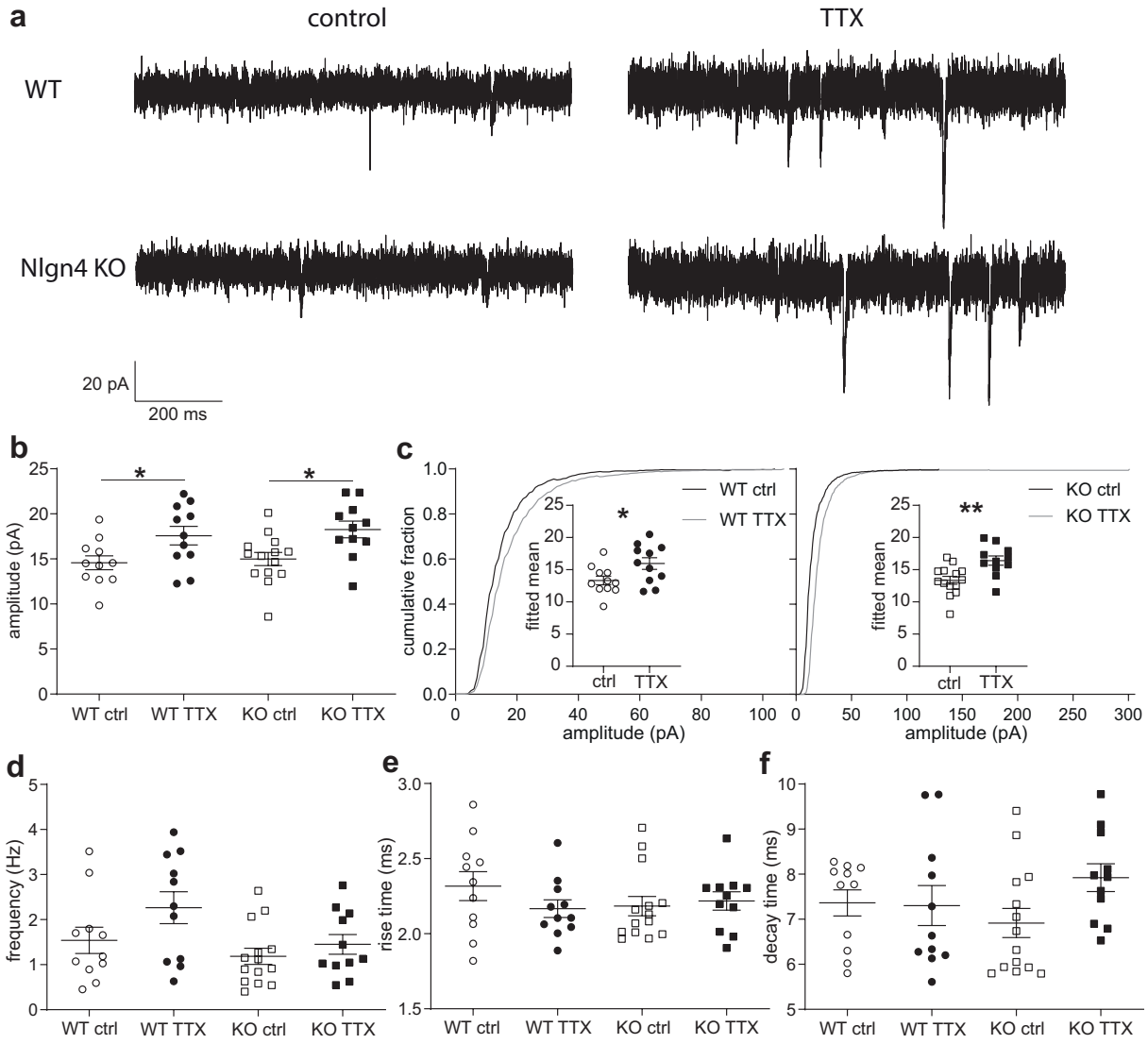


FIGURE 8: Homeostatic synaptic plasticity in dentate granule cells is not affected by the loss of Nlgn4. (a) Representative granule cell mEPSC traces from control and TTX-treated cultures prepared from WT and Nlgn4 KO mice. (b) mEPSC amplitudes were increased in TTX-treated cultures compared to control cultures from both WT ($n = 11$ control and 11 TTX) and KO ($n = 14$ control and 11 TTX) mice ($*p < 0.05$, two-way ANOVA with Bonferroni's multiple-comparison post-tests). (c) Cumulative plots reveal a shift towards higher amplitudes in the TTX-treated cultures which was quantified by the mean of the Gaussian function used to fit the individual curves (unpaired $t$-test with Welch's correction, $p = 0.031$ for WT, $p = 0.0037$ for KO). (d) The mEPSC frequency differed between genotypes, but not treatments (two-way ANOVA with Bonferroni's multiple-comparison post-tests, $p = 0.066$ for treatment, $p = 0.031$ for genotype, $p = 0.39$ for interaction). Neither the (e) mEPSC rise time (two-way ANOVA with Bonferroni's multiple-comparison post-tests, $p = 0.42$ for treatment, $p = 0.57$ for genotype, $p = 0.20$ for interaction) nor the (f) mEPSC decay time (two-way ANOVA with Bonferroni's multiple-comparison post-tests, $p = 0.18$ for treatment, $p = 0.81$ for genotype, $p = 0.13$ for interaction) differed based on the treatment or the genotype

TABLE 2: Granule cell mEPSC amplitudes (in pA) measured in control and TTX-treated slice cultures prepared from WT and Nlgn4 KO mice.

| | control | | | TTX | | | |
|---|---|---|---|---|---|---|---|
| | mean | 95% CI | n | mean | 95% CI | n | adjusted p-value |
| WT | $14.58 \pm 0.78$ | 12.84, 16.31 | 11 | $17.58 \pm 1.04$ | 15.27, 19.89 | 11 | 0.043 |
| KO | $14.99 \pm 0.73$ | 13.41, 16.57 | 14 | $18.26 \pm 0.93$ | 16.20, 20.33 | 11 | 0.018 |

TABLE 3: Granule cell mEPSC frequencies (in Hz) measured in control and TTX-treated slice cultures prepared from WT and Nlgn4 KO mice.

| | WT | | | KO | | | |
|---|---|---|---|---|---|---|---|
| | mean | 95% CI | n | mean | 95% CI | n | adjusted p-value |
| control | $1.54 \pm 0.29$ | 0.89, 2.19 | 11 | $1.19 \pm 0.18$ | 0.80, 1.58 | 14 | 0.66 |
| TTX | $2.27 \pm 0.35$ | 1.48, 3.06 | 11 | $1.45 \pm 0.22$ | 0.96, 1.94 | 11 | 0.077 |

## Discussion

E-I imbalance is one of the most widely studied mechanistic explanations of ASD [37]. We found that the Nlgn4 KO mouse, a construct- and face-valid autism model, exhibits a unique E-I imbalance in the hippocampal dentate gyrus (inhibition exceeding excitation), likely related to changes in the intrinsic excitability of dentate granule cells. To rule out other possible mechanisms for the observed E-I imbalance, such as impaired homeostatic plasticity or inhibitory synaptic transmission, we extended our approach to an in-depth analysis *in vitro*. Taken together, our data indicate that the Nlgn4 loss leads to subtle defects in the intrinsic excitability of dentate granule cells, which is reflected in a lower population spike amplitude and increased network inhibition *in vivo*.

Previous studies have shown that the four neuroligin proteins regulate different aspects of synaptic transmission and network excitability in mice. Remarkably, each of the four neuroligins (Nlgn1-4) exerts a characteristic effect on both intrinsic cellular and network activity in the dentate gyrus *in vivo* [24, 28, 39] (Figure 9a). The granule cell output, measured by the amplitude of the population spike, is determined by the complex interplay of the excitatory synaptic strength (quantified by the fEPSP slope), the intrinsic neuronal excitability of the granule cells, and feedback and feedforward inhibition from local interneurons (assessed with the PPI protocol, Figure 9b). Thus, the population spike can be used as a readout of the dentate E-I balance [40]. Nlgn1 KO mice exhibit a reduction in both the fEPSP slope and PPI, but an unchanged population spike output, thus preserving the network E-I balance [24]. Synaptic strength measured by the fEPSP slope is unchanged in Nlgn2 KO mice, but PPI is strongly decreased and the population spike output is strongly increased, leading to an increase in network excitation [39]. Nlgn3 KO mice also exhibit a reduction in the fEPSP slope, but show a tendency towards increased, rather than decreased, PPI; indicating that the unchanged population spike output is the result of a compensatory increase in the intrinsic excitability [28]. In the present work, we show that Nlgn4 KO mice exhibit no differences in excitatory synaptic transmission, a slight decrease in population spike output and an increase in PPI (Figure 4) that was more pronounced than in the Nlgn3 KO, leading to an overall decrease in network excitation.

The mechanisms underlying the reduction in PPI in the Nlgn1 and Nlgn2 KO mice are relatively straightforward to understand: the effect on PPI can be explained by a reduction in excitatory synaptic strength onto inhibitory interneurons in Nlgn1 KO mice and a reduction in inhibitory synaptic strength in granule cells in Nlgn2 KO mice. In contrast, the reason for the increase in PPI observed in the Nlgn3 and Nlgn4 KO mice is less clear. In Nlgn3 KO mice, a disruption of tonic endocannabinoid signaling from granule cells to inhibitory interneurons might result in increased inhibition, as has been demonstrated for the cholecystokinin-expressing interneuron-CA1 pyramidal cell synapse [41]. Perhaps Nlgn4 also regulates endocannabinoid signaling, but the available evidence indicates that the loss of Nlgn4 leads to a decrease in inhibitory transmission, rather than an increase, in other brain regions [8–10]. It was previously shown that increased network inhibition *in vivo* could also be caused by a reduction of voltage-gated sodium channels in the axon initial segment, thereby impairing the ability of neurons to generate action potentials [32], but our *in vitro* analysis did not indicate any changes in the properties of individual action potentials. However, we observed slight differences in the spike frequency adaptation and probability to enter depolarization block (Figure 5e+i).

Depolarization block is mediated by the interplay between the transient sodium and delayed-rectifier potassium currents [42] and may serve an important purpose in preventing network hyperexcitability. While somatic current injections do not represent normal physiological activity, currents in excess of 1 nA could be generated by the convergent input from only 3% of excitatory synapses on a CA1 pyramidal neuron [42], so current injections up to 500 pA are well within the physiological range. A different modeling study showed that the same currents that mediate de-

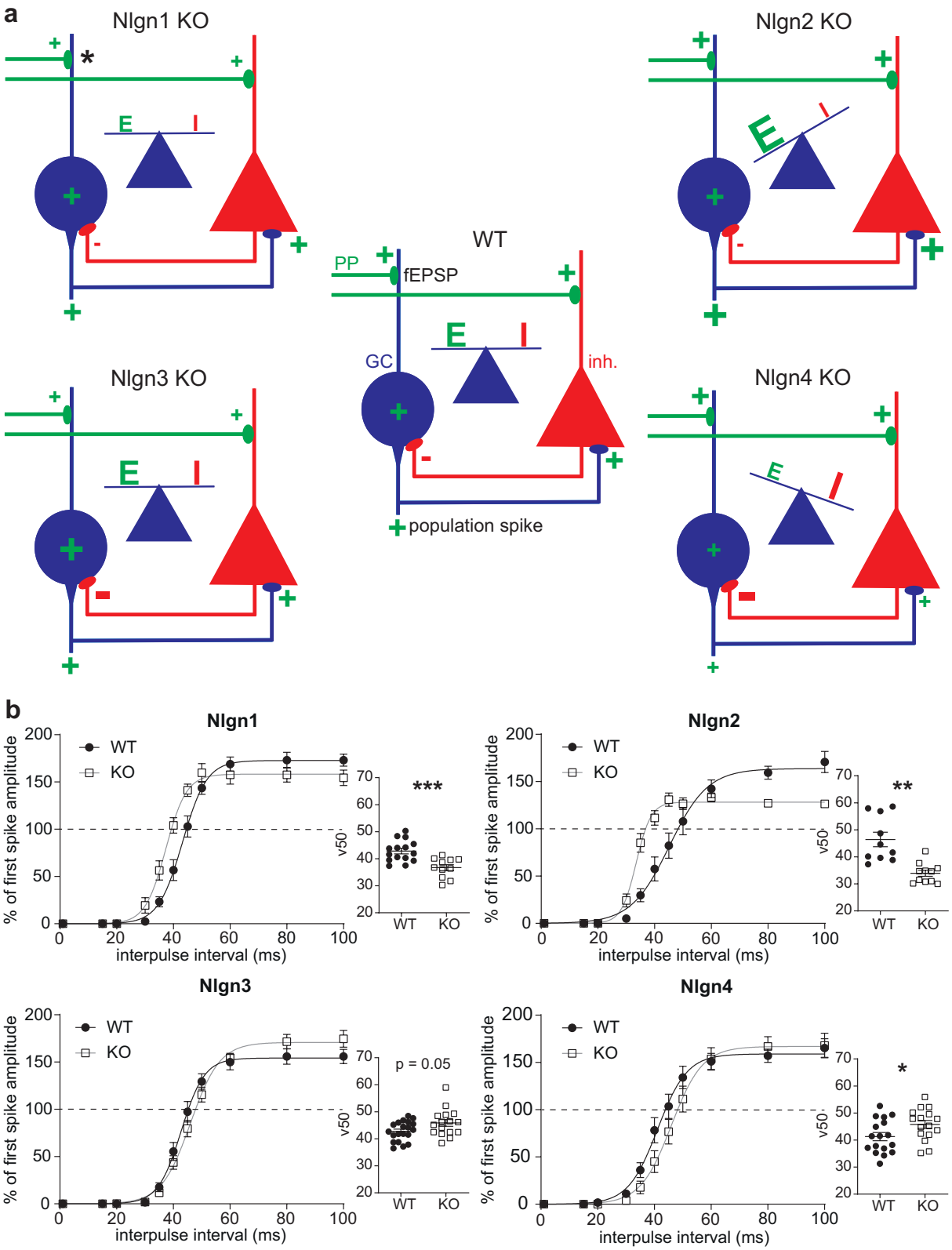


FIGURE 9: Neuroligins differentially affect E-I balance in the dentate gyrus. (a) In the wildtype (WT) dentate gyrus, excitation (E) and inhibition (I) are carefully balanced. In Nlgn1 knockout (KO) mice, both excitation and inhibition are reduced, so the net effect on the granule cell population spike output is zero [24]. In Nlgn2 KO mice, excitation is unchanged but inhibition is reduced, resulting in an increase in the granule cell excitability and an E-I imbalance [39]. In Nlgn3 KO mice, the reduced excitatory input and slightly increased inhibition is compensated by an increase in the intrinsic neuronal excitability of the granule cells, thereby preserving the E-I balance [28]. (*continued on next page*)

FIGURE 9: (*continued from last page*) In Nlgn4 KO mice, excitatory inputs are unchanged but inhibition is increased and the intrinsic granule cell excitability is slightly decreased, leading to a reduction in the population spike output and an E-I imbalance. *Of note, the only defect in the induction of long-term potentiation at perforant path-granule cell synapses was observed in Nlgn1 KO mice. GC = granule cell, inh. = inhibitory interneuron, PP = perforant path (b) Paired-pulse inhibition (PPI) of the granule cell population spike induced by double-pulse stimulation at the maximal stimulation intensity (800 µA) is reduced in Nlgn1 KO and Nlgn2 KO mice, but slightly enhanced in Nlgn3 KO mice and significantly enhanced in Nlgn4 KO mice compared to WT littermate controls. The shift in the PPI curve was quantified by the v50 parameter of the Boltzmann fit (unpaired *t*-test with Welch's correction, $*p < 0.05$, $**p < 0.01$, $***p < 0.001$)

polarization block give rise to bistability, that is, the ability of neurons to exhibit different modes of firing, such as tonic and phasic firing [43]. We also observed a slight, but not significant, increase in the interspike interval ratio of Nlgn4-deficient granule cells, reflecting a tendency towards weaker spike frequency adaptation (Figure 5m). Spike frequency adaptation is hypothesized to stabilize neuronal network dynamics [44] and could play a role in the generation of gamma oscillations [45]. Interestingly, a recent modeling study showed that extrasynaptic NMDAR activity reduces neuronal excitability but increases bistability by activating calcium-activated potassium channels [46], which could explain the seemingly contradictory results we obtained of slightly increased excitability at lower current intensities accompanied by an earlier entry into depolarization block.

To our surprise, we did not observe any defects in inhibitory synaptic transmission (sIPSCs) in granule cells (Figure 6). Both GABAergic [8–10] and glycinergic [6, 7] transmission have been shown to be regulated by Nlgn4 in other brain regions, so our findings might reflect a regional differentiation of Nlgn4 function. The model systems and the age of the animals also differed: we used organotypic slice cultures prepared from P5 mice whereas the other studies used acute slices from young mice between P12 and P30; however, we allowed the slice cultures to mature *in vitro* for three weeks before performing experiments. Importantly, our *in vivo* findings support our *in vitro* results in that the network inhibition was increased, rather than decreased, in adult Nlgn4 KO mice. In contrast, the previous studies reported a decrease in the amplitude or frequency of IPSCs, which would be expected to decrease the level of network inhibition. Therefore, our results are consistent with a regional difference in Nlgn4 function.

Likewise, we found no evidence of Nlgn4 involvement in excitatory synaptic transmission or plasticity *in vivo* or *in vitro*. Both presynaptic plasticity and perforant path-granule cell synaptic strength were unchanged in the Nlgn4 KO mice (Figure 1), and we detected no differences in the degree of LTP induction between KO and WT littermates (Figure 2). The absence of an LTP deficit is consistent with the previously reported absence of learning deficits in hippocampal-dependent tasks [14]. While we did observe a decrease in sEPSC rise times measured with the potassium-gluconate intracellular solution (Supplementary Figure 2), this finding could not be replicated with a cesium-based intracellular solution which improves the space clamp and therefore provides a more accurate reflection of the sEPSC kinetics (Figure 6d). Furthermore, our analysis of the synaptic scaling experiments revealed no genotype differences in the amplitude of mEPSCs (Figure 8), and the significant genotype effect on the mEPSC frequency might reflect differences in the variances rather than significant differences in the means (see the non-significant *post hoc* comparisons detailed in Table 3). However, we cannot exclude a function for Nlgn4 at excitatory synapses since all these experiments used constitutive KO mice which potentially suffer from confounding developmental or homeostatic compensation. Other studies of murine Nlgn4 found evidence for an involvement in excitatory synaptic transmission, but these results were obtained from cortical recordings [8, 10], and the synaptic localization of Nlgn4 might differ between the hippocampus and the cortex.

Unlike previous studies which reported a decrease in the E-I ratio of Nlgn4 KO mice [8, 10],

we measured evoked excitatory and inhibitory postsynaptic currents in the same cell, so each cell acted as its own control. We also found no difference in the E-I ratio of spontaneous currents, i.e., the mean sEPSC amplitude divided by the mean sIPSC amplitude of each cell (data not shown). These findings lend support to the hypothesis that the increased inhibition we observed at the network level *in vivo* could be caused by a decrease in the intrinsic excitability of granule cells, rather than an increase in inhibitory transmission.

Overall, the differences we observed in the Nlgn4 KO mice compared to WT littermates were very small relative to the differences observed in other neuroligin KOs. One possible explanation for these weak effects is the compensation of Nlgn4 function by other neuroligins, but the most parsimonious explanation is that Nlgn4 is expressed at fewer synapses as it makes up only 3% of the total neuroligin protein in the adult mouse brain [5]. Nevertheless, even small changes in the E-I balance of individual neurons can have profound effects on the network activity, as demonstrated by the decrease in gamma oscillations observed in the hippocampal subregion CA3 of Nlgn4-deficient mice [9]. A cell-specific deletion of Nlgn4 might help reduce the variability and increase the power to detect such small, but important, differences in future experiments.

Our results further underscore the differences between murine Nlgn4 and human NLGN4X, which was predominantly expressed at excitatory synapses in the brain regions and cell types studied thus far [17–20]. While these differences could be specific to certain brain areas or cell types, differences in glycosylation could also be responsible for the differential synaptic localization because the murine Nlgn4 lacks an additional glycosylation site which is preserved in all human neuroligins [17]. Nevertheless, even if the synaptic localization of Nlgn4 differs in human and murine neurons, common mechanisms might be involved in the generation of the behavioral symptoms observed in humans with ASD-related Nlgn4 mutations and Nlgn4 KO mice.

In conclusion, we provide evidence for an increased level of network inhibition in the dentate gyrus of adult Nlgn4 KO mice and alterations in the intrinsic excitability of cultured granule cells obtained from newborn (P5) mice. Intriguingly, the deletion of the fellow autism candidate gene Nlgn3 also leads to a slight increase in network inhibition in the dentate gyrus and a possibly homeostatic increase in the granule cell intrinsic excitability [28], which suggests that increased inhibition and modifications of the intrinsic excitability might underlie some of the behavioral symptoms observed in Nlgn3 and Nlgn4 KO mice and individuals with autism-associated neuroligin mutations. Our results show that even in the absence of synaptic deficits, alterations of the intrinsic excitability can impair the E-I balance in neuronal networks.

## References


1. Südhof TC (2017) Synaptic Neurexin Complexes: A Molecular Code for the Logic of Neural Circuits. Cell 171:745–769. https://doi.org/10.1016/j.cell.2017.10.024

2. Irie M, Hata Y, Takeuchi M, et al (1997) Binding of neuroligins to PSD-95. Science 277(5331): 1511–1515. https://doi.org/10.1126/science.277.5331.1511

3. Bolliger MF, Frei K, Winterhalter KH, Gloor SM (2001) Identification of a novel neuroligin in humans which binds to PSD-95 and has a widespread expression. Biochem J 356:581–588. https://doi.org/10.1042/0264-6021:3560581

4. Poulopoulos A, Aramuni G, Meyer G, et al (2009) Neuroligin 2 Drives Postsynaptic Assembly at Perisomatic Inhibitory Synapses through Gephyrin and Collybistin. Neuron 63:628–642. https://doi.org/10.1016/j.neuron.2009.08.023

5. Varoqueaux F, Aramuni G, Rawson RL, et al (2006) Neuroligins Determine Synapse Maturation and Function. Neuron 51:741–754. https://doi.org/10.1016/j.neuron.2006.09.003

6. Zhang B, Gokce O, Hale WD, et al (2018) Autism-associated neuroligin-4 mutation selectively impairs glycinergic synaptic transmission in mouse brainstem synapses. J Exp Med 215:1543–1553. https://doi.org/10.1084/jem.20172162

7. Hoon M, Soykan T, Falkenburger B, et al (2011) Neuroligin-4 is localized to glycinergic postsynapses and regulates inhibition in the retina. Proc Natl Acad Sci U S A 108:3053–3058. https://doi.org/10.1073/pnas.1006946108

8. Delattre V, La Mendola D, Meystre J, et al (2013) Nlgn4 knockout induces network hypoexcitability in juvenile mouse somatosensory cortex in vitro. Sci Rep 3:2897. https://doi.org/10.1038/srep02897

9. Hammer M, Krueger-Burg D, Tuffy LP, et al (2015) Perturbed Hippocampal Synaptic Inhibition and $\gamma$-Oscillations in a Neuroligin-4 Knockout Mouse Model of Autism. Cell Rep 13:516–523. https://doi.org/10.1016/j.celrep.2015.09.011

10. Unichenko P, Yang J-W, Kirischuk S, et al (2017) Autism Related Neuroligin-4 Knockout Impairs Intracortical Processing but not Sensory Inputs in Mouse Barrel Cortex. Cereb Cortex 1–14. https://doi.org/10.1093/cercor/bhx165

11. Jamain S, Quach H, Betancur C, et al (2003) Mutations of the X-linked genes encoding neuroligins NLGN3 and NLGN4 are associated with autism. Nat Genet 34:27–29. https://doi.org/10.1038/ng1136

12. Kopp N, Amarillo I, Martinez-Agosto J, Quintero-Rivera F (2020) Pathogenic paternally inherited NLGN4X deletion in a female with autism spectrum disorder: Clinical, cytogenetic, and molecular characterization . Am J Med Genet Part A. https://doi.org/10.1002/ajmg.a.62025

13. Yan J, Oliveira G, Coutinho A, et al (2005) Analysis of the neuroligin 3 and 4 genes in autism and other neuropsychiatric patients. Mol Psychiatry 10:329–332. https://doi.org/10.1038/sj.mp.4001629

14. Jamain S, Radyushkin K, Hammerschmidt K, et al (2008) Reduced social interaction and ultrasonic communication in a mouse model of monogenic heritable autism. Proc Natl Acad Sci U S A 105:1710–1715. https://doi.org/10.1073/pnas.0711555105

15. El-Kordi A, Winkler D, Hammerschmidt K, et al (2013) Development of an autism severity score for mice using Nlgn4 null mutants as a construct-valid model of heritable monogenic autism. Behav Brain Res 251:41–49. https://doi.org/10.1016/j.bbr.2012.11.016

16. Ju A, Hammerschmidt K, Tantra M, et al (2014) Juvenile manifestation of ultrasound communication deficits in the neuroligin-4 null mutant mouse model of autism. Behav Brain Res 270:159–164. https://doi.org/10.1016/j.bbr.2014.05.019

17. Cast TP, Boesch DJ, Smyth K, et al (2021) An Autism-Associated Mutation Impairs Neuroligin-4 Glycosylation and Enhances Excitatory Synaptic Transmission in Human Neurons. J Neurosci 41:392–407. https://doi.org/10.1523/JNEUROSCI.0404-20.2020

18. Marro SG, Chanda S, Yang N, et al (2019) Neuroligin-4 Regulates Excitatory Synaptic Transmission in Human Neurons. Neuron 103:617-626.e6. https://doi.org/10.1016/j.neuron.2019.05.043

19. Chanda S, Aoto J, Lee SJ, et al (2016) Pathogenic mechanism of an autism-associated neuroligin mutation involves altered AMPA-receptor trafficking. Mol Psychiatry 21:169–177. https://doi.org/10.1038/mp.2015.20

20. Zhang C, Milunsky JM, Newton S, et al (2009) A neuroligin-4 missense mutation associated with autism impairs neuroligin-4 folding and endoplasmic reticulum export. J Neurosci 29:10843–10854. https://doi.org/10.1523/JNEUROSCI.1248-09.2009

21. Bemben MA, Nguyen Q-A, Wang T, et al (2015) Autism-associated mutation inhibits protein kinase C-mediated neuroligin-4X enhancement of excitatory synapses. Proc Natl Acad Sci U S A 112:2551–2556. https://doi.org/10.1073/pnas.1500501112

22. Kesner RP (2018) An analysis of dentate gyrus function (an update). Behav Brain Res 354:84–91. https://doi.org/10.1016/j.bbr.2017.07.033

23. Krook-Magnuson E, Armstrong C, Bui A, et al (2015) In vivo evaluation of the dentate gate theory in epilepsy. J Physiol 593:2379–2388. https://doi.org/10.1113/JP270056

24. Jedlicka P, Vnencak M, Krueger DD, et al (2015) Neuroligin-1 regulates excitatory synaptic transmission, LTP and EPSP-spike coupling in the dentate gyrus in vivo. Brain Struct Funct 220:47–58. https://doi.org/10.1007/s00429-013-0636-1

25. Franklin KBJ, Paxinos G (1997) The Mouse Brain in Stereotaxic Coordinates, 1st ed. Academic Press, San Diego

26. Del Turco D, Deller T (2007) Organotypic entorhino-hippocampal slice cultures–a tool to study the molecular and cellular regulation of axonal regeneration and collateral sprouting in vitro. Methods Mol Biol 399:55–66. https://doi.org/10.1007/978-1-59745-504-6_5

27. Le Prieult F, Thal SC, Engelhard K, et al (2017) Acute Cortical Transhemispheric Diaschisis after Unilateral Traumatic Brain Injury. J Neurotrauma 34:1097–1110. https://doi.org/10.1089/neu.2016.4575

28. Muellerleile J, Vnencak M, Ippolito A, et al (2021) Neuroligin-3 Regulates Excitatory Synaptic Transmission and EPSP-Spike Coupling in the Dentate Gyrus In Vivo. Mol Neurobiol. https://doi.org/10.1007/s12035-021-02663-9

29. Taube JS, Schwartzkroin PA (1988) Mechanisms of long-term potentiation: EPSP/spike dissociation, intradendritic recordings, and glutamate sensitivity. J Neurosci 8:1632–1644. https://doi.org/10.1523/jneurosci.08-05-01632.1988

30. Lopez-Rojas J, Heine M, Kreutz MR (2016) Plasticity of intrinsic excitability in mature granule cells of the dentate gyrus. Sci Rep 6:21615. https://doi.org/10.1038/srep21615

31. Sloviter RS (1991) Feedforward and feedback inhibition of hippocampal principal cell activity evoked by perforant path stimulation: GABA-mediated mechanisms that regulate excitability In Vivo. Hippocampus 1:31–40. https://doi.org/10.1002/hipo.450010105

32. Winkels R, Jedlicka P, Weise FK, et al (2009) Reduced excitability in the dentate gyrus network of $\beta$IV-spectrin mutant mice in vivo. Hippocampus 19:677–686. https://doi.org/10.1002/hipo.20549

33. Madison BYD V, Nicoll RA (1984) Control of the Repetitive Discharge of Rat CA1 Pyramidal Neurones In Vitro. J Physiol 354:319–331

34. Kole MHP, Stuart GJ (2012) Signal Processing in the Axon Initial Segment. Neuron 73:235–247. https://doi.org/10.1016/j.neuron.2012.01.007

35. Hestrin S, Nicoll RA, Perkel DJ, Sah P (1990) Analysis of excitatory synaptic action in pyramidal cells using whole-cell recording from rat hippocampal slices. J Physiol 422:203–225

36. Turrigiano G (2012) Homeostatic synaptic plasticity: Local and global mechanisms for stabilizing neuronal function. Cold Spring Harb Perspect Biol 2012;4:a005736. https://doi.org/10.1101/cshperspect.a005736

37. Nelson SB, Valakh V (2015) Excitatory/Inhibitory Balance and Circuit Homeostasis in Autism Spectrum Disorders. Neuron 87:684–698. https://doi.org/10.1016/j.neuron.2015.07.033

38. Vlachos A, Becker D, Jedlicka P, et al (2012) Entorhinal denervation induces homeostatic synaptic scaling of excitatory postsynapses of dentate granule cells in mouse organotypic slice cultures. PLoS One 7:e32883. https://doi.org/10.1371/journal.pone.0032883

39. Jedlicka P, Hoon M, Papadopoulos T, et al (2011) Increased dentate gyrus excitability in neuroligin-2-deficient mice in vivo. Cereb Cortex 21:357–367. https://doi.org/10.1093/cercor/bhq100

40. Jedlicka P, Muellerleile J, Schwarzacher SW (2018) Synaptic Plasticity and Excitation-Inhibition Balance in the Dentate Gyrus: Insights from in Vivo Recordings in Neuroligin-1, Neuroligin-2, and Collybistin Knockouts. Neural Plast. https://doi.org/10.1155/2018/6015753

41. Földy C, Malenka RC, Südhof TC (2013) Autism-associated neuroligin-3 mutations commonly disrupt tonic endocannabinoid signaling. Neuron 78:498–509. https://doi.org/10.1016/j.neuron.2013.02.036

42. Bianchi D, Marasco A, Limongiello A, et al (2012) On the mechanisms underlying the depolarization block in the spiking dynamics of CA1 pyramidal neurons. J Comput Neurosci 33:207–225. https://doi.org/10.1007/s10827-012-0383-y

43. Dovzhenok A, Kuznetsov AS (2012) Exploring neuronal bistability at the depolarization block. PLoS One 7:e42811. https://doi.org/10.1371/journal.pone.0042811

44. Barranca VJ, Huang H, Li S (2019) The impact of spike-frequency adaptation on balanced network dynamics. Cogn Neurodyn 13:105–120. https://doi.org/10.1007/s11571-018-9504-2

45. Kilpatrick ZP, Ermentrout B (2011) Sparse gamma rhythms arising through clustering in adapting neuronal networks. PLoS Comput Biol 7:e1002281. https://doi.org/10.1371/journal.pcbi.1002281

46. Gall D, Dupont G (2020) Tonic activation of extrasynaptic NMDA receptors decreases intrinsic excitability and promotes bistability in a model of neuronal activity. Int J Mol Sci 21:206. https://doi.org/10.3390/ijms21010206

## Statements and Declarations

**Authors' Contributions** Conceptualization, P.J. and S.W.S.; Methodology, P.J.; Software, J.M., M.V. and T.J.; Formal Analysis, J.M., M.V. and T.J.; Investigation, J.M., M.V., V.S. and P.J.; Writing – Original Draft Preparation, J.M.; Writing – Review & Editing, J.M., P.J., S.W.S. and T.J.; Visualization, J.M.; Supervision, P.J.; Project Administration, P.J. and S.W.S.; Funding Acquisition, P.J. and S.W.S.

**Acknowledgments** We thank Charlotte Nolte-Uhl and Masuda Sader-Miri for excellent technical assistance. We thank Nils Brose (MPI for Experimental Medicine, Göttingen) for providing the Nlgn4 KO mouse line and helpful comments on the manuscript. We thank Thomas Deller (Institute of Clinical Neuroanatomy, Frankfurt) for helpful comments on the manuscript and his continuous support.

**Funding** This research was supported by the German Research Foundation (Deutsche Forschungsgemeinschaft), grant numbers JE 528/6–1 (to P.J.) and SCHW 534/6–1 (to S.W.S.).

**Conflict of Interest** The authors declare no competing interests.

**Availability of Data and Material** All data are available upon request from the corresponding author.

**Code Availability** Custom code is available upon request from the corresponding author.

**Ethics Approval** Animal experiments were conducted in accordance with the German law regarding the use of laboratory animals (Tierschutz-Versuchstierverordnung) and approved by the Regierungspräsidium Darmstadt and the animal welfare officer responsible for the institute.

**Consent to Participate** Not applicable.

**Consent for Publication** Not applicable.

# Supplementary Information

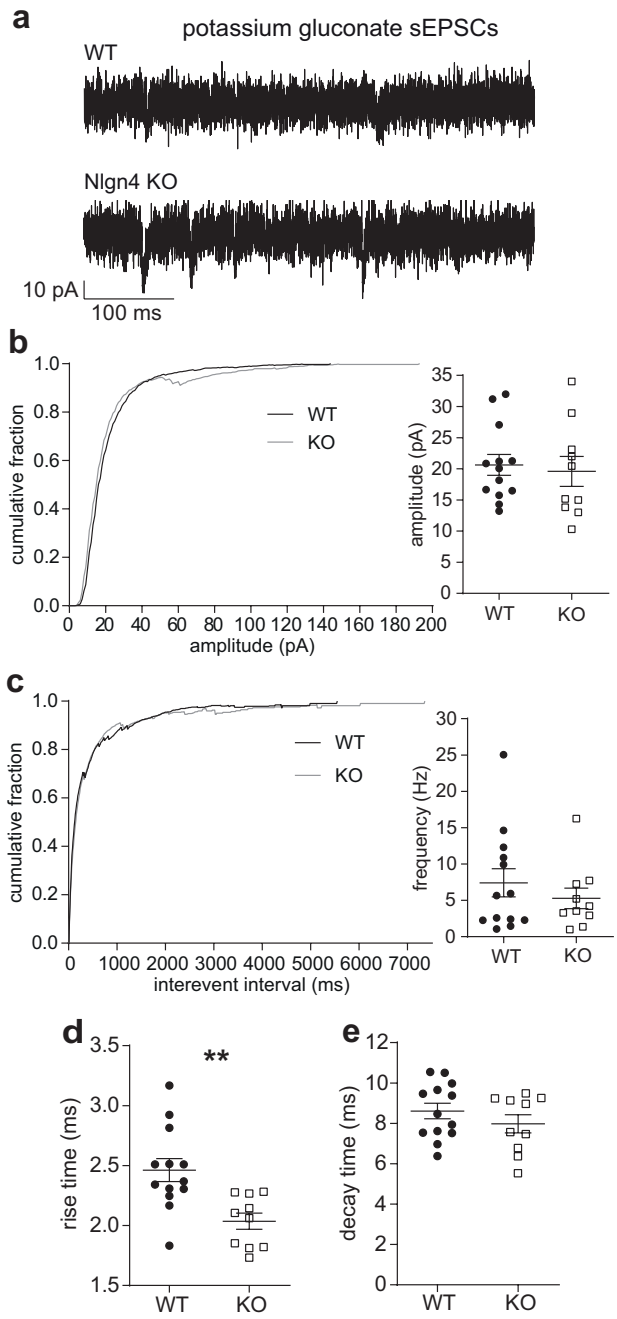


FIGURE S1: No difference in sEPSC amplitude or frequency, but decreased rise time, in Nlgn4-deficient granule cells using the potassium gluconate-based intracellular solution. (a) Representative sEPSC traces from one WT and one Nlgn4-deficient granule cell. (b) Cumulative plots and mean-error plots reveal no difference between WT ($20.63 \pm 1.68$ pA, 95% CI [16.97, 24.29], $n = 13$) and Nlgn4 KO ($19.59 \pm 2.40$ pA, 95% CI [14.16, 25.02], $n = 10$) sEPSC amplitude (unpaired $t$-test with Welch's correction, $p = 0.73$). (c) Cumulative plots reveal a similar distribution of the sEPSC interevent interval and mean-error plots show no differences between WT ($7.42 \pm 1.94$ Hz, 95% CI [3.19, 11.64]) and Nlgn4 KO ($5.27 \pm 1.41$ Hz, 95% CI [2.10, 8.45]) sEPSC frequency (Mann-Whitney test, $p = 0.74$). (d) Significant difference in the sEPSC rise time (WT: $2.46 \pm 0.10$ ms, 95% CI [2.25, 2.67]; KO: $2.04 \pm 0.07$ ms, 95% CI [1.88, 2.19]; unpaired $t$-test with Welch's correction, $p = 0.0017$), but not the (e) decay time (WT: $8.61 \pm 0.38$ ms, 95% CI [7.77, 9.45]; KO: $7.98 \pm 0.45$ ms, 95% CI [6.96, 9.00]; unpaired $t$-test with Welch's correction, $p = 0.30$).